



UNIVERSITÀ DEGLI STUDI DI MILANO
FACOLTÀ DI SCIENZE DEL FARMACO

Department of Pharmaceutical Sciences PhD
Course in Pharmaceutical Sciences (XXXIV Cycle)

**Heterocyclic β -amino acids as molecular tools for peptidomimetic
synthesis and organocatalysis**

Tutor: Prof. Maria Luisa GELMI
Coordinator: Prof. Giancarlo ALDINI

PhD Thesis of:
Francesco Vaghi R12318

Academic year 2020/2021

Contents

Table of Abbreviations.....	7
Introduction	9
β -Amino Acids	9
Carbocyclic β-amino acids.....	10
Secondary structure mimics.....	12
Pharmaceutical applications	16
Electrospinning Applications.....	17
Nanomaterials applications	20
Organocatalysis applications	22
Aim of the Thesis.....	26
Synthesis of non-natural 3-Arylmorpholino-β-amino Acid as a PPII Helix Inducer.....	28
Aim of the work.....	28
Computational studies.....	30
Synthesis of the new scaffold 2.....	32
Foldamer synthesis.....	33
NMR characterization	35
IR characterization.....	37
Simulation of (3S)-4 in a biological complex.....	38
Experimental part	40
General information.	40
Synthesis of (2S,6S)-4-Boc-6-methoxy-N-(quinolin-7-yl)-morpholine-2-carboxamide (+)-7	41
Synthesis of (2S,3S,6S)-4-Boc-6-methoxy-3-(4-methoxyphenyl)-N-(quinolin-7-yl)-morpholine-2-carboxamide (+)-8	42
Synthesis of (2S,3S,6S)-4-Boc-6-methoxy-3-(4-methoxyphenyl)-N-Boc-N'-(quinolin-7-yl)-morpholine-2-carboxamide (+)-9.....	43
Synthesis of (2S,3S,6S)-4-Boc-6-methoxy-3-(4-methoxyphenyl)-2-carboxylic acid (-)-2	44
Synthesis of N-Boc-(-)-3-(4-Methoxyphenyl)-β-Morph-(L)-Leu-(L)-Val-OBn(-)-3	46
Synthesis of CF ₃ CO ₂ H NH ₂ (-)-3-(4-Methoxyphenyl)-β-Morph-L-Leu-L-Val-OBn (+)-11	50
Synthesis of N-Boc-(-)-3-Ar-β-Morph-L-Leu-L-Val-OH (-)-12	51
Synthesis of N-Boc-(-)-3-Ar-β-Morph-(L)-Leu-(L)-Val-(-)-3-Ar-β-Morph-(L)-Leu-(L)-Val-OBn (-)-4	52
Synthesis of electrospun fibers using model peptide containing morpholino-β-amino AA	57
Introduction	57
Aim of the work.....	57
Foldamer synthesis.....	58
Electrospinning studies	61
SEM Analysis	63

Biological studies	65
Conclusions	65
Experimental part	67
General informations	67
Synthesis of (2 <i>S</i> ,6 <i>S</i>)-4-(<i>tert</i> -butoxycarbonyl)-6-methoxymorpholine-2-carboxylic acid (+)-1	68
Synthesis of (2 <i>S</i> ,3 <i>S</i> ,6 <i>S</i>)-4-(<i>tert</i> -butoxycarbonyl)-6-methoxy-3-(4-methoxyphenyl)morpholine-2-carboxylic acid (-)-2	68
Synthesis of N-Boc-(+)- β -Morph-(L)-Leu-(L)-Val-OBn-(+)-14	69
Synthesis of N-Boc-(+)- β -Morph-(L)-Leu-(L)-Val-(+)- β -Morph-(L)-Leu-L-Val-OBn-(+)-15	69
Synthesis of N-Boc-(+)- β -Morph-(L)-Leu-(L)-Val-NH ₂ -(+)-13	70
Synthesis of N-Boc-(+)- β -Morph-(L)-Leu-(L)-Val-(+)- β -Morph-(L)-Leu-(L)-Val-NH ₂ -(-)-5	70
Synthesis of N-Boc-(-)-3-(4-Methoxyphenyl)- β -Morph-(L)-Leu-(L)-Val-OBn-(-)-3	71
Synthesis of N-Boc-(-)-3-Ar- β -Morph-(L)-Leu-(L)-Val-(-)-3-Ar- β -Morph-(L)-Leu-(L)-Val-OBn-(-)-4	71
Nucleobase morpholino β amino acids as molecular chimeras for the preparation of photoluminescent materials from ribonucleosides	73
Introduction	73
Aim of the work	74
Scaffold synthesis	74
Peptides synthesis	76
Self-assembly studies	77
Photophysical characterizations	80
Experimental part	83
General information	83
Synthesis of (2 <i>S</i> ,6 <i>R</i>)-2-(hydroxymethyl)-6-(5-methyl-2,4-dioxo-3,4-dihydropyrimidin-1(2 <i>H</i>)-yl)morpholin-4-ium chloride (3a)	84
Synthesis of (2 <i>R</i> ,6 <i>S</i>)-2-(6-amino-9 <i>H</i> -purin-9-yl)-6-(hydroxymethyl)morpholin-4-ium chloride (3b)	85
Synthesis of (9 <i>H</i> -fluoren-9-yl)methyl (2 <i>S</i> ,6 <i>R</i>)-2-(hydroxymethyl)-6-(5-methyl-2,4-dioxo-3,4-dihydropyrimidin-1(2 <i>H</i>)-yl)morpholine-4-carboxylate (4a)	86
Synthesis of (9 <i>H</i> -fluoren-9-yl)methyl (2 <i>R</i> ,6 <i>S</i>)-2-(6-amino-9 <i>H</i> -purin-9-yl)-6-(hydroxymethyl)morpholine-4-carboxylate (4b)	87
Synthesis of (2 <i>S</i> ,6 <i>R</i>)-4-(((9 <i>H</i> -fluoren-9-yl)methoxy)carbonyl)-6-(5-methyl-2,4-dioxo-3,4-dihydropyrimidin-1(2 <i>H</i>)-yl)morpholine-2-carboxylic acid (1a)	88
Synthesis of (2 <i>S</i> ,6 <i>R</i>)-4-(((9 <i>H</i> -fluoren-9-yl)methoxy)carbonyl)-6-(6-amino-9 <i>H</i> -purin-9-yl)morpholine-2-carboxylic acid (1b)	89
General condition for peptide coupling reaction	90
Synthesis of (9 <i>H</i> -fluoren-9-yl)methyl (2 <i>S</i> ,6 <i>R</i>)-2-(((<i>S</i>)-1-(((<i>S</i>)-1-methoxy-1-oxo-3-phenylpropan-2-yl)amino)-1-oxo-3-phenylpropan-2-yl)carbonyl)-6-(5-methyl-2,4-dioxo-3,4-dihydropyrimidin-1(2 <i>H</i>)-yl)morpholine-4-carboxylate (6a)	91
Synthesis of (9 <i>H</i> -fluoren-9-yl)methyl (2 <i>R</i> ,6 <i>S</i>)-2-(6-amino-9 <i>H</i> -purin-9-yl)-6-(((<i>S</i>)-1-(((<i>S</i>)-1-methoxy-1-oxo-3-phenylpropan-2-yl)amino)-1-oxo-3-phenylpropan-2-yl)carbonyl)morpholine-4-carboxylate (6b)	92
Self-assembly studies	93
DLS analysis	95
Photoluminescence (PL) studies	99
Synthesis of non -natural amino acids with Morpholine core as organocatalysts for enantioselective reactions	104
Introduction	104

Aim of the work	110
Scaffold synthesis	112
5-Metoxyl- β -Morph AA synthesis.....	112
3-Aryl- β -Morph AA synthesis	112
Peptide Synthesis	114
Organocatalyst Screening	116
Peptide organocatalysts	116
Amino acids organocatalysts	122
Experimental part	129
General information	129
General procedure for amino alcohol synthesis	130
Synthesis of (R)-2-amino-2-phenylethan-1-ol (16a)	130
Synthesis of (R)-2-amino-3-phenylpropan-1-ol (16b).....	131
Synthesis of (R)-2-amino-3-phenylpropan-1-ol (16c).....	132
Synthesis of (R)-2-amino-3-(naphthalen-2-yl)propan-1-ol (16d).....	133
General procedure for Benzyl-amino alcohol synthesis (17a-d)	134
Synthesis of (R)-2-(benzylamino)-2-phenylethan-1-ol (17a)	134
Synthesis of (R)-2-(benzylamino)-3-phenylpropan-1-ol (17b).....	135
Synthesis of (S)-2-(benzylamino)-3-phenylpropan-1-ol (17c).....	136
Synthesis of (R)-2-(benzylamino)-3-(naphthalen-2-yl)propan-1-ol (17d).....	137
General procedure for benzyl-morpholino amino alcohol synthesis (18a-d)	138
Synthesis of ((2S,5R)-4-benzyl-5-phenylmorpholin-2-yl)methanol (18a).....	138
Synthesis of ((2S,5R)-4,5-dibenzylmorpholin-2-yl)methanol (18b)	139
Synthesis of ((2S,5R)-4,5-dibenzylmorpholin-2-yl)methanol (18c).....	140
Synthesis of ((2S,5R)-4-benzyl-5-(naphthalen-2-ylmethyl)morpholin-2-yl)methanol (18d)	141
General procedure for Boc-morpholino amino alcohol synthesis (19a-d)	142
Synthesis of tert-butyl (2S,5R)-2-(hydroxymethyl)-5-phenylmorpholine-4-carboxylate (19a)	142
Synthesis of tert-butyl (2S,5R)-5-benzyl-2-(hydroxymethyl)morpholine-4-carboxylate (19b).....	143
Synthesis of tert-butyl (2S,5S)-5-benzyl-2-(hydroxymethyl)morpholine-4-carboxylate (19c)	144
Synthesis of tert-butyl (2S,5R)-2-(hydroxymethyl)-5-(naphthalen-2-ylmethyl)morpholine-4-carboxylate (19d)	145
General procedure for Boc-morpholino amino acid synthesis (20a-d)	146
Synthesis of (2S,5R)-4-(tert-butoxycarbonyl)-5-phenylmorpholine-2-carboxylic acid (20a).....	146
Synthesis of (2S,5R)-5-benzyl-4-(tert-butoxycarbonyl)morpholine-2-carboxylic acid (20b)	147
Synthesis of (2S,5R)-5-benzyl-4-(tert-butoxycarbonyl)morpholine-2-carboxylic acid (20c).....	148
Synthesis of (2S,5R)-4-(tert-butoxycarbonyl)-5-(naphthalen-2-ylmethyl)morpholine-2-carboxylic acid (20d) ...	149
General procedure deprotection of morpholino amino acid (7a-d)	150
Synthesis of (2S,5R)-5-phenylmorpholine-2-carboxylic acid TFA salt (7a)	150
Synthesis of (2S,5R)-5-BenzylMorpholine 2-carboxylic acid TFA salt (7b).....	151
Synthesis of (2S,5S)-5-BenzylMorpholine 2-carboxylic acid TFA salt (7c)	152
Synthesis of (2S,5R)-5-(naphthalen-2-ylmethyl)Morpholine 2-carboxylic acid TFA(7d)	153
General solid phase synthesis (SPPS) for peptides containing morpholino amino acid scaffold (Peptide 1-6)	154
Synthesis of (2S,6S)-6-Methoxy-2-Morph-(L)-Pro-(L)-Glu-NH ₂ (1)	155
Synthesis of (2S,6S)-6-Methoxy-2-Morph-Gly-(L)-Glu-NH ₂ (2)	155
Synthesis of (2S,6S)-6-Methoxy-2-Morph-(L)-Glu-NH ₂ (3)	156
Synthesis of 3(S)-Aryl (2S,6S)-6-Methoxy-2-Morph-Gly-(L)-Glu-NH ₂ (4)	156
Synthesis of (2S, 5R) 5-Phenyl 2-Morph-Gly-(L)-Glu-NH ₂ (5)	157
Synthesis of (2S, 5S) 5-Benzyl 2-Morph-Gly-L-Glu-NH ₂ (6)	157
Synthesis and Analytical Data of γ-Nitroaldehydes	158
Synthesis of (2R,3S)-2-methyl-4-nitro-3-phenylbutanal (23b)	159
Synthesis of (2R,3S)-2-ethyl-4-nitro-3-phenylbutanal (23a).....	160

Synthesis of (R)-2-((S)-2-nitro-1-phenylethyl)pentanal (23c)	161
Synthesis of (2R,3S)-2-isopropyl-4-nitro-3-phenylbutanal (23d).....	162
Synthesis of (R)-2-((S)-2-nitro-1-phenylethyl)hexanal (23e)	163
Synthesis of (2S,3S)-4-nitro-2,3-diphenylbutanal (23f)	164
Synthesis of (R)-1-(2-nitro-1-phenylethyl)cyclopentane-1-carbaldehyde (23g).....	165
Synthesis of (2R,3S)-3-(4-methoxyphenyl)-2-methyl-4-nitrobutanal (23h)	166
Synthesis of (R)-2-((S)-1-(4-methoxyphenyl)-2-nitroethyl)pentanal (23i)	167
Synthesis of (2R,3R)-2-methyl-4-nitro-3-(thiophen-2-yl)butanal (23l).....	168
Synthesis of non-natural amino acid with isoxazoline core for the preparation of peptidomimetics	169
Introduction	169
Aim of the work.....	170
Scaffold synthesis	171
Peptides synthesis	176
NMR characterization	180
Conclusion	184
Experimental part	185
General information	185
Synthesis of methyl 2-(azidomethyl)acrylate (2).....	185
Synthesis of N-hydroxybenzimidoyl chloride (4).....	186
Synthesis of methyl 5-(azidomethyl)-3-phenyl-4,5- dihydroisoxazole-5-carboxylate (5).....	187
Synthesis of methyl 5-(aminomethyl)-3-phenyl-4,5- dihydroisoxazole-5-carboxylate (6)	188
Synthesis of methyl 5-(((S)-2-((tert-butoxycarbonyl)amino)-4- methylpentanamido)methyl)-3-phenyl-4,5- dihydroisoxazole-5- carboxylate (7)	189
Synthesis of methyl 5-(((S)-2-amino-4-methylpentanamido)methyl) -3-phenyl-4,5-dihydroisoxazole-5- carboxylate (8a).....	190
Synthesis of methyl 5-(((S)-2-amino-4-methylpentanamido)methyl) -3-phenyl-4,5-dihydroisoxazole-5- carboxylate (8b).....	191
Synthesis of N-Boc-(L)-Val-(L)-Leu-β-(R)-Isox-MetOMe (9a)	192
Synthesis of N-Boc-(L)-Val-(L)-Leu-β-(S)-Isox-MetOMe (9b)	194
Synthesis of N-Boc-(L)-Val-(L)-Leu-β-(R)-Isox-MetOH (10a)	196
Synthesis of N-Boc-(L)-Val-(L)-Leu-β-(S)-Isox-MetOH (10b)	197
Synthesis of N-Boc-(L)-Val-(L)-Leu-β-(R)-Isox-MetOMe (11a)	198
Synthesis of N-Boc-(L)-Val-(L)-Leu-β-(S)-Isox-MetOMe (11b)	201
Photochemistry cyclization peptide	204
Introduction	204
Aim of the work.....	205
Bibliography.....	207

Table of Abbreviations

AAs = Amino acids

ACHC = *trans*-2-aminocyclohexanecarboxylic acid

ACPC = Pentacyclic *trans*-2- aminocyclopentanecarboxylic acid

Aib = 2-Aminoisobutyric acid

APC = *trans*-3-amino-pyrrolidine-4- carboxylic acid

BIAB = (Diacetoxyiodo)benzene

DCHC = *trans*-2,5-diaminocyclohexanecarboxylic acid

θ_p = Degree of pyramidalization

d.e. = diastereomeric excess

DLS = Dynamic Light Scattering

DMEM =Dulbecco's Modified Eagle Medium

e.e = Enantiomeric excess

ESP = Electrospinning

FBS = Fetal Bovine Serum

Gly = glycine

Glu = Glutamic acid

HFIP = Hexafluoro-2-propanol

HPP = Human platelet profilin

IP1 = Ionization potential

Leu = Leucine

L-Pro10 =Poly-L-proline decamer

MTT = [3-(4,5-dimethylthiazol-2-yl)-2,5-diphenyltetrazolium bromide]

Phe-Phe = Diphenylalanine

PL = Photoluminescence

PPIs = Protein-protein interactions

PPII = Polyproline II helix

Pro = Proline

SEM = Scanning electron microscope

SPPS = Solid-Phase Peptide Synthesis

TDC = Target distance collector

TFE = 2,2,2-Trifluoroethanol

TEMPO = (2,2,6,6-Tetramethylpiperidin-1-yl)oxyl

T3P = Propanephosphonic acid anhydride

Val = Valine

Introduction

Peptides and protein are made by amino acids (AAs). Even if they are simple molecules, having at least one carboxylic and one amino group, they are at the molecular basis of the living world. These very simple molecules can be easily used to build structures with high complexity and variability, making them attractive tools for different applications, ranging from catalysis to electrochemistry, biology and nanomedicine.

Nature has optimized their structures to absolve numerous functions in almost all the biological processes. In nature, 21 AAs are present and they are α -AA.

β -Amino Acids

β -AAs are analogues of α -AAs with a difference: an additional carbon atom between the carboxylic and amine groups (Figure 1).

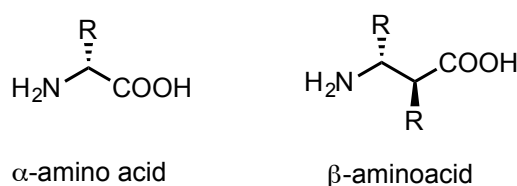


Figure 1 Difference between α/β amino acid

Seebach¹ and co-workers propose a nomenclature system to identify positional isomers for β -amino acids. In particular the superscript after β symbol (β^2 , β^3 , $\beta^{2,3}$, $\beta^{2,2}$...) indicates the position of the side chain substituent/s respect to the carboxylic function (Figure 2).

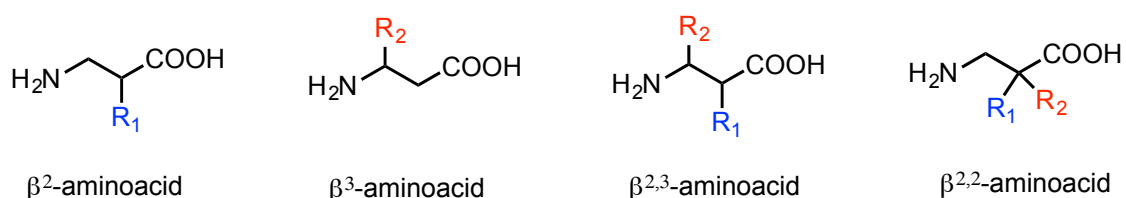


Figure 2 Representation of Seebach numeration of β -amino acid's side chain substituent

β -AAs are commonly considered not natural amino acids, although there are some examples of this class in nature as secondary metabolites or as components of complex natural products. Moreover, β -AAs moiety is often recurrent in biological active compounds, such as β -lactam antibiotics, Taxol and bleomycin derivatives as anticancer agents (Figure 3).

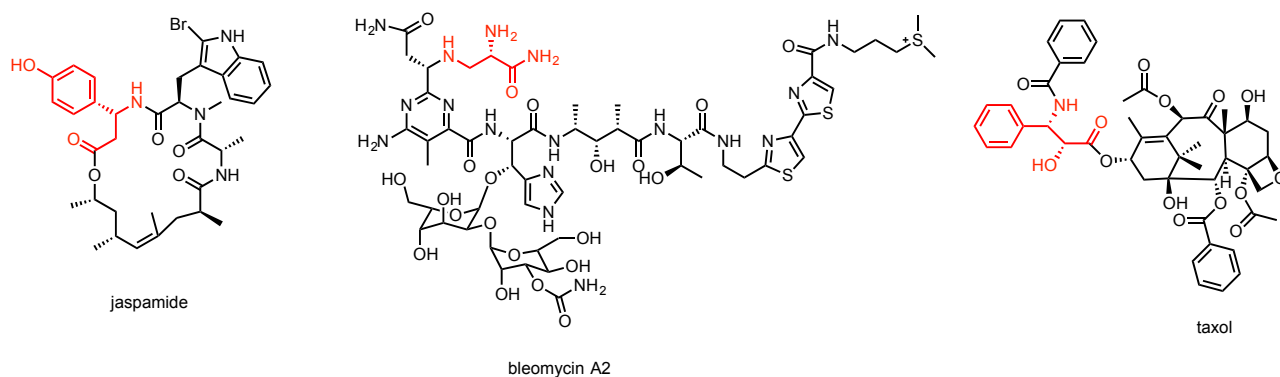


Figure 3 Biologically active compounds containing a β -AA motif

Being not natural AAs, when they are inserted in a peptide structure they can confer major proteolytic stability to the system compared to natural AAs.² In fact, human peptidases do not recognize β -amino acids and are not able to hydrolyze peptide bond. Moreover β -peptides and α/β hybrid peptides can induce a predictable and well-defined secondary structure, such as helices, strands and loops that may be residue-controlled and biologically active.

Carbocyclic β -amino acids

In the last decades cyclic β -amino acids received considerable interest especially in pharmaceutical chemistry. These moieties can be found in various bioactive natural products as gougertin oxetin and cispentacin (Figure 4).³ Despite these simple cyclic β -amino acids have a very simple structure, they show very marked biological activities.

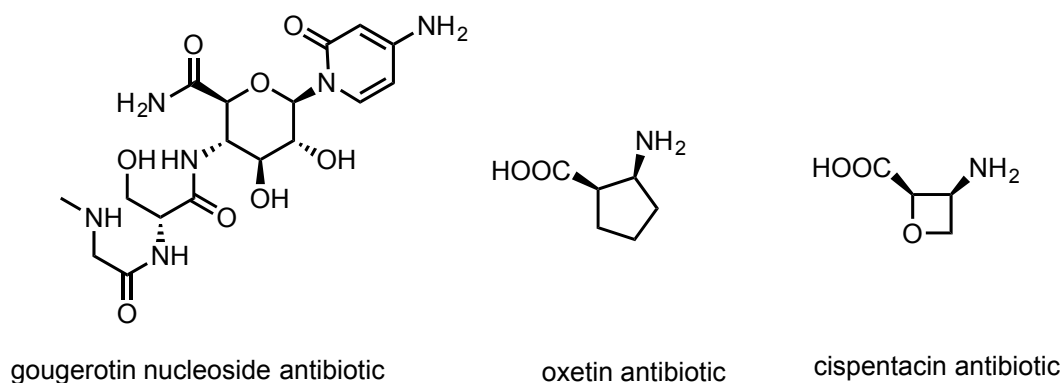


Figure 4 Bioactive molecules and peptides foldamers containing cyclic β -amino acids

Starting from the compounds described before, recently many pharmaceutical companies produce new drug candidate containing synthetic cyclic β -amino acid into their scaffold (BAY9379, Tilidin, and oryzoxymycin). The idea is to start from a structure known for its biological activity and try to modify the ring in order to increase power and effectiveness (CEP-28122, VX-787, VLA-4 Antagonist, and 11-methoxytabersonine (Figure 5)).⁴

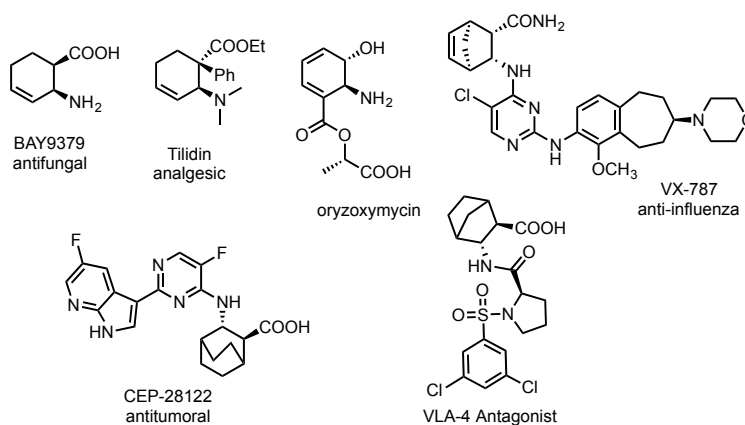


Figure 5 Synthetic pharmaceutical drug containing cyclic β -amino acids

Conformation of cyclic β -AA, compared to acyclic β -AA, present a higher constraint due to the presence of the ring. Moreover, the ring size influences the $\text{C}_2\text{-C}_3$ torsional angle which can potentially influence the β -peptide secondary structure.

Due to their conformally restricted structure, cyclic β -AAs have been studied for decades to induce stable peptide secondary structures. Studies are mostly focused on β -AAs like *trans*-2-aminocyclohexanecarboxylic acid (ACHC)^{5,6} *trans*-2,5-diaminocyclohexanecarboxylic acid (DCHC)⁷, Pentacyclic *trans*-2-aminocyclopentanecarboxylic acid (ACPC), *trans*-3-amino-pyrrolidine-4-carboxylic acid (APC)⁸ and *cis*-pentacine⁹ (Figure 6).

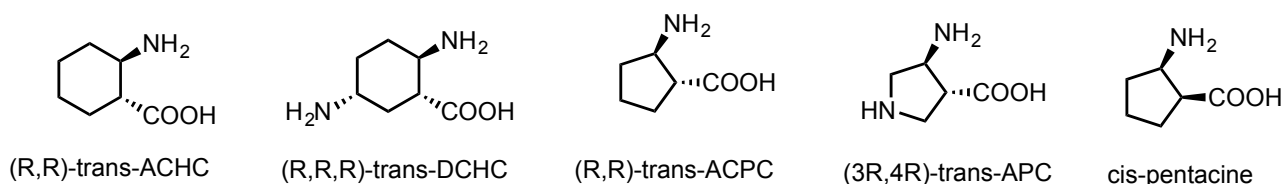


Figure 6 Conformally restricted cyclic β -amino acids

These cyclic β -amino acids are known to stabilize various secondary structure motifs in synthetic oligomers. Their ability to stabilize specific secondary structures when inserted into peptide sequences will be illustrated in the next chapter.

Secondary structure mimics

Protein-protein interactions (PPIs) are involved in many biological functions and play a key role in several pathological disorder.¹⁰ By the analysis of the full set of helical protein interfaces in the Protein Data Bank it has been seen that about 62% of the helical interfaces contribute to protein-protein interactions. However, as said before, peptides with high degrees of freedom lose their secondary structure in solution: for this reason, several strategies have been developed to obtain compounds able to mimic the natural peptides in their exact bioactive conformation.

The most common peptide secondary structure is the helix, that is formed by repetitive sequences stabilized by intramolecular hydrogen-bonds between sequential residues (Figure 7).

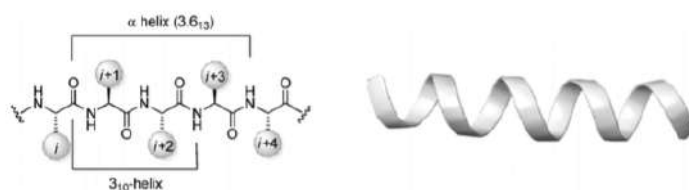


Figure 7 Helix conformation

Helical secondary structures in α/β - and β -peptides depend on the length of the chain. α -Peptides require at least 8-12 residues for a stable helix-conformation while β -peptides need only six residues (Figure 8).

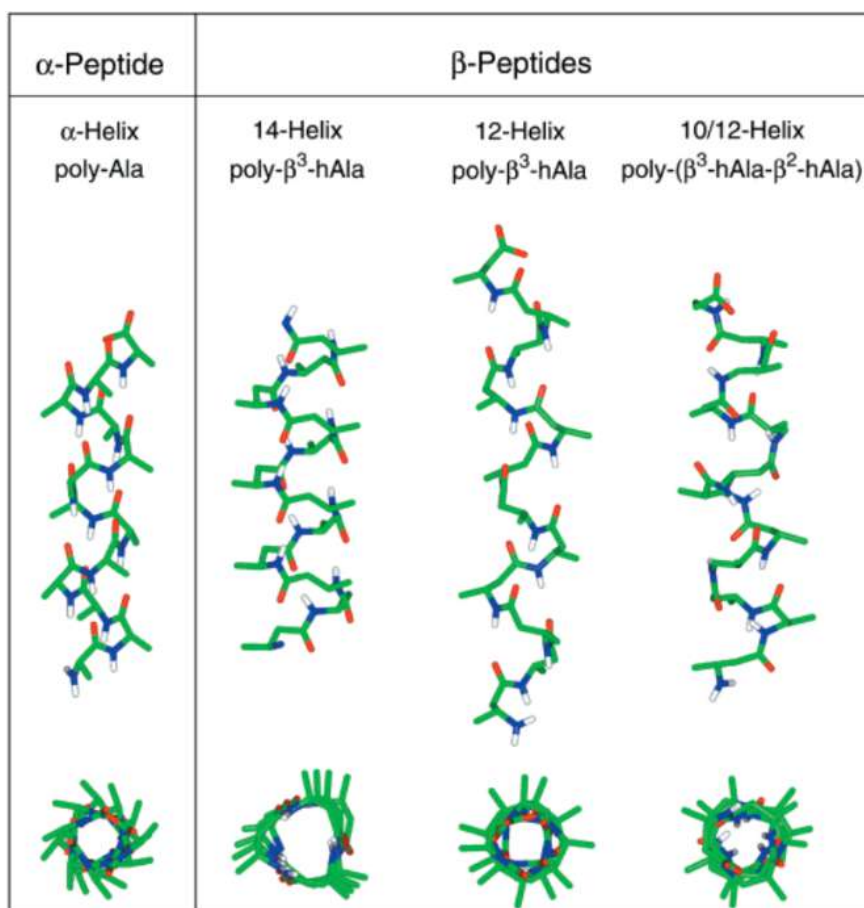


Figure 8 Structure of the α -helix, 14-helix, 12-helix, and 10/12-helix¹¹

β -peptide helix conformations could be classified as follows (Figure 9):

- 14-helix, forming series of 14-membered: it is stabilized by hydrogen bonds between the amide proton at position (i) and the carbonyl at position ($i+2$);
- 12-helix, with repetitions every 2.5 residues: it is stabilized by hydrogen bonds between amide carbonyl groups at position (i) and amide protons at position ($i+3$);
- 10/12-helix: there is a twist between networks of 10 and 12-member-helices stabilized by hydrogens bonds. The amides, surrounded by methylene hydrogens, bond one to another ($i, i+2$), forming the 10-membered rings, while the 12-atom rings are formed between amides surrounded by side chains ($i+1, i+3$);
- 8-helix (less recurring): it is formed by turns composed of eight-member pseudo-rings.

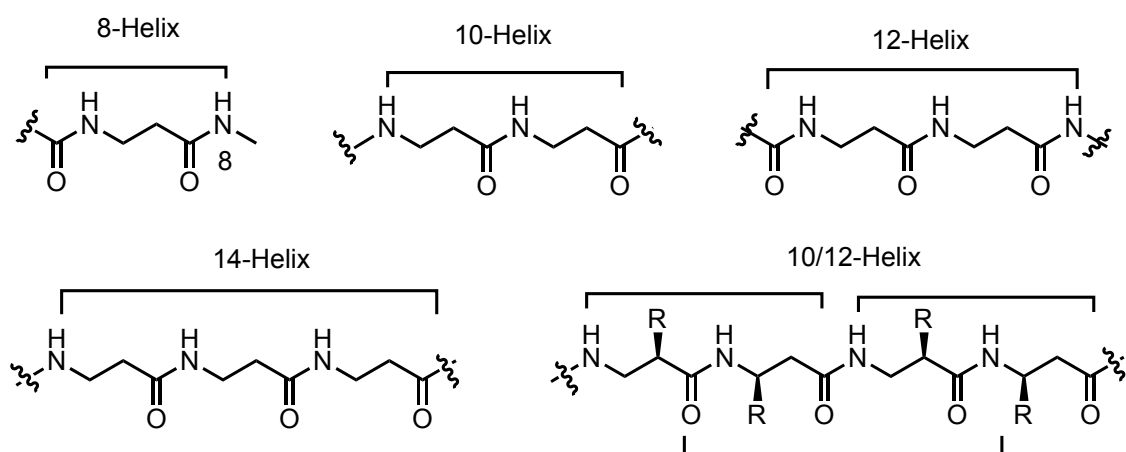


Figure 9 Nomenclature for β -peptide helices based on hydrogen-bonding patterns

The β -sheet is a common motif of regular secondary structure in proteins. β -Sheets have a crucial role in the formation of the three-dimensional structures in peptides, and this is the reason why they represent interesting structural elements for the development of peptidomimetics, especially in the field of CNS diseases.¹²

There are two types of conformation of the β sheet for peptides containing β -AA: anti and gauche. Their structure depends on the torsion angle C_2-C_3 ¹³, as shown in Figure 10. In the anti-type sheet β we can see the formation of a net dipole; in fact, each carbonyl group is oriented in the same direction. In the gauche type, on the other hand, the dipole described above does not exist, in fact the carbonyl groups are alternated.

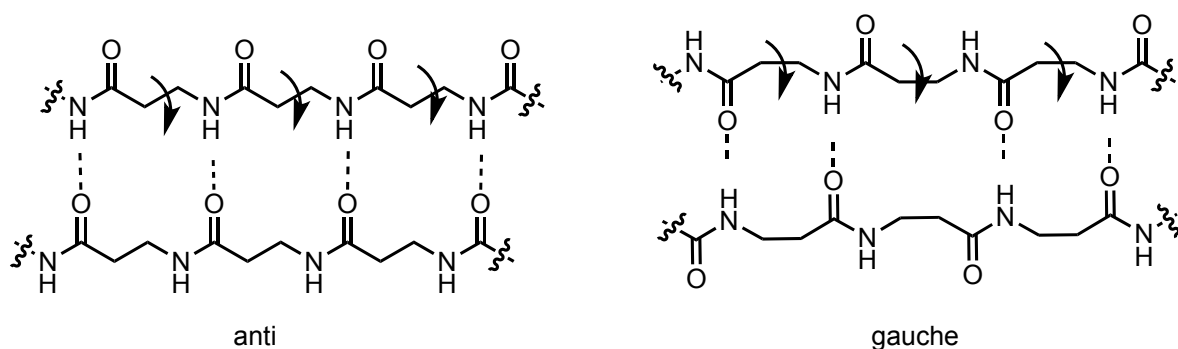


Figure 10 Type of β -sheet anti and gauche

Moreover, they can be classified on the basis of parallel or antiparallel alignment. In the parallel, the two strands have the same orientation, so that the nitrogen atoms and carbonyl groups are slightly shifted between each another. In the antiparallel, the consecutive β -strands alternate directions, thus the N -terminus of one strand is nearby to the C -terminus

of the next one. The antiparallel alignment allows the strongest bonding with planar interactions, meanwhile the parallel alignment introduces non-planarity in the inter strand hydrogen-bonding pattern, so that are less stable Figure 11.

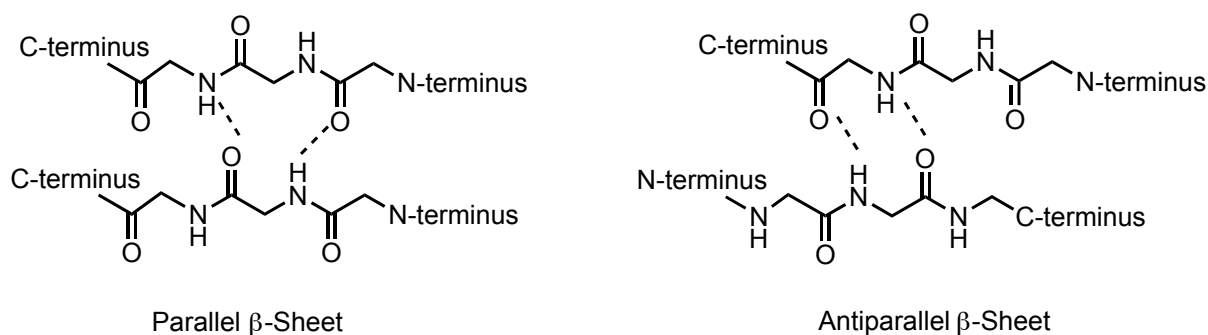


Figure 11 Parallel/Antiparallel β -sheets

Two antiparallel β -strands connected through a turn lead to an antiparallel β -hairpin structure, which is stabilized by an extended pattern of inter strand hydrogen-bonds (Figure 12). Turn- inducing amino acids, such as L-ornithine or the dipeptides D-Pro/L-Pro and D-Pro/L-Gly, are privileged motifs used to stabilize a β -hairpin, by allowing the nucleation of peptides into the secondary structure.¹⁴

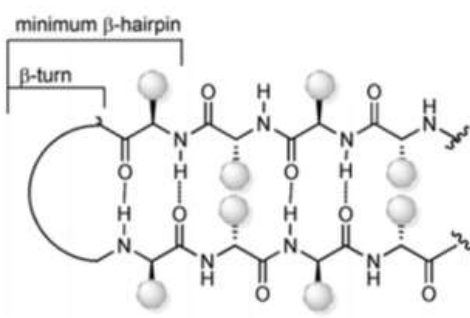


Figure 12 β -hairpin structure¹³

Turn motifs, which are highly recurrent in loop regions, play a relevant role in PPIs.¹⁵ They consist of irregular secondary structures characterized by non-repetitive dihedral angles of their backbones, so the peptide chain fold back on itself. There are different types of turns, classified depending on the length and on the hydrogen-bonding pattern between the carbonyl group at position i and the amide proton at position $i+n$ (Figure 13). Among the

different families, β -turn, composed by four amino acids ($n = 3$) and a hydrogen-bond forming a *pseudo* ten-membered ring, plays a significant role in many biological recognition systems, such as in several peptide-antibody interactions and in the binding interactions between peptide ligands and proteins.¹⁶ Besides β -turn, the other most common turn types are γ - and α -turns, while δ -turns are rare. In particular, γ -turns involve three amino acids and is characterized by a *pseudo* seven-membered ring formed by an H-bond between i and $i+2$ residue, whilst in the α -turns the H-bond is between i and $i+4$ residue with the involvement of four amino acids. δ -Turns are rarely authenticated and characterized by a *cis*-amide bond, which allow the formation of an eight-membered *pseudo*-cyclic structure, stabilized by an H-bond between i and $i+1$ residue.

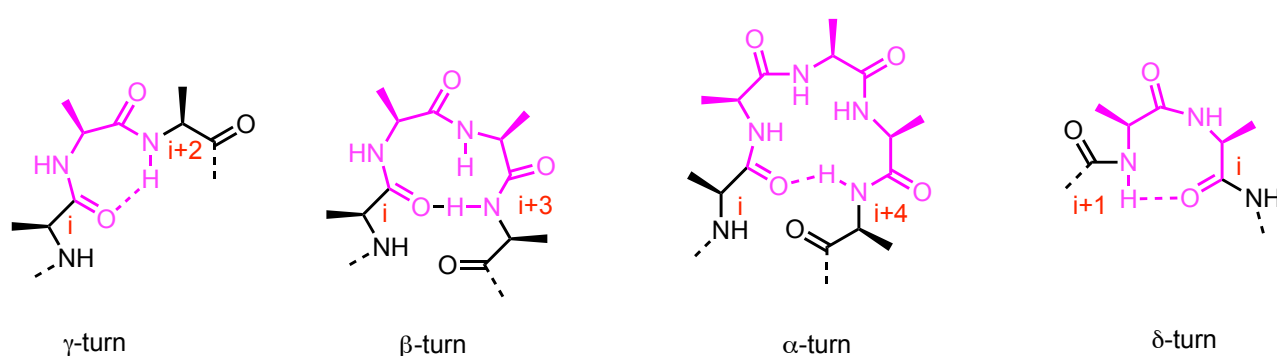


Figure 13 Structures of different turn types

Pharmaceutical applications

As previously mentioned, the major problem in using natural peptides in pharmaceutical field is their degradation caused by human peptidases. The presence of a not natural amino acids, such as β - AAs, confers proteolytic stability to the system because the peptidases can't recognize them.¹⁷ For this reason, mimetics peptide like α/β hybrid-peptides are very appealing for pharmaceutical applications.

Mulzer group reported the synthesis of a GnRH Mimetic. A cispentacin-derived bicyclic - amino acid (Bic) (Figure 14) has been synthesized and incorporated into the 6-position of GnRH.¹⁸

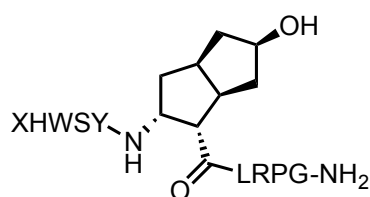


Figure 14 Structures of different turn types

The analogue is more rigid but keeping the structural requirements for biological activity at the receptor. Moreover, the incorporation of Bic results in enhanced stability against enzymatic cleavage.

Another example of a molecule that mimics a non-natural amino acid is used in inhibition of PPI comes from my research group. In particular, the synthesis and conformational analysis of β -hairpin peptidomimetics, built on a piperidine-pyrrolidine semi-rigid β -turn inducer and bearing two small recognition peptide sequences, was performed designed on oligomeric and fibril structures of A β 1-42. According to these peptide sequences, a stable β -hairpin or a dynamic equilibrium between two possible architectures was observed (Figure 15). These original constructs are able to greatly delay the kinetics of A β 1-42 aggregation process, inhibiting the formation of toxic oligomers. Furthermore, compounds protect against toxic effects of A β on neuroblastoma cells.¹⁹



Figure 15 Structure of piperidine-pyrrolidine semi-rigid β -turn inducer(left); structure of the most populated clusters obtained of computational analyse of β -amyloid mimic (right).¹⁹

Electrospinning Applications

Electrospinning is a technique used for the fabrication of continue ultrafine fibers, having diameters from ten nanometers to a few microns, commonly known as nanofibers. So far, this technique is considered as the only one that can produce nanofibers on an industrial scale with a length up to several meters. This procedure uses an electrical field as the trigger to create nanofibers. In fact, a solid fiber is generated as the electrified jet composed by a

highly viscous polymer solution, that is continuously stretched due to the electrospinning repulsions between the surface charges and the evaporation of solvent (Figure16).

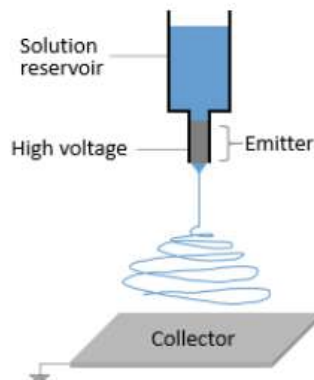


Figure 16 Schematic illustration of the basic set up for electrospinning process

The morphology, diameter and directions of the fiber can be controlled, depending on materials by instrument setup and process parameters. The principle way is based on applying a high voltage (kV range) to a high viscosity fluid, which forms a jet that can be collected in dry form on grounded substrate.

The electrospinning process can be divided in two phases:

- - in the first phase the solution droplet is charged above a critical high voltage, resulting in the formation of Taylor cone shape (Figure 17).
- - the second phase concerns the ejecting of the jet that travels to a grounded collector. Further away from the cone, the solution jet is nonstable until it meets the electronic field. At this point, the jet rapidly elongates forming the long fiber on the collector.

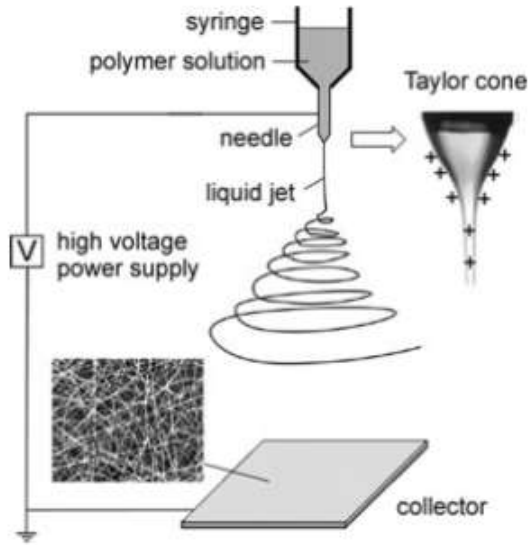


Figure 17 Illustration show the cone Taylor and a typical SEM image of the nanofibers deposited on the collector

The concentration of spinning solution is one of the most important parameters of electrospinning. In Hongyan's group, to determine the optimal spinning concentration, PPV precursors/GO nanofibers exhibiting different GO contents (2.0, 3.0, 5.0 and 10.0 wt %) were electrospun under constant voltage (12 kV), spinneret diameter (0.51 mm), and receiving distance (18 cm). The morphology of synthesized nanofibers was characterized through the SEM images and diameter distribution histograms of PPV precursor/GO composite nanofibers at different concentrations. The concentration significantly impacted the diameter of electrospun fibers (Figure 18).²⁰

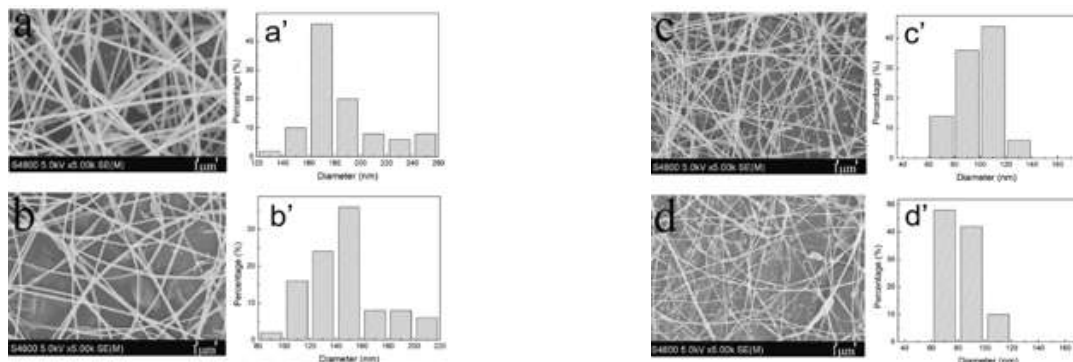


Figure 18 SEM images and the corresponding diameter histogram of PPV precursor/GO nanofibers with different GO content: (a) 2.0 wt%, (b) 3.0 wt%, (c) 5.0 wt% and (d) 10.0 wt%²⁰

The structures obtained with this technique are versatile and can be used in different application, such as the building of membranes, filters and biomaterials, important also in pharmaceutical industry thanks to their chemical and physical characteristics. In particular, they found applications in tissue engineering and drug delivery. Electrospinning affords also great flexibility in selecting materials for drug delivery applications. Either biodegradable or non-degradable materials can be used as drug delivery system, where the release can occur via diffusion with or without fiber degradation.

Peptide nanofibers structures can be produced by using electrospinning (ESP). In material production, synthetic polymers offer several advantages such as ease of availability, processing without difficulty, reproducible results, excellent mechanical properties but they usually show lack of cell recognition sites and lack of cell affinity due to low hydrophilicity. For these reasons, peptides can be interesting tools to overcome some of these drawbacks, mostly in tissue engineering, where biodegradable scaffolds are required to direct tissue repair and regeneration, also providing structural support. Indeed, there is the possibility to tune AA sequences and produce a hydrophobic or hydrophilic surface with specificity for different biological targets. The fact that they do not suffer from denaturation issues is one of their advantages together with the compatibility with nonaqueous solvents and the easy large-scale preparation due to the limited length and complexity. Peptides can be used in ESP: 1) in combination with natural or synthetic polymers and 2) alone, as reported for poly- and oligopeptides.²¹ To obtain uniform electrospun fibers is important the presence of sufficient intermolecular interactions, while high molecular weight is not essential. Some small molecules able to self-assemble have been electrospun from solution into fibers and, among them, there are peptides containing both natural and non-natural amino acids. Nowadays, the use of peptides for this purpose is not that common, but it is gaining increasingly interest.²²

Nanomaterials applications

In nature, complex and well-defined structures are constructed by the self- assembly of biomolecules. The self-assembly of peptide-based molecular systems is especially complex and difficult to control because of their intrinsic conformational flexibility and diverse side-chain functionality.²³ β -peptide foldamers (oligomers of β -amino acids) are excellent candidates for a model system that meets the minimum requirements of rigidity and predictability because, in solution, they adopt rigid and controllable secondary structures. It's already known that cyclic β -peptide, β -peptide foldamers or hybrid α/β -peptides with different lengths can self- assemble into three dimensional molecular architectures thanks to their rigid and predictable secondary conformation.

In particular, peptides based on their design can assemble into different kinds of supramolecular architectures (Figure 19) such as nanotubes and monolayers with a nanoscale order and as vesicular structure. Nanostructures have been developed from different types of peptides including cyclic peptides, amphiphilic peptides, peptides containing β -sheeted motifs, helical structures, or β -turns.

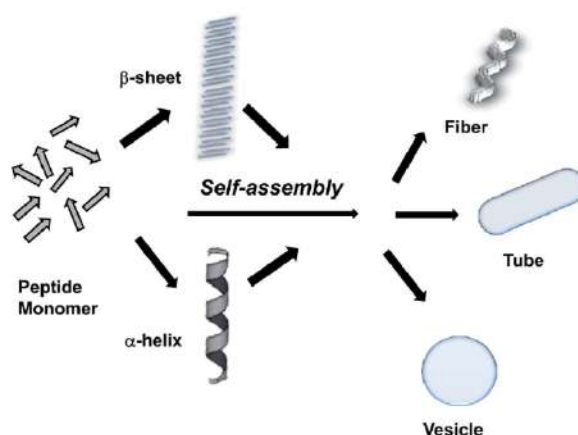


Figure 19 Self-assembly of peptides into different types of nanostructures

Over the last several years, self-assembled peptides attracted considerable attention as new materials with potential application in research and industry. Natural and synthetic peptides with strong self-assembly propensity give the possibility to access a wide range of different nanostructures and the corresponding properties. Numerous applications have been studied including 3D cell culture and tissue regeneration, drug delivery, biosensing, bioimaging, and microbiology and in the elaboration of new materials (Figure 20).

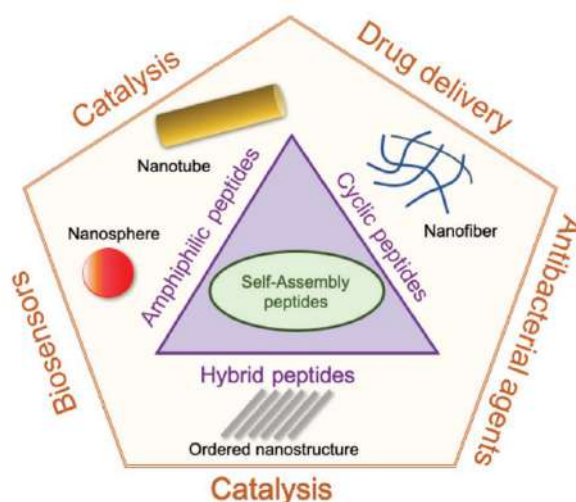


Figure 20 Schematic illustration of peptide nanostructures and possible applications by self-assembly²⁴

Nowadays scientists are trying to discover new nanomaterials that can find application in different fields.²⁴

Organocatalysis applications

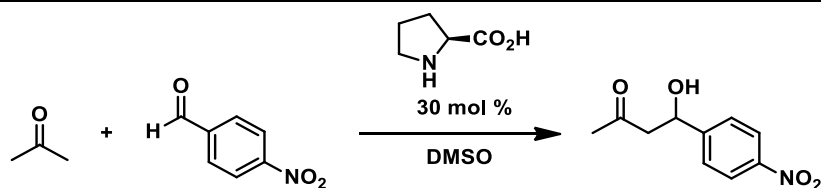
The efficacy and versatility of organocatalysis lay the groundwork of the organic synthesis since the late 1990s. Organic chemists, impressed by the Nature with its biocatalytic processes, gave birth to organocatalysis, using very simple molecules bearing the minimal functionalities to mimic biocatalysts and effect asymmetric reactions.^{25,26}

Before List's and Mcmillan's publications as the pioneers of organocatalysis, Breslow and coworkers already in 1958 proposed a groundbreaking paper in which a Thiamine could act as organocatalyst forming an intermediate acyl carbanion $R-CO^-$, inverting the polarity of a carbonyl group and thus obtaining a so called 'active aldehyde' (Figure 21).

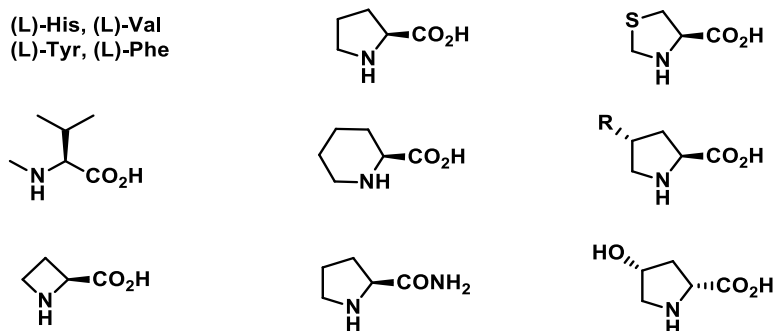
Later on, Eder, Sauer and Wiecherst discovered the huge potential of Proline as effective asymmetric catalyst for the synthesis of 7a-alkyl-5,6,7,7a-tetrahydro-1,5-indandiones and 8a-alkyl-1,2,3,4,6,7,8,8 a-octahydro-1,6-naphthalenediones, optically active intermediates for the total synthesis of steroids. They used Proline as chirality inducer in an aldol reaction²⁷. Since then, the use of the Proline continued over the years. Actually, Proline is a chiral organic compound that can be used as a catalyst in many reactions such as aldol condensation, Mannich reactions, or Michael additions. Proline is nontoxic, inexpensive, and readily available in both enantiomeric forms. Reactions with Proline do not require inert conditions, as do so many organometal catalysts, and most reactions carried out with this compound can be at r.t. Proline is an example of a green alternative to classic organocatalysts.

In 2000, List *et al.* for the first time focuses his attention on the use of the Proline analogues to promote aldol reaction to form new C-C bond. At that time, the most used method to perform this reaction was the formation of the enolate using a metal that entered in the catalytic cycle together with a chiral catalyst. Being inspired from the class I of aldolases, using enamine-based mechanism, they synthesized different Proline analogues as asymmetric catalyst for the direct aldol reactions (Scheme 1)

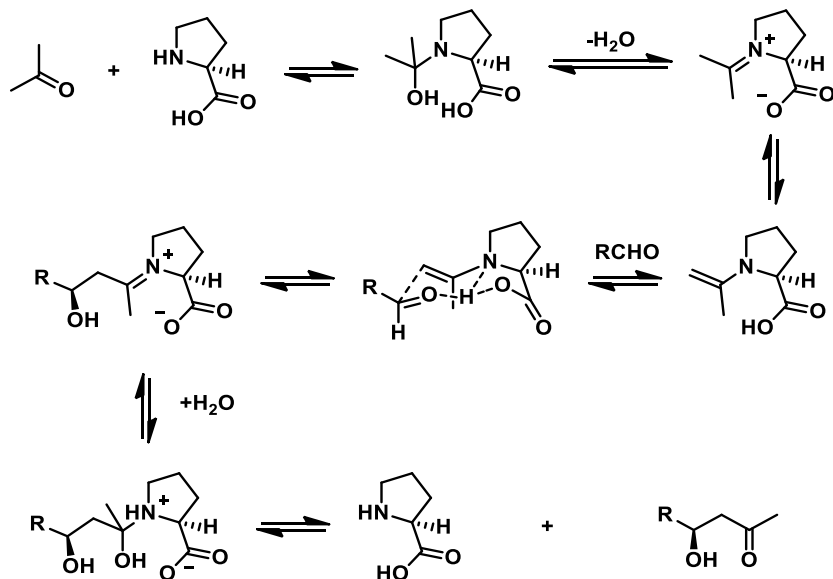
(a) Aldol reaction Proline catalyzed between acetone and 4-nitro benzaldehyde



(b) Amino Acid Derivatives Tested as Catalysts for the Asymmetric Aldol Reaction of Acetone with 4-Nitrobenzaldehyde

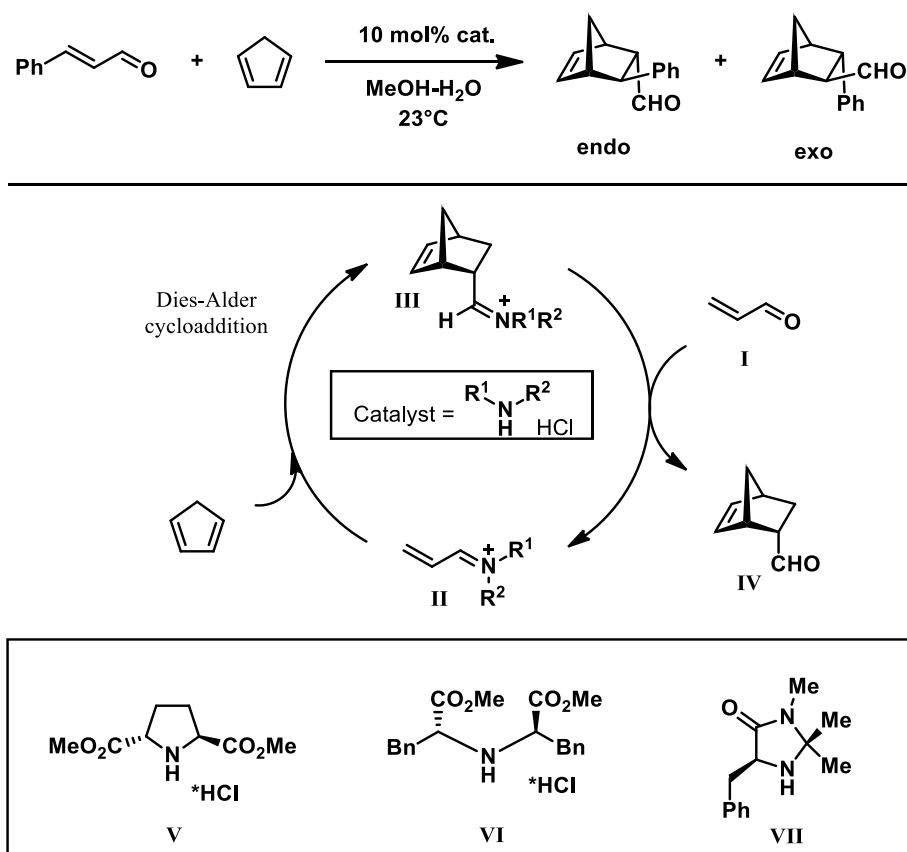


(c) Proposed Enamine Mechanism of the Proline-Catalyzed Asymmetric Aldol Reaction



Scheme 1 Proline analogues in promote aldol reaction

In the same year, MacMillan and coworker published the use of MacMillan catalyst (**VII**, Scheme 2) as an analogue of Proline for reactions going through the formation of iminium ions from α,β -unsaturated aldehydes. To prove the efficacy of the catalyst, they firstly focused on Diels-Alder reaction between α,β -unsaturated aldehydes and various dienes obtaining high enantioselectivity.



Scheme 2 Diels-Alder reaction between α,β -unsaturated aldehydes and cyclopentadiene and mechanism.

As outlined in Scheme 2, the condensation of aldehyde (I) with an enantiopure amine (i.e., V, VI, VII) lead to the formation of an iminium ion (II) that is sufficiently activated to engage a diene reaction partner. As a matter of fact, it was already known at that time that α,β -unsaturated iminium ions are significantly more reactive as dienophiles than the corresponding α,β -unsaturated aldehydes. Accordingly, Diels-Alder cycloaddition would lead to the intermediate (III), which upon hydrolysis would provide the enantioenriched cycloadduct (IV) regenerating the chiral amine catalyst.²⁸

These last two publications mark the beginning of the organocatalysis and thus the use of organocatalysts as appealing molecules as key reagents for enantioselective syntheses.

From the early 2000, the research of the perfect organocatalyst represents a milestone for the synthesis of enantiopure intermediates, that otherwise would be prepared with a lot of synthetic steps and expensive chiral auxiliaries.

Continuing our journey in the Organocatalysis field, the Hayashi-Jorgensen catalyst need to be underlined. In 2007, Hayashi and Jorgensen, independently, developed the same catalyst that then was called Hayashi-Jorgensen catalyst (Figure 21). This catalyst is more

active and more soluble in organic solvents than prototypical Proline catalyst. Compared with the MacMillan catalysts, that are used often in iminium-mediated reactions, the Hayashi-Jørgensen catalysts tends to be more effective in enamine-mediated reactions. Since the first publication, in which Jørgensen group presented this catalyst with the capability of forming five definite stereocenters in one reaction²⁹, Hayashi-Jørgensen catalyst, as the McMillan's one, are commercially available.

Recently, different short peptide catalysts were designed. Among of all, in 2008 Wennemers group proposed conformationally stable tripeptides with Proline at *N-terminus* to be used in addition reactions of aldehydes to nitroolefins.

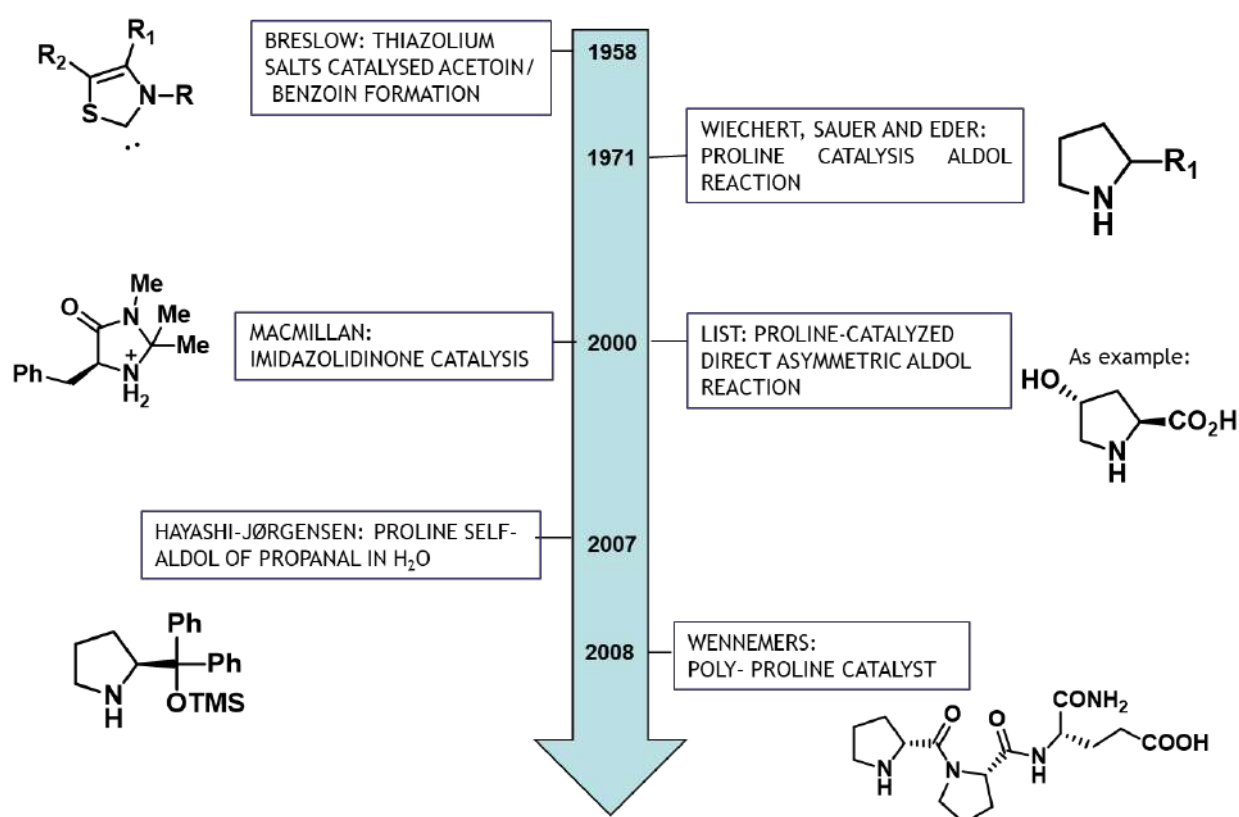
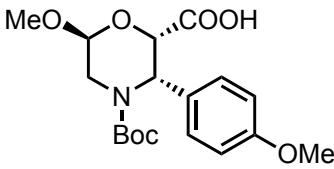
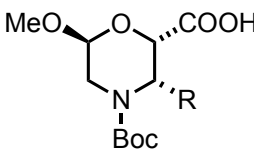
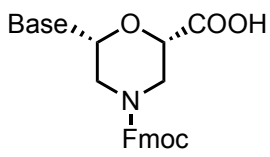
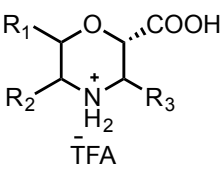
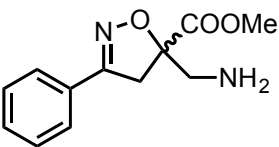


Figure 21 Overview of the most important catalyst used for organocatalysis reaction

Aim of the Thesis

During the PhD activity the synthesis of non-natural cyclic β -amino acids has been performed. Each of these has been used for different applications as shown in the Table below.

Table 1 Different applications of non-natural cyclic β -amino acids

 <p>Chapter 1</p>	<p>Synthesis of non-natural 3-Arylmorpholino-β-amino Acid as a PPII Helix Inducer</p>
 <p>R = H, pOMePh</p> <p>Chapter 2</p>	<p>Synthesis of electrospun fibers using model peptide containing morpholino-β-amino acid scaffolds</p>
 <p>Base : = Thymine, Adenine</p> <p>Chapter 3</p>	<p>Synthesis of nucleobase morpholino β amino acids from ribonucleosides as molecular chimeras for the preparation of photoluminescent materials</p>
 <p>R₁ = -OMe R₂ = -CH₂Ph R₃ = -pOMePh R₂ = -Ph R₂ = -CH₂Naphtyl</p> <p>Chapter 4</p>	<p>Synthesis of non-natural amino acids with Morpholine core as organocatalysts for enantioselective Aldol-condensation reactions</p>
	

<p>Chapter 5</p>	<p>Synthesis of non-natural amino acid with isoxazoline core as β-turn inducer for the preparation of peptidomimetics</p>
<div data-bbox="363 376 555 629" data-label="Chemical-Block"> </div> <p>Chapter 6</p>	<p>Photochemistry cyclization peptide. This part of my thesis was performed during my visiting period at University of Manchester (UK) in Leonori Group.</p>

Synthesis of non-natural 3-Arylmorpholino- β -amino Acid as a PPII Helix Inducer

Aim of the work

The polyproline II helix (PPII) is the less abundant among the ubiquitous secondary structures in folded proteins such as α -helices, 3,10-helices, and β -sheets.³⁰ The PPII helix is characterized by ϕ and ψ torsional angles of about -75° and 150° , respectively, and, contrary to PPI, is left-handed with trans peptide bonds.³¹ It is involved in biological systems such as cell motility, bacterial and viral pathogenesis.³² Moreover, it is also at the basis of the collagen triple helix, formed by three PPIIs that coil into each other thanks to intermolecular hydrogen bonds.

In general, non-natural amino acids (AAs)³³ could be commonly used as inducers of a particular secondary structure. Despite the large number of protocols involving β -AAs for locking peptides into helices and β -strand conformations, their use for generating mimics of PPII structures is absent in the literature.³⁴

Recently, my research group reported on the synthesis of a morpholino β -AA, named β -Morph **1**, that was inserted in peptide model ($n = 1, 2$; $R = H$; Figure 22) containing Leu-Val dipeptide (prone to give an extended conformation) in order to evaluate the ability of compound **1** to induce a specific conformation.³⁵

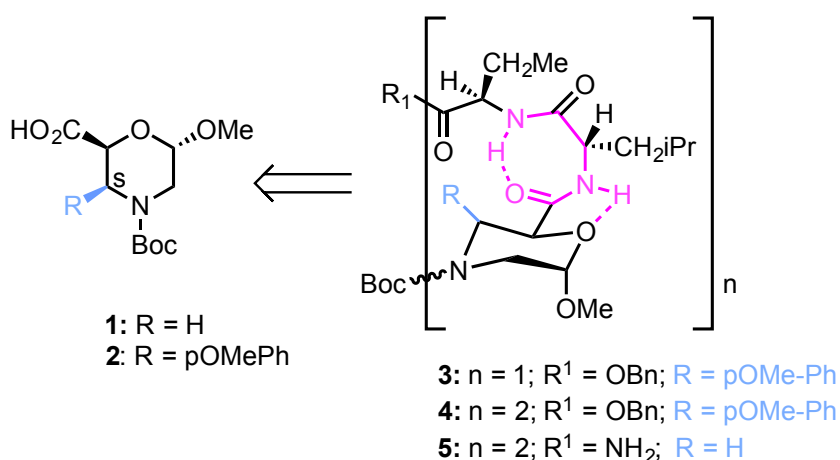


Figure 22 Peptides containing β -MorpholinoAA

Due to the formation of a strong H-bond between the oxygen of the morpholino ring and NH of amino acid $i+1$, γ -turn/s stabilized by a H-bond between C=O and NH at positions i and $i+2$ can be formed. Interestingly, the hexapeptide **4** (Figure 23) showed an equilibrium between α - and PP-helices as secondary structures. The shift between the two geometries, stabilized by the γ -turn (described in pink), is possible thanks to the rotation of the tertiary amide bond (underlined with green ring).

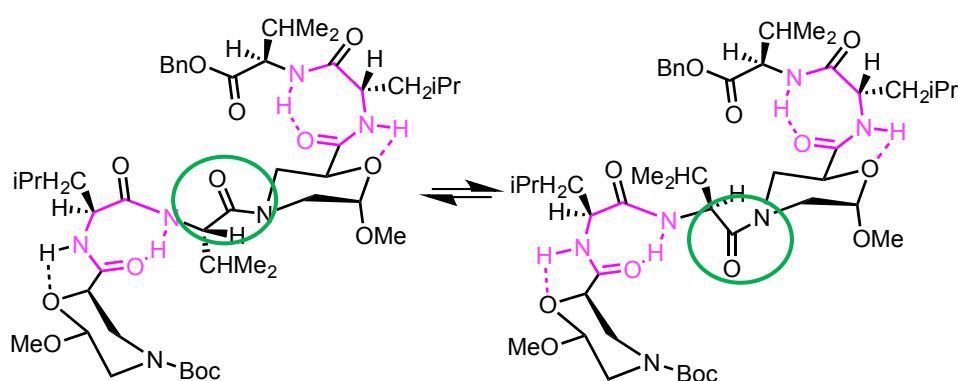


Figure 23 Equilibrium of model peptide containing β -Morpholino AA

In order to block this rotation, we evaluated the possibility of introducing a bulky group in the α -position of the tertiary amide bond on the morpholino ring, thus stabilizing only the PPII helix as reported in Figure 24. In particular the p -OMe substituent on the aryl group has been chosen because it could be involved in PPI as hydrogen bond acceptor.

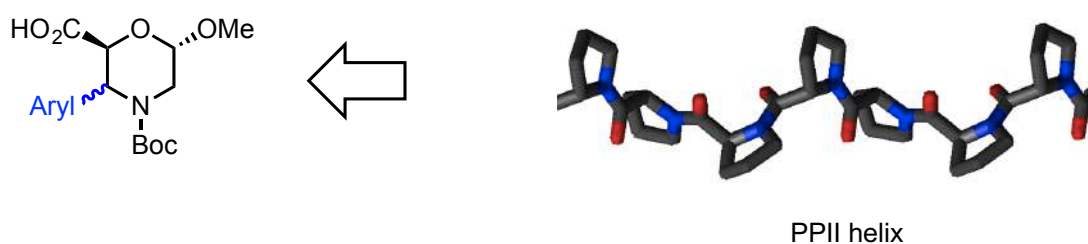


Figure 24 Idea for the stabilization of PPII helix.

Computational studies

H-REMD simulations were performed by Prof. Contini (Department of Pharmaceutical Science, University of Milano) in order to evaluate the role of the *p*-OMe-Ph group at C-3 and the stereochemical configuration at the same carbon in the conformational preferences of N-Boc-[(S/R)-Ar- β Morph-Leu-Val]₂-OBn hexapeptide **4**. As expected, the insertion of the aryl group at C-3 induced a significant change in the conformational stability of peptides (3S)- or (3R)-Ar- β Morph containing hexapeptides, named (3S)-**4** and (3R)-**4**, respectively, compared to **5** (Figure 25).

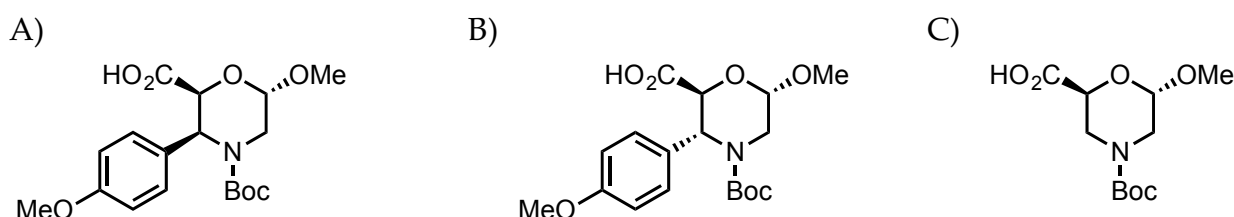


Figure 25 Hexapeptides containing: A) (3S)-4 Ar- β Morph, B) (3R)-4 Ar- β Morph, C) β Morph 5

A different stability was observed depending on the stereochemistry at C-3 of Ar- β Morph. The population of the main conformational cluster is different for (3S)-**4** and (3R)-**4** (67.3% and 29.2%, respectively; Tables 2) suggesting that the former is conformationally more stable.

Table 2 Dihedral values taken from the most representative conformation of the main cluster *c0*

	(3S)-4	(3R)-4
φ_1	-54.8 ± 43.4	-111.0 ± 17.0
ψ_1	135.8 ± 28.0	-33.0 ± 9.7
φ_2	-75.8 ± 27.7	-128.5 ± 8.9
ψ_2	152.4 ± 21.1	82.7 ± 11.1
φ_3	-86.9 ± 25.6	-72.0 ± 11.0
ψ_3	147.0 ± 49.4	-6.9 ± 18.2
φ_4	-75.4 ± 26.5	-80.8 ± 18.6
ψ_4	127.9 ± 29.1	122.8 ± 12.1
<i>c0</i> pop (%)	67.3	29.2

Moreover, for (3S)-**4**, the average φ and ψ dihedrals of the cluster (*c0*) population match with the typical PPII-helices range (about -75° and 150° , respectively; Table 2 and Figure 26).

A disordered conformation was obtained for **(3R)-4**, where the average φ and ψ dihedrals of c0 do not match any well-defined secondary structure.

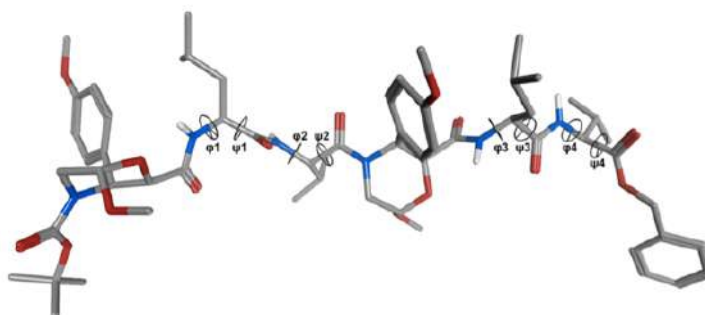


Figure 26 Representative geometry of the most populated cluster for c0 for **(3S)-4**

The different behavior of **(3S)-4**, **(3R)-4**, and **5** is also well described by the heatmaps (Figure 27) obtained from the analysis of the last 500 ns of the H-REMD trajectory, representing the conformational free energy surfaces derived from the Boltzmann distributions of selected dihedral pairs. Indeed, a deep well at about $\varphi_1 = -80^\circ$ and $\psi_1 = 150^\circ$ can be observed for **(3S)-4**. Conversely, for **(3R)-4**, an additional and rather wide low energy region is observed at about $\varphi_1 = -100^\circ$ and $\psi_1 = -50^\circ$. Furthermore, the region corresponding to the left-handed helix ($30^\circ \leq \varphi \leq 130^\circ$ and $-50^\circ \leq \psi \leq 100^\circ$) also is energetically more accessible, compared to **(3S)-4**. In conclusion from computational studies, β -Morph **2** seems to favor both PP- and α -helix geometries, as well as the transition region between them represented by the inverse γ turn region ($\varphi \approx -80^\circ$ and $\psi \approx 70^\circ$). Conversely, **(3R)-Ar- β -Morph** still induces α - and PP-helices, but with a less favored inverse γ -turn region.³⁶

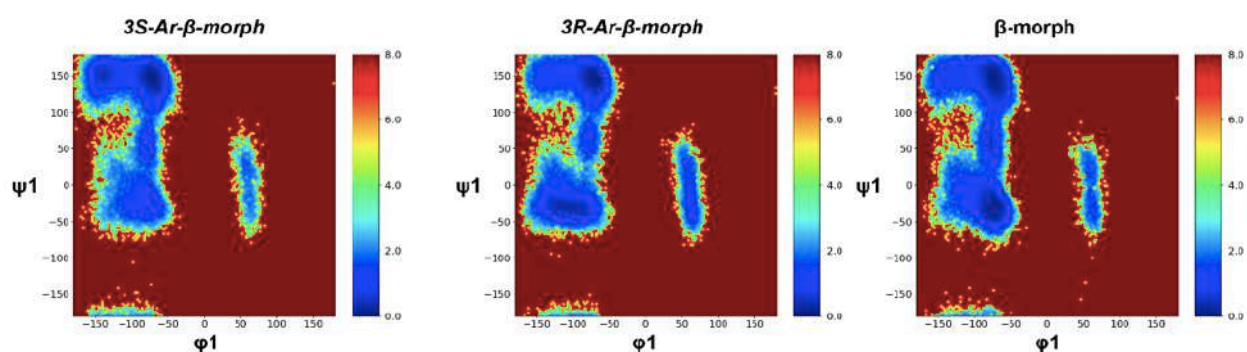
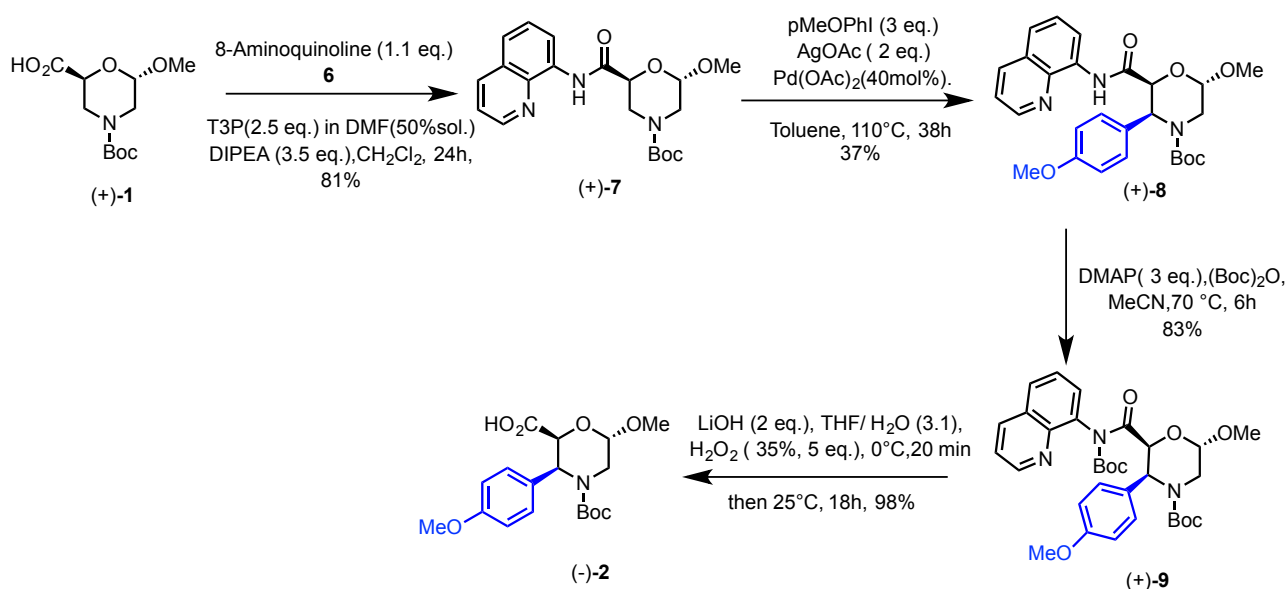


Figure 27 Heatmaps describing the relative free energy (kcal/mol) associated with different values for the φ_1/ψ_1 dihedral pair for peptides **(3S)-4**, **(3R)-4**, and **5**, 24 containing **3S-Ar- β -Morph**, **3R-Ar- β -Morph**, and **β Morph**, respectively.

Synthesis of the new scaffold 2

According to the computational data (3S)-Ar- β Morph was then synthesized to verify its ability to stabilize the PPII helix starting from the enantiopure β Morph (+)-**1** (Figure 22, R = H). It was prepared from the commercially available glucose according a known procedure.³⁵ First, **1** was transformed into amide **7** by reaction with 8-aminoquinoline (**6**) because it is reported that a regio and diastereoselective Pd-catalyzed C(sp³)H-arylation could be mediated by the Pd-coordinating nitrogen of quinoline ring. Amide **7** (43%) was prepared by using a reported protocol.³⁷ On the other hand, a strong improvement in the yield was achieved by activation of **1** with propylphosphonic anhydride [T3P, 2.5 equiv; 50% DMF solution in CH₂Cl₂, DMAP (3.5 equiv), 0 °C, 1 h; then 24 h at 25 °C] followed by reaction with **6** (1.1 equiv, 25 °C, 24 h) giving (+)-**7** in 81% yield (Scheme 3).



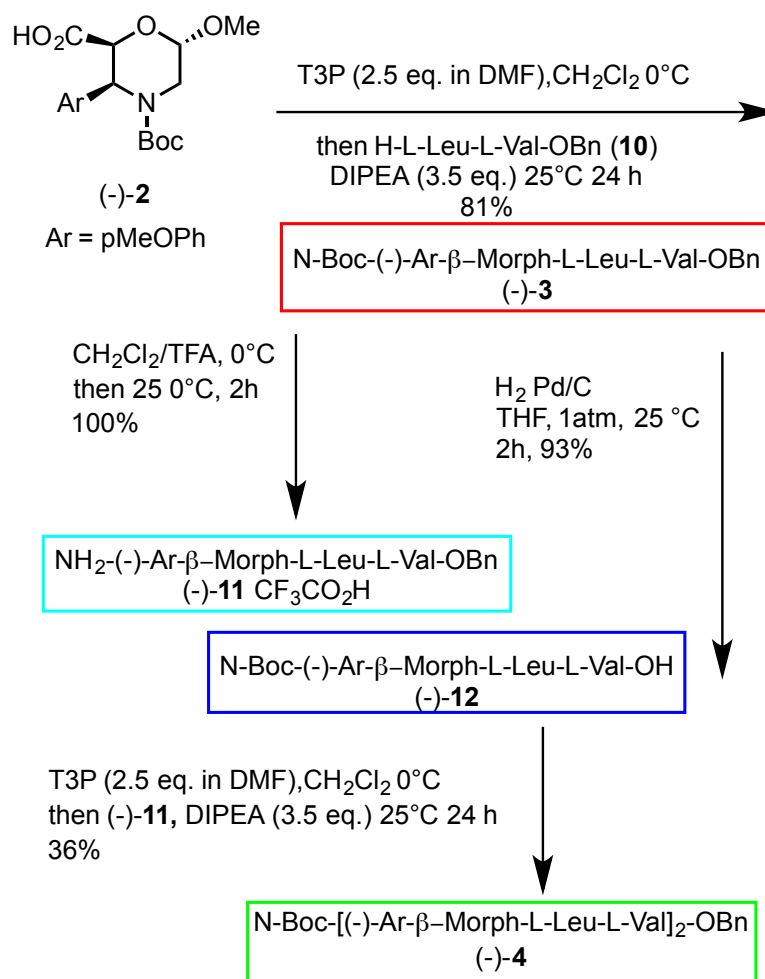
Scheme 3 Synthesis of 3-Ar- β -Morph (-)AA 2

The arylation at C-3 for a similar compound of **7** (10% yield) is reported in literature [Pd(OAc)₂ (0.1 equiv), AcOAg (2 equiv), MeOPhI (3 equiv) toluene, reflux, 38 h].³⁸ The same protocol, starting from **7** and p-iodoanisole, gave analogous yields of **8**. Several attempts were performed to optimize this procedure. While the use of toluene was found to be crucial (other solvents inhibit the reaction), incrementing the amount of Pd(OAc)₂ from 0.2 to 0.4 equiv. increased the yield up to 37% (63% recovery starting material). Unfortunately, no improvement was observed by changing the catalyst (Cu(OAc)₂, Cu(TFA)₂, Pd(TFA)₂, PdCl₂) or the oxidant (AgTFA instead of AcOAg). The reaction is regio- and diastereoselective, affording only compound (+)-**8** having the aryl moiety in cis relationship with the carbonyl group. To synthesize the deprotected carboxylic acid **2**, N-Boc amide (+)-

9 was first prepared [(Boc)₂O (20 equiv), DMAP (3 equiv), MeCN, 70 °C, 6 h; 83%]. Its hydrolysis [LiOH·H₂O (2 equiv)/ H₂O₂ (35%, 5 equiv), THF/H₂O (3:1), 25 °C, 18 h] gave (-)-**2** (98%).

Foldamer synthesis

Different coupling agents were used for the foldamer syntheses (Scheme 4). T3P (DMF/DMAP solution) was chosen as the most efficient coupling agent, giving tripeptide (-)-**10** in 81% yield. It was selectively deprotected (TFA, CH₂Cl₂, 25 °C, 2 h), affording (-)-**11** (quantitative yield). Debenzoylation reaction of (-)-**3** (H₂, Pd/C, THF, 1 atm., 25 °C, 2 h) provided (-)-**12** (93%). For the final coupling of **11** with **12** we used first HOBt/EDC or HOBt [(1.1 equiv)/EtCN-oxime (1.1 equiv)/ DIPEA (2.1 equiv)] but low yield of hexapeptide **4** (17 and 8%, respectively) were detected. In a third attempt, T3P was selected resulting the best coupling agent, improving the yield of (-)-**4** (36%).



Scheme 4 Synthesis of Tripeptide (-)-**3** and Hexapeptide (-)-**4**

NMR characterization

NOESY experiments were used for the stereochemistry assignment of (-)-**2** at C-3. The trans disposition of H-2/ H-3 is excluded by the J value (5.1 Hz), and a distorted morpholino chair is suggested ($J_{5_{ax},6} = 8.9$ Hz, $J_{5_{eq},6} = 5.4$ Hz). NOEs were detected between H-2/Boc (w) and aryl group with H-2, H-3, and H-5_{ax}, indicating the pseudo-axial disposition of the aryl moiety cis with respect to the carboxylic function (Figure 28).

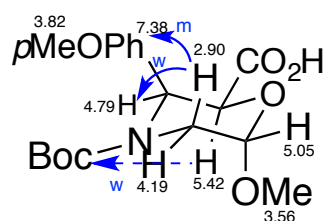


Figure 28 NOEs NMR of morpholino ring protons (blue arrows)

Tripeptides (-)-**3** and hexapeptide (-)-**4** were characterized by NMR (^1H , ^{13}C , COSY, TOCSY, HMBC, HMQC, NOESY; 600 MHz) in CD_3CN solution, and δ values of morpholino and α -AA protons were assigned. For the tripeptide **3** a γ -turn is present at C-terminus. As reported in Figure 29, weak NOEs are those between NH_{Leu} with $\text{OMe}_{\text{Morph}}$, H-6, and H-2, indicating its orientation toward the oxygen region of the ring. The formation of the γ -turn is supported by the spatial proximity of NH_{Val} with the leucine moiety.

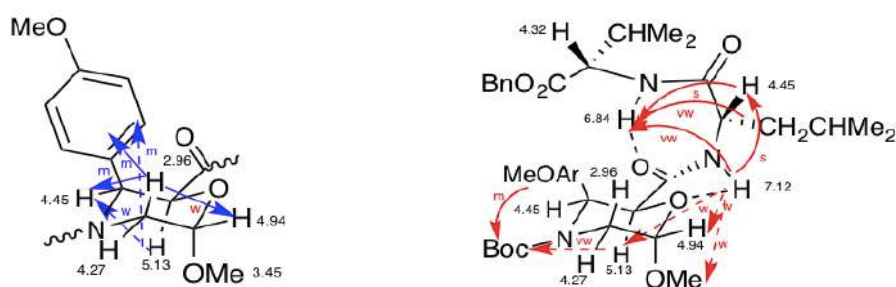


Figure 29 NOEs NMR of morpholino ring protons (blue arrows) and between the different AAs (red arrows) and H-bonds (dotted lines) for tripeptide

Furthermore, low $\delta\Delta/\Delta T$ values (273–323 K; Figure 30) for NH_{Val} (-1.8 ppb K^{-1}) and NH_{Leu} (-2.2 ppb K^{-1}) were detected. Accordingly, a H-bond between NH_{Val} and $\text{C}=\text{O}_{\text{Morph}}$ is suggested, driven by a second strong H-bond between NH_{Leu} and the oxygen of the ring.

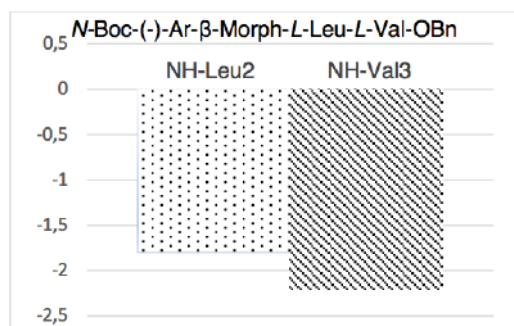


Figure 30 NMR data for tripeptide (-)-3: $\Delta\delta/\Delta T$ NH values (273–333 K)

Moreover, the NMR analysis of (-)-4 showed the presence of two conformers in 80:20 ratio. Very low $\delta\Delta/\Delta T$ values (273–333 K) (Figure 31) for all NHs ranging from -2.8 to -2 ppb K^{-1} were found for the main isomer, supporting a strong H-bond network, as indicated for 3.

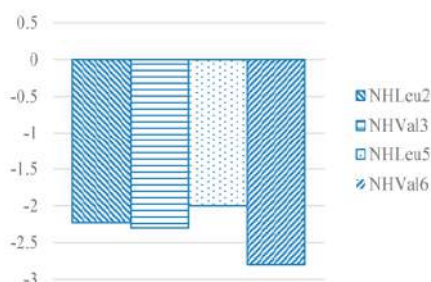


Figure 31 NMR data for hexapeptide (-)-4: $\Delta\delta/\Delta T$ NH values (273–333 K).

NOEs of compound (-)-4 are shown in Figure 32. Similar spatial proximities between NH_{Leu2} and NH_{Leu5} with the acetal region of the corresponding morpholine ring at positions 1 and 4 are present, supporting the formation of two γ -turns. Spatial proximities between CH_{Val3} and protons of morpholine-4 are diagnostic for the prediction of the main conformer.

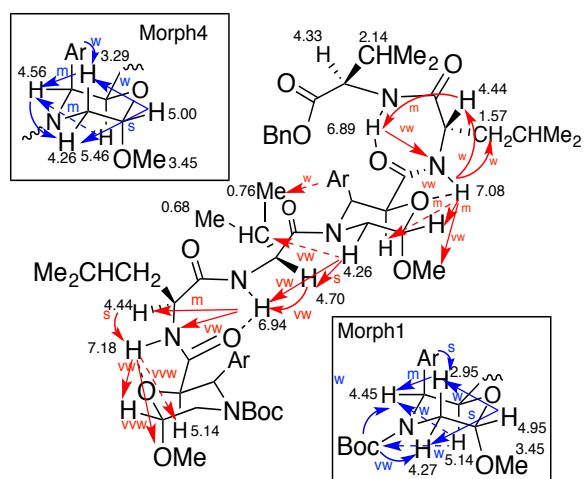


Figure 32 NOEs NMR of compound 4 protons (blue arrows) and between the different AAs (red arrows) and H-bonds (dotted lines)

NOEs were detected between CH_{Val3} and $\text{H}_{\text{eq-5Morph4}}$ but not with $\text{H-3}_{\text{Morph4}}$ (Figure 33), thus indicating the orientation of $\text{C}=\text{O}$ toward the aryl region. As a result, the E-conformer is suggested for the tertiary amide bond.

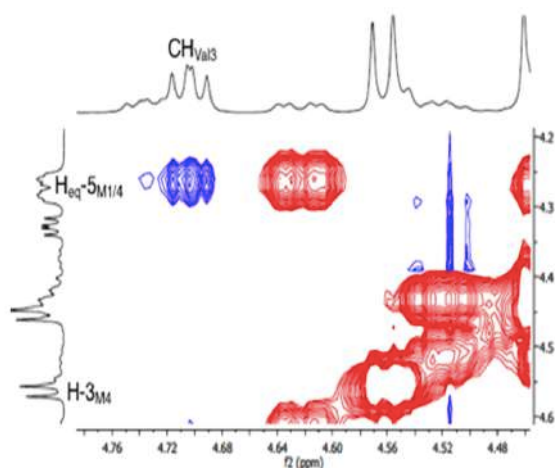


Figure 33 Zoom of Val3/Morph4 region for hexapeptide 4

IR characterization

FTIR studies were performed on a solid sample of (-)-4. The PPII helix conformation was confirmed thanks to the presence of a peak around 1640 cm^{-1} , corresponding to the PPII characteristic $\text{C}=\text{O}$ stretching frequency (Figure 34).³⁹

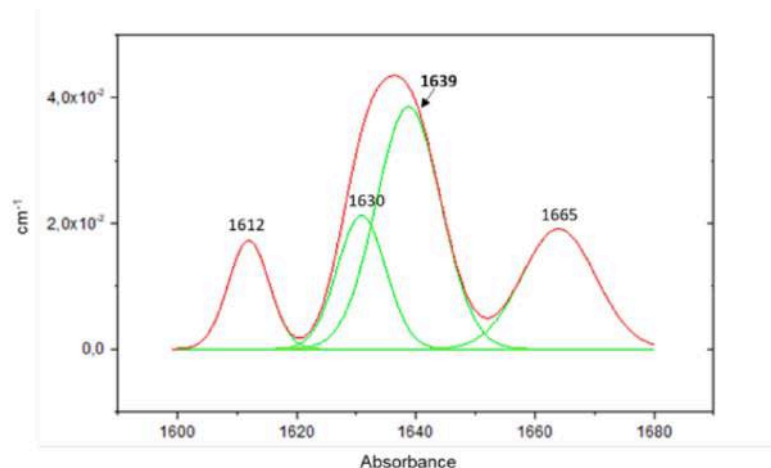


Figure 34 FTIR spectra for peptide 4

Simulation of (3S)-4 in a biological complex

Considering these promising results, we investigated on the possibility for peptide (3S)-4 to mimic a PPII helix within a biological complex. As a reference, we chosen the structure of the complex between human platelet profilin (HPP) and a poly-L-proline decamer (L-Pro10).⁴⁰ The complex is formed by two molecules of HPP bound to L-Pro10, where this latter adopts a PPII helix. We performed MD simulations (100 ns) of both the HPP: L-Pro10 and HPP:(3S)-4 complexes, the latter obtained by a protein-protein docking approach. The binding energy of both L-Pro10 and (3S)-4 was then computed using the Nwat-MMGBSA method⁴¹ are reported in the Table 3

Table 3 Average Energies^a (kcal/mol) and Standard Deviations Computed by Analyzing the 90-100 ns Segment of the MD trajectory of HPP:(3S)-4 and HPP:L-Pro10

	HPP:(3S)-4		HPP:L-Pro10	
	N _{wat} =0	N _{wat} =30	N _{wat} =0	N _{wat} =30
E _{tot} Complex	-25505.1 ± 48.6	-25790.9 ± 49.9	-25879.6 ± 50.8	-26150.8 ± 50.6
E _{tot} Receptor	-25032.4 ± 48.0	-25291.6 ± 49.2	-25089.3 ± 51.2	-25329.1 ± 52.4
E _{tot} Ligand	-408.1 ± 6.6	-408.1 ± 6.6	-741.4 ± 4.2	-741.4 ± 4.2
ΔE _{binding}	64.5 ± 4.9	-91.2 ± 9.6	-48.9 ± 6.5	-80.3 ± 10.5

Results confirmed that peptide (3S)-4 can actually behave as a PPII mimic in a biological complex (Figure 35).

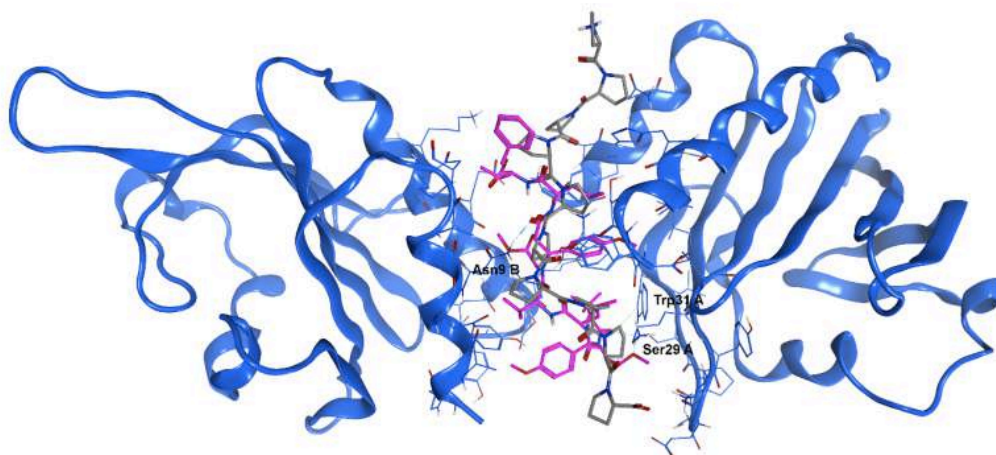


Figure 35 Representative geometry of the most populated cluster c0 obtained from the analysis of the last 50 ns of the 100 ns MD trajectory of HPP:(3S)-4 (peptide (3S)-4 carbons are colored in magenta). HPP:L-Pro10 was subjected to the same protocol and the representative geometry of the most populated cluster was superposed to HPP:(3S)-4; but only LPro10 is shown (grey carbon atoms)

In conclusion, starting from our previous work where scaffold **1** was able to generate a mixture of α and PPII-like helices when it was inserted in a model peptide, we designed the new scaffold (-)-**2** with the idea to stabilize only the PPII structure. We demonstrated by computational, IR and NMR data that the 3-Aryl β -Morph AA **2** represents the first β -AA able to induce a PPII helix when inserted in a model foldamer due to the presence of a hindered aryl-substituent at C-3 that blocks the rotation of the tertiary amide bond favoring the trans-conformation.

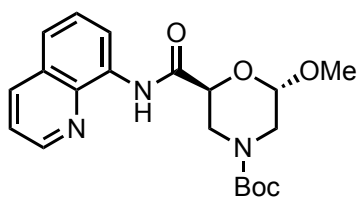
The results of these researches were published on *Organic Letters ACS*⁴²

Experimental part

General information.

Chemicals were purchased from Sigma Aldrich and were used without further purification. Mass spectra were recorded on an LCQESI MS and on a LCQ Advantage spectrometer from Thermo Finnigan and a LCQ Fleet spectrometer from Thermo Scientific. The NMR spectroscopic experiments were carried out either on Varian MERCURY 300 MHz (300 and 75 MHz for ^1H and ^{13}C , respectively), or Bruker Avance I 500 MHz spectrometers (500 and 125 MHz for ^1H and ^{13}C , respectively). Optical rotations were measured on a Perkin-Elmer 343 polarimeter at 20 °C (concentration in g/100 mL). Chemical shifts (δ) are given in ppm relative to the CHCl_3 internal standard, and the coupling constants J are reported in Hertz (Hz).

Synthesis of (2S,6S)-4-Boc-6-methoxy-N-(quinolin-7-yl)-morpholine-2-carboxamide (+)-7



To a solution of compound **1** (277 mg, 1.06 mmol, 1 equiv.) in anhydrous CH_2Cl_2 (15 mL) at 0 °C, a propylphosphonic anhydride (T3P) (2.65 mmol, 2.5 equiv. 1.7 mL of 50% DMF solution), 8-aminoquinoline (168.23 mg, 1.16 mmol, 1.1 equiv.) and DIPEA (647 μL , 3.71 mmol, 3.5 equiv.) were added. The reaction mixture was stirred for 24 h at 25 °C. The organic layer was washed with a solution of KHSO_4 (5%, 25 mL), a saturated solution of NaHCO_3 (25 mL) and brine (25 mL). After drying over Na_2SO_4 , the solvent was removed under reduced pressure. Purification of the crude product by silica gel flash chromatography (*n*hexane/ AcOEt 8:2) afforded the amide **7** oil in 81% (334 mg, 0.86 mmol).

^1H NMR (CDCl_3 , 300 MHz) δ 10.81 (s, 1H), 8.88 (dd, J = 4.2, 1.6 Hz, 1H), 8.84-8.80 (m, 1H), 8.20 (dd, J = 8.3, 1.6 Hz, 1H), 7.57 (d, J = 4.5 Hz, 2H), 7.49 (dd, J = 8.3, 4.2 Hz, 1H), 5.01 (brs, 1H), 4.66 (dd, J = 10.8, 3.3 Hz, 1H), 4.47 (brs, 1H), 4.08 (brs, 1H), 3.53 (s, 3H), 3.25-2.97 (m, 2H), 1.51 (s, 9H);

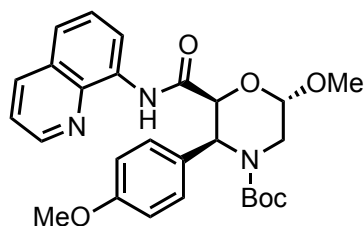
^{13}C NMR (75 MHz, CDCl_3) δ 167.8, 154.9, 148.4, 138.7, 136.0, 133.6, 128.1, 127.4, 122.3, 121.0, 117.3, 96.8, 77.5, 69.3, 55.3, 46.0, 45.3, 28.4 (x3);

HRMS (ESI-TOF) m/z : $[\text{M}+\text{Na}]^+$ Calcd for $\text{C}_{20}\text{H}_{25}\text{N}_3\text{O}_5\text{Na}$ 410.1692; Found 410.1697.

Anal. Calcd for $\text{C}_{20}\text{H}_{25}\text{N}_3\text{O}_5$: C, 62.00; H, 6.50; N, 10.85. Found C, 61.88; H, 6.60; N, 10.79.

$[\alpha]_{\text{D}}^{20} = +43.6$ (c 0.2 in CHCl_3)

Synthesis of (2S,3S,6S)-4-Boc-6-methoxy-3-(4-methoxyphenyl)-N-(quinolin-7-yl)-morpholine-2-carboxamide (+)-8



Operating in a sealed tube amide **7** (1.4 g, 3.4 mmol, 1.0 equiv.) was dissolved in toluene (65 mL) and AgOAc (1.13 g, 6.8 mmol, 2.0 equiv.), 4-iodoanisole (2.4 g, 10.2 mmol, 3.0 equiv.), Pd(OAc)₂ (305.3 mg, 1.36 mmol, 0.4 equiv.) were added. The tube was flushed with argon and sealed, then placed in a preheated oil bath to 110 °C (oil bath) and stirred for 38 h. The reaction mixture was cooled at 25 °C and EtOAc (10 mL) was added. The resulting solution was filtered through a Celite pad, that was washed with EtOAc (10 mL). The solvent was removed in vacuo, and the crude material was purified by flash column chromatography (n-hexane/AcOEt, 8:2) affording pure compound **8** as a yellow oil (606 mg, 0.86 mmol, 37%).

¹H NMR (300 MHz, CDCl₃) δ 10.84 (s, 1H), 8.83-8.66 (m, 2H), 8.19 (dd, J = 8.3, 1.6 Hz, 1H), 7.56-7.41 (m, 3H), 7.47, 6.88 (AA'XX' system, J = 8.8 Hz, 4H), 5.59 (d, J = 6.3 Hz, 1H), 5.12 (dd, J = 8.5, 5.2 Hz, 1H), 4.90 (d, J = 6.3 Hz, 1H), 4.33 (dd, J = 14.4, 5.2 Hz, 1H), 3.82 (s, 3H), 3.72 (s, 3H), 3.04 (dd, J = 14.4, 8.5 Hz, 1H), 1.43 (s, 9H);

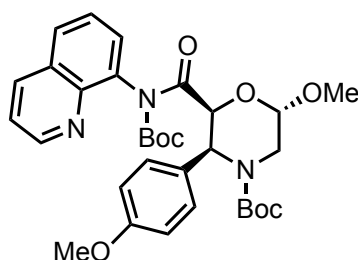
¹³C NMR (75 MHz, CDCl₃) δ 167.7, 159.5, 155.2, 148.7, 139.1, 136.7, 134.3, 131.7, 129.3(x2), 128.4, 127.7, 122.4, 122.1, 117.1, 114.2(x2), 98.5, 81.1, 74.2, 56.6, 55.8, 55.6, 42.2, 28.7(x3);

HRMS (ESI-TOF): m/z [M+H]⁺ Calcd for C₂₇H₃₂N₃O₆ 494.2291; Found 494.2294.

Anal. Calcd for C₂₇H₃₁N₃O: C, 65.71; H, 6.33; N, 8.51. Found C, 65.49; H, 6.49; N, 8.39.

[α]_D²⁰ = +33.6 (c 0.3 in CHCl₃).

Synthesis of (2S,3S,6S)-4-Boc-6-methoxy-3-(4-methoxyphenyl)-N-Boc-N'-(quinolin-7-yl)-morpholine-2- carboxamide (+)-9



Compound **8** (606 mg, 1.22 mmol, 1.0 equiv.) was dissolved in MeCN (30 mL). DMAP (413.4 mg, 3.68 mmol, 3.0 equiv.) and (Boc)₂O (5.3 g, 24.5 mol 20.0 equiv.) were added at 25 °C. The reaction mixture was stirred at 70 °C (oil bath) for 6 h. After cooling at 25 °C, the reaction mixture was concentrated in vacuo. The crude mixture was purified by flash chromatography (*n*hexane/AcOEt, 6:4) affording pure compound **9** as an oil (604 mg, 1.01 mmol, 83%)

¹H NMR (300 MHz, CDCl₃) δ 8.90 (dd, J = 4.1, 1.6 Hz, 1H), 8.19 (dd, J = 8.5, 1.6 Hz, 1H), 7.87-7.82 (m, 1H), 7.60-7.47 (m, 4H), 7.43 (dd, J = 8.4, 4.4 Hz, 1H), 6.92 (d, J = 8.9 Hz, 2H), 6.14 (brs, 1H), 5.74 (brs, 1H), 5.39 (brs, 1H), 4.16-4.03 (m, 1H), 3.84 (s, 3H), 3.53 (s, 3H), 2.85 (dd, J = 13.6, 9.4 Hz, 1H), 1.45 (s, 9H), 1.23 (s, 9H);

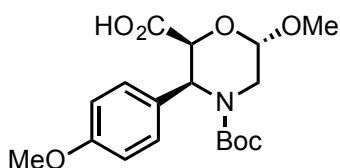
¹³C NMR (75 MHz, CDCl₃) δ 159.4, 155.1, 152.8, 150.8, 144.6, 137.1, 136.4, 131.3, 129.4(x2), 129.3, 129.1, 128.7, 126.5, 121.9, 114.2(x2), 97.4, 83.8, 80.8, 75.9, 56.8, 55.7, 54.6, 42.4, 28.7(x3), 27.9(x3);

HRMS (ESI-TOF): m/z [M+Na]⁺ Calcd for C₃₂H₃₉N₃O₈Na 616.2635; Found 616.2639.

Anal. Calcd for C₃₂H₃₉N₃O₈: C, 64.74; H, 6.62; N, 7.08. Found: C, 64.63; H, 6.70; N, 7.00.

[α]_D²⁰ = +25.8 (c 0.2 in CHCl₃).

Synthesis of (2*S*,3*S*,6*S*)-4-Boc-6-methoxy-3-(4-methoxyphenyl)-2-carboxylic acid (-)-**2**



A solution of compound **9** (450 mg, 0.758 mmol, 1.0 equiv.) in THF/H₂O (10 mL, 3:1) was cooled at 0 °C. LiOH H₂O (63.6 mg, 1.51 mmol, 2 equiv.) and H₂O₂ (35%, 128.9 mg, 3.79 mmol, 5 equiv.) were added and the reaction mixture was stirred for 20 min at 0 °C. After warming at 25 °C, the stirring was continued for 18 h. The reaction was extracted with Et₂O to remove the organic impurities and then the aqueous layer was acidified with 1 M HCl to pH = 6 and extracted with EtOAc (3 x 10 mL). The combined organic layers were washed with brine (3 x 10 mL), dried over Na₂SO₄. The solvent was removed and the acid **2** was obtained as an oil and was used without further purification (271.6 mg 0.74 mmol, 98%). Detailed NMR data are reported in Table 4 and Figure 36.

HRMS (ESI-TOF): *m/z* [M+Na]⁺ Calcd for C₁₈H₂₅NO₇Na 390.1529; Found 390.1532.

Anal. Calcd for C₁₈H₂₅NO₇: C, 58.85; H, 6.86; N, 3.81. Found: C, 58.63; H, 6.90; N, 3.65.

[α]_D²⁰ = -12.24 (c 1.24 in CHCl₃)

Table 4 ^1H , ^{13}C NMR (CDCl_3 , $750\mu\text{L}$, 0.036 mM , 300 MHz ,) and NOEs (600 ms) data for (-)-Boc-3-Ar- β -Morph 2

AA	Atom	^1H δ	Multiplicity J (Hz)	^{13}C δ	Noesy
ArMorph	COOH			173.9	
	CH-2	5.42	d J 5.1	55.3	Boc(w), Ar(7.38,m), H-3 (m)
	CH-3	4.79	d J 5.1	72.7	H-2 (m), H _{ax} -5 (w), H _o (m), ArOMe(vvw)
	CH ₂ -5	H _{eq} 4.19	brd J 14.0, 5.4	41.9	H _{ax} -5(s), H-6(m)
		H _{ax} 2.90	dd J 14.0, 8.9		H _{eq} -5(vs), H-3(w), H-6(vw), Ar(7.38,m)
	CH-6	5.05	dd, J 8.5, 5.4	97.5	OMe-6 (s), H-5(_{seq} ; vW _{ax})
	OMe	3.56		56.3	H-2(w), H-6 (m)
	MeOAr	MeO: 3.82	s	55.2	MeO: H _m (s)
H _m : 6.89		dd, J 8.8	113.9	H _m : ArOMe(s)	
H _o : 7.38			128.7	H _o : Boc (w), H-3(m), H-2(m), H _{ax} -5(m)	
			C _q 130.1, 159.2		
Boc	1.37		28.3, 81.0, 154.7	H-2 (w), H _o (w)	

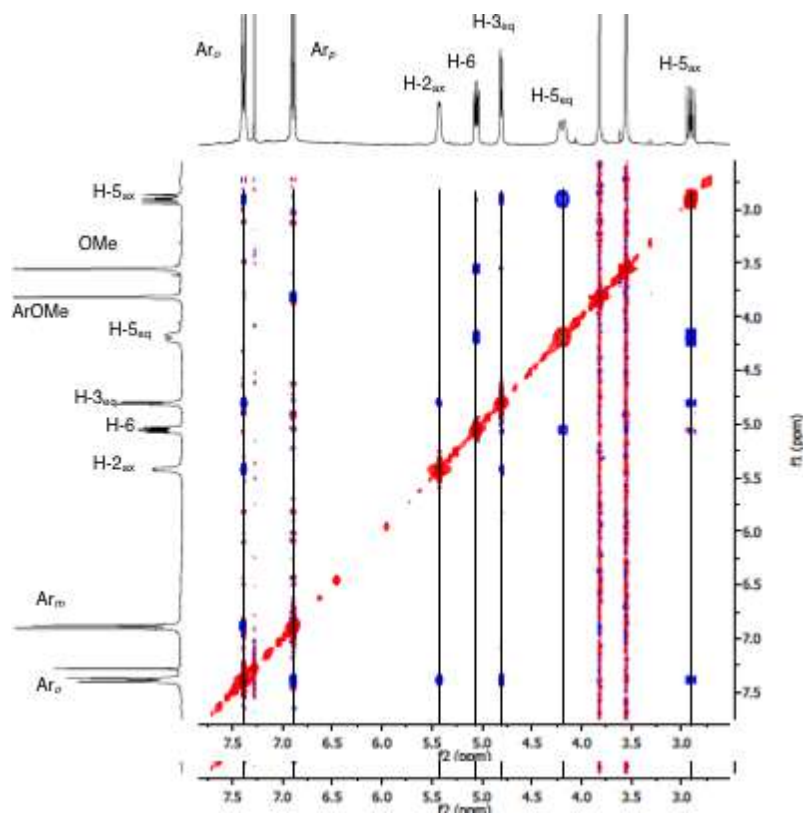
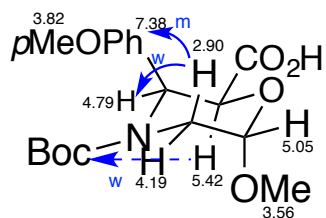
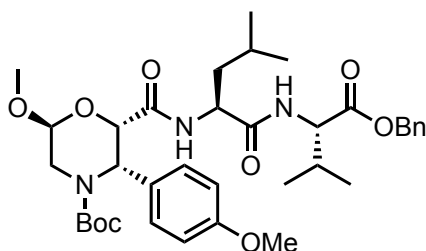


Figure 36 NOEs (CDCl_3 , 300 MHz , 600 ms) of Boc-3-Ar-morpholino acid 2.

Synthesis of N-Boc-(-)-3-(4-Methoxyphenyl)- β -Morph-(L)-Leu-(L)-Val-OBn(-)-3



To a solution of acid **2** (50 mg, 0.13 mmol, 1 equiv.) in CH_2Cl_2 (2.5 mL) at 0 °C, propylphosphonic anhydride solution (T3P) (50% solution in DMF, 215 μL , 0.34 mmol, 2.5 equiv.), dipeptide **10** (65 mg, 0.15 mmol, 1.1 equiv.) and DIPEA (71.1 μL , 0.40 mmol, 3.5 equiv.) were added. The reaction mixture was stirred for 24 h at 25 °C. The organic layer was washed with a solution of KHSO_4 (5%, 25 mL), a saturated solution of NaHCO_3 (25 mL) and brine (25 mL). After drying over Na_2SO_4 , the solvent was removed under reduced pressure. Purification of the crude product by silica gel flash chromatography (*n*hexane/ AcOEt , 7:3) afforded tripeptide **3** as a colorless oil (67.5 mg, 0.1 mmol, 81%). Detailed NMR data are reported in Table 5 and Figure 37.

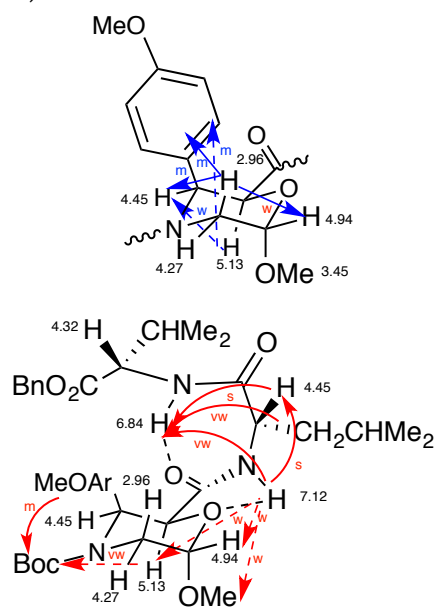
HRMS (ESI-TOF): m/z $[\text{M}+\text{Na}]^+$ Calcd for $\text{C}_{36}\text{H}_{51}\text{N}_3\text{O}_9\text{Na}$ 692.3523; Found 692.3528.

$[\alpha]_{\text{D}}^{20} = -24.13$ (c 0.7 in CHCl_3)

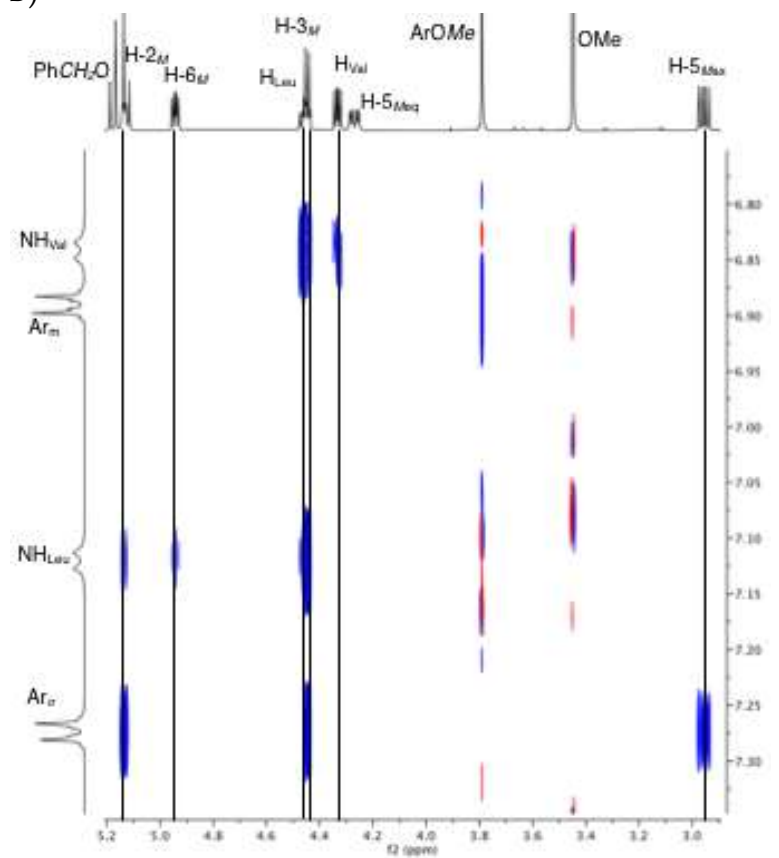
Table 5 ^1H , ^{13}C NMR (CD_3CN , $750\mu\text{L}$ 0.020 mM , 600 MHz ,) and NOEs (600 ms) data for *N*-Boc(-)-*Ar*- β -*Morph*-*L*-*Leu*-*L*-*Val*-*OBn* (**3**)

AA	Atom	^1H δ	Moltepicity <i>J</i> (Hz)	^{13}C δ	Noesy
ArMorf-1	CO			168.5 ^a	
	CH-2	5.13	d <i>J</i> 8.0	56.8	Boc(vw), NH _{Leu} (w), H _o (m), H-3(w)
	CH-3	4.45	d <i>J</i> 8.0	72.1	H-2 (w), H _{ax} -5(m), ArOMe (w), H _o (m)
	CH ₂ -5	H _{eq} 4.27	dd <i>J</i> 14.6, 5.5	41.7	H-6(m), H _{ax} -5(s)
		H _{ax} 2.96	d <i>J</i> 14.6, 8.2		----- H _{eq} -5(s), H-3(m), H- 6(w), H _o (m)
	CH-6	4.94	dd, <i>J</i> 8.2, 5.5	97.8	OMe (m), NH _{Leu} (w) H-5(m _{eq} , w _{ax})
	OMe	3.45		55.0	NH _{Leu} (w), H-6(m)
	MeOAr	MeO: 3.79 H _m : 6.89 H _o : 7.27	s AA'BB' system <i>J</i> 8.7	54.7	H _m (s)
113.5				H _m : ArOMe (s)	
128.5 C _q 131.3, 159.1				H _o : Boc(m), H-3(m), H _{ax} - 5(m), H-2(m)	
Boc	1.37		27.6, 80.0 154.6	H-2 (vw), H _o (m)	
Leu-2	CO			171.2 ^a	
	CH	4.47-4.43	m	51.3	NH _{Val} (s), Me ₂ CHCH ₂ (m)
	CH	1.71-1.64	m	24.5	Me _{Leu} (s), NH(w)CH _{Leu} vw),
	CH ₂	1.60-1.59	m	40.8	NHCH _{Leu} (m), Me _{Leu} (m) NH _{Val} (w)
	Me	0.93	d <i>J</i> 6.0	21.0	NCH(s), CHCH ₂ (s)
		0.95	d <i>J</i> 6.4		
NH	7.12	d <i>J</i> 8.6		CH(s)CH ₂ (w), NH _{Val} (vw), H-6(w), H-2(w), OMe(w)	
Val-3	CO			171.8 ^a	
	CH	4.32	m	57.6	Me ₂ CH(s), NH _{Val} (m)
	CH	2.16-2.10	m	30.5	CH _{Val} (m), NH _{Val} (vw)
	Me	0.90	d <i>J</i> 6.8	18.3	NH _{Val} (m) Me ₂ CHCH (s)
		0.88	d <i>J</i> 6.7	17.5	
	NH	6.84	d, <i>J</i> 7.8		CH ₂ Leu ₂ (vw), CH _{Leu} (s), NH _{Leu} (vw), Me ₂ CH _{Val} (w), CH _{Val} (m), Me _{Val} (m)
	OBn	OCH ₂ 5.17, 5.12 Ph 7.27, 7.89	AB system <i>J</i> 12.2	66.5 136.0, 128.5, 128.3, 128.2	Ph(w) 7.27: OCH ₂ (s), Me _{Val} (m)

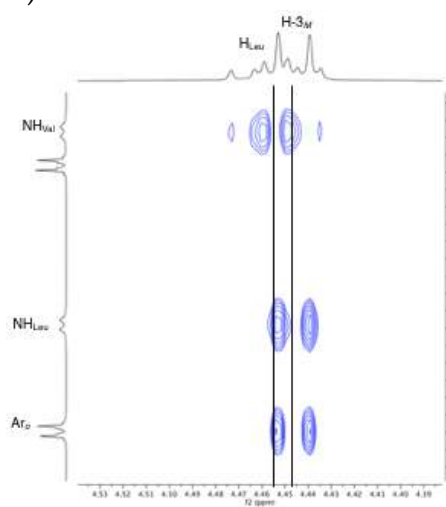
A)



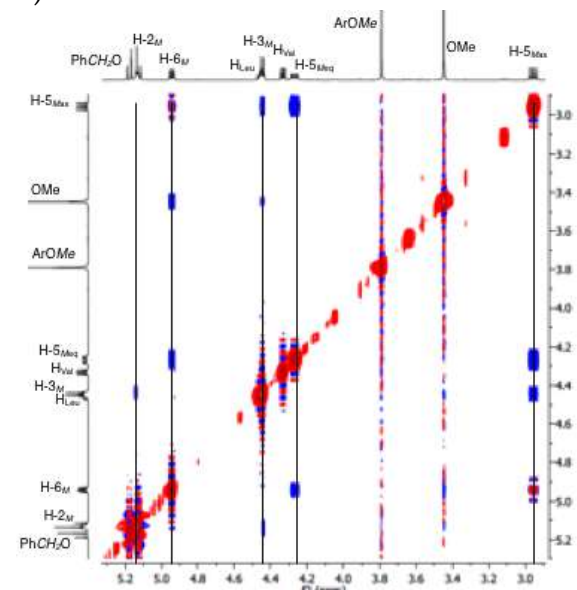
B)



C)



D)



E)

F)

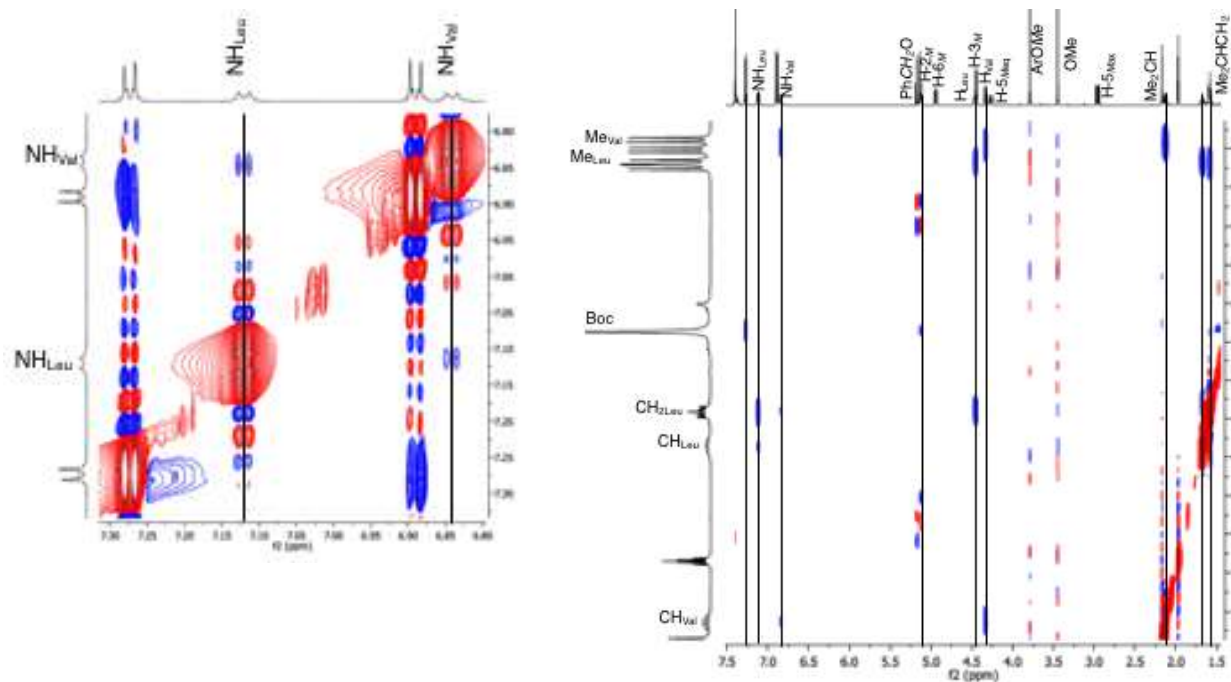
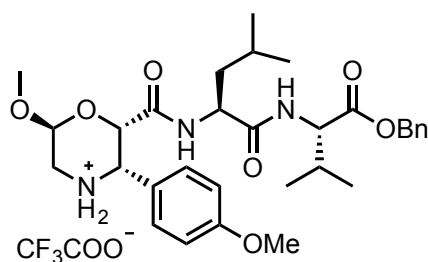


Figure 37 NOESY for tripeptide (-)-3 (CD₃CN, 600 MHz, 600ms): A) NOEs of morpholino ring protons (blue arrows) and between the different amino acids (red arrows). H-bonds (dotted lines). B) CH/Ar and CH/NH region. C) Zoom of CH-NH region. D) CH/CH region. E) zoom NH/NH region. F) High field/all protons region.

Synthesis of CF₃CO₂H NH₂(-)-3-(4-Methoxyphenyl)-β-Morph-L-Leu-L-Val-OBn (+)-11



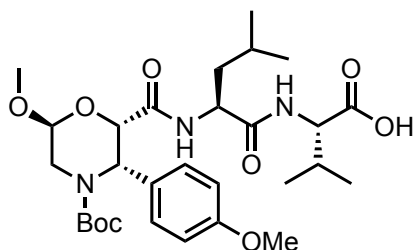
Operating in a round-bottom flask equipped with magnetic stirrer, compound **3** (26 mg, 0.04 mmol) was dissolved in CH₂Cl₂ (2 mL). The solution was cooled to 0 °C and TFA (2 mL) was slowly dropped. The solution was stirred at 25 °C for 2 h. The solvent was removed under reducing pressure affording compound **11** as CF₃CO₂H salt, obtained in quantitative yield (23.3 mg), that was used without further purification.

¹H NMR (300 MHz, CDCl₃) δ 7.33 (m, 7H), 6.91 (d, *J* = 7.4 Hz, 1H), 6.83 (s brs, 2H), 6.30 (d, *J* = 8.5 Hz, 1H), 5.13 (dd, *J* = 25.7, 12.2 Hz, 2H), 4.80 (m, 2H), 4.44 (dd, *J* = 8.5, 4.9 Hz, 1H), 4.29 (s brs, 1H), 4.15 (s brs, 1H), 3.76 (s, 3H), 3.45 (s, 3H), 3.10 (s, brs 1H), 2.82 (s brs, 1H), 2.09 (m, 1H), 1.66 – 1.39 (m, 3H), 0.96 – 0.61 (m, 12H).

¹³C NMR (75 MHz, CDCl₃) δ 171.56, 166.43, 161.02, 135.60, 130.59, 129.00, 128.90, 128.78, 123.78, 114.64, 94.35, 77.83, 77.40, 76.98, 70.69, 67.48, 60.51, 57.59, 55.98, 55.55, 51.65, 45.85, 41.04, 31.44, 25.03, 23.13, 22.36, 19.21, 17.88.

[α]_D²⁰ = +22.5 (c 0.32 in CHCl₃).

Synthesis of N-Boc-(-)-3-Ar-β-Morph-L-Leu-L-Val-OH (-)-12



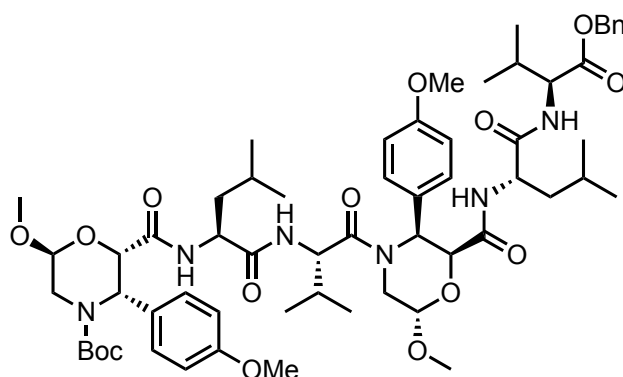
Operating in a round-bottom flask equipped with a magnetic stirrer, compound **3** (52 mg, 0.077 mmol) was dissolved in THF (5 mL) and Pd/C (50 mg, 10% loading) was added to the solution. The suspension was stirred under H₂ (1 atm) at 25 °C for 2 h. The catalyst was filtered over a Celite pad. The solvent was removed under reduced pressure and the obtained clear oil was dissolved in CH₂Cl₂ (20 mL) and washed with a saturated solution of NaHCO₃ (20 mL). The aqueous layer was then acidified with 37% HCl until pH 2. The product was extracted with CH₂Cl₂ (2 x 20 mL). The organic layer was concentrated under vacuum, affording compound **12** (41.4 mg, 0.071mmol, 93%) as colourless oil.

¹H NMR (300 MHz, CDCl₃) δ 7.29 – 7.26 (m, 2H), 6.99 (d, J = 8.9 Hz, 1H), 6.92 – 6.77 (m, 3H), 5.13 (d, J = 8.1 Hz, 1H), 4.91 (dd, J = 7.8, 5.9 Hz, 1H), 4.60 (m, 1H), 4.50 (m, 2H), 4.30 (dd, J = 14.1, 5.7 Hz, 1H), 3.78 (s, 3H), 3.44 (s, 3H), 2.96 (dd, J = 14.7, 8.1 Hz, 1H), 2.18 (m, 1H), 1.74 – 1.54 (m, 3H), 1.37 (s, 9H), 1.02 – 0.77 (m, 12H).

¹³C NMR (75 MHz, CDCl₃) δ 174.56, 172.00, 169.72, 159.51, 155.24, 131.24, 128.92, 114.19, 98.34, 81.20, 72.19, 57.99, 57.45, 56.16, 55.59, 51.75, 42.31, 41.16, 31.45, 28.64(x3), 25.20, 23.23, 22.57, 19.26, 17.98.

$[\alpha]_D^{20} = -15.75$ (c 0.36 in CHCl₃).

Synthesis of N-Boc-(-)-3-Ar-β-Morph-(L)-Leu-(L)-Val-(-)-3-Ar-β-Morph-(L)-Leu-(L)-Val-OBn (-)-4



According to procedure reported for peptide **3**, tripeptide **12** (1 equiv.) was made to react with **11** (1.1 equiv.). The purification of the crude product by silica gel flash chromatography (*n*hexane/ AcOEt 1:1) afforded **4** (36%) as colorless oil. Detailed NMR data are reported in Table 6 Figure 38.

HRMS (ESI-TOF): m/z $[M+Na]^+$ Calcd for $C_{60}H_{86}N_6O_{15}Na$ 1153.6049; Found 1153.6052.

$[\alpha]_D^{20} = -41.3$ (c 0.36 in $CHCl_3$)

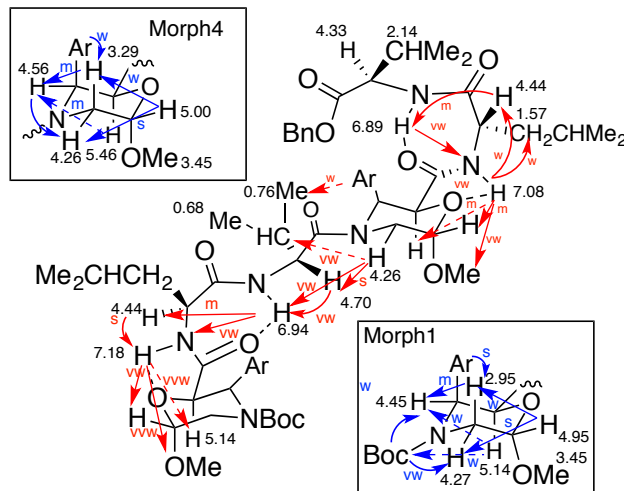
Table 6 ¹H, ¹³C NMR (CD₃CN, 750 μL 0.021 mM, 500 MHz,) and NOEs (600 ms) data for N-Boc(-)-Ar-β-Morph-L-Leu-L-Val(-)-Ar-β-Morph-L-Leu-L-Val-OBn (4)

AA	Atom	¹ H δ	Molteplcity J (Hz)	¹³ C δ	Noesy
ArMorf-1	CO			168.7	
	CH-2	5.14	d J 7.6	56.9	Boc(w), NH _{Leu2} (w), Ar(7.28,s), H-3 _{M1} (w)
	CH-3	4.45	d J 7.6	72.3	H-2 _{M1} (w), H _{ax-5M1} (m), H _o (s), OMe(w)
	CH ₂ -5	H _{eq} 4.27 H _{ax} 2.95	Overl. dd J 14.4, 8.0	41.8	----- H _{eq-5M1} (vs), H-3 _{M1} (m), H-6 _{M1} (w), Ar(7.28,m)
	CH-6	4.95	dd, J 8.0, 5.7	97.8	OMe (vs), NH _{Leu2} (w), H-5 _{M1} (4.27,s; 2.96,w)
	6-OMe	3.45	s	^a	H-6 _{M1} (s), H-3 _{M1} (w)
	MeOAr	^b	^b		OMe: H _m (s), H-3 _{M1} (s) H _m : OMe (s) H _o : Boc (w), H-3 _{M1} (m), H _{ax-5M1} (m), H _{2M1} (s), H _m (s)
	Boc	1.37		27.5, 80.1 154.7	H-2 _{M1} (w), H _{eq-5M1} (vw), Ar _o (w)
Leu-2	CO			171.5	
	CH	4.44	Overl.	51.5	
	CH	1.69	m	24.6	CH _{Leu} (m), Me _{Leu} (s)
	CH ₂	1.63	m	40.7	Me _{Leu} (s)
	Me	0.94 0.98	d J 6.2 d J 6.7	22.5	CHCH ₂ (s)CHN (m) CH _{2Leu} (s)
NH	7.17	d J 8.5		CH(w)CH ₂ (m)CHN _{Leu} (s), NH _{Val3} (vw) OMe(vvw), H-6 _{M1} (vw), H-2 _{M1} (vw)	
Val-3	CO			170.7	
	CH	4.70	dd J 8.5, 6.8	53.6	H _{eq-5M4} (s), Me ₂ CH(m), NH _{Val3} (vw)
	CH	1.95	m	30.8	Me _{Val} (m), H-5 _{eqM4} (vw), NHCH _{Val} (s)
	Me	0.76 0.68	d J 7.0 d J 6.5	18.7 16.6	Ar _o (w), Me ₂ CHCH(m), Me ₂ CHCHNH _{Val} (m)
	NH	6.94	d, J 8.5		CH ₂ (vw)CH(m)NH(vw) _{Leu2} , H _{eq-5M4} (vw) CHCHN _{Val2} (w), Me(0.69,m)
ArMorf-4	CO			168.3	
	CH-2	5.46	d J 8.9	55.9	NH _{Leu5} (vw), H _o (s), H-3 _{M4} (m)
	CH-3	4.56	d J 8.9	71.8	H-2 _{M4} (m), H _{ax-5M4} (m), OMe (3.45, w) Ar(7.28,s)
	CH ₂ -5	H _{eq} 4.26 H _{ax} 3.29	Overl. dd J 14.6, 8.1	44.0	----- H _{eq-5M4} (s), H-3 _{M4} (m), H _o (w), H-6 _{M4} (w)
	CH-6	5.00	dd, J 8.1, 6.0	97.9	OMe (vs), H-5 _{M4} (4.27s; 3.29w), NH _{Leu} (vw)
	OMe	3.45	s	^a	H-6 _{M4} (s), H-3 _{M4} (w)
	MeOAr	^b	^b	^b	OMe: H _m (s) H _m : OMe (s) H _o : H-3 _{M4} (s), H _{ax-5M4} (w), H-2 _{M4} (s), H _m (s) Me _{Val3} (w)
Leu-5	CO			171.8	
	CH	4.44	Overl.	51.5	
	CH	1.66	m	24.6	CH _{Leu} (m), Me _{Leu} (s)
	CH ₂	1.57	m	40.9	Me _{Leu} (s)
	Me	0.93 0.91	d J 6.5 d J 6.7	21.0	NCH(m), CHCH ₂ (s)

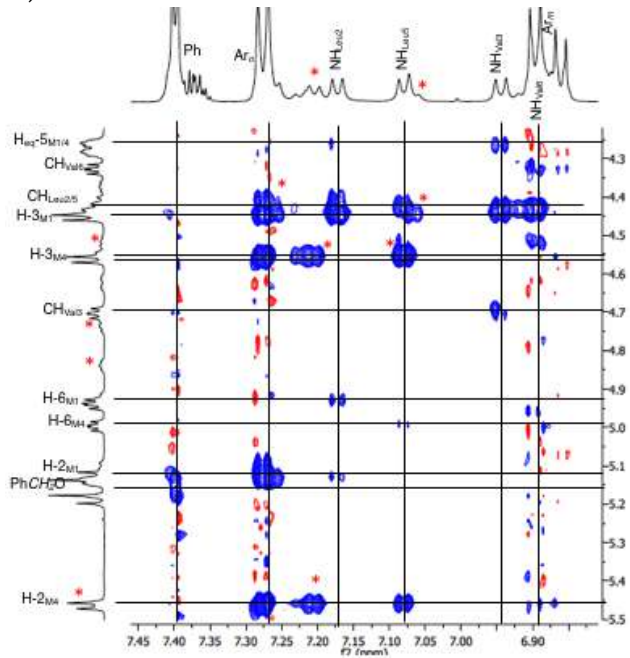
	NH	7.08	d J 8.3		<i>Me</i> (0.93w) <i>CHCH</i> ₂ (w), <i>CH</i> (m) _{Leu4} , NH _{Val} (vw) OMe(vw), H-6 _{M4} (m), H-2 _{M4} (m)
Val-6	CO			170.7	
	CH	4.33	dd J 8.3, 5.9	57.6	<i>Me</i> ₂ <i>CH</i> (s), NH _{Val} (w)
	CH	2.14	m	30.4	<i>Me</i> (s) <i>CHNH</i> (m) _{Val6}
	Me	0.89 0.87	d J 6.9	18.4	<i>Me</i> ₂ <i>CH</i> (s) <i>CH</i> (w) <i>NH</i> (w) _{Val6}
			d J 6.9	17.6	
	NH	6.89	Overl.		<i>Me</i> ₂ (s) <i>CH</i> (w) <i>CHN</i> (m) _{Leu5} , NH _{Leu5} (vw)
OBn	OCH ₂ 5.19, 5.12 Ph 7.42-7.34	AB system	66.5	Ph(m)	
		J 12.3 m	C _q 136.2, 128.8- 128.3	OCH ₂ (m)	

^aδ_{OMe}: 55.2, 55.1; ^bδ_{ArOMe}: 3.78 (OMe); AA'BB' system, 6.86 (113.6), 7.28 (128.7), J 8.7; 3.79, AA'BB' system, 6.90 (113.8), 7.28 (128.7), J 8.5; C_q(159.9, 131.4, 130.4).

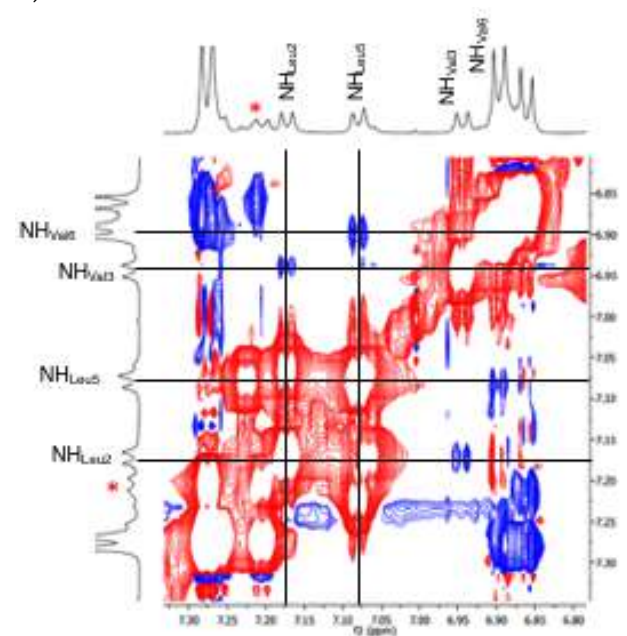
A)



A)

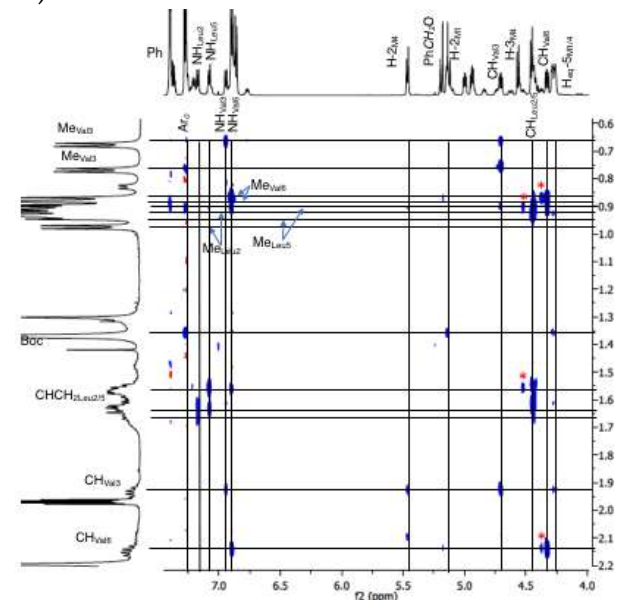


B)



C)

D)



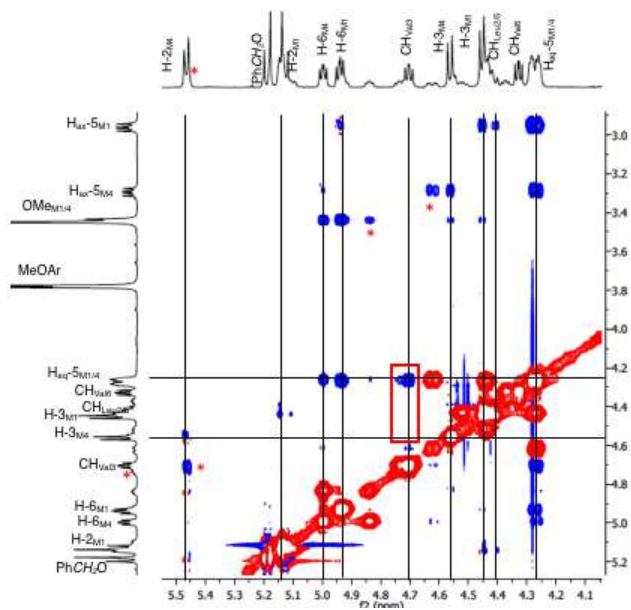


Figure 38 NOESY for hexapeptide (-)-4 (CD_3CN , 0.021 mM, 600 MHz, 500 ms): A) NOEs of morpholino ring protons (blu arrows) and between the different amino acids (red arrows); H-bonds (dotted lines). B) CH/Ar and CH/NH region. c) Zoom of NH-NH region. D) CH/CH region. High field/medium field CH region.

Synthesis of electrospun fibers using model peptide containing morpholino- β -amino AA

Introduction

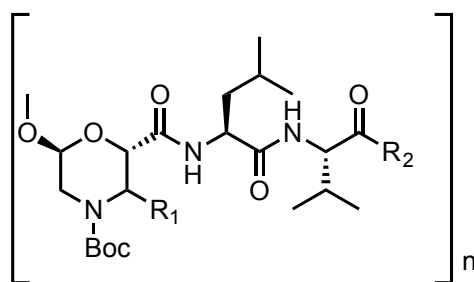
With recent developments in electrospinning, both synthetic and natural polymers can be produced as nanofibers with diameters ranging from tens to hundreds of nanometers. Synthetic polymers offer several advantages such as ease of availability, processing without difficulty and with reproducible results. Usually, synthetic polymers have excellent mechanical properties but, in some cases, they show lack of cell recognition sites and lack of cell affinity due to low hydrophilicity⁴³ For these reasons' peptides can be interesting tools to overcome some of these drawbacks, mostly in tissue engineering, where biodegradable scaffolds are required to direct tissue repair and regeneration, also providing structural support.⁴⁴

Currently, only few reports of the electrospinning of short peptide sequences have been published²². In particular, they are focused on short peptides containing aromatic amino acids, it being known that π - π interactions play a vital role in stabilizing the structures of the bulk crystal and of fibers. Diphenylalanine (Phe-Phe)⁴⁵ is very well studied in materials science due to its capability to self-assemble into various architectures.

More in general, it was found that peptides which naturally self-assemble into fibers or tubes are also prone to forming electrospun fibers. It is important emphasize that advances in peptide electrospun nanofibers have brought significant information on the forces involved in peptide assembly. Compared to "natural self-assembly", electrospinning is based on a "forced" assembly, because the trigger for the formation of the material is the application of an electrical field.^{46,47}

Aim of the work

Starting from these considerations, we decide to use the electrospinning technique to obtain nanomaterials on model peptides containing our Morph β -AA (Figure 39), indeed it's well known that peptides and foldamers having Morph β -A scaffold are able to assume well-defined conformation⁴² and self-assemble³⁵ in supramolecular architectures.⁴⁸



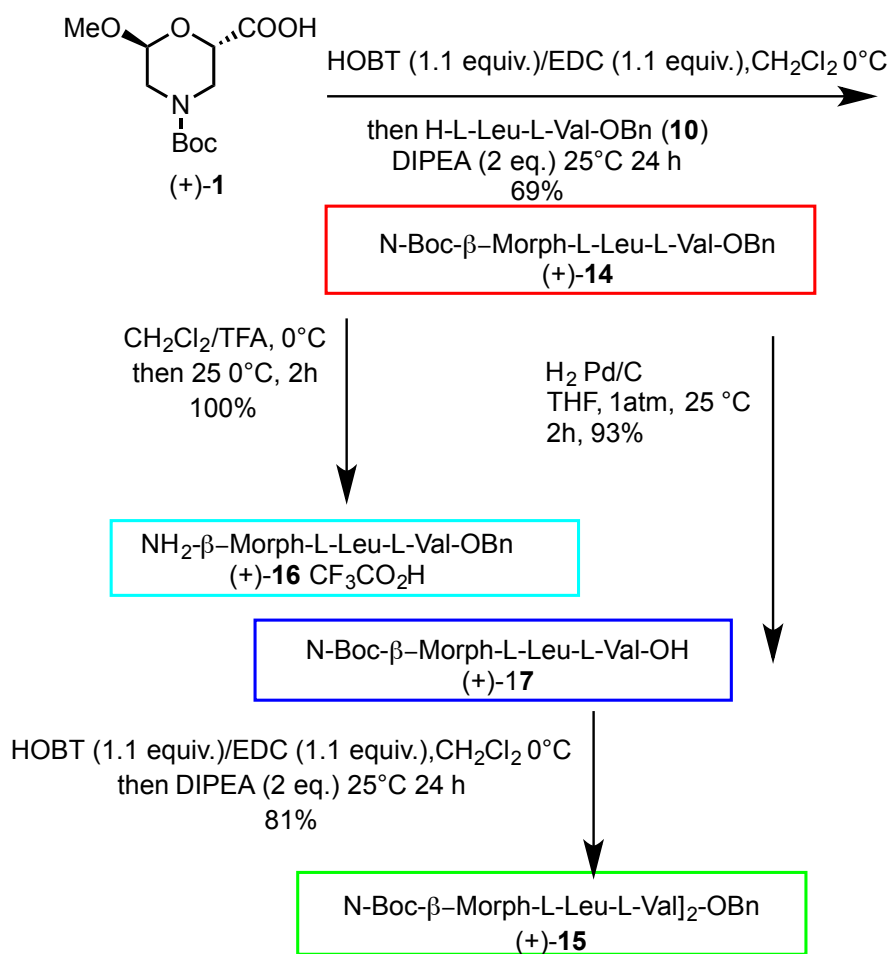
- 3** : $n = 1$; $R_1 = \text{pMeOPh}$; $R_2 = \text{OBn}$
4 : $n = 2$; $R_1 = \text{pMeOPh}$; $R_2 = \text{OBn}$
5 : $n = 2$; $R_1 = \text{H}$; $R_2 = \text{NH}_2$
13 : $n = 1$; $R_1 = \text{H}$; $R_2 = \text{NH}_2$
14 : $n = 1$; $R_1 = \text{H}$; $R_2 = \text{OBn}$
15 : $n = 2$; $R_1 = \text{H}$; $R_2 = \text{OBn}$

Figure 39 Model peptide containing β -Morpholino scaffold

First of all, we wanted to evaluate the influence of C-terminus (ester and amide) of the peptide and of the substitution pattern of the ring to stabilize electrospun fibers. Last but not least, the stability and toxicity of the new materials was investigated. Preliminary results are presented in the thesis, but further studies are ongoing to synthesize and characterize different ordered architectures with this new technique.

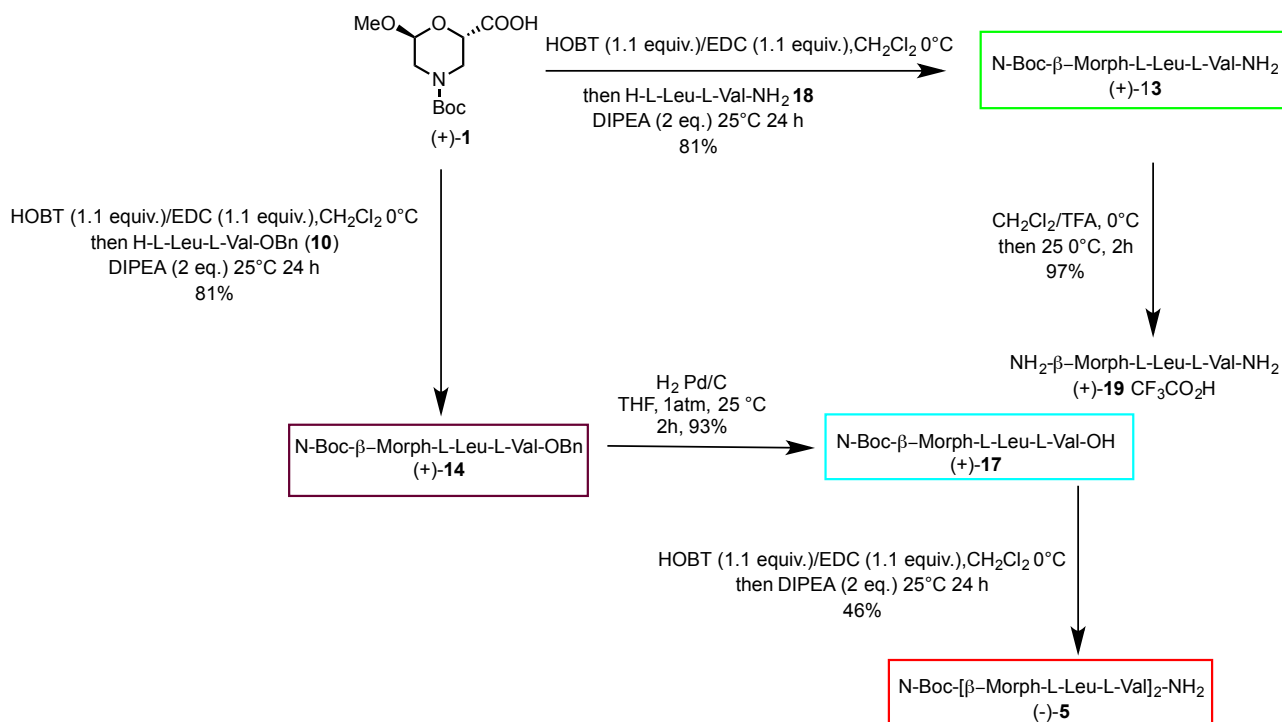
Foldamer synthesis

The tripeptide **14** and hexapeptide **15** was synthesized according a known procedure³⁵ using standard protocols (Scheme 5). The condensation reactions were performed by activation of the carboxylic acid (1 equiv.) with HOBT (1.1 equiv.) and EDC (1.1 equiv.) in CH_2Cl_2 (0 °C, 1 h). Free amine (1 equiv.) was then dissolved in CH_2Cl_2 and added to the reaction mixture together with DIPEA (2 equiv.; overnight stirring at 25 °C). By applying these conditions, compound (+)-**1** was coupled with dipeptide $\text{NH}_2\text{-L-Leu-L-Val-OBn}$ (**10**) leading to tripeptide *N*-Boc-(+)- β -Morph-*L*-Leu-*L*-Val-OBn [(+)-**14**; 69%]. Hexapeptide *N*-Boc-(+)- β -Morph-*L*-Leu-*L*-Val-(+)- β -Morph-*L*-Leu-*L*-Val-OBn [(+)-**15**, 50%] was obtained through Boc deprotection of compound (+)-**16** (95%) and coupling with *N*-Boc-(+)- β -Morph-*L*-Leu-*L*-Val-OH (+)-**17**. This last compound was obtained by carboxylic function of (+)-**17** deprotection under H_2 atmosphere (10% Pd/C, THF, 25 °C, 2 h, 93%).



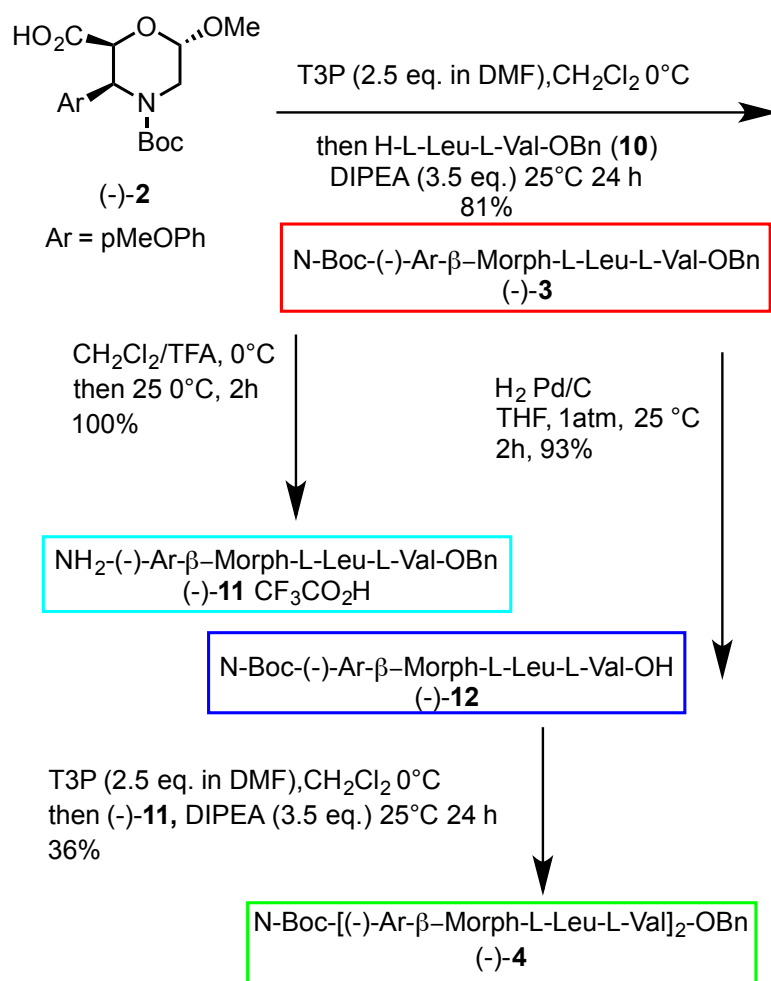
Scheme 5 General reaction scheme for tripeptide 14 and hexapeptide 15

The dipeptide NH₂-Leu-Val-NH₂ (**18**) was condensed with compound **1**, to obtain tripeptide N- Boc-Morph β -L-Leu-L-Val-NH₂ [(+)-**13**, 81%]. The condensation reaction was performed by activation of the carboxylic acid (1 equiv.) with HOBT (1.1 equiv.) and EDC (1.1 equiv.) in CH₂Cl₂ (0 °C, 1 h). After N-terminus deprotection, compound (+)-**19** was isolated in 97%. The N-Boc-Morph β -Leu-Val-OH (+)-**17** (93%) was synthesized by reduction of compound (+)-**14** under H₂ atmosphere, using Pd/C (10% loading, THF, 2h). The condensation between **17** and **19** gave N-Boc- Morph β -Leu-Val-Morph β -Leu-Val-NH₂ (-)-**5** in 46 % yield. Each peptide was purified by flash chromatography (Scheme 6)



Scheme 6 General reaction scheme for tripeptide **13** and hexapeptide **5**

As described above T3P (in DMF solution) was chosen as the most efficient coupling agent for the tripeptide foldamer's synthesis (-)-**3** (81% yield) as reported in Scheme 7. It was selectively deprotected (TFA, CH₂Cl₂, 25 °C, 2 h), affording (+)-**11** (quantitative yield). Debenzylation reaction of **3** (H₂, Pd/C, THF, 1 atm., 25 °C, 2 h) provided (-)-**12** (93%). For the final coupling of **11** with **12** we used, T3P was selected resulting the best coupling agent, (-)-**4** (36%)⁴².



Scheme 7 General reaction scheme for tripeptide 3 and hexapeptide 4

Electrospinning studies

Electrospinning studies were performed in collaboration with Prof.ssa Ida Genta (Department of Pharmaceutical Science, University of Pavia). For the manufacture of the nanofibers, samples of **3**, **4**, **5**, **13**, **14** and **15** were dissolved in HFIP to obtain the final concentration of 30% w/w. Solutions were loaded into 1mL B Braun Injekt syringes and each one was inserted in the appropriate housing connected to the pump. The solution is extruded through a 20 G needle (Nordson EFD, internal diameter of 0.61 mm) and the fibers were deposited on square glass plates (22 x 22 mm, 0,13-0,17 mm of thickness) placed on the flat collector (Figure 40).

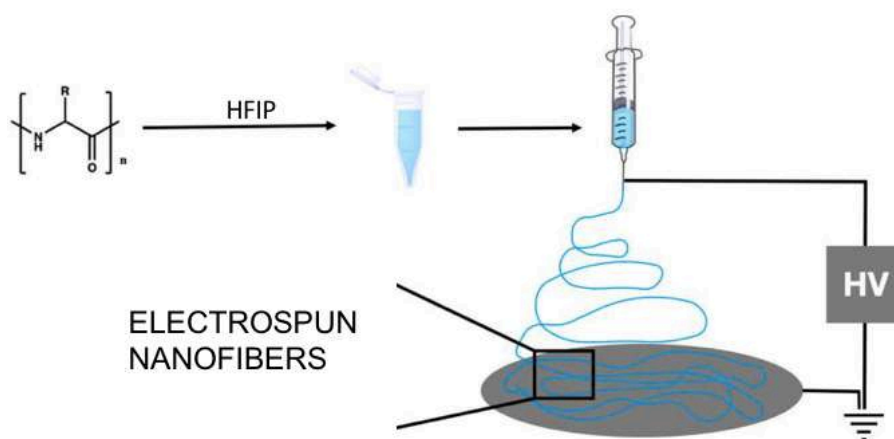


Figure 40 Overview of electrospinning technique

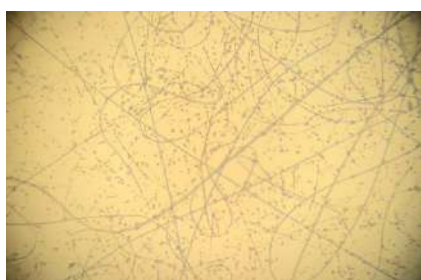
The electrospinning parameters were:

- target distance collector (TDC) of 15 cm;
- applied voltage of 25 kV for compound **13** and 28 kV for compound **5**;
- flow rate of the solution was set at 0.2 mL/h for compound **13** and at 0.8 ml/h for compound **5**;

The experiments were performed under controlled environmental conditions of temperature and humidity for a set time of 3 minutes.

In Figure 41 we can clearly see the morphology of the fibers obtained from solution of compound **13** (Figure 41a) and **5** (Figure 41b) after 1 minute of electrospinning.

A)



B)



Figure 41 Fibers of compound **13** and **5** after 1 minute of electrospinning

Electrospinning studies on compounds **3,4, 14** and **15** did not give rise to fibers.

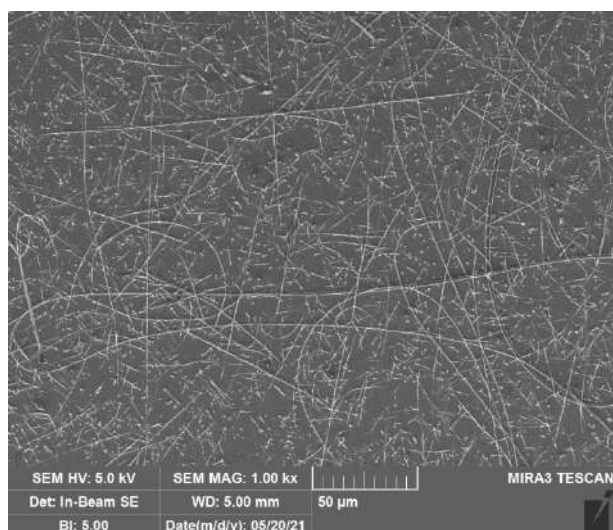
After obtaining the electrospun fibers of compound **5** and **13**, they were analyzed in inverted optical microscopy Leica DM IL LED (Leica Microsystems, Milan, Italy) using 20X of magnification in order to evaluate the fibers morphology. Images were acquired for each sample and subsequently processed by ImageJ software to evaluate the diameters of the

fibers. Fibers obtained with **5** and **13** showed average diameters of $1,10 \pm 1,203 \mu\text{m}$ and $0,73 \pm 0,12 \mu\text{m}$ respectively and for both samples, a mixed morphology of fibers and beads is observed.

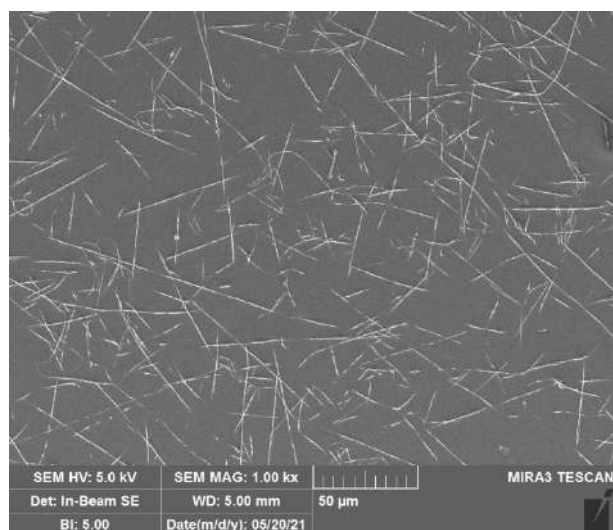
SEM Analysis

The first analyses of electrospun fibers are performed using Scanning Electron Microscopy (SEM). Fibers of compound **5** (Figure 42b) are much more fragmented and aren't curved like those of compound **13** (Figure 42a). Moreover, fibers of compound **13** (Figure 42a) have higher density and are more frequently longer than fibers of compound **5** (Figure 42b).

A)



B)



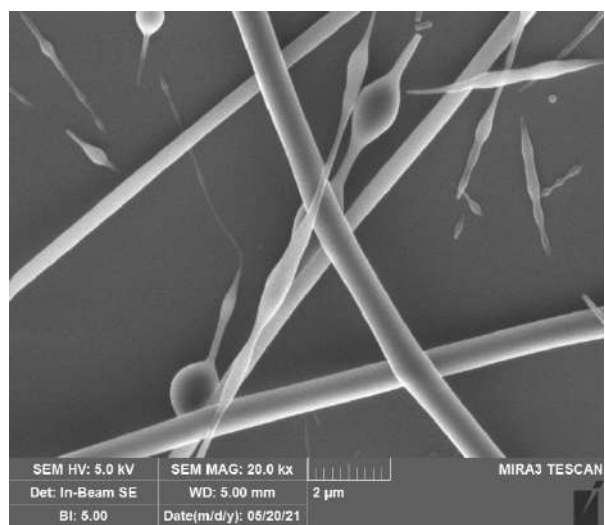
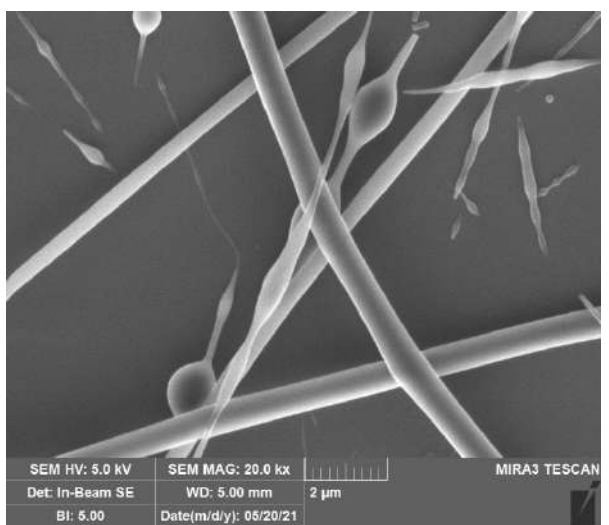
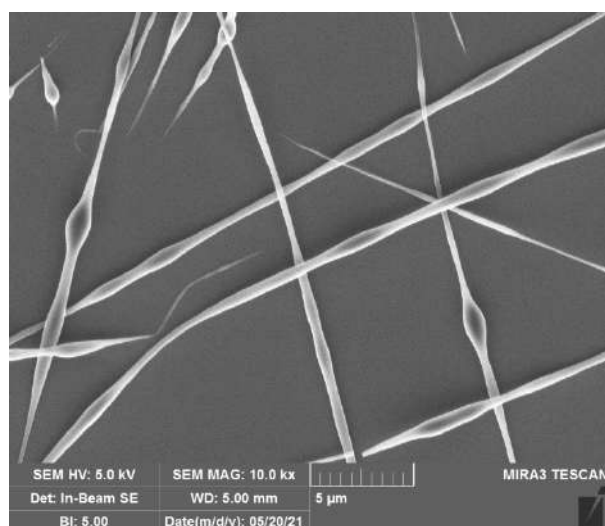
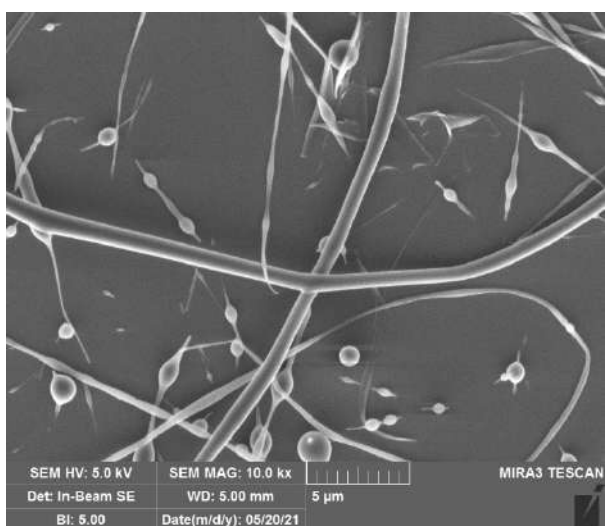
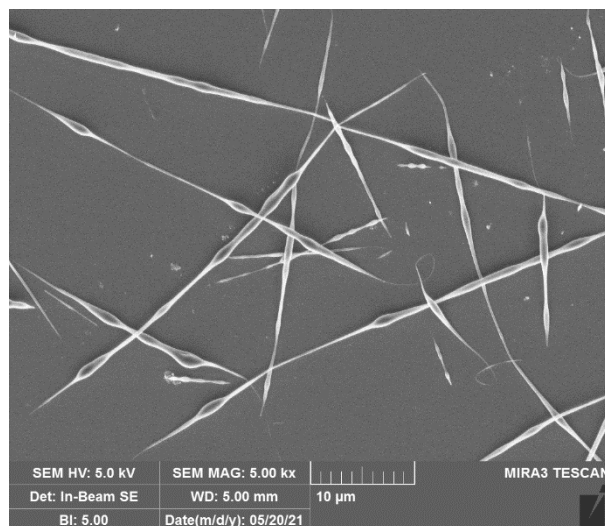
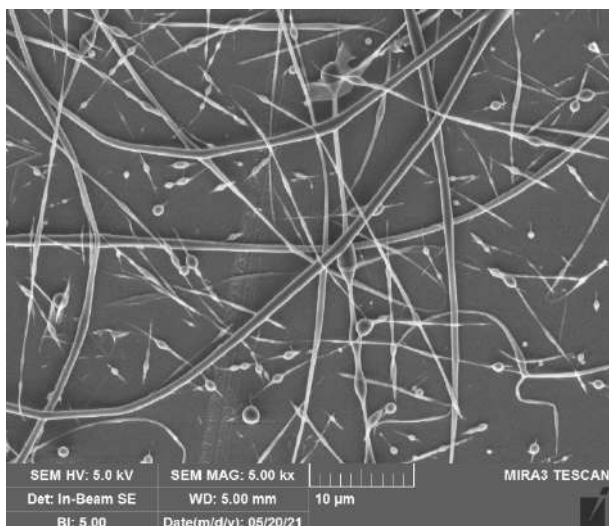


Figure 42 A) SEM images, fibers of compound 13; B) SEM images, fibers of compound 5

Biological studies

Biological tests for compound **5** and **13** were performed using fibroblasts of adult human dermis as a model, derived from primary culture (International PBI, Milan, Italy). Cells were cultivated in DMEM (Dulbecco's Modified Eagle Medium) containing 20% v/v of FBS (Fetal Bovine Serum) and 1% v/v of mixture of antibiotics (100 $\mu\text{g mL}^{-1}$ of penicillin, 100 $\mu\text{g mL}^{-1}$ of streptomycin) at 37°C, 5% CO₂. The cytotoxicity study was performed on the incubation medium at pH 7 and 7.2, collected every 1, 2, 4 and 6 hours. 1x10⁴ cells were seeded on a 96-well plate, diluted with 100 μL of complete culture medium and then incubated at 37°C and 5% of CO₂. Cells exposed with 200 μL of fresh medium were used as positive control (ctrl) incubated at 37°C and 5% of CO₂. After 1, 2, 4 and 6 hours, culture medium was aspirated and then MTT [3-(4,5-dimethylthiazol-2-yl)-2,5-diphenyltetrazolium bromide] assay was performed. Results for compound **5** and **13** (Figure 43) indicate a slightest reduction of the cell vitality compared to control for degradation medium at pH 7 after 1 and 2 hours of incubation; however, cell vitality remains above 62%. About degradation medium at pH 7.2, at every timing no significant effect was observed.

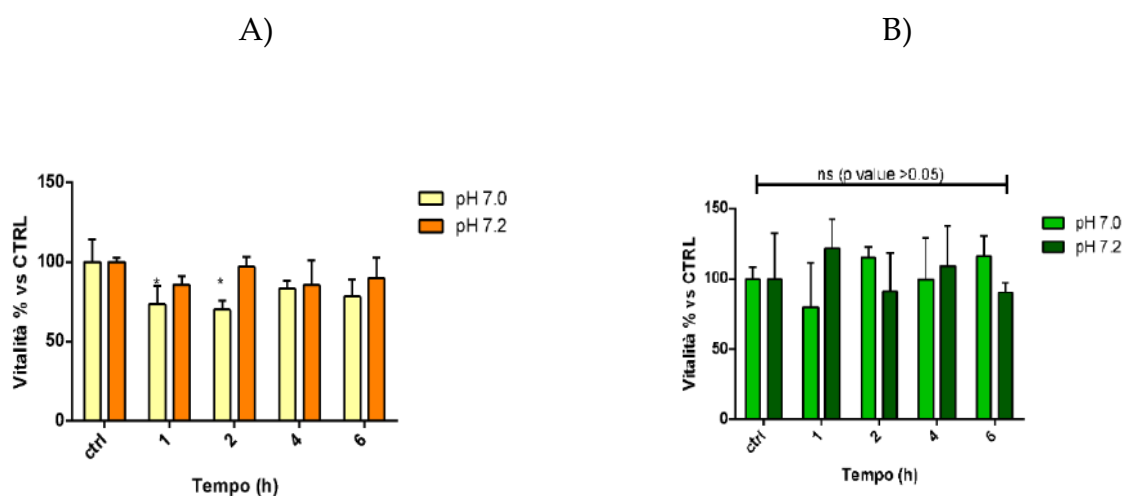


Figure 43 A) MTT test for compounds 13 and B) MTT test for compounds 5

Conclusions

In conclusion, starting from our previous knowledge electrospinning studies were performed. We were able to obtain fibers using foldamers **5** and **13**. These two peptides don't have the aryl group in their structures, but they are the only ones able to spin. Even if generally this ability is characteristic of structures rich in aryl groups, we can say that in our case the structure stabilization is the most important goal to effectively obtain nanofibers

with electrospinning technique. The biological tests revealed that compounds **5** and **13** aren't toxic to the cell vitality. These data suggest a potential use of those nanofibers in the area of pharmaceutical from tissue and bio surface engineering to drug delivery systems, from components for biosensing to bioanalytical devices.

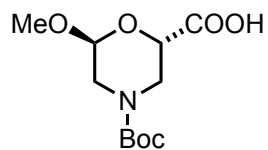
Since one of the recent topics in our research group is the preparation of electrospun fibers using peptides and peptidomimetics, we wrote a review published in *Acta Biomaterialia*²¹.

Experimental part

General informations

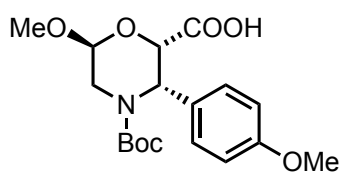
Melting points were determined with a Stuart Scientific melting point apparatus in open capillary tubes and are uncorrected. Chemicals were purchased from Sigma Aldrich and were used without further purification. HPLC analysis were performed on Jasco PU-980 pump equipped with a UV-vis detector Jasco UV-975 (wavelength: 220 nm) and on a Kromasil 5-AmyCoat column (4.6 mm i.d. × 250 mm, 5 μm, AkzoNobel). Mass spectra were recorded on an LCQESI MS were recorded on a LCQ Advantage spectrometer from Thermo Finningan and a LCQ Fleet spectrometer from Thermo Scientific. The NMR spectroscopic experiments were carried out either on a Varian MERCURY 200 MHz (200 and 50 MHz for ¹H and ¹³C, respectively), Varian MERCURY 200 MHz (300 and 75 MHz for ¹H and ¹³C, respectively), or Bruker Avance I 500 MHz spectrometers (500 and 125 MHz for ¹H and ¹³C, respectively). Optical rotations were measured on a Perkin-Elmer 343 polarimeter at 20°C (concentration in g/100 mL). Chemical shifts δ are given in ppm relative to the CHCl₃ internal standard, and the coupling constants J are reported in Hertz (Hz). The instrument Nanon-01A (MEEC Instruments, Ltd., Ogori-shi, Fukuoka, Japan) was used for the electrospinning. The synthesis of dipeptides NH₂-Leu-Val-CONH₂ (**18**), NH₂-Leu-Val-OBn (**10**)⁴⁹ are reported in literature.

Synthesis of (2*S*,6*S*)-4-(*tert*-butoxycarbonyl)-6-methoxymorpholine-2-carboxylic acid (+)-1



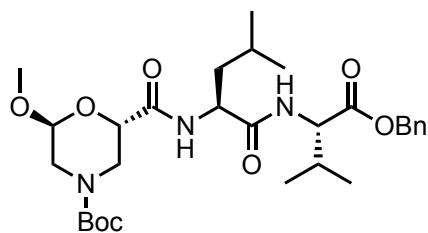
The synthesis of compound **1** is reported in literature.³⁵

Synthesis of (2*S*,3*S*,6*S*)-4-(*tert*-butoxycarbonyl)-6-methoxy-3-(4-methoxyphenyl)morpholine-2-carboxylic acid (-)-2



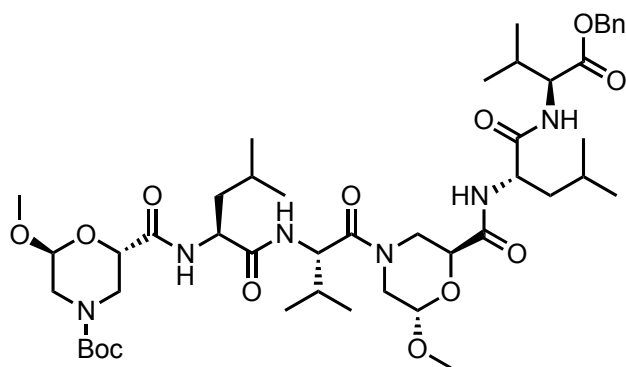
The synthesis of compound **2** is reported in literature⁴²

Synthesis of N-Boc-(+)- β -Morph-(L)-Leu-(L)-Val-OBn-(+)-14



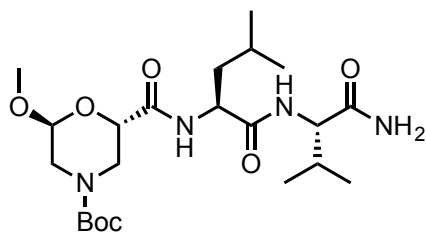
The synthesis of compound **14** is reported in literature³⁵

Synthesis of N-Boc-(+)- β -Morph-(L)-Leu-(L)-Val-(+)- β -Morph-(L)-Leu-L-Val-OBn-(+)-15



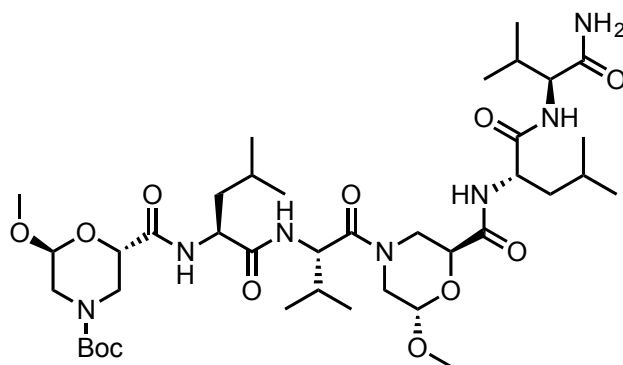
The synthesis of compound **15** is reported in literature³⁵

Synthesis of N-Boc-(+)- β -Morph-(L)-Leu-(L)-Val-NH₂-(+)-13



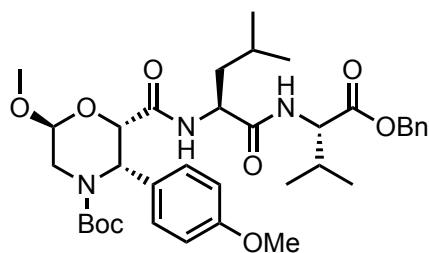
The synthesis of compound **13** is reported in literature³⁵

Synthesis of N-Boc-(+)- β -Morph-(L)-Leu-(L)-Val-(+)- β -Morph-(L)-Leu-(L)-Val-NH₂ -(-)-5



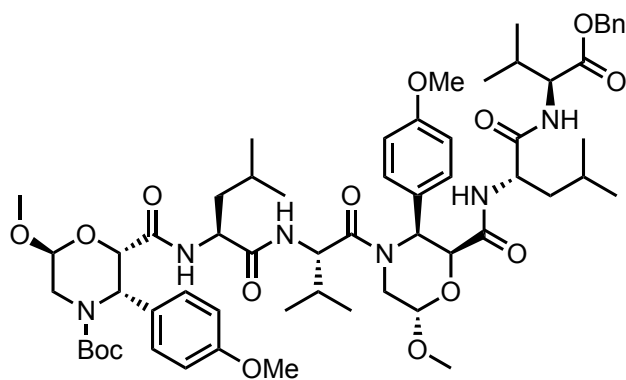
The synthesis of compound **5** is reported in literature³⁵

Synthesis of N-Boc-(-)-3-(4-Methoxyphenyl)- β -Morph-(L)-Leu-(L)-Val-OBn-(-)-3



The synthesis of compound **3** is reported in literature⁴²

Synthesis of N-Boc-(-)-3-Ar- β -Morph-(L)-Leu-(L)-Val-(-)-3-Ar- β -Morph-(L)-Leu-(L)-Val-OBn-(-)-**4**



The synthesis of compound **4** is reported in literature⁴²

Nucleobase morpholino β amino acids as molecular chimeras for the preparation of photoluminescent materials from ribonucleosides

Introduction

In the last ten years, bioinspired smart materials represent a tremendously growing research field and the obtainment of new building blocks is at the molecular basis of this technology progress. Nanomaterials are thus expected having a strong impact on societal change owing to their wide applications ranging from clean energy to biomedicine.^{50,51,52}

Natural macromolecules (proteins and nucleic acids) result to be able to create a wide range of nanomaterials. Being amino acids and nucleotides at the molecular level of this high complexity, in the recent years many studies have been focused on the development of bioinspired building blocks that self-assemble into preferred architectures.^{53,54,55,56,57,58,59}

In literature it is well known that the dipeptide diphenylalanine can build up different morphologies depending on the environment conditions and functionalization (Figure 44).^{60,61} The driving force of self-assembly is the π - π stacking interactions between the phenyl groups that are then enforced by hydrogen bonds stabilizing the final architectures.

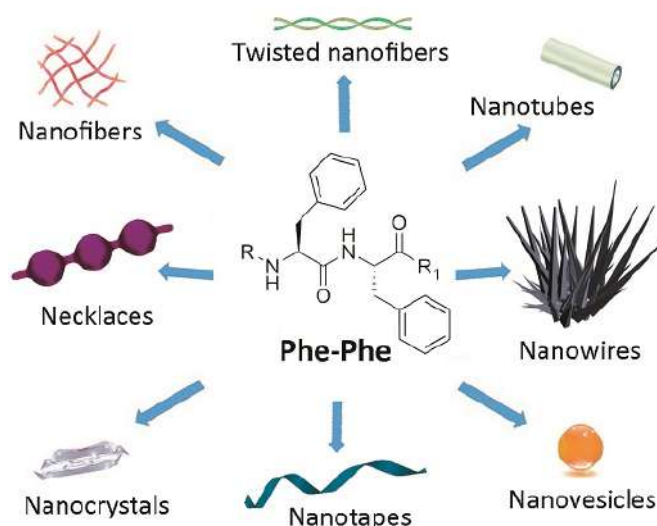


Figure 44 Phe-Phe different nanomaterials

Moreover, amino acids (AAs) and peptides are normally able to form supramolecular structures thanks to H-bonding, van der Waals force and π - π interactions.^{62,63} On the other

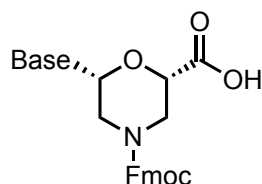
hand, nucleotide-based architectures are formed due to Watson–Crick interactions allowing specific molecular recognition and base-pairing complementarity.

Nucleopeptides⁶⁴ containing both nucleobases and amino acids, are still underexploited in the development of functional materials. Indeed, only few examples are reported in the literature. In these cases, the environment polarity drives the self-assembly of helical Aib based nucleo-foldamers⁶⁵ and diphenylalanine nucleopeptides hydrogels.⁶⁶ In both examples, the nucleobases are linked to the C- and/or N-terminus of the peptides.

Aim of the work

Starting from the information's written above, our idea was to combine peptides and nucleic acids for the design of novel self-organized materials with enhanced properties and features.

Specifically, a new class of β amino acids **1** (Figure 45) containing a morpholino ring and a nucleobase were our new starting materials. Nucleo amino acids **1** were then used for the preparation of ultra-short peptides containing the dipeptide Phe-Phe in order to evaluate self-aggregation propensity. Last but not least, photoluminescence (PL) studies have been performed on the synthesized ultra-short peptide aggregates.



Base **1a** = Thymine
1b = Adenine

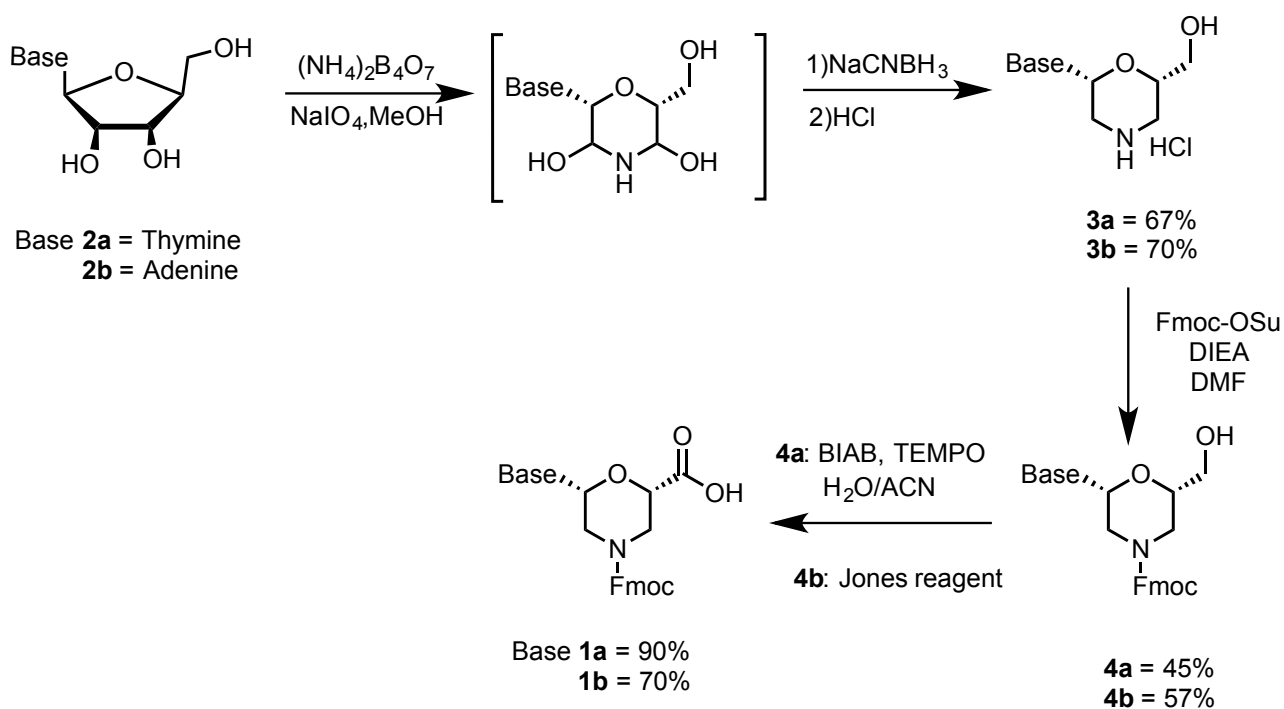
Figure 45 β -Morph-nucleobase amino acid scaffold

Scaffold synthesis

Nucleo amino acids **1** were prepared in enantiopure form taking advantage of alcohol intermediates **3** which synthesis was reported in 1993 by Summerton in a patent. Starting from nucleosides **2a** and **2b**, a “one-pot” oxidative ring-opening of the ribose sugar followed by a reductive amination leads the morpholino ring (Scheme 8). Several modifications of this procedure have been reported in the last years.^{67,68,69,70} Here, we started from unprotected ribonucleosides **2a** and **2b**, using the Summerton's procedure with different work up conditions. Briefly, the sugar ring is converted into the corresponding morpholino

through a “one-pot” oxidation/amination reaction using a mixture of NaIO₄ and (NH₄)₂B₄O₇ in MeOH. The intermediates were directly treated with NaCNBH₃ in MeOH affording compounds **3**. The reaction was quenched with HCl and the products **3a** and **3b** were isolated as hydrochloride salts by crystallization from polar solvents (**3a**: MeOH, 67%; **3b**: ACN, 70%).

Firstly, the protection of the endocyclic nitrogen was required to avoid side reactions on the free amine during the oxidation reaction. The Fmoc protecting group was selected for the synthesis of compound **1a,b** and then for the preparation of nucleopeptide materials. Fmoc group is indeed known to favor self-assembly through π - π stacking.⁷¹ The reaction was carried out directly on the crude **3a,b** obtained in the previous reaction (Scheme 8) simply adding Fmoc-OSu and DIEA in DMF affording **4a,b** in good yields.



Scheme 8 General scheme for synthesis of nucleobase **1a** and **1b**

We investigated the oxidation reaction of the hydroxyl function to the corresponding carboxylic one. Several oxidants were then tested on the compounds **4a** and **4b** (Table 7).

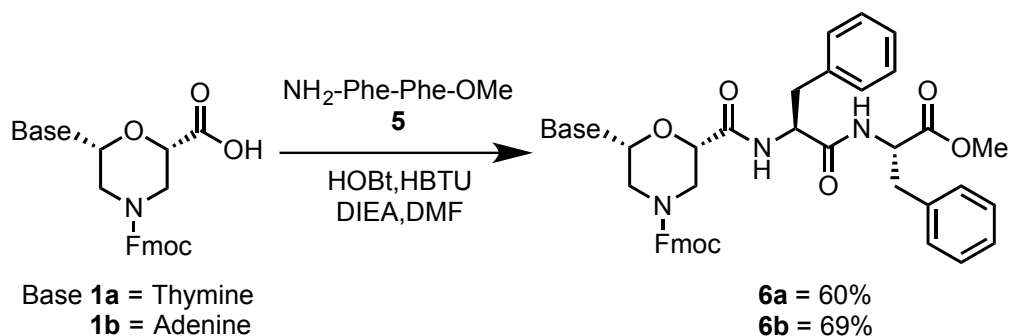
Table 7 Overview of different oxidant reagents used to obtain acids 1

Entry	Compound	Oxidants	Yield
1	4a	10% NaOCl, TEMPO, KBr, TBABr	Traces
2	4a	BIAB, TEMPO	90%
3	4a	CrO ₃	Not reproducible
4	4a	RuO ₄	-
5	4a	KMnO ₄	20%
6	4b	BIAB, TEMPO	15% ^a
7	4b	KMnO ₄	-
8	4b	CrO ₃	70%

For compound **4a** the combination BIAB/TEMPO³⁵ was found the most effective, obtaining compound **1a** in 90% yield, while acid **1b** was thus obtained by Jones oxidation with CrO₃ in 70%.

Peptides synthesis

Thymine and adenine nucleoside amino acids **1a,b** were used for the preparation of ultra-short nucleopeptides containing diphenylalanine dipeptide (Phe-Phe). HOBt/HBTU was chosen as best condensing agents for the reaction of **1** with the dipeptide H₂N-Phe-Phe-OMe leading to compounds **6a,b** (Scheme 9).



Scheme 9 Tetrapeptides **6a** and **6b**

Self-assembly studies

The self-assembly behavior of both compounds **6a,b** was studied using the solvent displacement method where a 'non-solvent' is added to the solution of peptide to form a colloidal suspension (Figure 46). A solution of compound **6a,b** in hexafluoroisopropanol (HFIP, 100 mg/mL) was diluted with different solvents (distilled water, EtOH, 50% EtOH, MeOH, isopropanol, chloroform) to a final concentration of 2 mg/mL. The formation of sub-micrometric aggregates was observed by drop-casting on silicon wafers for recording SEM after 30 min and after 24 h.

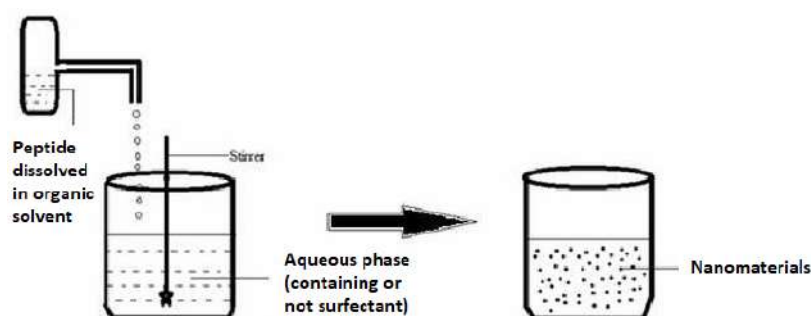


Figure 46 Solvent displacement method analysis

In water, both compounds **6a** and **6b** exhibited spherical aggregates (Figure 47) whose size ranged from a few tens of nanometers to less than a micron. In chloroform, isopropanol and HFIP no aggregates were observed.

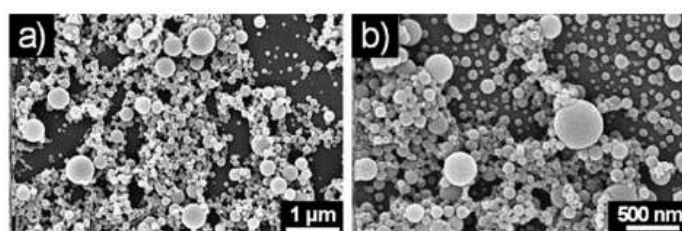


Figure 47 SEM micrographs of the self-assembled structures formed by **6a** (a) and **6b** (b) in pure water

In EtOH and MeOH, **6a** and **6b** had a different behavior. Compound **6a** exhibited indeed spherical macroaggregates in 50% EtOH, while **6b** self-aggregates in ordered spherical structures both in EtOH and MeOH (Figure 48 and Figure 54 S.I.).

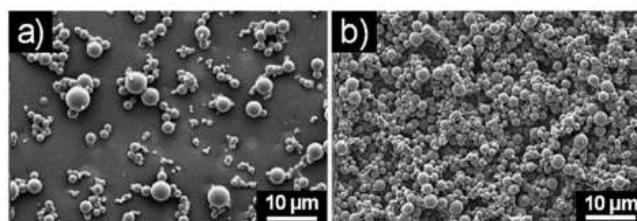


Figure 48 SEM micrographs of the self-assembled structures formed by **6b** (a) in EtOH and (b) MeOH

Considering the promising results obtained in HFIP/ H₂O, we performed DLS analysis on **6a** and **6b** at different HFIP/H₂O ratios. Our results suggested that the quantity of water is fundamental for determining the formation of aggregates, their size and their distribution. At the lowest water content (HFIP/H₂O, 70:30) the formation of nanocolloidal clusters of 5-6 nm was observed together with larger agglomerates (Figure 49).

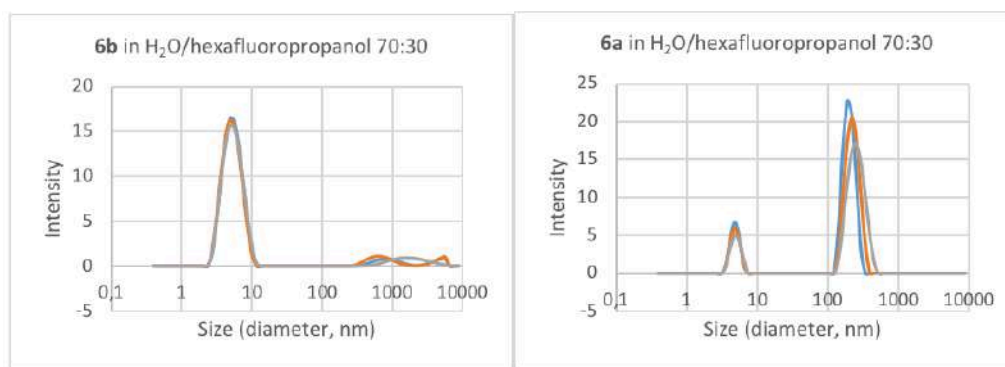


Figure 49 DLs analysis of the self-assembled structures formed by **6a** and **6b**

An enhancement in the size of the aggregates was obtained increasing the water amount, although the distribution was not optimal. When only 2% of HFIP was used, **6a** and **6b** suspensions showed only one sharp peak centered at 200 nm, indicating the formation of a monodispersed colloidal suspension (Figure 50).

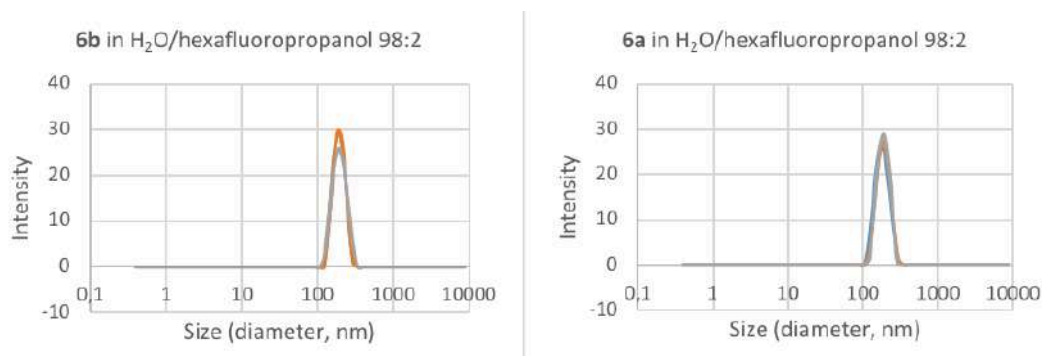


Figure 50 DLS analysis of the self-assembled structures formed by **6a** and **6b** H₂O/HFIP 98:2

In the case of **6a**, an increase of the size of the agglomerates was observed by measurements repeated after 24 h and 48 h. A negative ζ -potential was detected for both **6a** and **6b**, suggesting a protonated state of the nucleobases with a consequent formation of a tight ion pair due to the presence of acidic HFIP (Table 8).

Table 8 Hydrodynamic diameter by DLS and ζ -potential of **6a** and **6b** aggregates

H ₂ O/HFIP	6a	6b
98:2 t=0	190 ± 60 nm	190 ± 91 nm
98:2 t=24h	342 ± 120 nm	220 ± 100 nm
98:2 t=48h	342 ± 150 nm	220 ± 100 nm
ζ -potential	-47 mV	-16 mV

The stability of **6a** and **6b** water aggregates was examined at different pH and upon heating at 120°C. Both aggregates were not stable at high temperature and at acidic pH. At basic pH (pH=10), a change of the morphology was observed (Figure 51).

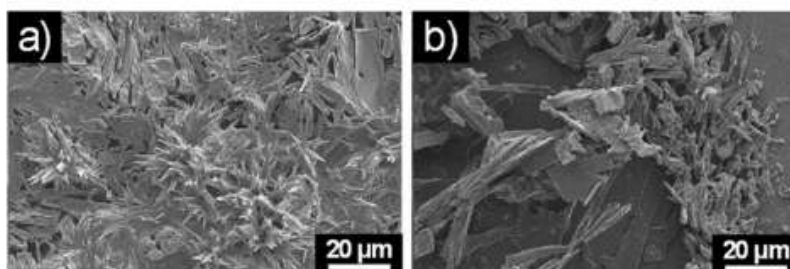


Figure 51 SEM micrographs of the self-assembled structures formed at basic pH by (a) **6a** and (b) **6b**

To understand the molecular conformation of the self-assembled structure of **6a** and **6b**, FT-IR experiments were performed (Figure 52). In both cases, the minima at 1688 cm⁻¹ in the

amide-I region and 1540 cm^{-1} in the amide-II region suggested the presence of β -sheet conformations. We thus hypothesized that the closer of sheets along the two axes results in the formation of the spherical structure³⁴. The other minima in the spectrum (1652 cm^{-1} for **6a** and 1660 cm^{-1} for **6b**) are ascribable to adenine (A) and thymine (T) residues, respectively (Figure 55 S.I.).

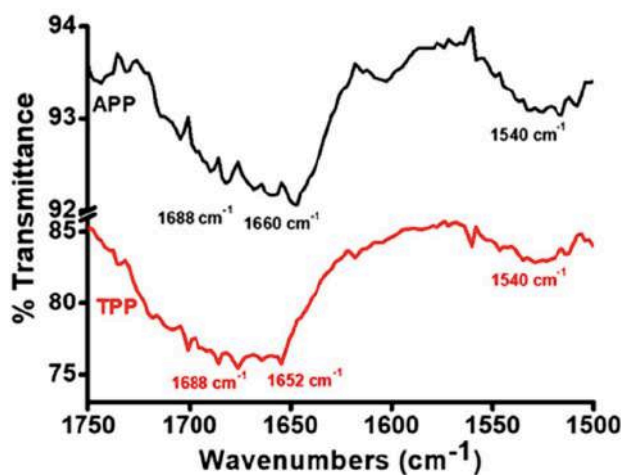


Figure 52 FT-IR spectra of the amide I and amide II regions of **6a** (red) and **6b** (black)

Photophysical characterizations

Photophysical characterizations were performed on diluted solutions ($1\text{--}2\times 10^{-5}\text{ M}$) of the tripeptides **6a** and **6b** (self-assembled materials in water, obtained from HFIP/ H_2O (98:2 v/v) at the concentration of $5\times 10^{-5}\text{ M}$) (Figure 53).

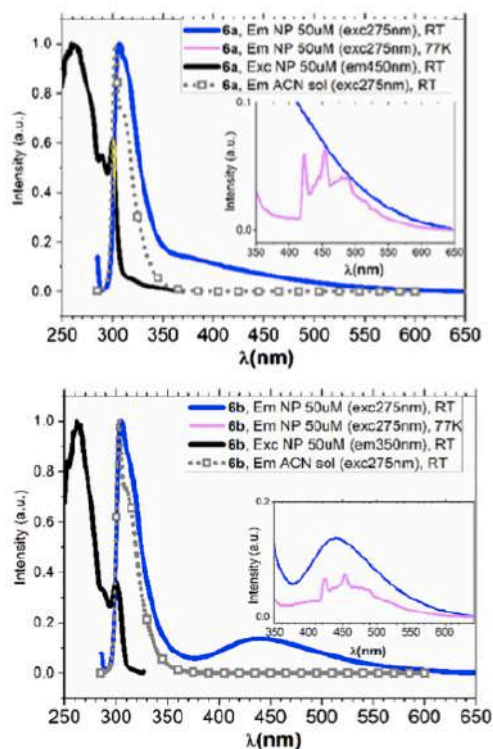


Figure 53 Emission and excitation spectra of **6a** (top panel) and **6b** (bottom panel) as diluted solution in ACN and as self-assembled NP at both RT and 77 K glass matrix

Both compound aggregates of **6a,b** showed similar characteristics. In particular while the solutions showed only an emission peak around 300 nm, the colloidal suspension showed not only the classical band around 300 nm, but also a new emission band between 400-600 nm with maximum at 440 nm. The peak could be attributed to the fluorescence emission linked to the restricted intramolecular rotation of the backbone as previously reported in the literature for the Phe-Phe system.

Upon cooling the colloidal suspensions of compounds **6a,b** at 77 K (pink curve in Figure 53) a new emission appeared in the visible range between 420 and 550 nm. The band is characterized by structurally resolved features. These emissions had a long radiative lifetime of 4.2 and 4.1s for **6a** and **6b**, respectively, thus indicating a process originated from a triplet state. To understand the origin of the phosphorescence emission, PL studies were performed on the isolated building blocks to generate compounds **6** (Figure 61 and 62 S.I.) [i.e. H₂N-Phe-Phe-OMe **5** (Figure 63 S.I.) and the Fmoc protected **1** (Figure 64-66 S.I.)]. As shown in Figure 53, a structured emission above 400 nm is only observed in nucleobases containing compounds **1**, thus allowing the attribution of the phosphorescence observed in the tripeptide systems to the adenine or thymine unit (Table 10 S.I.)⁷².

In conclusion, a new class of β amino acids containing a morpholino ring and a nucleobase has been developed starting from ribonucleosides. Their synthesis takes advantage from a

“one-pot” oxidative ribose ring-opening and reductive amination, followed by the oxidation of the primary alcohol of the sugar. The so obtained β amino acids was used for the functionalization of Phe-Phe dipeptide leading to sub-micrometric aggregates possessing photoluminescent features of both fluorescence and phosphorescence type. It was proved that the here presented tripeptides possess the photoluminescent properties given by the β -AA and the self-assembly behavior induced by the presence of Phe-Phe. They hence represent promising tools for the development of bioinspired functional materials with applications not only in the biotechnology field but also in non-biological optoelectronic ones.

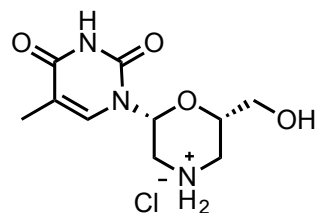
These results have been published in *Scientific Report*⁵⁵

Experimental part

General information

Chemicals were purchased from Sigma Aldrich and were used without further purification. HPLC analysis were performed on Jasco PU-980 pump equipped with a UV-vis detector Jasco UV-975 (wavelength: 220 nm) and on a Kromasil 5-AmyCoat column (4.6 mm i.d. × 250 mm, 5 μ m, AkzoNobel). Mass spectra were recorded on an LCQESI MS were recorded on a LCQ Advantage spectrometer from Thermo Finningan and a LCQ Fleet spectrometer from Thermo Scientific. The NMR spectroscopic experiments were carried out either on Varian MERCURY 300 MHz (300 and 75 MHz for ^1H and ^{13}C , respectively), or Bruker Avance I 500 MHz spectrometers (500 and 125 MHz for ^1H and ^{13}C , respectively). Chemical shifts δ are given in ppm relative to the CHCl_3 internal standard, and the coupling constants J are reported in Hertz (Hz).

Synthesis of (2S,6R)-2-(hydroxymethyl)-6-(5-methyl-2,4-dioxo-3,4 dihydropyrimidin-1(2H)-yl)morpholin-4-ium chloride (3a)



In a round bottom flask, thymidine (1 g, 4.1 mmol) was dissolved in MeOH (70 mL). NaIO₄ (0.9 g, 4.14 mmol) and (NH₄)₂B₄O₇ (0.9 g, 4.7 mmol) were added. After 2h the mixture was filtered, the white solid was washed abundantly with methanol (200 mL). The liquid phase was treated with NaCNBH₃ (1.3 eq., 0.3 g, 5.3 mmol). After 20 min, others 0.4 eq. of NaCNBH₃ (0.1g, 1.6 mmol) were added to the mixture that was left reacting for 15 min. Subsequently, a quenching with HCl was done, until the pH 3. Finally, the solution was concentrated under reduced pressure. Pure compound **3a** (yield: 60%, 0.68 g, 2.46 mmol) was obtained after crystallization with MeOH.

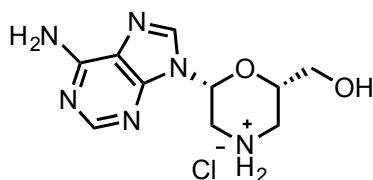
¹H NMR (300 MHz, D₂O) δ 7.54 (s, 1H), 5.93 (dd, *J* = 4.34, 2.29 Hz, 1H), 4.15-4.10 (m, 1H), 3.74-3.62 (m, 2H), 3.47-3.22 (m, 2H), 3.20-3.00 (m, 2H), 1.8 (s, 3H) ppm;

¹³C NMR (75 MHz, D₂O) δ 166.2, 150.9, 136.7, 112.1, 77.3, 74.4, 61.1, 43.7, 42.5, 11.5 ppm;

MS (ESI): calcd for C₁₀H₁₅N₃O₄ 241.11, found [M + H]⁺ 242.20.

Elemental Analysis: calcd for C₁₀H₁₆ClN₃O₄ C, 43.25; H, 5.81; N, 15.13, found C, 43.15; H, 5.93; N, 15.03

Synthesis of (2R,6S)-2-(6-amino-9H-purin-9-yl)-6-(hydroxymethyl)morpholin-4-ium chloride (**3b**)



In a round bottom flask, adenosine (1 g, 3.7 mmol) was dissolved in MeOH (70 mL). NaIO₄ (0.8 g, 3.74 mmol) and (NH₄)₂B₄O₇ (1.3 g, 4.3 mmol) were added. After 2h the mixture was filtered, the white solid was washed abundantly with methanol (200 mL). The liquid phase was treated with NaCNBH₃ (1.3 eq., 0.3 g, 4.7 mmol). After 20 min, others 0.4 eq. of NaCNBH₃ (0.1g, 1.5 mmol) were added to the mixture, that was left reacting for 15 min. Subsequently, a quenching with HCl was done, until the pH nd 3. Finally, the solution was concentrated under reduced pressure. Pure **3b** (yield: 70%, 0.74 g, 2.6 mmol) was obtained after crystallization with MeCN.

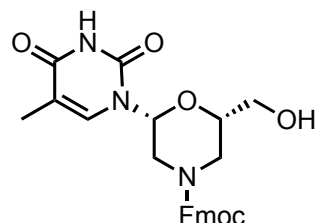
¹H NMR (300 MHz, D₂O) δ 8.49 (s, 1H), 8.40 (s, 1H), 6.30-6.26 (m, 1H), 4.33-4.28 (m, 1H), 3.81-3.65 (m, 4H), 3.51-3.46 (m, 2H) ppm;

¹³C NMR (75 MHz, D₂O) δ 150.1, 148.0, 144.9, 143.9, 118.7, 77.7, 74.5, 61.1, 44.0, 42.7 ppm;

MS (ESI): calcd for C₁₀H₁₄N₆O₂ 250.13, found [M + Na]⁺ 274.43.

Elemental Analysis: calcd for C₁₀H₁₅ClN₆O₂ C, 41.89; H, 5.27; N, 29.31, found C, 41.71; H, 5.39; N, 29.25

Synthesis of (9H-fluoren-9-yl)methyl (2S,6R)-2-(hydroxymethyl)-6-(5-methyl-2,4-dioxo-3,4-dihydropyrimidin-1(2H)-yl)morpholine-4-carboxylate (4a)



Compound **3a** (0.5 g, 2 mmol) was dissolved in DMF (10 mL) and the solution was cooled to 0 °C. Fmoc-Succinimide (0.7 g, 2 mmol) and DIEA (0.5 g, 4 mmol, 0.7 mL) were added and the solution was slowly warmed up to r.t. and kept under stirring for 3 h. The solvent was removed under reduced pressure and the crude product was purified by flash chromatography (DCM:MeOH = gradient 0-100%) affording **4a** as white solid (yield: 85%, 0.79 g, 1.7 mmol).

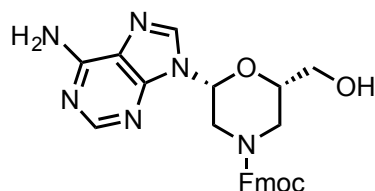
^1H NMR (300 MHz, CDCl_3) δ 8.86 (brs, 1H), 7.77-7.74 (m, 2H), 7.55-7.53 (m, 2H), 7.42-7.30 (m, 4H), 7.2 (brs, 1H), 5.65 (brs, 1H), 4.62-4.26 (m, 2H), 4.22-4.10 (m, 2H), 3.86-3.60 (m, 4H), 2.85-2.79 (brs, 2H), 1.93 (s, 3H) ppm;

^{13}C NMR (75 MHz, CDCl_3) δ 163.3, 154.8, 149.6, 143.7, 143.6, 141.3, 134.9, 127.8, 127.2, 125.0, 120.0, 111.4, 79.0, 77.2, 72.2, 67.7, 67.1, 62.8, 47.2, 46.3, 43.9, 14.2, 12.5 ppm;

MS (ESI): calcd for $\text{C}_{25}\text{H}_{25}\text{N}_3\text{O}_6$ 463.17, found $[\text{M} + \text{Na}]^+$ 486.94.

Elemental Analysis: calcd for $\text{C}_{25}\text{H}_{25}\text{N}_3\text{O}_6$ C, 64.79; H, 5.44; N, 9.07; found C, 64.68; H, 5.57; N, 9.01.

Synthesis of (9H-fluoren-9-yl)methyl (2R,6S)-2-(6-amino-9H-purin-9-yl)-6-(hydroxymethyl)morpholine-4-carboxylate (**4b**)



Compound **3b** (0.5 g, 2 mmol) was dissolved in DMF (10 mL) and the solution was cooled to 0 °C. Fmoc-Succinimide (0.7 g, 2 mmol) and DIEA (0.5 g, 4 mmol, 0.7 mL) were added and the solution was slowly warmed up to r.t. and kept stirring for 3 h. The solvent was removed under reduced pressure and the crude product was purified by flash chromatography (DCM:MeOH = 10:1 with 1% AcOH) affording **4b** as white solid (yield: 55%, 0.52 g, 1.1 mmol).

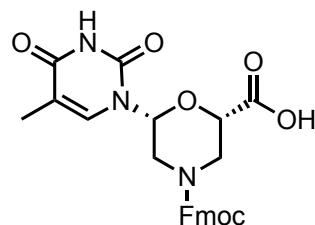
¹H NMR (300 MHz, DMSO) δ 8.35 (s, 1H), 8.22 (brs, 1H), 7.99-7.78 (m, 2H), 7.70-7.60 (m, 2H), 7.49-7.26 (m, 6H), 5.72 (d, *J* = 10.3, 1H), 4.97-4.92 (m, 1H), 4.57-4.28 (m, 3H), 4.25-3.86 (m, 2H), 3.80-3.57 (m, 2H), 3.55-3.42 (m, 2H) ppm;

¹³C NMR (75 MHz, DMSO) δ 157.2, 156.6, 154.8, 153.3, 150.0, 144.2, 141.2, 139.9, 139.2, 129.1, 127.6, 125.6, 120.5, 119.1, 110.2, 78.8, 76.9, 67.5, 61.9, 47.3, 46.4, 45.1 ppm;

MS (ESI): calcd for C₂₅H₂₄N₆O₄ 472.19, found [M + H]⁺ 473.42.

Elemental Analysis: calcd for C₂₅H₂₄N₆O₄ C, 63.55; H, 5.12; N, 17.79; found C, 63.12; H, 5.25; N, 17.70

Synthesis of (2S,6R)-4-(((9H-fluoren-9-yl)methoxy)carbonyl)-6-(5-methyl-2,4-dioxo-3,4-dihydropyrimidin-1(2H)-yl)morpholine-2-carboxylic acid (1a)



Compound **4a** (0.3 g, 0.6 mmol) was dissolved in a mixture of MeCN/H₂O (1:1; 10 mL) and the solution was cooled to 0 °C. TEMPO (0.03 g, 0.18 mmol) and (Diacetoxyiodo)benzene (0.43 g, 1.32 mmol) were added and the solution was slowly warmed up to r.t.. After 5h the solvent was removed under reduced pressure and the crude was purified by flash chromatography (DCM:MeOH = gradient 0-100%) affording the pure **1a** as white solid (yield: 90%, 0.26 g, 0.54 mmol).

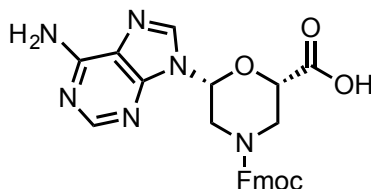
¹H NMR (300 MHz, CDCl₃) δ 9.66 (brs, 1H), 7.74-7.71 (m, 2H), 7.53-7.51 (m, 2H), 7.39-7.25 (m, 4H), 6.2 (brs, 1H), 5.80-5.60 (m, 1H), 4.46-4.31 (m, 2H), 4.23-4.11 (m, 4H), 3.00-2.86 (m, 2H), 1.88 (s, 3H) ppm;

¹³C NMR (75 MHz, CDCl₃) δ 169.9, 164.1, 154.7, 149.8, 143.5, 143.4, 141.34, 141.3, 135.3, 127.8, 127.2, 124.93, 124.92, 120.1, 111.7, 110.0, 78.9, 74.2, 68.2, 60.5, 47.1, 44.2, 29.6, 14.16, 12.4 ppm;

MS (ESI): calcd for C₂₅H₂₃N₃O₇ 477.15, found [M + Na]⁺ 499.94; [M - H]⁻ 476.34.

Elemental Analysis: calcd for C₂₅H₂₃N₃O₇ C, 62.89; H, 4.86; N, 8.80; found C, 62.95; H, 4.93; N, 8.72.

Synthesis of (2S,6R)-4-(((9H-fluoren-9-yl)methoxy)carbonyl)-6-(6-amino-9H-purin-9-yl)morpholine-2-carboxylic acid (**1b**)



Compound **4b** (0.47g, 0.4 mmol) was placed in a round bottom flask with a stirrer bar. Under N_2 flow, Acetone (5 mL) was added and the suspension was cooled to 0 °C. Jones reagent (0.7 mL) was added and the reaction was warmed up to r.t. and kept stirring for 3h. The solvent was removed under reduced pressure and the crude product was purified by flash chromatography (DCM:MeOH = 10:1 with 1% AcOH) affording the product **1b** as white solid (yield: 70%, 0.14 g, 0.28 mmol).

1H NMR (300 MHz, DMSO) δ 13.20 (brs, 1H), 8.33 (s, 1H), 8.18 (brs, 1H), 7.88-7.80 (m, 2H), 7.68-7.58 (m, 2H), 7.39-7.20 (m, 4H), 5.79-5.76 (m, 1H), 4.60-4.0 (m, 4H), 3.72-3.60 (m, 1H), 3.48-3.34 (m, 2H), 3.03-3.20 (m, 1H) ppm;

^{13}C NMR (75 MHz, $CDCl_3$) δ 169.5, 157.0, 155.0, 153.8, 150.0, 144.6, 141.6, 139.7, 128.5, 128.4, 128.0, 127.9, 125.9, 121.0, 119.4, 78.7, 76.7, 74.2, 68.1, 49.7, 47.5, 46.2, 45.0, 29.9, 29.5 ppm;

MS (ESI): calcd for $C_{25}H_{22}N_6O_5$ 486.17, found $[M + Na]^+$ 511.12

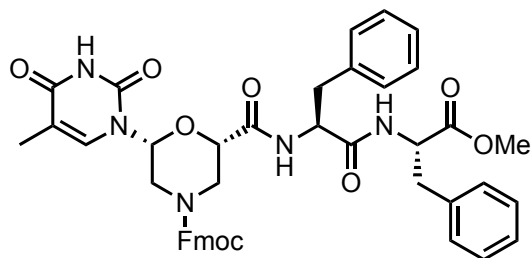
Elemental Analysis: calcd for $C_{25}H_{22}N_6O_5$, C, 61.72; H, 4.56; N, 17.28; found C, 61.62; H, 4.60; N, 17.21.

General condition for peptide coupling reaction

The Morph- β AA **1a/1b** (1 eq.) was dissolved in DMF (0.1 M) and the solution was cooled to 0 °C. HOBT (1.1 eq) and HBTU (1.1 eq.) were added and the solution was kept stirring for 1h. After that, NH₂-PhePheCOOMe **5** (1 eq.) and DIEA (2.2 eq.) were added and the reaction was warmed up to r.t. and kept stirring overnight.

The solvent was removed under reduced pressure and the obtained yellow solid was dissolved in EtOAc and washed three times with water. The organic layer was dried over NaSO₄ and concentrated under reduced pressure. The crude mixture was purified by chromatography column with *n*-Hexane:AcOEt (gradient 0-100%) affording the tripeptides **6** as white solids.

Synthesis of (9H-fluoren-9-yl)methyl (2S,6R)-2-(((S)-1-(((S)-1-methoxy-1-oxo-3-phenylpropan-2-yl)amino)-1-oxo-3-phenylpropan-2-yl)carbamoyl)-6-(5-methyl-2,4-dioxo-3,4-dihydropyrimidin-1(2H)-yl)morpholine-4-carboxylate (6a)



yield: 82%; *m.p.* = 130 °C.

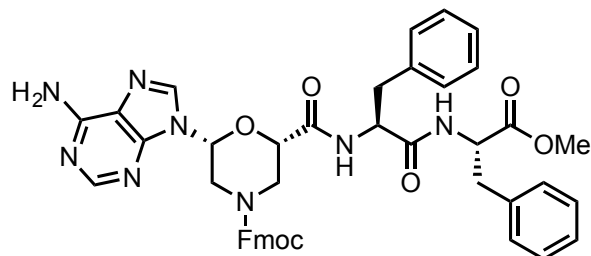
¹H NMR (500 MHz, CD₃CN) δ 9.19 (brs, 1H), 7.85 (d, *J* = 5.35, 2H), 7.64 (d, *J* = 6.91, 2H), 7.48-7.12 (m, 14H), 7.04-6.60 (m, 2H), 5.77-5.72 (m, 1H), 4.75-4.55 (m, 2H), 4.55-4.40 (m, 2H), 4.36-4.25 (m, 1H), 4.20-3.90 (m, 2H), 3.70 (s overlapped, 3H), 3.67-3.59 (m overlapped, 1H), 3.23-3.08 (m, 3H), 3.07-2.25 (m, 3H), 2.64-2.46 (m, 1H), 1.96 (s, 3H) ppm;

¹³C NMR (125 MHz, CD₃CN) δ 171.9, 170.6, 167.1, 163.7, 154.9, 150.3, 144.4, 141.6, 137.4, 137.0, 135.9, 129.9, 129.7, 128.8, 128.7, 128.1, 127.6, 127.2, 127.1, 125.5, 117.6, 111.0, 96.4, 78.9, 75.7, 67.7, 66.0, 55.5, 53.9, 53.7, 52.2, 47.5, 45.6, 44.7, 43.4, 37.4, 12.3 ppm.

MS (ESI): calcd for C₄₄H₄₃N₅O₉ 785.31, found [M + H]⁺ 786.34.

Elemental Analysis: calcd for C₄₄H₄₃N₅O₉ C, 67.25; H, 5.52; N, 8.91; found C, 67.15; H, 5.55; N, 8.83.

Synthesis of (9H-fluoren-9-yl)methyl (2R,6S)-2-(6-amino-9H-purin-9-yl)-6-(((S)-1-(((S)-1-methoxy-1-oxo-3-phenylpropan-2-yl)amino)-1-oxo-3-phenylpropan-2-yl)carbamoyl)morpholine-4-carboxylate (6b)



yield: 75%; *m.p.* = 137 °C.

¹H NMR (500 MHz, CD₃CN) δ 8.34 (brs, 1H), 8.10 (brs, 1H), 7.94 (d, *J* = 8.42, 1H), 7.84-7.77 (m, 1H), 7.72 (d, *J* = 8.42, 1H), 7.64 (d, *J* = 6.87, 1H), 7.56 (t, *J* = 6.87, 1H), 7.50-7.31 (m, 3H), 7.31-7.07 (m, 10 H), 7.04 (d, *J* = 8.42, 1H), 6.91 (d, *J* = 7.73, 1H), 6.48 (brs, 2H), 5.75 (brs, 1H), 4.71-4.48 (m, 3H), 4.36-4.25 (m, 1H), 4.19-3.97 (m, 1H), 3.70 (m, 1H), 3.67 (s, 3H), 3.55-3.42 (m, 1H), 3.22-2.75 (m, 4H) 2.66-2.53 (m, 1H) ppm.

¹³C NMR (125 MHz, CD₃CN) δ 171.5, 170.1, 167.0, 155.1, 154.5, 151.60, 149.5, 146.4, 144.0, 141.1, 139.4, 137.0, 136.6, 129.4, 129.3, 129.2, 128.4, 128.3, 128.2, 127.7, 127.2, 127.1, 126.7, 126.6, 126.5, 125.0, 125.03, 124.4, 120.0, 119.1, 118.6, 109.7, 78.5, 74.8, 70.2, 67.3, 55.0, 53.56, 53.3, 51.8, 47.2, 46.0, 44.5, 37.0. ppm.

MS (ESI): calcd for C₄₄H₄₂N₈O₇ 794.32, found [M + Na]⁺ 817.12.

Elemental Analysis: calcd for C₄₄H₄₂N₈O₇ C, 66.49; H, 5.33; N, 14.10, found C, 66.41; H, 5.40; N, 14.00.

Self-assembly studies

6a or **6b** were dissolved in 1,1,1,3,3,3-Hexafluoro-2-propanol (HFP) at a concentration of 100 mg/mL. The peptide in HFP was diluted in different solvents (TDW, EtOH, 50% EtOH in TDW, MeOH, isopropanol, chloroform, TDW with NaOH pH = 10, TDW with HCl pH = 2) to a final concentration of 2 mg/mL: A drop from each sample was placed on a glass for SEM analysis at time = 0 (right after dilution) and at time = 24 (after overnight incubation). After overnight incubation of APP\TPP in TDW, the temperature stability of the assemblies (the dried assemblies on a glass were heated to 120°C for 2 hours) and the PH stability (the right amount of base\acid was added to the solution of the assemblies until 1M concentration of NaOH and HCl and the samples were left for an additional day of incubation) were studied by SEM analysis.

SEM images were taken using a Sirion high resolution scanning electron microscope or extra-high-resolution scanning electron microscope, MagellanTM400L, operating at 5kV.

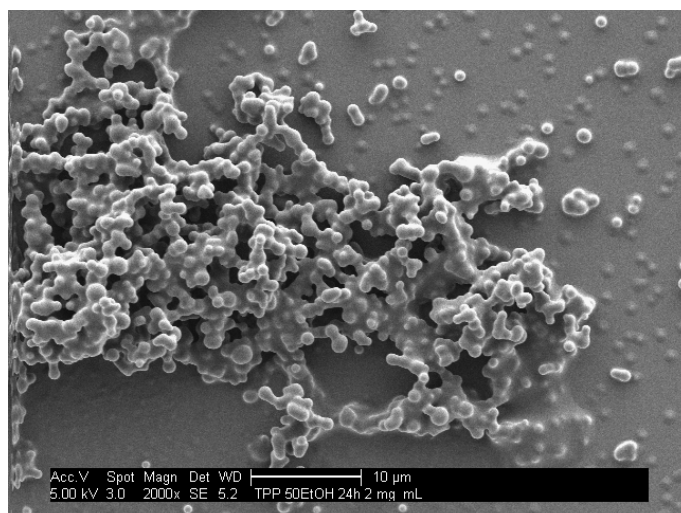


Figure 54 Spherical aggregates of 6a in 50% EtOH in water

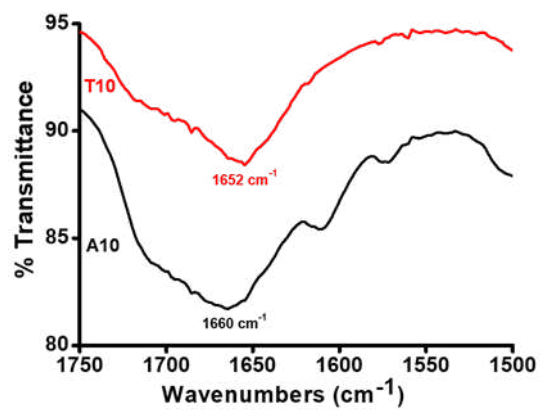


Figure 55 FT-IR spectra of Adenine (black) and thymine (red).

DLS analysis

The Dynamic Light Scattering (DLS) measurements were performed using a Malvern Zetasizer Nano ZS instrument at 25° C, equipped with a 633 nm solid state He-Ne laser at a scattering angle of 173°. Analyses were performed in water (viscosity: 0.8872 Cp, refractive index: 1.33). The size measurements were averaged from at least three repeated measurements.

6b and **6a** were separately dissolved in hexafluoropropanol/H₂O in 30:70 (Figure 56), 20:80 (Figure 57), 10:90 and 2:98 (Figure 58), ratios respectively, such that the final concentration of **6a** or **6b** was equal to 50 mM for all the samples.

DLS showed some differences between **6a** and **6b**. In particular, at the lowest water content, the DLS size distribution by intensities for **6b** showed one peak centred at ca 5-6 nm attributable at few molecules forming small clusters, while in the case of **6a**, besides the peak at 5-6 nm, there was a second peak centred at 200-300 nm. Anyhow, this second population can be ascribed to a few aggregates already present, which accounts for a very minor part of the whole molecules present in the mixture, so that they can be neglected.

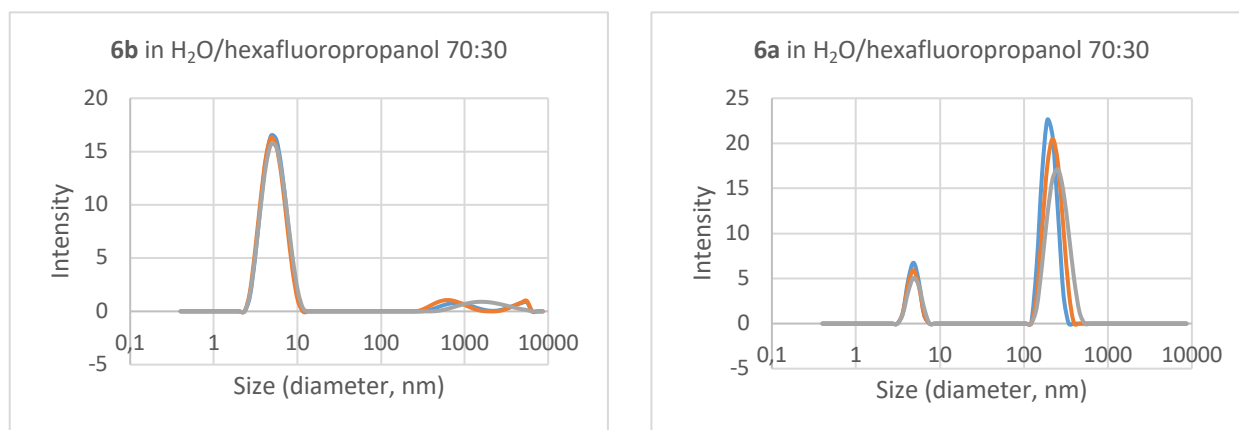


Figure 56 DLS analysis using hexafluoropropanol/H₂O in 30:70

This condition was observed for **6b** only increasing the water in the mixture up to the 80%, while at the ratio 20:80 the **6a** already showed the bigger peak at ca 200 nm only, suggesting a more favourable aggregation capacity (Figure 57).

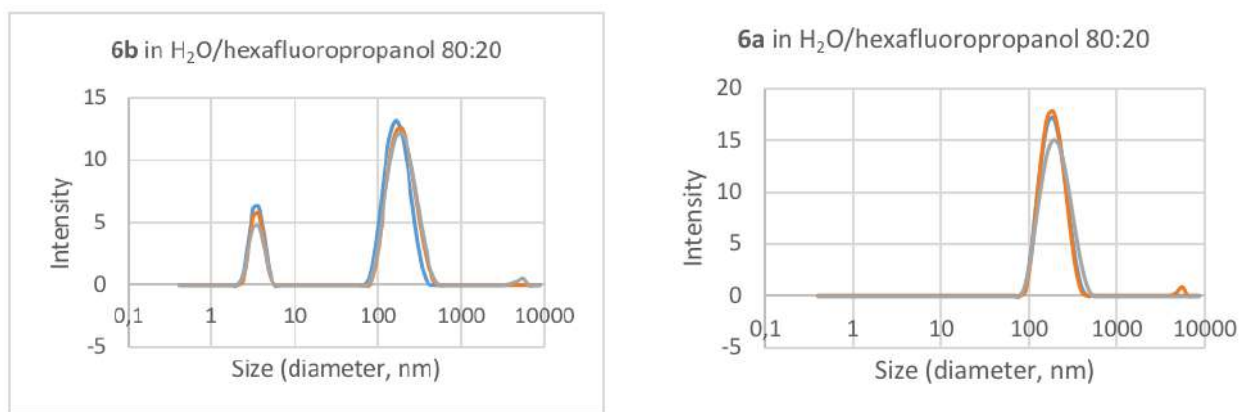


Figure 57 DLS analysis using hexafluoropropanol/H₂O in 20:80

Both the two samples showed a huge increase in the size of the aggregates further increasing the water content at 10:90 ratio. Nevertheless, in this condition, the fitting of the correlation function was poor, so that the distribution output should not be considered reliable.

When the content of hexafluoropropanol was decreased to 2% (Figure 58) only the two suspensions showed one peak only centred at 200 nm for both **6a** and **6b**, suggesting that at time 0, the two nucleo-dipeptides behave at the same way. Moreover, compared to the peaks observed at 20:80 ratio, the peaks are sharper, indicating a more monodispersed situation.

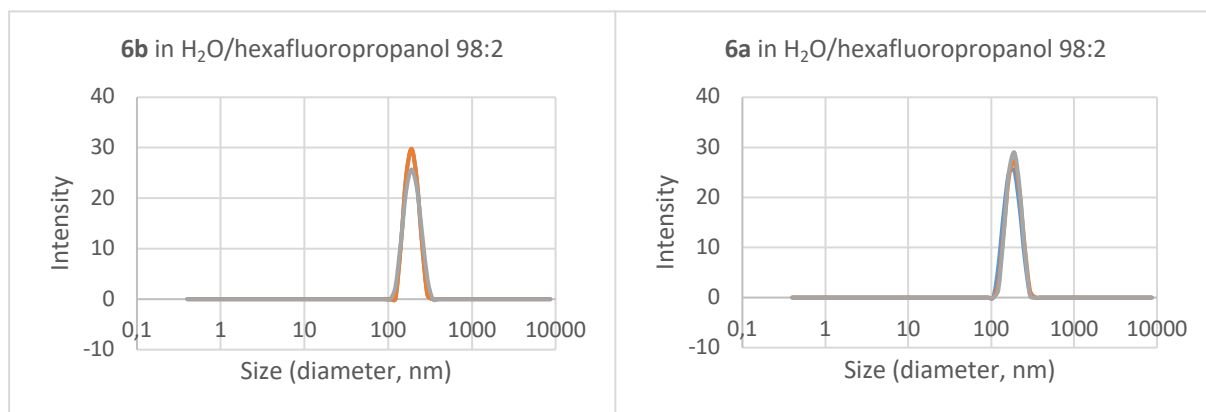


Figure 58 DLS analysis using H₂O/hexafluoropropanol in 98:2

The stability of the aggregates over time was investigated acquiring a measurement at 24 h and 48 h (Figure 59). In the table below, a summary of DLS analysis are reported. Moreover, in the graphic is describe the ζ -potential (Figure 60 and Table 9).

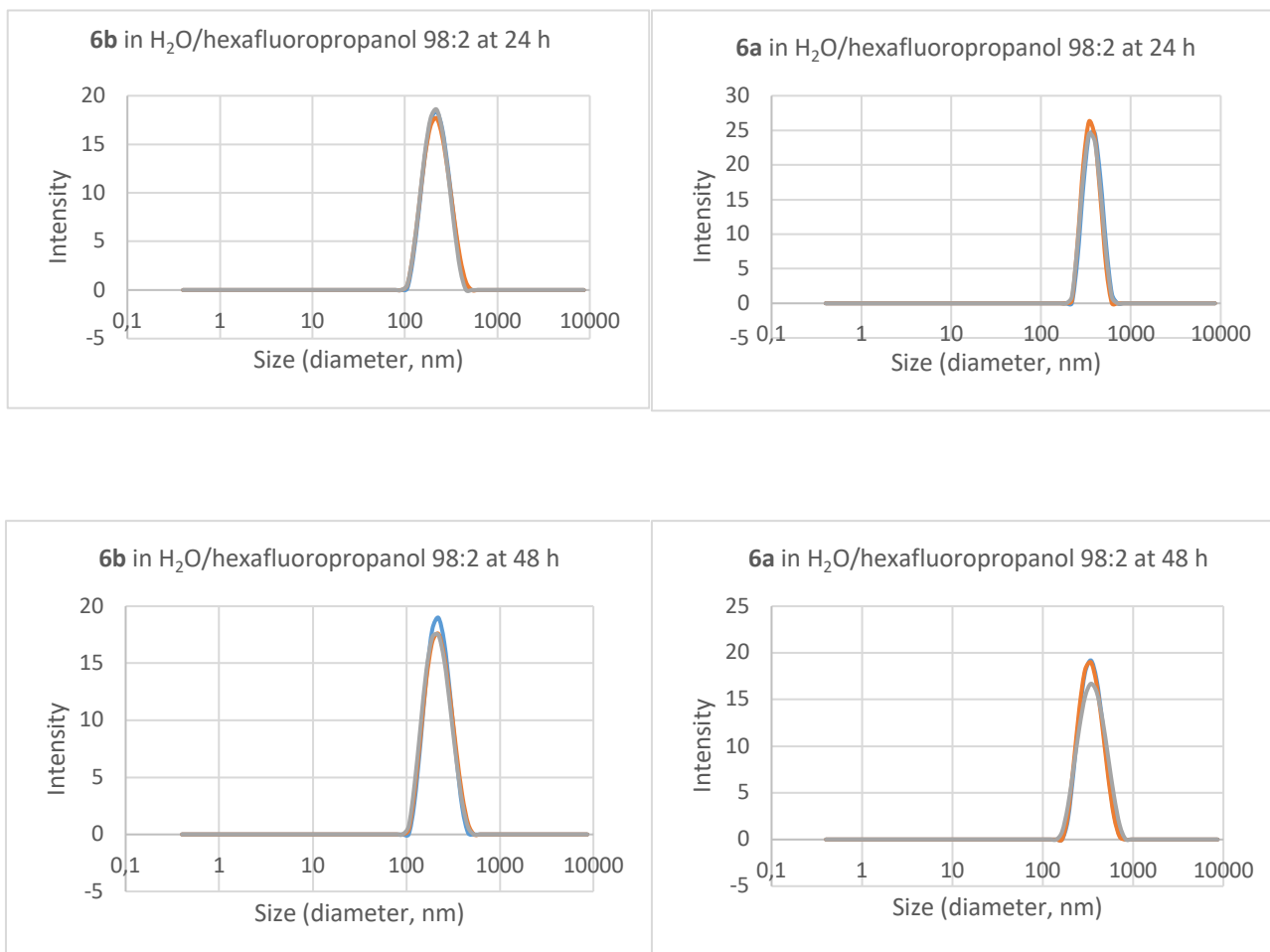


Figure 59 DLS analysis using H₂O/hexafluoropropanol in 98:2 after 24h and 48h

Table 9 Summary of DLS analysis

H ₂ O/hexafluoropropanol	6a	6b
70:30	5.6 nm ± 2.0 (+ 260 ± 90 nm)	5.6 ± 2.5 nm
80:20	200 ± 98 nm	3.6 ± 1.5 nm (+ 200 ± 85 nm)
90:10	---	---
98:2 t=0	190 ± 60 nm	190 ± 91 nm
98:2 t=24h	342 ± 120 nm	220 ± 100 nm
98:2 t=48h	342 ± 150 nm	220 ± 100 nm
ζ-potential	-47 mV	-16 mV

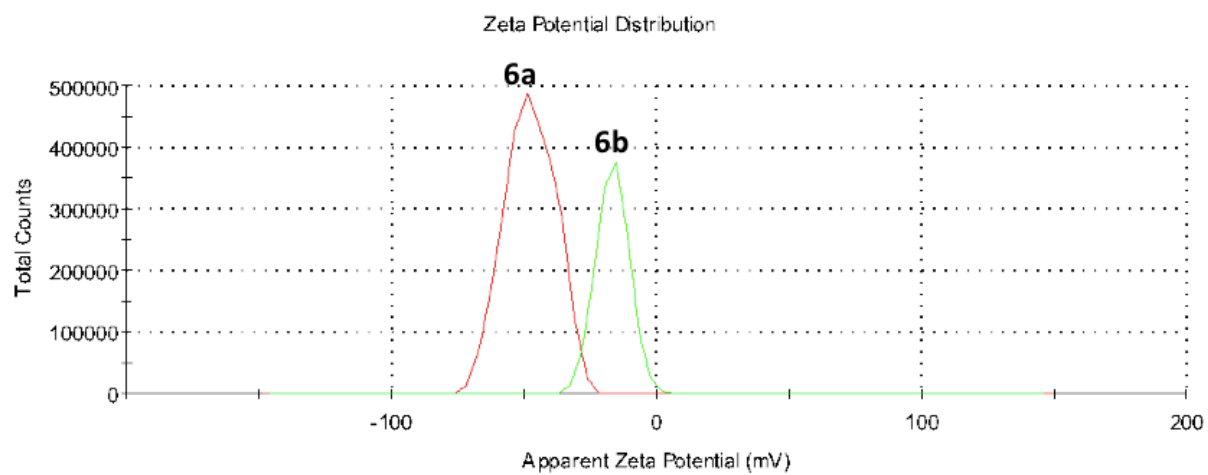


Figure 60 ζ -potential of tripeptide 6a and 6b

Photoluminescence (PL) studies

UV/Vis absorption spectra were obtained on Shimadzu UV-Vis-NIR 3600 Spectrophotometer in 1 cm path length quartz cell. Photoluminescence quantum yields were measured with a C11347 Quantaury-QY Absolute Photoluminescence Quantum Yield Spectrometer (Hamamatsu Photonics U.K), equipped with a 150 W Xenon lamp, an integrating sphere and a multi-channel detector. Steady state emission and excitation spectra and photoluminescence lifetimes were obtained with a FLS 980 spectrofluorimeter (Edinburg Instrument Ltd.). Continuous excitation for the steady state measurements was provided by a 450 W Xenon arc lamp. Photoluminescence lifetime measurements were determined by TCSPC (time-correlated single-photon counting) method, were performed using an Edinburgh Pulsed Diode PLED-300 (Edinburg Instrument Ltd.), with central wavelength 300 nm and repetition rates 100ps or greater or for the long phosphorescence components by decay kinetics.

Photoluminescence experiments at room temperature were carried out in various solvent solution at $1-2 \times 10^{-5}$ mol L⁻¹ including acetonitrile (ACN), dimethylsulphoxyde (DMSO), water, methanol-ethanol (MeOH-EtOH) mixture. Measurements at 77 K were performed in MeOH-EtOH 4/1 mixture frozen matrix or by cooling the colloidal suspension obtained from HFIP-water at the concentration of 5×10^{-5} mol L⁻¹.

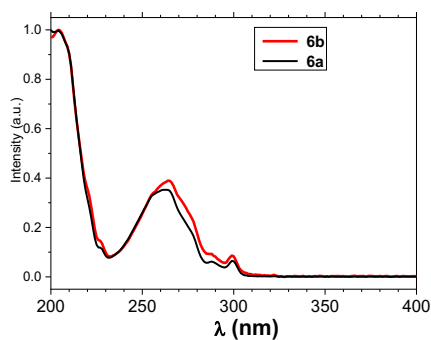


Figure 61 Absorption spectra of compounds 6a and 6b in acetonitrile (ACN) solution

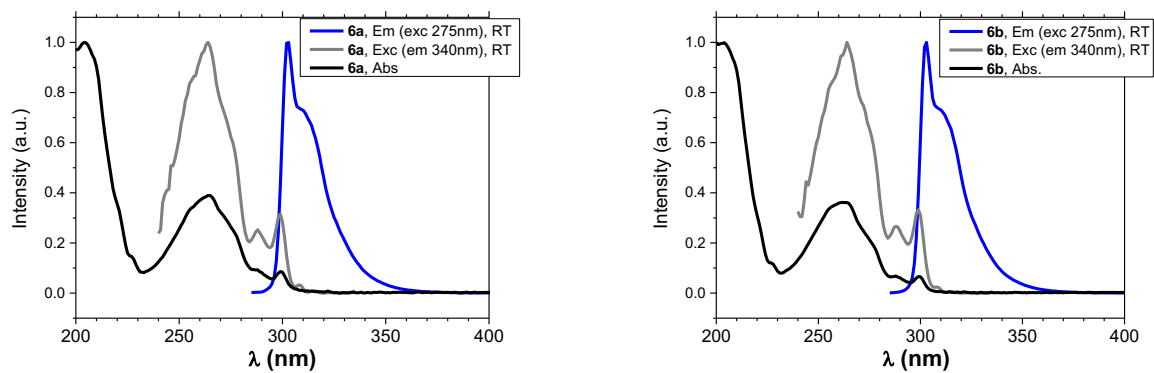


Figure 62 Emission, excitation and absorption spectrum of **6a** (left) and **6b** (right) in ACN solution at RT.

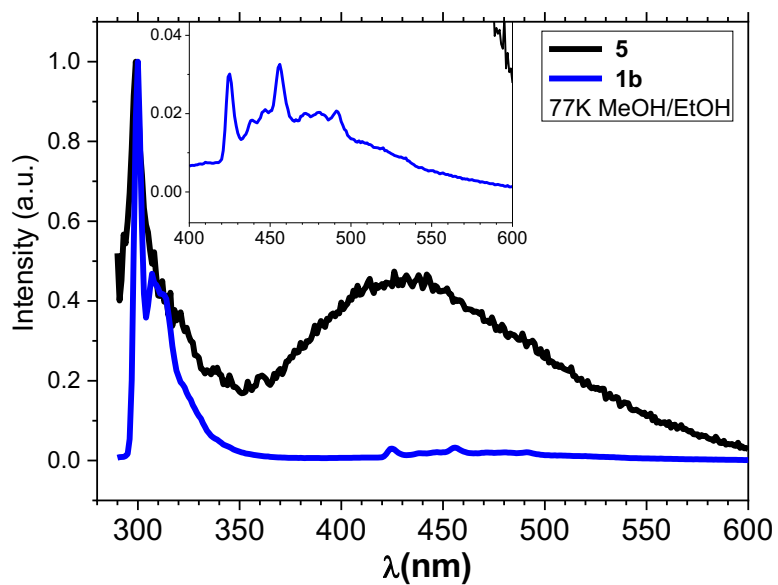


Figure 63 Emission spectra of building blocks **5** and the **1b**, 77K glassy matrix in MeOH/EtOH solution

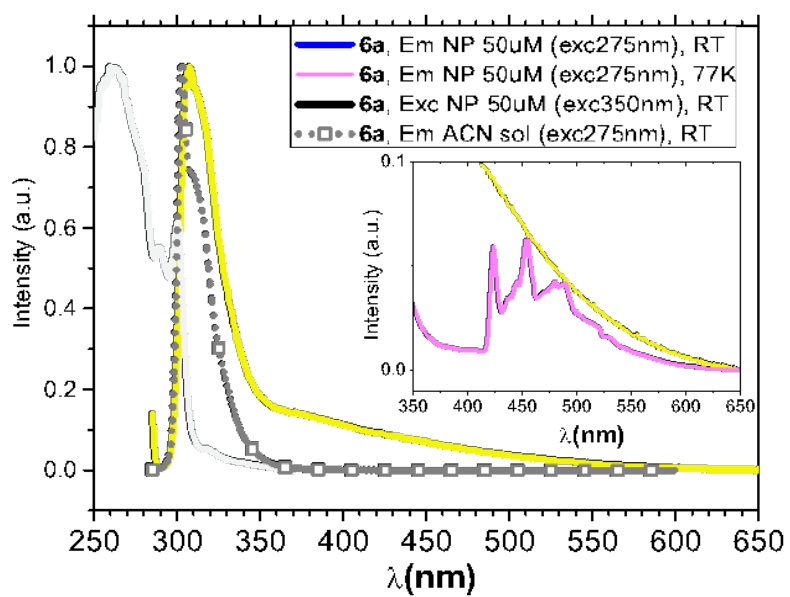
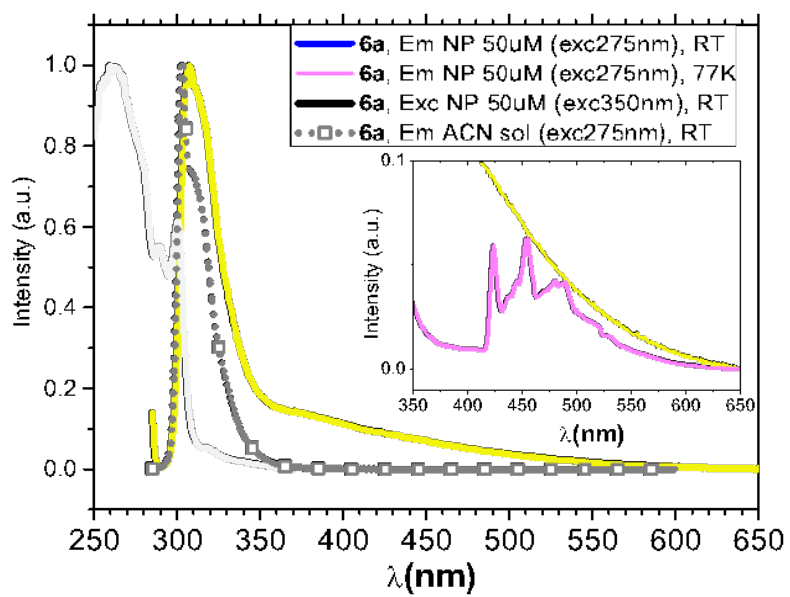


Figure 64 Emission spectra of **6a** and **6b** in diluted ACN solution excitation and emission of the aggregated NP at RT and in frozen matrix t 77K.

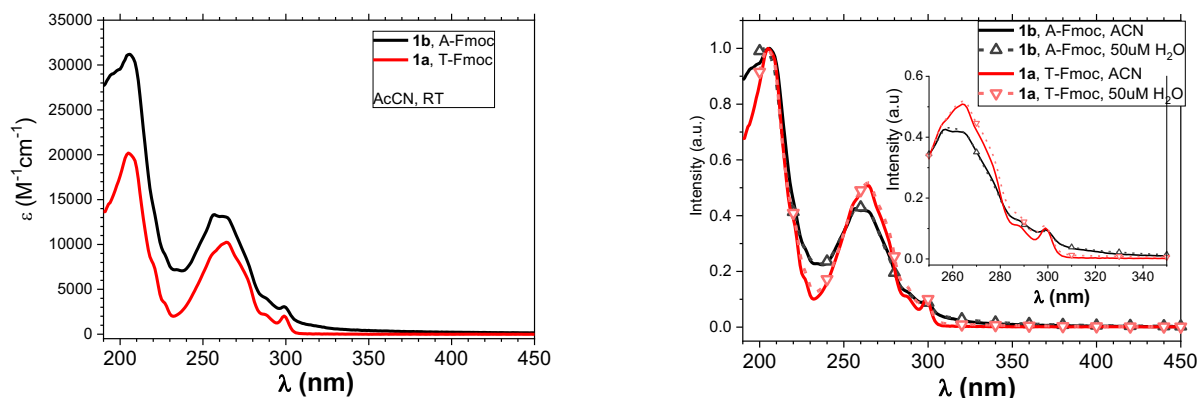


Figure 65 Absorption spectra of compounds **1a** and **1b**: left, molar absorptivity in acetonitrile (ACN) solutions; right, normalized ACN spectra (solid lines) compared to those obtained from a 98/2 v/v HFIP-water mixture at 50 μ M concentration (dashed lines with drawings).

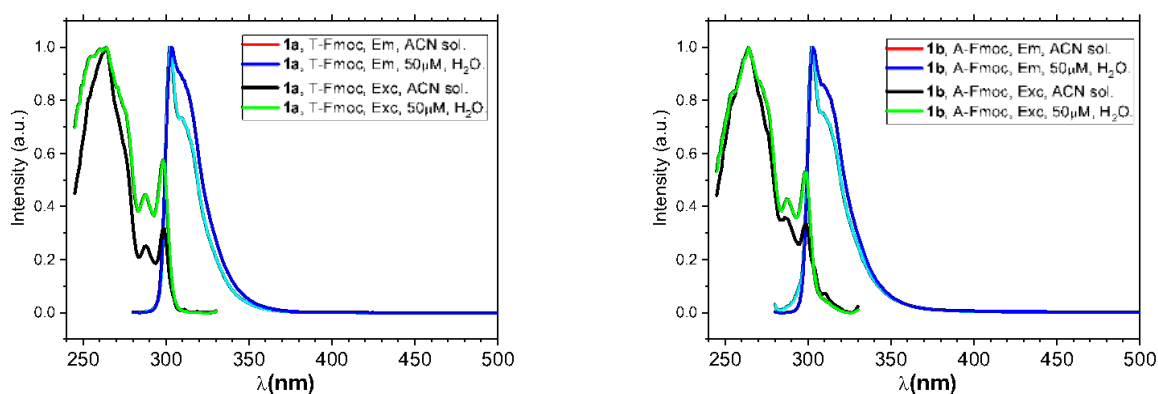


Figure 66 emission and excitation spectra of compounds **1a** (left) and **1b** (right): in both case are compared the curves collected from a diluted CAN solution and those obtained from a 98/2 v/v HFIP-water mixture at 50 μ M concentration

Table 10 Photoluminescent emission properties in diluted ACN solutions and in 98/2 v/v HFIP-water mixture at 50 μ M concentration

Compound (solvent)	QY	τ (%) / ns
1a , ACN solution	0.137	4.34
1a , 98/2 v/v HFIP-water mixture at 50 μ M concentration		1.54(79%); 3.94(21%)
1b , ACN solution	0.08	0.32(12%); 4.75(88%)
1b , 98/2 v/v HFIP-water mixture at 50 μ M concentration		0.55(26%); 5.73(74%)

Synthesis of non-natural amino acids with Morpholine core as organocatalysts for enantioselective reactions

Introduction

Organocatalysts are metal-free organic compounds able to promote a reaction in a sub-stoichiometric amount.⁷³ They have to be easy to prepare and easily accessible in enantiopure form and very often they come from a natural source. In general, organocatalysts play two functions: 1) activate the substrate in the reactions and 2) induce enantioselectivity.

The success in using organocatalysis has been the invention or identification of generic modes in which the catalyst is involved. A generic activation model describes a reactive species that can participate in many reaction types inducing high enantioselectivity (as opposed to one or two unique transformations). Such reactive species arise from the interaction of a single chiral catalyst with a functional group (such as a ketone, aldehyde, alkene or imine) in a highly organized and predictable manner. Even if more than a hundred organocatalytic reactions have been reported since 1998, only six activation modes were identified.⁷⁴

The mode of action of the most used organocatalysts are reported in Table 11. The use of Proline in reactions *via* enamine mechanism is shown in entry 1. Basically, enamine catalysis could be better described as bifunctional catalysis because the amine-containing catalyst typically interacts with a ketone/aldehyde substrate to form an enamine intermediate but simultaneously engages with an electrophilic reaction partner through either hydrogen bonding or electrostatic attraction. This activation mode has been used in a wide range of enantioselective carbonyl α -functionalization processes.⁷⁵

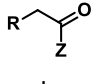
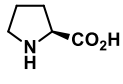
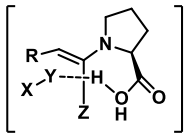
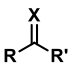
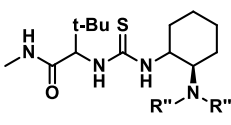
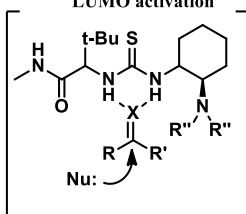
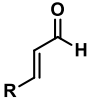
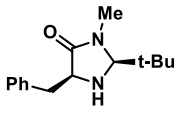
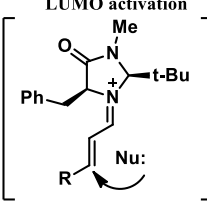
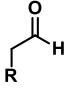
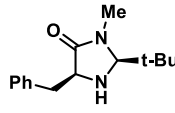
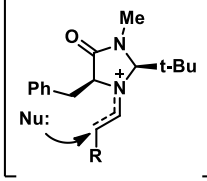
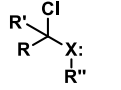
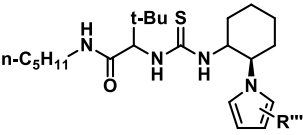
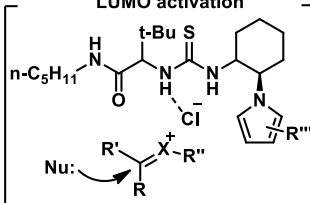
Thiourea-based catalysts are described in entry 2 and entry 5. These molecules can interact with the substrate *via* H-bond or catalyze the reaction *via* counterion. Jacobsen⁷⁶ and Corey⁷⁷ describe for the first time H-bonding mode of action. They independently reported an asymmetric variant of the Strecker reaction that used well-defined hydrogen-bonding organocatalysts that activate imine electrophiles. Four years later, Jacobsen showed as the thiourea catalysts could be used for other synthetic reactions, launching the generic use of enantioselective hydrogen-bonding catalysis. The thiourea catalysts, is able to form strong complexes with halide ions (entry 5). Thanks to the weak carbon–chlorine bonds of Chloroamides and Chloroacetals, they generate an electrophilic transient intermediate. The

resultant anionic catalyst–chloride complex functions as a chiral counterion, biasing the approach of nucleophiles to a single face of one enantiomer of the transient α -hetero atom-stabilized cationic species.⁷⁸

MacMillan catalyst could be used as iminium catalyst or a SOMO one (entry 3 and 4). The idea of iminium catalyst is based on the capacity of chiral amines to function as enantioselective catalysts for several transformations (entry 3). The concept was founded on the mechanistic hypothesis that the reversible formation of iminium ions from α,β -unsaturated aldehydes and chiral amines might emulate the equilibrium dynamics and π -orbital electronics that are inherent to Lewis acid catalysis (lowest-unoccupied molecular orbital (LUMO)-lowering activation).

More recently McMillan group introduced the concept of SOMO catalysis. It is based on the idea that one-electron oxidation of an electron-rich enamine selectively generates a reactive radical cation with three π -electrons. The electrophilicity of the singly occupied molecular orbital (SOMO) of this intermediate allows it to react readily with a variety of weakly nucleophilic carbon-based 'SOMOphiles' at the α -carbon of the parent enamine, resulting in formal alkylation products.

Table 11 Generic activation modes

Entry	Substrate	Catalyst	Activation mode
1	<p>Enamine catalyst</p>  <p>+ X=Y</p> <p>R= any organic chain or ring system X= C, N, O, S Y= generic organic atom Z= alkyl, H</p>		<p>HOMO activation</p> 
2	<p>Hydrogen-bonding catalysis</p>  <p>X= O, NR R, R', R''= alkyl, aryl</p>		<p>LUMO activation</p> 
3	<p>Iminium catalysis</p>  <p>R= alkyl, aryl</p>		<p>LUMO activation</p> 
4	<p>SOMO catalysis</p>  <p>R= alkyl, aryl</p>		<p>SOMO activation</p> 
5	<p>Counterion catalyst</p>  <p>X= O, NR R, R', R''= alkyl, aryl</p>		<p>LUMO activation</p> 

In reaction involving enamine catalysis transition state (Figure 67), the deprotonation of the iminium ion provides the enamine nucleophilic intermediate, with increased HOMO energy, able to attack an electrophile.

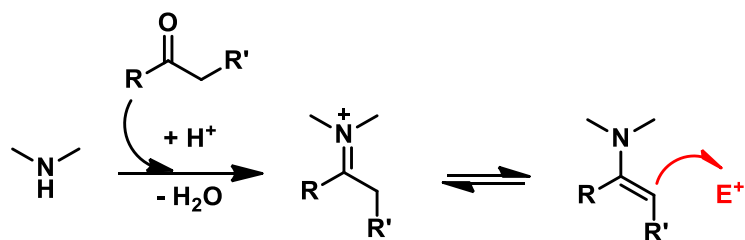


Figure 67 Enamine catalysis

The asymmetric addition of ketones and aldehydes to Michael acceptors can be catalyzed by chiral amines thanks to the transformation of the carbonyl group into enamine intermediate, as it is explained in the catalytic cycle (Figure 68).

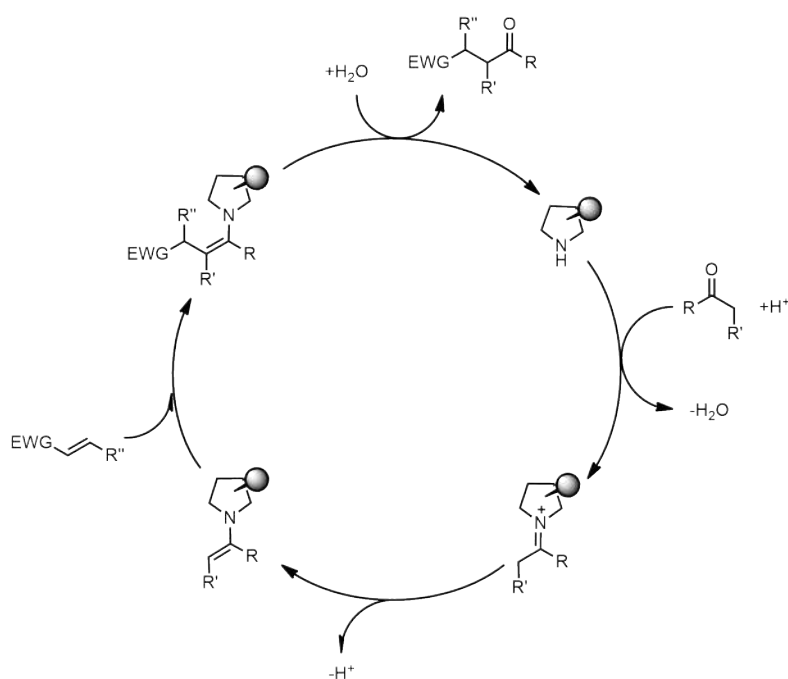


Figure 68 Catalytic cycle of asymmetric conjugate addition of ketones and aldehydes to Michael acceptors

The iminium ion is generated by the reaction of a chiral secondary amine catalyst with a carbonyl compound. Enamine intermediate reacts with the electron poor olefin to create the new C–C bond. The hydrolysis of the α -modified iminium ion give the Michael adduct and the amino catalyst, which is now ready for a new catalytic cycle.

Intermolecular conjugate addition selectivity depends on electronic and/or steric interactions so, the catalyst structure would determinate the geometry of the enamine (E or Z).⁷⁹

Comparing different types of enamine and different electrophiles, the relative reactivities of enamines is related to the amino moiety and generally decrease in the order Pyrrolidine > Piperidine > Morpholine (Figure 69).

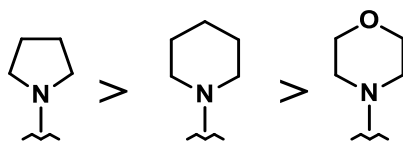


Figure 69 Relative reactivities of enamines

The higher reactivity of pyrrolidine enamine compared to piperidine analogues could be explained by the higher π -character of the nitrogen lone-pair in a five-membered ring compared with a six-membered ring. As a result, a lower first vertical ionization potential (IP1) of pyrrolidine compared to piperidine compounds is observed (Figure 70), indicating a higher nucleophilicity of pyrrolidine derivatives. Replacement of the 4-CH₂ group in piperidine by the more electro-negative oxygen further increases the ionization potential and consequently reduces nucleophilicity.⁸⁰

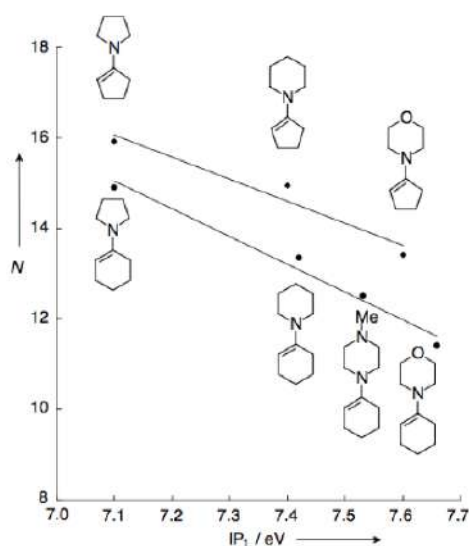


Figure 70 Correlation of the nucleophilic reactivities *N* with the first vertical ionization potentials IP₁ for cyclic enamines

Different enamine reactivity could be also attributed to a difference in degree of pyramidalization (θ_p : defined as the difference between 90° and the angle between the in-plane and out-of-plane bonds in the trigonal configuration as shown in Figure 71.⁸¹

$$\text{Pyramidalization Angle } p = (\theta - 90)^\circ$$

TRIGONAL

TETRAHEDRAL

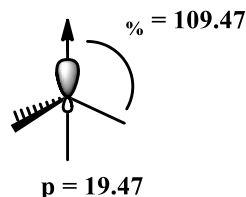
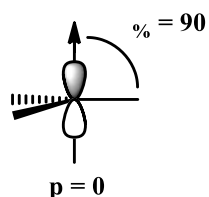


Figure 71 Definition of the pyramidalization angle θ_p

The decrease in degree of pyramidalization at N is reflected in a little shortening of the enamine N-C distance. As reported in Figure 72 there is an increase of the angle for the first to third one that reduces the reactivity of enamine comparing pyrrolidine, morpholine and piperidine.

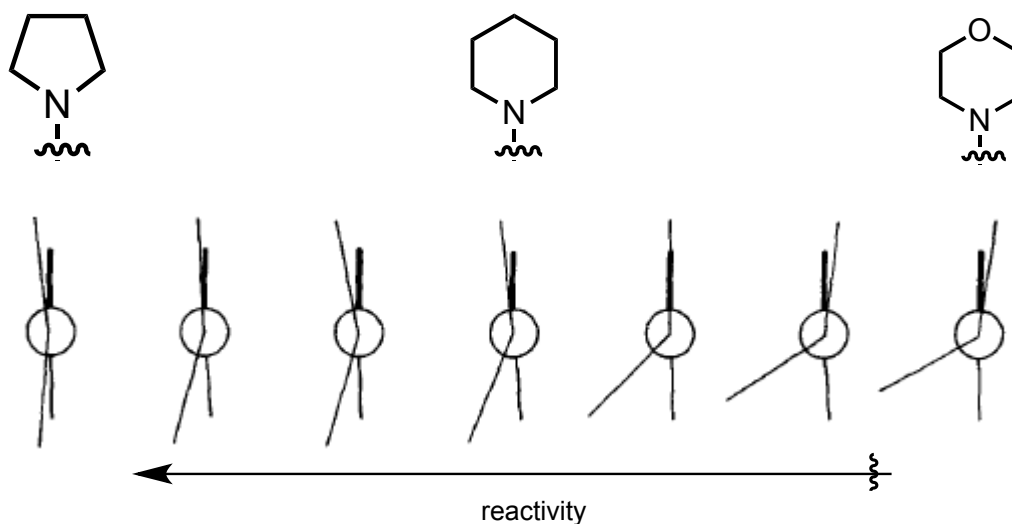


Figure 72 Newman projections of enamines looking down the N-C(sp^2) bond. The C=C bond is maintained in the vertical position

Substituents at the β -carbon atom of enamine (site of electrophilic attack) can influence the reactivity of enamines. Electron-withdrawing substituents like ethoxy-carbonyl instead electron-donor substituents (methyl group) reduce the reactivity of β -C-substituted morpholino by a factor of about 700 (calculated for $(pfa)_2CH^+$, CH_2Cl_2 , $20^\circ C$).

Reporting the N-parameters versus the σ_p values of the β -substituents of these enamines, a linear correlation is shown (Figure 73).⁸⁰

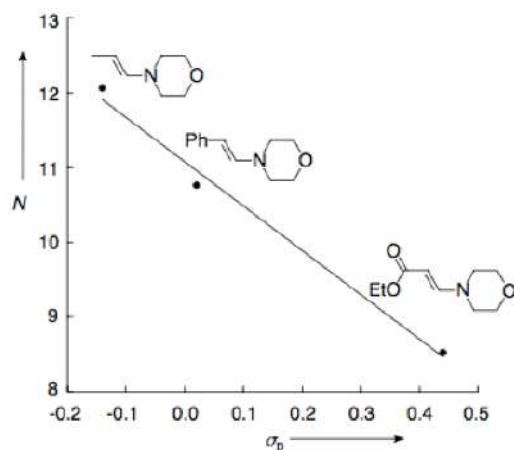


Figure 73 Correlation of N with σ_p for β C-substituted (*E*)-morpholinoethenes

Aim of the work

As underlined above, because of its ionization potential and low enamine nucleophilicity, morpholine presents disadvantages in terms of reactivity as organocatalyst when compared to catalysts such as Hayashi-Jorgensen and MacMillan, with pyrrolidine core. With this background, it was extremely stimulating to develop new catalysts containing morpholine core for asymmetric reactions and challenging in term of yields and enantioselectivity to overcome the results obtained with proline, toward the same reaction.

Starting from commercially available amino acids (AAs), our research group synthesized a series of new non-natural β -Morph-AAs as catalysts able to promote asymmetric reaction (Figure 74).

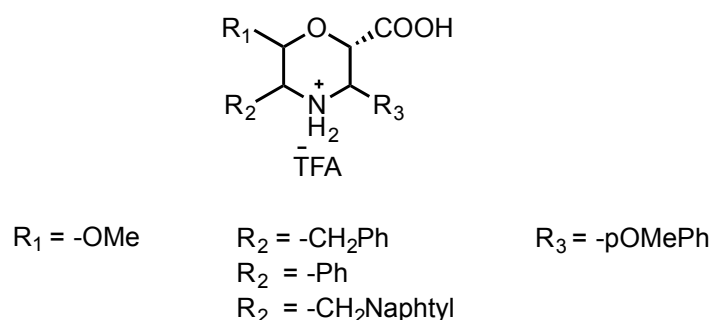


Figure 74 New β -Morph AAs catalyst

In particular, we tested the Michael reaction using (Figure 75):

- first our β -Morph AAs as the *N*-terminus of different ultra-short tripeptides, taking inspiration from Wennemers' catalysts.⁸²
- subsequently, we turned our attention on a series of β -Morph AAs as organocatalysts with simpler structure, investigating the best reaction conditions and the performance in function of the substitution pattern and stereochemistries.

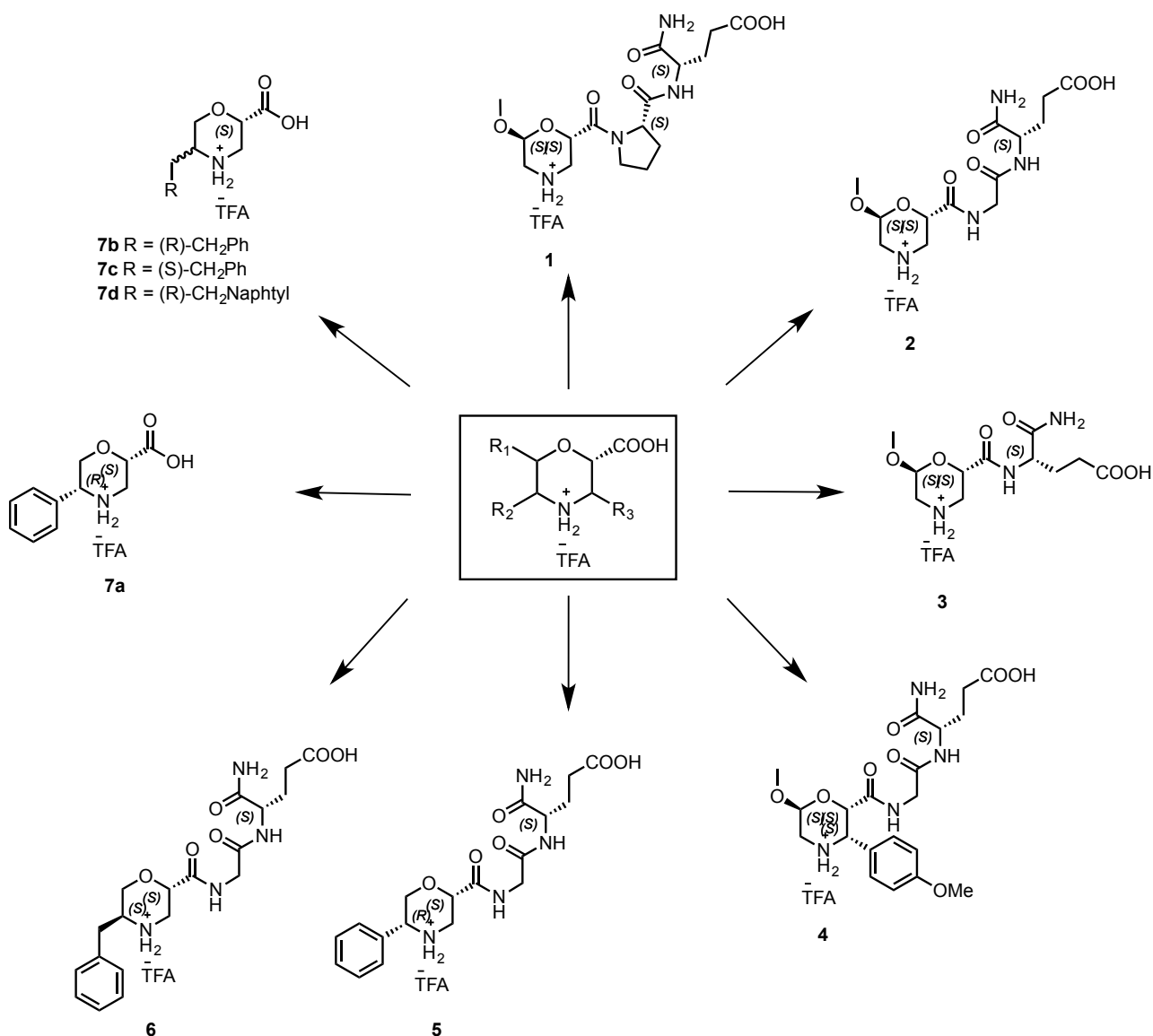
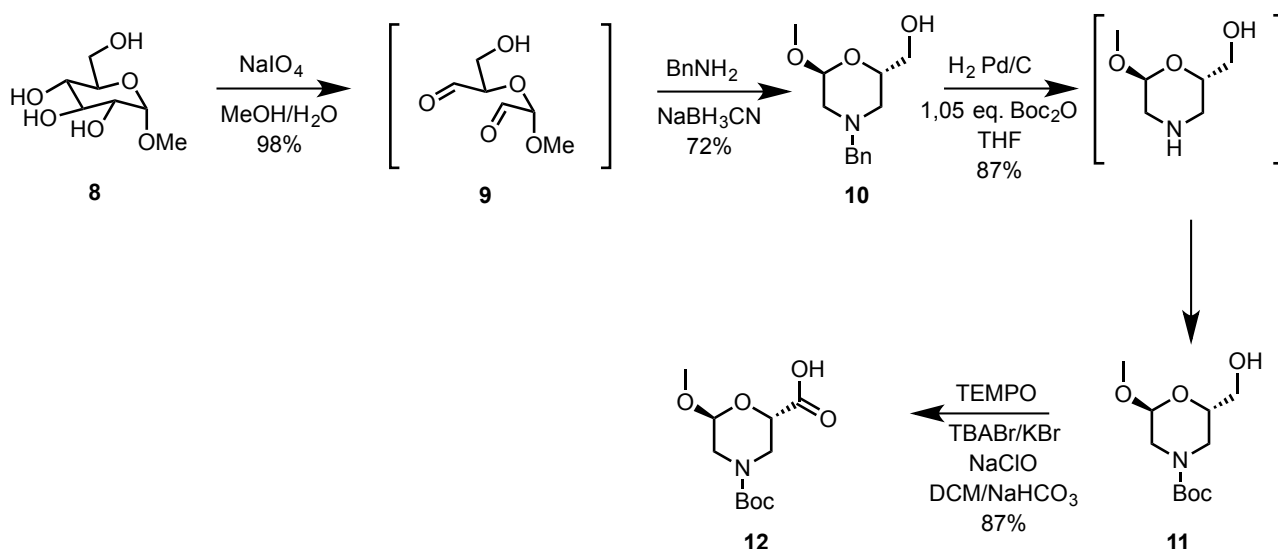


Figure 75 New catalysts containing Morph core for asymmetric Michael reaction.

Scaffold synthesis

5-Metoxyl- β -Morph AA synthesis

5-Metoxyl- β -Morph AA (**12**) was synthesized according a known procedure³⁵ from the commercially available α -D-glucopyranose (Scheme 10). The first two synthetic steps to obtain compound **10** consist in an oxidative step, using an excess of NaIO₄, and after work-up a reductive amination reaction of di-aldehyde **9** with NaBH₃CN and benzylamine, pH was adjusted to pH 7 with dropwise of AcOH. Another bunch of benzylamine was added after 12 h, affording product **10** in a good overall yield (78% from **9**). A one-pot nitrogen deprotection/Boc-protection reaction of amine intermediate **10** was performed with Pd/C and Boc₂O in THF under H₂ atmosphere (1 atm) at 25°C affording compound **11** in good yields (87%). With a phase-transfer oxidation procedure (TEMPO, NaClO, TBABr, KBr) operating in 1 M solution of NaHCO₃ and DCM at r.t., the oxidation of the alcohol function was performed, giving the N-Boc- β -AA **12** in a very good yield (83%).

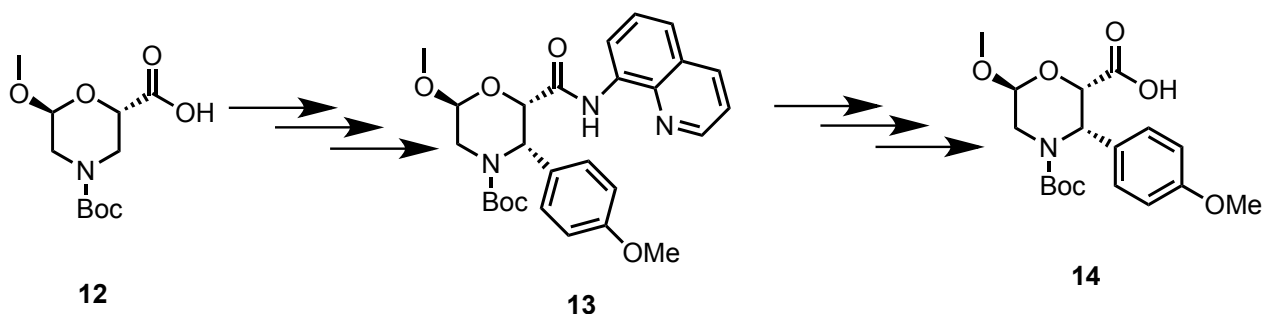


Scheme 10 General scheme for the synthesis of β -Morph AA 12

3-Aryl- β -Morph AA synthesis

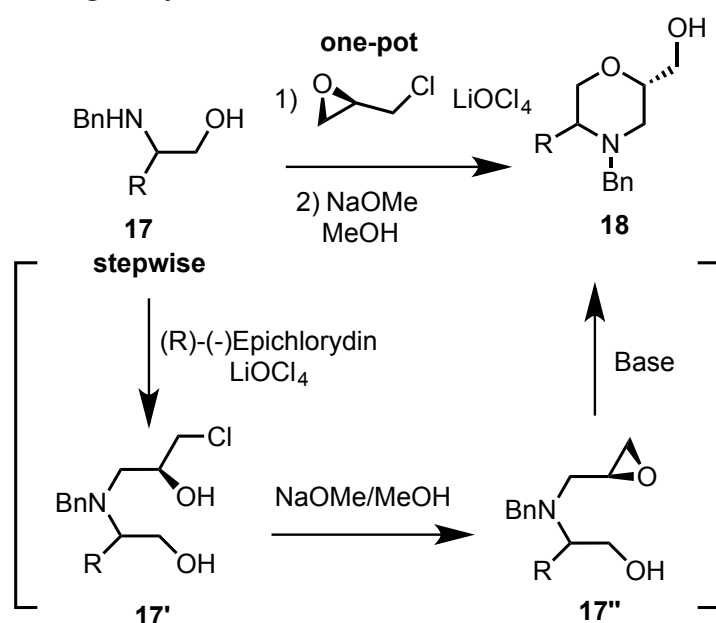
As described before in Chapter 1, we converted the β -Morph **12** into 3-Aryl- β -Morph AA **14** thanks to a regio and diastereoselective Pd-catalyzed C(sp³) H-arylation reaction.⁴² The

key step is the transformation mediated by the Pd-coordinating nitrogen of quinoline ring as described in Scheme 11.³⁷



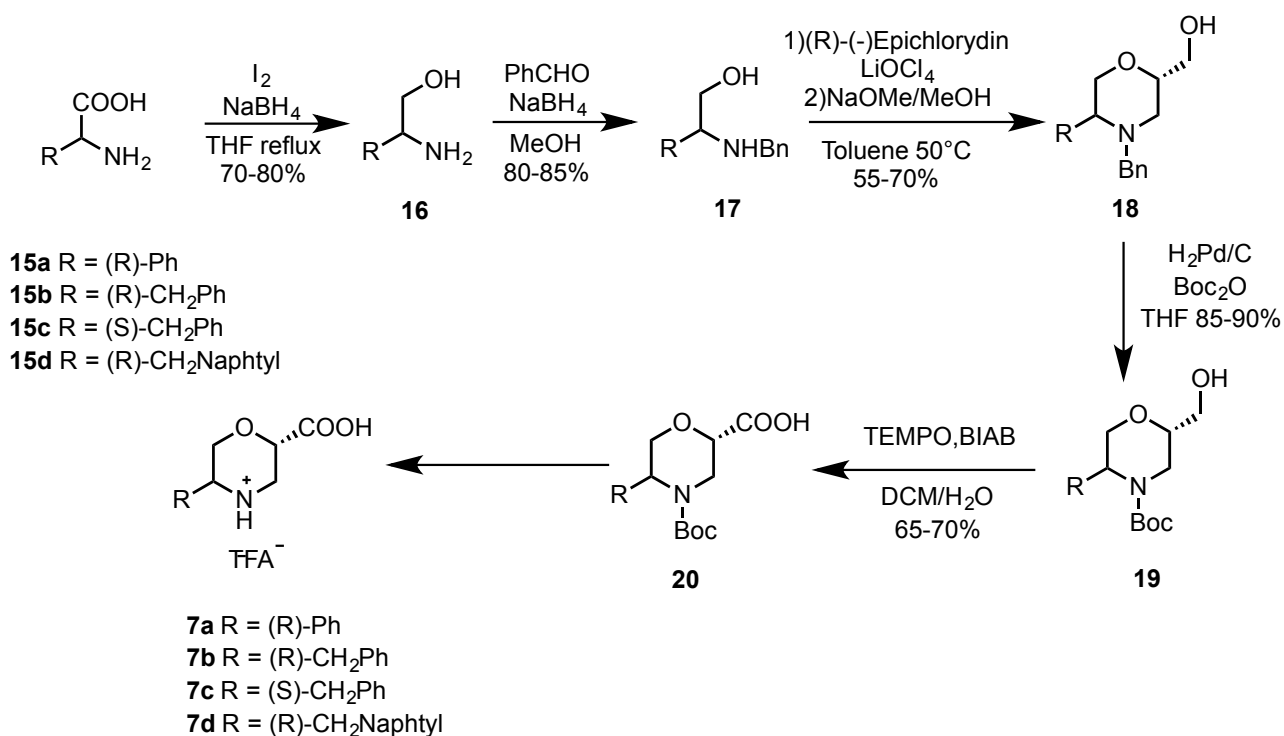
Scheme 11 General scheme for the synthesis of β -Morph AA 14

5-Substituted β -Morphs were synthesized from commercially available α -AAs (Scheme 4). Treatment of several amino acids (**15a-c**) with sodium borohydride (2,5 equiv.), Iodine (1 equiv.) in THF afforded the corresponding amino alcohols (**16**) in 80% yields after recrystallization. Subsequent reaction between amine group of **16** and benzaldehyde (1,3 equiv.) generate the enamine that is reduced to secondary amine **17** with NaBH_4 (3 equiv.). The one-pot synthesis of enantiomerically pure hydroxymethyl-morpholines **18** from amino alcohol was reported in literature (Scheme 12).⁸³ The addition of the amino alcohol **17** to enantiomerically pure (R)-epichlorohydrin (1,3 equiv.) in presence of Lewis acid (LiClO_4 , 1,3 equiv.) in toluene gave the chloro alcohol **17'**. A base-induced cyclization (MeONa , 2,5 equiv.) provides the intermediate epoxide **17''** and its final ring closure delivered the desired morpholine **18** in good yields (70%).



Scheme 12 Key intermediate for the synthesis of β -Morph AA 18

Starting from **18**, a one-pot nitrogen deprotection/Boc-protection reaction of amine intermediate **18** was performed with Pd/C (10% loading) and Boc₂O (1.05 eq.) in THF, under H₂ atmosphere (1 atm), at 25°C for 2h affording compound **19** in good yields (85%). Oxidation of alcohol function in **2** to carboxylic acid with TEMPO and BIAB in CH₂Cl₂/H₂O 2:1 provide the desired β-Morph AAs **8a-d**.

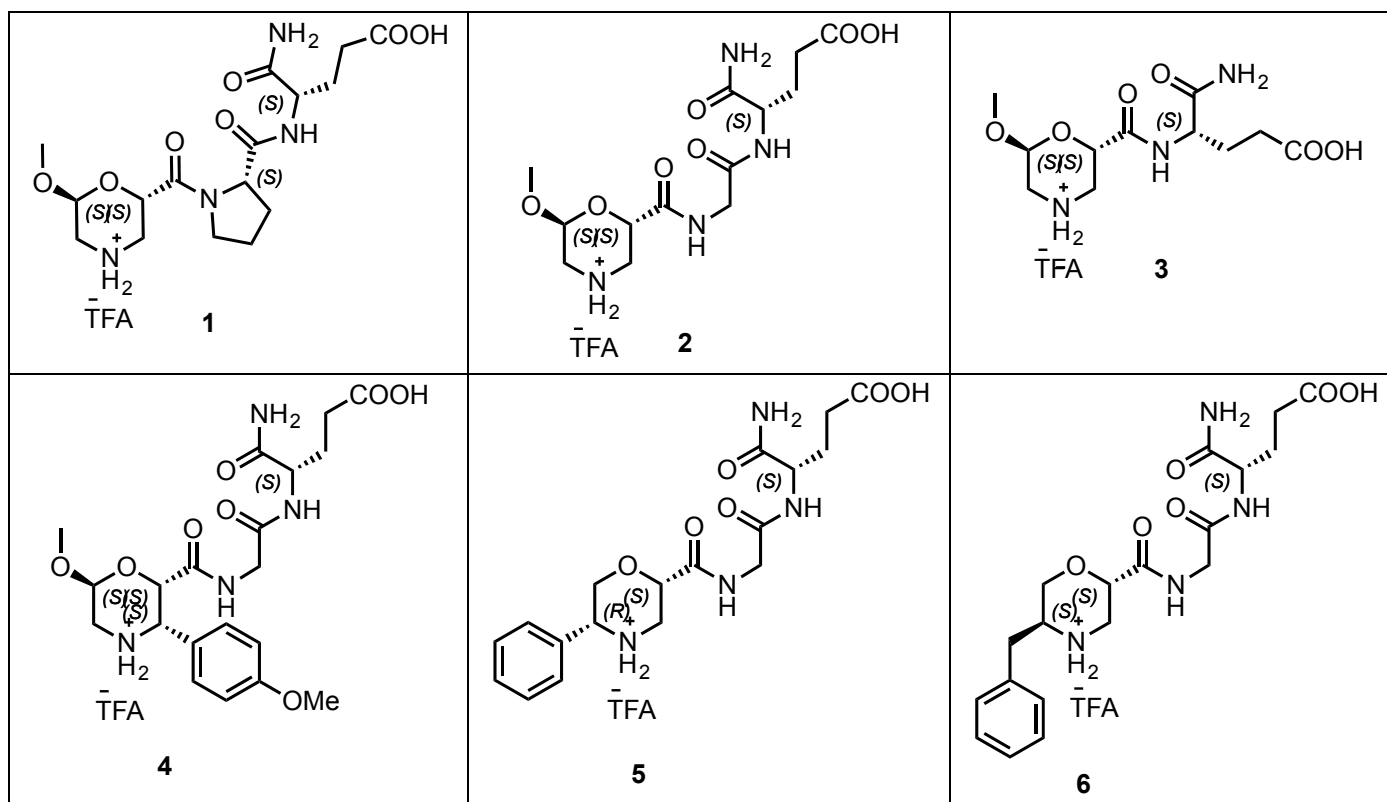


Scheme 13 General scheme for the synthesis of β-Morph AA 7a-d

Peptide Synthesis

The β-Morph AA scaffold (obtained as described above) has been used for the synthesis of the corresponding peptides derivative (Table 12).

Table 12 new peptide catalysts containing β-Morph AA scaffold



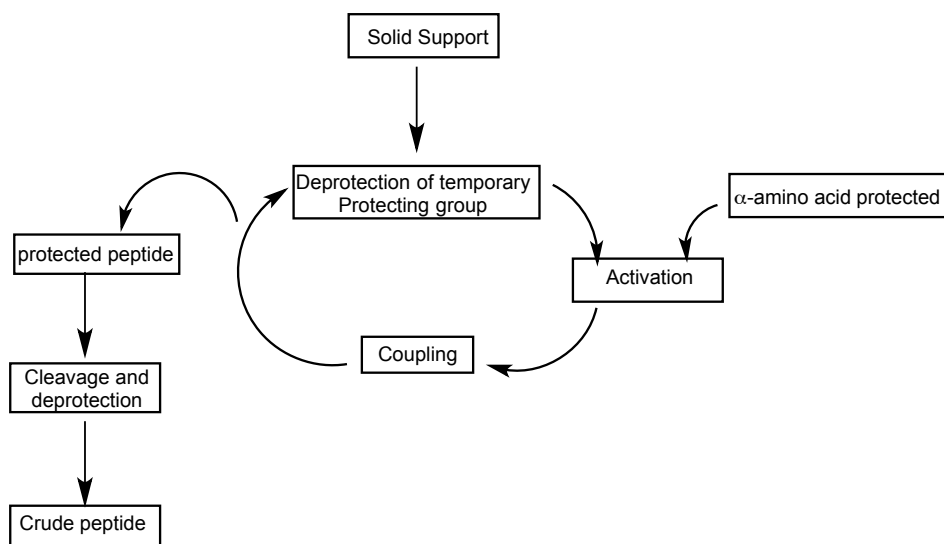
All peptides were prepared on solid phase synthesis (SPPS) using Rink Amide resin. The protocol for Fmoc/tBu peptide synthesis was followed according to the general procedures reported below (Scheme 14). The procedure is focused on the linkage of amino acid chains to a solid support, usually named resin or bead.

The first coupling starts from a N-protected amino acid linked to the resin from its carboxylic function and the synthesis proceed C → N terminus. Solid phase synthesis shows a lot of advantages compare to liquid synthesis: 1) reaction time are reduced, 2) it is easier to separate the main product from any remaining reagent, 3) yields are usually increase.

Coupling reaction are realized using DMF as solvent. In order to achieve the formation of the peptide bond, the carboxylic group needs to be activated. To promote the coupling reaction is activated into the corresponding activated ester. In our case 1-Ethyl-3-(3-dimethylaminopropyl)carbodiimide (EDC) and 1-Hydroxybenzotriazole (HOBT) resulted to be the best coupling reagents. The free amine from the elongating peptide chain can then attack the carbonyl and, displacing the activator group, form the peptide bond.

By-product generated during the reaction are soluble both in water and organic solvent and can therefore be easily eliminated.

Lastly, cleavage from the resin is carried out using a cleavage solution containing TFA and various scavenger as tri-isopropyl silane, thioanisole and phenol (to prevent cleaved protecting group can reacts with the peptide side chain).

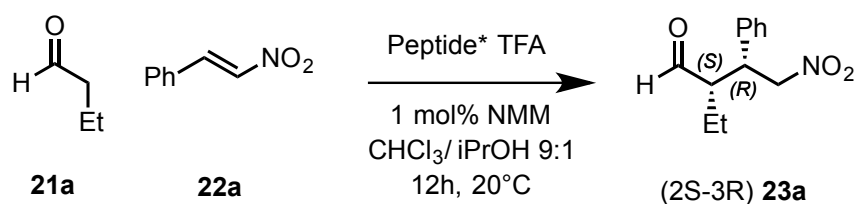


Scheme 14 Solid-Phase Peptide Synthesis (SPPS) general scheme

Organocatalyst Screening

Peptide organocatalysts

In a recent work published by Wennemers group, it was analyzed the catalytic effect of tripeptide sequences in a classical Michael reaction (Scheme 15). Theoretically two diastereomers can be obtained (*syn* and *anti* products), each of which is present as a pair of enantiomers.

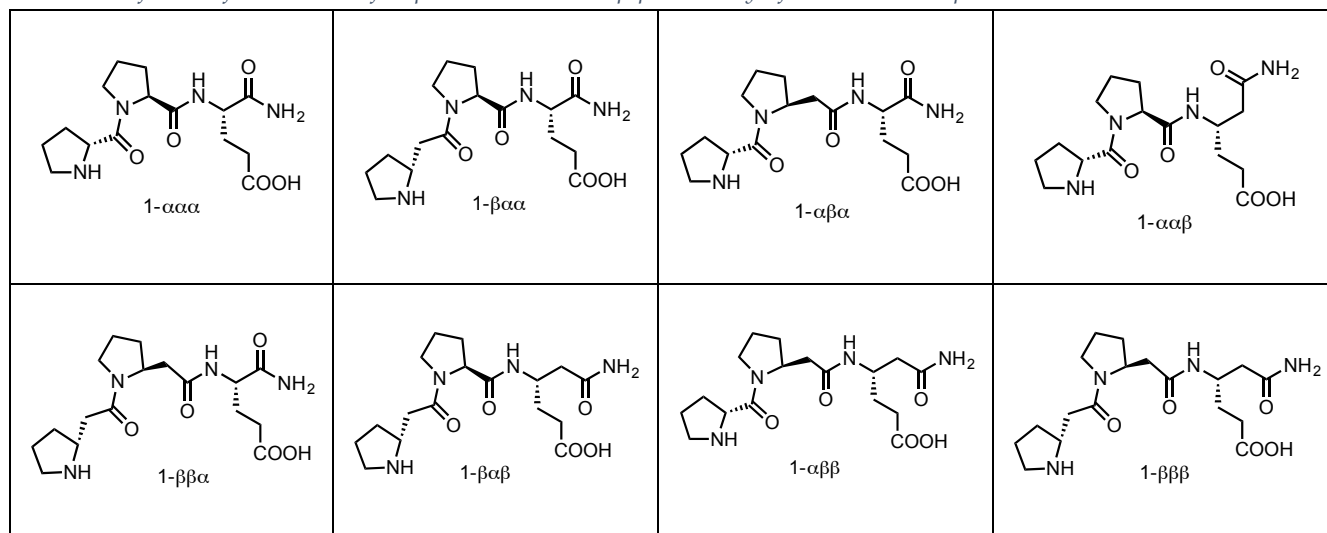


Scheme 15 General Micheal addiction reaction scheme

Several tripeptides catalysts were used containing α AAs (Pro and Glu) and/or β AAs (β Pro/ β Glu) exchanging the position of these AAs. This study showed that the replacement of the α - by a β -amino acid in the peptide catalyst is tolerated at the middle and C- terminus position but when located at N-terminus a severe negative effect on the stereoselectivity occurs. In particular, only when α -Pro is at the N-terminus a very good control of the enantioselection is achieved and excellent control was found by using H-DPro-Pro-Glu-NH₂

(1- $\alpha\alpha\alpha$) (Entry 1 Table 13).⁸² On the other hand, the presence of the β -Pro at N-terminus decrease dramatically the stereo control.

Table 13 Influence of substitution of α - β -amino acids in the peptidic catalyst for the reaction depicted in Scheme 15



Entry	Peptide	Conversion (%)	d.r (%)	e.e. (%)
1	1- $\alpha\alpha\alpha$	Quant.	98	97
2	1- $\beta\alpha\alpha$	81	85	-13
3	1- $\alpha\beta\alpha$	81	94	87
4	1- $\alpha\alpha\beta$	94	96	90
5	1- $\beta\beta\alpha$	96	85	-12
6	1- $\beta\alpha\beta$	85	5	4
6	1- $\alpha\beta\beta$	90	95	86
8	1- $\beta\beta\beta$	89	85	-14

Through computational analysis they understood how the inclusion of β -AAs in the structure of the catalyst **1- $\alpha\alpha\alpha$** at N-termini can drive the stereo selection of the proposed peptides (Figure 76a). As a matter of fact, the most flexible peptide conformation, due to the presence of more degree of β -AAs freedom, leads the generated enamine to be much further from the coordinating C-terminus. This loss of coordination negatively affects the selectivity of the catalyst (Figure 76b)

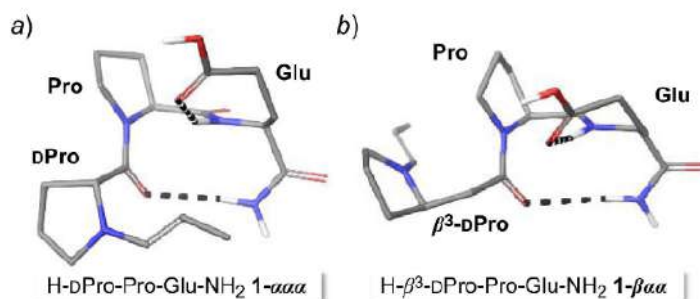


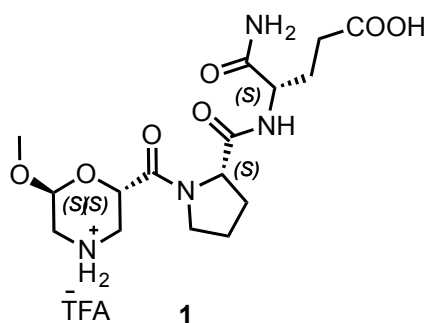
Figure 76 Lowest energy structures of the enamines from peptides 1- $\alpha\alpha\alpha$ and 1- $\beta\alpha\alpha$

To demonstrate that our β -Morph AAs could act as Pro-analogue in organo catalysis, analogues of tripeptide catalyst H-DPro-Pro-Glu-NH₂, bearing instead of the α -Pro or β -Pro at N-terminus our β -Morph AAs, were prepared and their reactivity and stereoselectivity was investigated in conjugate addition reactions of aldehydes to nitroolefins as reported in Scheme 15.

Using morpholine catalyst **1** the reaction was performed at the same conditions of the reference peptide catalyst **1- $\beta\alpha\alpha$** (Table 13, entry 2) to compare the reactivity of our catalysts.

The results obtained with our catalysts **1** showed a 70% conversion and a reversed selectivity [32% of enantiomeric excess in favor of (2S,3R)-enantiomer; Table 14; Entry 1]. Encouraged by this result, we performed the reaction changing solvents and temperature and by using 1% of the catalyst (Entries 2-5). Results showed quantitative conversion with enantiomeric excess (*e.e.*) between 28% and 42% and diastereomeric excess (*d.e.*) of 65%. The reaction was then tested at 15°C in CHCl₃/TFE 1:1 providing 50% of conversion but despite this, we found an increase of the enantiomeric and diastereomeric excess (Entry 6).

Table 14 Peptide **1** catalyzed conjugate addition reaction of butanal to (*E*)-nitrostyrene



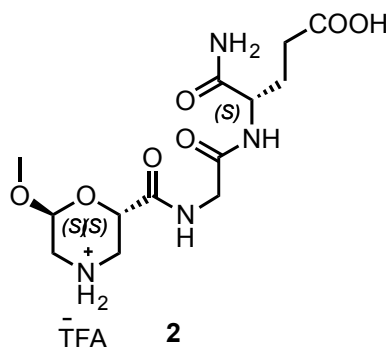
Entry	% Catalyst	Solvent	Time (h)	Temperature	Conversion ^(a)	<i>de</i> [%] ^(b)	<i>ee</i> [%] ^(b)
1	1%	CHCl ₃ /iPrOH 9:1	24h	25°C	70%	45%	32%

2	1%	CHCl ₃ /TFE 9:1	24h	40°C	Quant.	65%	42%
3	1%	CHCl ₃ /TFE 1:1	24h	40°C	Quant.	65%	41%
4	1%	ACN/TFE 9:1	24h	40°C	Quant.	65%	28%
5	1%	ACN/TFE 1:1	24h	40°C	Quant.	65%	33%
6	1%	CHCl ₃ /TFE 1:1	24h	15°C	50%	90%	47%

(a) Determinated by ¹H-NMR spectroscopy analysis of the crude reactions. (b) determinated by chiral stationary phase HPLC analysis.

Proline in position 2 was replaced with a Gly AA in order to provide a more conformational freedom of peptide (2) as shown in Table 15. A quantitative conversion was detected with catalyst 2 operating in different solvents and maintaining the temperature at 40 °C for 24 h (Entry 2). Moreover, the enantiomeric excess was a little bit improved in comparison with catalyst 1. More in general temperature and polar solvents are able to improve the yields, *d.e* and *e.e*. excess.

Table 15 Peptide 2 catalyzed conjugate addition reaction of butanal to (*E*)-nitrostyrene

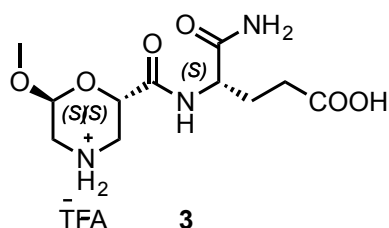


Entry	% Catalyst	Solvent	Time (h)	Temperature	Conversion ^(a)	<i>de</i> [%] ^(b)	<i>ee</i> [%] ^(b)
1	1%	CHCl ₃ /iPrOH 9:1	24 h	40°C	Quant.	72%	30%
2	1%	CHCl ₃ /TFE 9:1	24 h	40°C	92%	87%	45%
3	1%	CHCl ₃ TFE 1:1	24 h	40°C	Quant.	79%	51%
4	1%	ACN/TFE 9:1	24 h	40°C	97%	85%	24%
5	1%	ACN/TFE 1:1	24 h	40°C	Quant.	80%	45%
6	1%	ACN/HFIP 9:1	24 h	40°C	Quant.	80%	40%
7	1%	ACN/HFIP 1:1	24 h	40°C	Quant.	80%	50%
8	1%	HFIP	24 h	40°C	Quant.	80%	40%
9	1%	TFE	24 h	40°C	Quant.	80%	53%

(a) Determinated by ¹H-NMR spectroscopy analysis of the crude reactions. (b) determinated by chiral stationary phase HPLC analysis.

The synthesis of the dipeptide 3 was performed based on the theory that a shorter peptide would make the carboxylic function closer to the enamine intermediate, improving the coordination of nitrostyrene. As reported in Table 16, the results demonstrate that despite conversion remains high, there was a loss of enantioselectivity.

Table 16 peptide 3 catalyzed conjugate addition reaction of butanal to (E)-nitrostyrene



Entry	% Catalyst	Solvent	Time (h)	Temperature	Conversion ^(a)	<i>de</i> [%] ^(b)	<i>ee</i> [%] ^(b)
1	1%	CHCl ₃ /TFE 9:1	24 h	40°C	83%	83%	30%
2	1%	CHCl ₃ /TFE 1:1	24 h	40°C	Quant.	73%	40%
3	1%	ACN/TFE 9:1	24 h	40°C	83%	83%	16%
4	1%	ACN/TFE 1:1	24 h	40°C	Quant.	73%	34%
5	1%	ACN/HFIP 1:1	24 h	40°C	Quant.	80%	41%
6	1%	TFE	24 h	40°C	92%	73%	40%

(a) Determinated by ¹H-NMR spectroscopy analysis of the crude reactions. (b) determinated by chiral stationary phase HPLC analysis

In order to improve the *e.e.*, different bulky substituents were inserted on β -Morph AA ring. Tripeptides **4**, **5** and **6** were synthesized and in all of them the morpholino ring was functionalized with a bulky group in position 3 or 5 (Table 17)

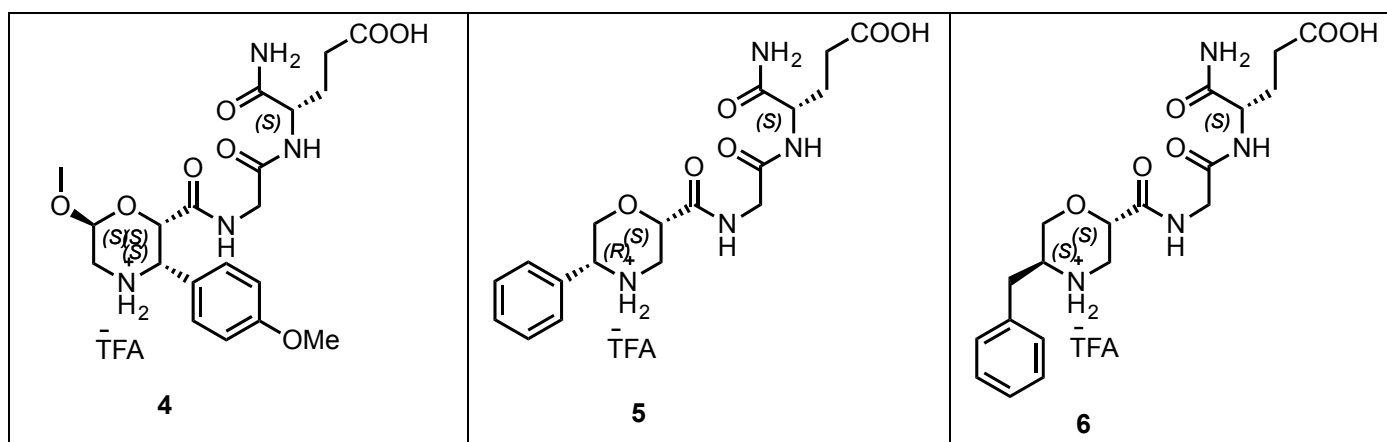
The reactions performed with catalyst **4** showed a significant reduction in term of selectivity (Table 17, Entries 1-5). The reduction of *e.e.* could be ascribed to the hindrance between the bulky substituent in position 3 and the carboxylic acid group of glutamic acid that probably prevent the coordination of the nitro group to the acidic function.

A bulky group in position 5 of morpholino ring in peptides **5** and **6** could avoid the coordination problem due to the aryl in position 3 of tripeptide **4**.

Results showed that catalyst **5** (Entries 6-7) gave the addition product with opposite stereochemistry. *2R,3S*-enantiomer was obtained but with low enantioselectivity.

The catalyst **6** (containing the benzyl group), was synthesized with the purpose of having a more freedom with respect to the phenyl one at C-5. For this catalyst we have the opposite stereochemistry at C-5 respect to catalyst **5** (Table 17). The results confirmed our theory (Entries 10-12) indeed, we obtain in general an enhancement of enantiomeric excess respect to catalyst **5**.

Table 17 Peptide 4,5 and 6 catalyzed conjugate addition reaction of butanal to (E)-nitrostyrene



Entry	Catalyst (%)	Solvent	Time (h)	Temperature	Conversion ^(a)	<i>de</i> [%] ^(b)	<i>ee</i> [%] ^(b)
1	4 (1%)	ACN	24h	40°C	80%	78%	6%
2	4 (1%)	CHCl ₃ /TFE 9:1	24h	40°C	89%	59%	rac.
3	4 (1%)	CHCl ₃ /TFE 1:1	24h	40°C	71%	36%	12%
4	4 (1%)	ACN/TFE 9:1	24h	40°C	77%	31%	2%
5	4 (1%)	ACN/HFIP 1:1	24h	40°C	85%	45%	5%
6	5 (1%)	THF/H ₂ O 1:1	24h	40°C	66%	76%	-20%
7	5 (1%)	CHCl ₃ /TFE 1:1	24h	40°C	73%	89%	-30%
8	6 (1%)	CHCl ₃ / <i>i</i> PrOH 9:1	24h	40°C	95%	81%	30%
9	6 (1%)	CHCl ₃ /TFE 1:1	24h	40°C	Quant.	54%	44%
10	6 (1%)	TFE	24h	40°C	Quant.	46%	27%
11	6 (1%)	ACN/HFIP 1:1	24h	40°C	Quant.	51%	58%
12	6 (1%)	HFIP	24h	40°C	80%	42%	44%

(a) Determinated by ¹H-NMR spectroscopy analysis of the crude reactions. (b) determined by chiral stationary phase HPLC analysis. A minus sign indicates that the (2*R*,3*S*) enantiomer was predominantly formed

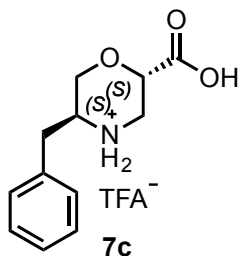
In conclusion, the analysis of this small library of tripeptides **1-7**, containing different morpholino scaffolds at *N*-terminus, confirms that the majority of them gives a quantitative conversion of reagents into the condensation product as mixture of 2*R*,3*S* and 2*S*,3*S* enantiomers. It is to point out that the presence of acidic protons of the solvent is fundamental for achieve good yields. In general, except for catalyst **4**, a satisfactory diastereoselection was obtained ranging from 80 to 90% in favor of syn product. Last but not least, it is possible to obtain the syn condensation products with opposite stereochemistry by playing with the stereochemistry of the bulky group in position 5 of the morpholino ring (see catalysts **5** and **6**). More in general, using our β-Morph AAs we are able to obtain better *ee* in comparison with 1-β $\alpha\alpha$ Wennemers catalyst (Entry 2, Table 13).

Amino acids organocatalysts

At this point we decide to simplify further the catalyst in order to remove the variability of the peptide side chain. Different catalysts containing only the β -Morph scaffold were prepared, characterized by different bulky groups at C-5 and different stereochemistries at both stereocenters.

The catalyst **7c**, bearing benzyl group in 5 and free carboxylic acid in 2 with opposite stereochemistry (Table 18), was tested in the above model reaction and showed surprising results.

Table 18 Catalyzed conjugate addition reaction of butanal to (*E*)-nitrostyrene



Entry	% Catalyst	Solvent	Time (h)	Temperature	Conversion ^(a)	<i>de</i> [%] ^(b)	<i>ee</i> [%] ^(b)
1	1%	CHCl ₃ /TFE 1:1	24h	40°C	Quant.	62%	58%
2	1%	ACN/HFIP 1:1	24h	40°C	Quant.	70%	59%
3	1%	ACN	24h	40°C	72%	56%	48%

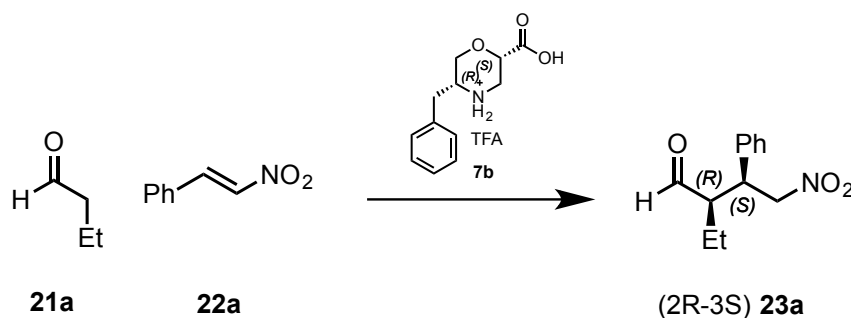
As reported in Table 18, the desiderate addition product was obtained even if peptide side chain is absent. From these results it seems that the peptidic side chain it is not necessary in the catalytic cycle influencing the formation of 2*S*,3*R*-enantiomer as the major one.

The catalyst **7b** (Table 19) was synthesized with opposite stereochemistry at C-5 to demonstrate that the difference in enamine's face hinderance provides a different enantiomer. Our hypothesis was confirmed and enantiomer 2*R*,3*S* was obtained

At the beginning the reaction was conducted with solvents previously investigated and 1% of catalyst (Table 19). Quantitative yields and high selectivity were obtained (Entries 2-3). Then, the reaction was conducted in *i*PrOH, giving a quantitative conversion as other solvents and 55% of e.e. (Entry 5). Trying to improve the selectivity, the reactions was tested at 0°C (Entries 6-7). Results showed that, despite a reduction in conversion, an improvement

in enantioselectivity was achieved especially with *i*PrOH. As reported in Entry 8 an increase of enantioselectivity was obtained. Motivated by these results, we investigated the reaction at lower temperature to confirm that it could favour an improvement of diastereo- and enantioselectivity. Only *i*PrOH showed a further increase in selectivity reaching 96% of *d.e.* and 92% of *e.e.* (Entry 11). *i*PrOH has been chosen as best solvent at -10°C giving the desiderate product with higer diastereo and enantioselectivity (Entry 11).

Table 19 Catalyst **7b** catalyzed conjugate addition reaction of butanal to (*E*)-nitrostyrene

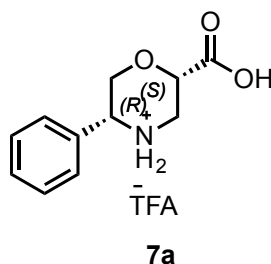


Entry	% Catalyst	Solvent	Time (h)	Temperature	Conversion ^(a)	<i>de</i> [%] ^(b)	<i>ee</i> [%] ^(b)
1	1%	ACN	12 h	40 °C	Quant.	49%	31%
2	1%	CHCl ₃ /TFE 1:1	12 h	40 °C	Quant	66%	52%
3	1%	ACN/HIFP	12 h	40 °C	Quant.	65%	67%
4	1%	Toluene	12 h	40 °C	Quant.	69%	32%
5	1%	<i>i</i> PrOH	12 h	40 °C	Quant.	74%	55%
6	1%	CHCl ₃ /TFE 1:1	12 h	0°C	86%	86%	65%
7	1%	ACN/HIFP	12 h	0°C	91%	92%	72%
8	1%	<i>i</i> PrOH	12 h	0°C	Quant	87%	80%
9	1%	CHCl ₃ /TFE 1:1	24 h	-10°C	88%	89%	60%
10	1%	ACN/HIFP	24 h	-10°C	93%	93%	75%
11	1%	<i>i</i> PrOH	24 h	-10°C	96%	96%	92%

(a) Determinated by ¹H-NMR spectroscopy analysis of the crude reactions. (b) determinated by chiral stationary phase HPLC analysis. A minus sign indicates that the (2*R*,3*S*) enantiomer was predominantly formed

Inspired by the very good results achieved with catalyst **7c**, we wanted to evaluate the role of the bulky group in position 5. The benzyl substituent was replaced by a phenyl group (catalyst **7a**) in order to decrease the freedom of the substituent C-5 (Table 20). Results show small reduction in conversion and diastereo selection (Entry 4) but lost of enantio selection.

Table 20 Addition reaction of butanal to (*E*)-nitrostyrene using catalyst **7a**



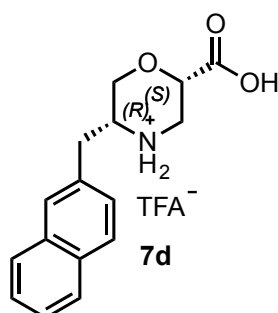
Entry	% Catalyst	Solvent	Time (h)	Temperature	Conversion ^(a)	<i>de</i> [%] ^(b)	<i>ee</i> [%] ^(b)
1	1%	CHCl ₃ /TFE	12h	40°C	84%	72%	21%
2	1%	ACN/HFIP 1:1	12h	40°C	83%	70%	24%
3	1%	ACN	12h	40°C	81%	70%	10%
4	1%	iPrOH	24h	-10°C	10%	99%	39%

(a) Determinated by ¹H-NMR spectroscopy analysis of the crude reactions. (b) determinated by chiral stationary phase

In a third step we test the catalyst **7d** characterized by freedom as catalysts **7b** but with an extended aromatic system (Table 21).

The reaction was carried out in iPrOH, that turned out to be an excellent solvent. The time was prolonged from 12h to 24-48h to increase the conversation. At first, we performed the reaction at 0°C with 1% of catalyst giving a 55% of yield (that is a substantial reduction from conversion with respect catalyst **7b**) and 73% of enantioselectivity with 99% of diastereo selectivity (Entry 1). Then the reaction was performed increasing the amount of the catalyst (5%) at -10°C for 48h that provided a quantitative conversion and 80% of enantioselectivity and 90% of diastereo selectivity (Entry 2).

Table 21 Conjugate addition reaction of butanal to (*E*)-nitrostyrene using catalyst **7d**



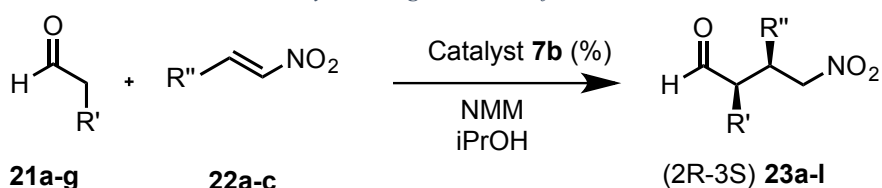
Entry	% Catalyst	Solvent	Time (h)	Temperature	Conversion ^(a)	<i>de</i> [%] ^(b)	<i>ee</i> [%] ^(b)
1	1%	iPrOH	24h	0° C	55%	99%	73%
2	5%	iPrOH	48h	-10 °C	Quant.	90%	80%

(a) Determinated by ¹H-NMR spectroscopy analysis of the crude reactions. (b) determinated by chiral stationary phase HPLC analysis.

In conclusion, compound **7b** is the best candidate as organocatalyst for the studied reaction between aldehydes and nitrostyrenes. *i*PrOH was found to be the perfect solvent and different temperatures were tried. In particular, when the reactions were carried out at 40 °C, the conversion was found to be quantitative in almost all the cases, however worse *e.e.* were observed. On the other hand, the enantioselectivity increased when the reactions were set up in a range of temperature between 0 and -10 °C.

At this point using our best catalyst **7b** we oriented our work expanding the scope of aldehyde and nitroolefin. The influence of the steric effect of aldehyde was investigated. The reaction was then performed using propanal (Table 22). The reaction was performed at -10°C, 1% of catalyst providing a quantitative conversion, 73% *e.e.*, and 90% *d.e.* (Entry 1). Considering the excellent conversion, we investigated if less amount of catalyst would provide good yield and selectivity. The reaction performed with 0.5% of catalyst demonstrates that this amount wasn't enough to provide good selectivity (Entry 2).

Table 22 Conjugate addition reactions between aldehydes **21a-g** and nitroolefins **22a-c**



Entry	21 a-g	22 a-c	Product 23 a-l Conversion (%)	Catalyst %	Time (h)	<i>d.e.</i> (%) ^[b]	<i>e.e.</i> (%) ^[c]
1	b = R':Me	a = R'':Ph	23 b Quant%	1%	24 h	90	72
2	b = R':Me	a = R'':Ph	23 b Quant%	0.5%	24h	94	73
3	a = R':Et	a = R'':Ph	23 a Quant%	1%	24h	99	92
4	c = R': <i>n</i> Pr	a = R'':Ph	23 c 90%	1%	48h	99	99
5	d = R': <i>i</i> Pr	a = R'':Ph	23 d	1%	48h	99	99

			68%				
6	d = R': <i>i</i> Pr	a = R'':Ph	23 d 91%	5%	48h	94	93
7	e = R': <i>n</i> Bu	a = R'':Ph	23 e 52%	1%	24h	98	78
8	e = R': <i>n</i> Bu	a = R'':Ph	23 e 60%	1%	48h	99	87
9	f = R':CH ₂ Ph	a = R'':Ph	23 f 40%	1%	48h	99	88
10	f = R':CH ₂ Ph	a = R'':Ph	23 f 76%	5%	48h	89	82
11	g = R': cyclopentyl	a = R'':Ph	23 g 53%	* 5%	48h*	-	30
12	b = R':Me	b = R'': <i>p</i> OMe-Ph	23 h Quant%	1%	48h	91	80
13	c = R': <i>n</i> Pr	b = R'': <i>p</i> OMe-Ph	23 i 74%	1%	48h	99	66
14	c = R': <i>n</i> Pr	b = R'': <i>p</i> OMe-Ph	23 i 74%	5%	48h	98	70
15	b = R':Me	c = R'': tiophenyl	23 l Quant.	1%	48h	89	67

Reaction condition: Aldehyde (1.0 eq.)/Nitrostyrene (1.5 eq.)/NMM (2% mol) [a] Conversion was determined by ¹H NMR of crude mixture. [b] d.e. was determined by ¹H NMR of crude mixture. [c] Enantioselectivities were determined by chiral HPLC analysis in comparison with authentic racemic material. * Entry 11 The reaction was performed at 40 °C

Then pentanal was used in order to test the reactivity of an aldehyde with a longer aliphatic chain. With 1% of catalyst we were able to obtain conversion of 90%, 99% of *d.e.* and 99% of

e.e. (Entry 4, Table 22). This result showed an increase of the enantioselectivity respect to previously listed aldehydes.

Other branched aldehydes were tested, i.e. isovaleraldehyde (Entries 5-6), a structural isomer of pentanal. With 1% of catalyst **7b** the reaction was performed with a temperature of -10°C for 48h, and results showed a 68% of conversion with an excellent 99% of enantiomeric and diastereomeric excess (Entry 5). To confirm the excellent results and trying to improve yields of the reaction we used 5% of catalyst of at -10°C for 48h but this setting of reaction didn't show an increase of yield and affected a little the selectivity (Entry 6).

The reaction with Hexanal as aldehyde was performed in order to investigate the effect of a higher hindered aldehyde (Entries 7-8 Table 22). At the beginning, the reaction with 1% of catalyst was conducted at 0°C for 24h and provided a low conversion (52%) with respect to results presented above, a discrete enantiomeric excess (78%) and excellent diastereomeric excess (98%) (Entry 7). The reaction was performed at -10°C for 48h and the results shows an increasing of enantiomeric excess (87%), a constant diastereomeric excess of 99% but a small increase in yield (Entry 8).

Aldehyde bearing an aromatic chain was tested in order to investigate the influence of an aromatic substituent (Entries 9-10). The reaction was performed at -10°C for 48h giving a 40% of conversion and high selectivity (Entry 9). Increasing the amount of catalyst to 5% (Entry 10) gave similar results.

To expand the scope of the reaction, we tested cyclopentanecarbaldehyde. We introduced a ramification in α position to study the effect of an increased steric hinderance near to the site of generation of enamine. The reaction carried out at -10°C at 0°C in 24 h showed absence of reactivity with catalyst **7b**. Only when temperature was increased to 40°C for 48h with 5% of catalyst, a 53% of yield was achieved (Entry 11). The low yield could be attributed to the high stability of the enamine intermediate⁸⁰ that react very slowly with nitrostyrene to provide the desiderated product.

At this point we moved to study how different nitroolefins could influence the reaction (Table 12 Entry 12). First, we tested propanal with an electro donating group a nitrostyrene, i.e. a methoxy group in para-position.

The same olefin was investigated with pentanal (Entry 13-14) to confirm the above positive results. The reaction with 1% of catalyst at -10°C provide a conversion of 52%, excellent *d.e.* and 66% *e.e.* (Entry 13). Again, the increase of the catalyst (5%) does not benefit the reaction (Entry 14) both for conversion and selectivity.

Finally, the electrophile was then subject to a radical modification with the introduction of the strongly electron-rich thiophen instead of an aryl and its reactivity was studied with Propionaldehyde (Entry 15). The reaction performed with 1% of catalyst for 24h at -10°C showed reduction in yield and selectivity with respect the reaction with the classical nitrostyrene.

In conclusion, we confirmed the possibility of using β -Morph as proline analogue in catalytic applications despite all the disadvantages previously reported. we were able to obtain a series of catalysts with a simple synthetic pathway and achievable from commercially available α -AA. Through the study of different functionalization/stereochemistry of the catalyst, we understood how to obtain the highest performing catalyst and the desired product. Their use in the above-mentioned Michael reaction provided high yields of the adduct with a strong control of diastereo- and enantioselectivity. In addition, we investigated a broad spectrum of expanding the scope of the studied reaction.

Experimental part

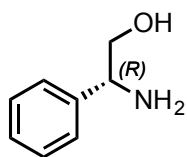
General information

Chemicals were purchased from Sigma Aldrich and were used without further purification. Mass spectra were recorded on an LCQESI MS and on an LCQ Advantage spectrometer from Thermo Finnigan and a LCQ Fleet spectrometer from Thermo Scientific. The NMR spectroscopic experiments were carried out either on Varian MERCURY 300 MHz (300 and 75 MHz for ^1H and ^{13}C , respectively), or Bruker Avance I 500 MHz spectrometers (500 and 125 MHz for ^1H and ^{13}C , respectively). Optical rotations were measured on a Perkin-Elmer 343 polarimeter at 20 °C (concentration in g/100 mL). Chemical shifts (δ) are given in ppm relative to the CHCl_3 internal standard, and the coupling constants J are reported in Hertz (Hz). The synthesis of compound **12**³⁵ and **14**⁴² are reported in the literature.

General procedure for amino alcohol synthesis

A1-L three-neck round-bottom flask was fitted with a magnetic stirring bar, a reflux condenser, and an addition funnel. The flask was charged with (2.5 equiv.) sodium borohydride in THF. Amino acid (2.5 equiv.) was added in one portion. The remaining neck was sealed with a septum and nitrogen line attached, and the flask was cooled to 0 °C in an ice bath. A solution of iodine (1 equiv.) dissolved in THF was poured into the addition funnel and added slowly and dropwise over 30 min resulting in vigorous evolution of hydrogen. After addition of the iodine was complete and gas evolution had ceased, the flask was heated to reflux for 18 h and then cooled to room temperature. MeOH was added cautiously until the mixture became clear. After stirring 30 min, the solvent was removed by rotary evaporation leaving a white paste which was dissolved by addition of 20% aqueous KOH. The solution was stirred for 4 h and extracted three times with CH₂Cl₂. The organic extracts were dried over sodium sulfate and concentrated in vacuo, affording a white semisolid. The crude material was recrystallized from toluene to afford the final amino alcohol as colorless crystals.

Synthesis of (R)-2-amino-2-phenylethan-1-ol (16a)



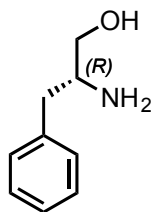
Yield: 60%

¹H NMR (400 MHz, CDCl₃) δ 7.59 – 7.12 (m, 5H), 4.07 (dd, *J* = 8.3, 4.4 Hz, 1H), 3.76 (dd, *J* = 10.8, 4.4 Hz, 1H), 3.58 (dd, *J* = 10.8, 8.3 Hz, 1H).

¹³C NMR (101 MHz, CDCl₃) δ 142.7, 128.6, 127.5, 126.4, 68.0, 57.3.

m/z [M]⁺ Calcd for C₁₄H₁₄O 198.10; Found 198.15

Synthesis of (R)-2-amino-3-phenylpropan-1-ol (16b)



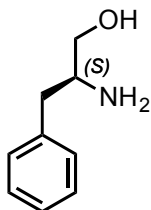
Yield: 91%

^1H NMR (400 MHz, CDCl_3) δ 7.92 – 6.40 (m, 5H), 3.66 (dd, $J = 10.7, 3.9$ Hz, 1H), 3.41 (dd, $J = 10.7, 7.2$ Hz, 1H), 3.21 – 3.07 (m, 1H), 2.82 (dd, $J = 13.5, 5.2$ Hz, 1H), 2.55 (dd, $J = 13.5, 8.6$ Hz, 1H), 2.03 (s, 1H).

^{13}C NMR (101 MHz, CDCl_3) δ 138.7, 129.2, 128.6, 126.4, 66.3, 54.2, 40.8.

m/z $[\text{M}+\text{Na}]^+$ Calcd for $\text{C}_9\text{H}_{13}\text{NO}$ 174.10; Found 174.13

Synthesis of (R)-2-amino-3-phenylpropan-1-ol (16c)



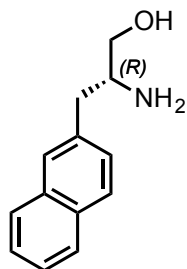
Yield: 58%

¹H NMR (400 MHz, CDCl₃) δ 7.62 – 6.77 (m, 5H), 3.66 (dd, J = 10.7, 3.8 Hz, 1H), 3.42 (dd, J = 10.7, 7.2 Hz, 1H), 3.24 – 3.00 (m, 1H), 2.82 (dd, J = 13.5, 5.2 Hz, 1H), 2.55 (dd, J = 13.5, 8.6 Hz, 1H), 2.16 (s, 3H).

¹³C NMR (101 MHz, CDCl₃) δ 138.6, 129.2, 128.6, 126.4, 66.1, 54.2, 40.7.

m/z [M+Na⁺]⁺ Calcd for C₉H₁₃NO 174.10; Found 174.11

Synthesis of (R)-2-amino-3-(naphthalen-2-yl)propan-1-ol (16d)



Yield:55%

$^1\text{H NMR}$ (300 MHz, CDCl_3) δ 7.89 – 7.71 (m, 3H), 7.64 (m, 1H), 7.54 – 7.39 (m, 2H), 7.33 (dd, $J = 8.3, 1.8$ Hz, 1H), 3.67 (dd, $J = 10.6, 3.9$ Hz, 1H), 3.44 (dd, $J = 10.6, 7.1$ Hz, 1H), 3.33 – 3.13 (m, 1H), 2.96 (dd, $J = 13.2, 5.1$ Hz, 1H), 2.68 (dd, $J = 13.2, 8.7$ Hz, 1H), 2.04 (s, 2H).

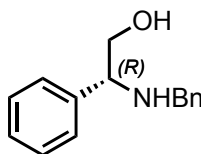
$^{13}\text{C NMR}$ (75 MHz, CDCl_3) δ 136.2, 133.5, 132.2, 128.2, 127.6, 127.6, 127.5, 127.4, 126.1, 125.4, 66.4, 54.0, 41.0.

m/z $[\text{M}^+]^+$ Calcd for $\text{C}_{13}\text{H}_{15}\text{NO}$ 201.12; Found 201.13

General procedure for Benzyl-amino alcohol synthesis (17a-d)

A solution of amino alcohol (mmol 1 equiv.) and benzaldehyde (1.3 equiv.) in absolute MeOH was stirred at 20 °C for 2 h. NaBH₄ (3 equiv.) was added at 0 °C, and stirring was continued for 1 h. CH₂Cl₂ and saturated aq. NH₄Cl were added, and the layers were separated. After extraction of the aqueous layer with CH₂Cl₂, the combined organic layers were washed with brine, dried with Na₂SO₄, and the solvent was removed in vacuo. The solvent was removed in vacuo, and the crude material was purified by flash column chromatography (*n*hexane/AcOEt,0-100%) affording pure compound as a white solid.

Synthesis of (R)-2-(benzylamino)-2-phenylethan-1-ol (17a)



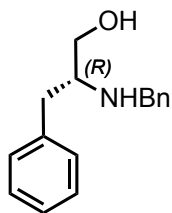
Yield: 85%

¹H NMR (300 MHz, CDCl₃) δ 7.89 – 7.71 (m, 3H), 7.64 (m, 1H), 7.54 – 7.39 (m, 2H), 7.33 (dd, *J* = 8.3, 1.8 Hz, 1H), 3.67 (dd, *J* = 10.6, 3.9 Hz, 1H), 3.44 (dd, *J* = 10.6, 7.1 Hz, 1H), 3.33 – 3.13 (m, 1H), 2.96 (dd, *J* = 13.2, 5.1 Hz, 1H), 2.68 (dd, *J* = 13.2, 8.7 Hz, 1H), 2.04 (s, 2H).

¹³C NMR (75 MHz, CDCl₃) δ 136.2, 133.5, 132.2, 128.2, 127.6, 127.6, 127.5, 127.4, 126.1, 125.4, 66.4, 54.0, 41.0.

m/z [M⁺]⁺ Calcd for C₁₅H₁₇NO 227.13; Found 227.16

Synthesis of (R)-2-(benzylamino)-3-phenylpropan-1-ol (17b)



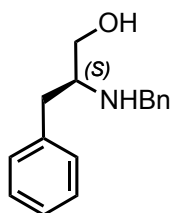
Yield: 56%

^1H NMR (400 MHz, CDCl_3) δ 7.62 – 6.81 (m, 10H), 3.81 (s, 2H), 3.68 (dd, $J = 10.8, 3.9$ Hz, 1H), 3.38 (dd, $J = 10.8, 5.3$ Hz, 1H), 3.00 (m, 1H), 2.82 (qd, $J = 13.6, 7.0$ Hz, 2H), 2.20 (s, 1H).

^{13}C NMR (101 MHz, CDCl_3) δ 139.9, 138.4, 129.2, 128.6, 128.5, 128.0, 127.1, 126.4, 62.4, 59.3, 51.1, 38.1

m/z $[\text{M}+\text{Na}]^+$ Calcd for $\text{C}_{16}\text{H}_{19}\text{NO}$ 264.15; Found 264.16

Synthesis of (S)-2-(benzylamino)-3-phenylpropan-1-ol (17c)



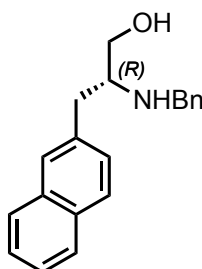
Yield: 64%

^1H NMR (400 MHz, CDCl_3) δ 7.62 – 6.95 (m, 5H), 3.81 (s, 2H), 3.68 (dd, $J = 10.8, 3.9$ Hz, 1H), 3.38 (dd, $J = 10.8, 5.3$ Hz, 1H), 3.05 – 2.94 (m, 1H), 2.91 – 2.73 (m, 2H), 2.17 (s, 2H).

^{13}C NMR (101 MHz, CDCl_3) δ 140.0, 138.4, 129.2, 128.6, 128.5, 128.0, 127.1, 126.4, 62.5, 59.3, 51.1, 38.1.

m/z $[\text{M}+\text{Na}]^+$ Calcd for $\text{C}_{16}\text{H}_{19}\text{NO}$ 264.15; Found 264.16

Synthesis of (*R*)-2-(benzylamino)-3-(naphthalen-2-yl)propan-1-ol (17d)



Yield: 80%

$^1\text{H NMR}$ (400 MHz, CDCl_3) δ 7.90 – 7.77 (m, 3H), 7.64 (s, 1H), 7.55 – 7.45 (m, 2H), 7.36 – 7.20 (m, 6H), 3.83 (s, 2H), 3.72 (dd, $J = 10.8, 3.8$ Hz, 1H), 3.44 (dd, $J = 10.8, 5.1$ Hz, 1H), 3.11 (m, 1H), 3.00 (m, 2H), 2.28 (s, 2H).

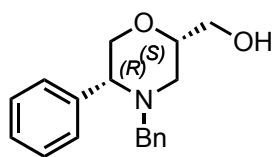
$^{13}\text{C NMR}$ (101 MHz, CDCl_3) δ 139.8, 135.9, 133.5, 132.2, 128.5, 128.2, 128.0, 127.6, 127.6, 127.53, 127.5, 127.1, 126.1, 125.5, 62.4, 59.2, 51.1, 38.2.

m/z $[\text{M}^+]^+$ Calcd for $\text{C}_{20}\text{H}_{21}\text{NO}$ 291.16 Found 291.15

General procedure for benzyl-morpholino amino alcohol synthesis (18a-d)

A solution of the amino alcohol (1 equiv.) in absolute toluene was treated with (R)-epi-chlorohydrin, (1.3 equiv.) and LiClO₄ (1.3 equiv.). After 24h at 60°C, NaOMe (25%v/v in MeOH) (2.5 equiv.) were added and stirring was continued for 24h. The reaction mixture was quenched with saturated aq. NH₄Cl, and the aqueous layer was extracted with EtOAc. The combined organic layers were extracted with brine, dried with Na₂SO₄, and the solvent was removed in vacuo. Chromatographic purification (silica gel; Et₂O/hexanes, 50:50) delivered the desired as transparent oil.

Synthesis of ((2S,5R)-4-benzyl-5-phenylmorpholin-2-yl)methanol (18a)



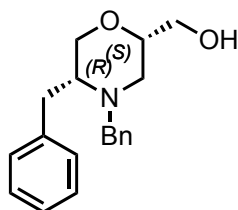
Yield 66%

¹H NMR (400 MHz, CDCl₃) δ 7.48 (m, 2H), 7.43 – 7.36 (m, 2H), 7.33 (m, 3H), 7.29 – 7.22 (m, 3H), 4.23 (dd, *J* = 11.7, 7.3 Hz, 1H), 4.05 (dd, *J* = 11.8, 9.3 Hz, 1H), 3.90 (m, 1H), 3.83 – 3.69 (m, 3H), 3.53 (dd, *J* = 9.3, 3.8 Hz, 1H), 3.06 (s, 1H), 2.93 (d, *J* = 13.4 Hz, 1H), 2.85 (dd, *J* = 12.1, 2.6 Hz, 1H), 2.52 (dd, *J* = 12.1, 4.1 Hz, 1H), 1.61 (s, 1H).

¹³C NMR (101 MHz, CDCl₃) δ 138.8, 137.9, 128.7, 128.6, 128.4, 128.0, 127.1, 73.2, 68.2, 66.7, 63.7, 59.1, 51.6.

m/z [M+Na]⁺ Calcd for C₁₈H₂₁NO₂Na 306.20 Found 307.19

Synthesis of ((2S,5R)-4,5-dibenzylmorpholin-2-yl)methanol (18b)



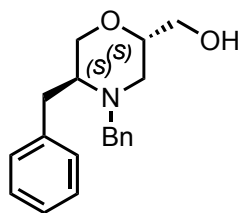
Yield 75%

^1H NMR (400 MHz, CDCl_3) δ 7.44 – 7.08 (m, 10H), 3.82 (dd, $J = 31.4, 13.3$ Hz, 2H), 3.76 – 3.69 (m, 2H), 3.68 – 3.65 (m, 2H), 3.61 (ddd, $J = 11.2, 2.7, 1.2$ Hz, 1H), 3.03 – 2.89 (m, 2H), 2.85 – 2.77 (m, 1H), 2.65 (dd, $J = 11.6, 10.2$ Hz, 1H), 2.50 (dd, $J = 11.7, 2.9$ Hz, 1H) 2.1(s, 1H).

^{13}C NMR (101 MHz, CDCl_3) δ 140.0, 138.4, 129.4, 128.8, 128.4, 128.4, 127.2, 125.9, 76.1, 67.6, 64.2, 59.1, 59.0, 47.9, 28.0.

m/z $[\text{M}^+]$ Calcd for $\text{C}_{19}\text{H}_{23}\text{NO}_2$ 297.17 Found 297.16

Synthesis of ((2S,SR)-4,5-dibenzylmorpholin-2-yl)methanol (18c)



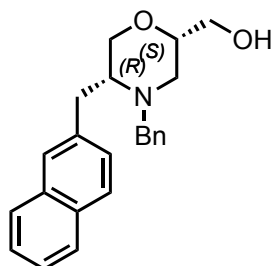
Yield 67%

¹H NMR (400 MHz, CDCl₃) δ 7.45 – 7.16 (m, 10H), 4.37 (d, *J* = 13.4 Hz, 1H), 3.73 (dd, *J* = 11.4, 3.3 Hz, 1H), 3.65-3.60 (m, 1H), 3.57-3.40 (m, 3H), 3.27 (dd, *J* = 13.9, 4.0 Hz, 1H), 3.20 (d, *J* = 13.4 Hz, 1H), 2.15 (s, 1H), 2.06 (dd, *J* = 11.6, 10.3 Hz, 1H).

¹³C NMR (101 MHz, CDCl₃) δ 138.4, 138.3, 129.1, 129.0, 128.5, 128.4, 127.1, 126.3, 76.1, 70.8, 64.0, 61.2, 58.4, 53.4, 36.1.

m/z [M⁺]⁺ Calcd for C₁₉H₂₃NO₂ 297.17 Found 297.16

Synthesis of ((2S,5R)-4-benzyl-5-(naphthalen-2-ylmethyl)morpholin-2-yl)methanol (18d)



Yield 68%

^1H NMR (400 MHz, CDCl_3) δ 7.85 – 7.72 (m, 3H), 7.60 (s, 1H), 7.52 – 7.30 (m, 7H), 7.22 (dd, J = 8.4, 1.6 Hz, 1H), 3.88 (dd, J = 34.7, 13.3 Hz, 2H), 3.80 – 3.67 (m, 3H), 3.65 – 3.59 (m, 2H), 3.13 (m, 2H), 2.92 (d, J = 10.6 Hz, 1H), 2.70 (m, 1H), 2.54 (dd, J = 11.7, 2.8 Hz, 1H), 2.08 (s, 1H).

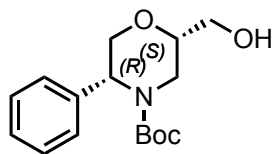
^{13}C NMR (101 MHz, CDCl_3) δ 138.4, 137.5, 133.5, 131.9, 128.8, 128.4, 128.0, 127.8, 127.8, 127.6, 127.3, 127.3, 126.0, 125.2, 76.2, 67.6, 64.3, 59.1, 59.0, 47.9, 28.1.

m/z $[\text{M}^+]^+$ Calcd for $\text{C}_{23}\text{H}_{25}\text{NO}_2$ 347.19 Found 347.19

General procedure for Boc-morpholino amino alcohol synthesis (19a-d)

Operating in a round-bottom flask equipped with magnetic stirrer, compound (1 equiv.) was dissolved in THF. Boc₂O (1.05 equiv.) and Pd/C (10% loading) were added to the solution. The suspension was stirred under H₂ (1 atmosphere) at 25 °C. After 24 h, the mixture was filtered on Celite pad. The solvent was evaporated, and the yellow oil was dissolved in CH₂Cl₂ washed with a 5% solution of KH₂O₄ and a saturated solution of NaCl. The organic layer was dried over Na₂SO₄, filtered and concentrated in vacuum. The purification of the crude by flash chromatography (*n*hexane / AcOEt, 1:1) afforded product as colorless oil.

Synthesis of tert-butyl (2S,5R)-2-(hydroxymethyl)-5-phenylmorpholine-4-carboxylate (19a)



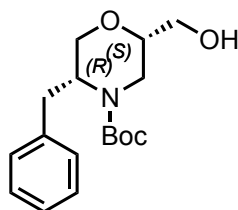
Yield 87%

¹H NMR (400 MHz, CDCl₃) δ 7.45 (d, *J* = 7.3 Hz, 2H), 7.41 – 7.34 (m, 2H), 7.33 – 7.21 (m, 1H), 5.14 (d, *J* = 55.9 Hz, 1H), 4.47 (d, *J* = 10.4 Hz, 1H), 3.98 (dd, *J* = 12.0, 3.7 Hz, 1H), 3.93 – 3.46 (m, 4H), 3.49– 3.11 (m, 1H), 2.88 (dd, *J* = 15.1, 8.5 Hz, 1H), 1.95 (s, 1H), 1.66 (s, 1H), 1.50 (s, 9H).

¹³C NMR (101 MHz, CDCl₃) δ 154.8, 139.1, 128.8, 128.5, 128.4, 127.5, 127.3, 127.2, 126.5, 126.4, 80.5, 78.6, 76.4, 73.7, 70.5, 68.9, 65.4, 63.7, 62.0, 61.1, 56.2, 40.0, 36.6, 29.7, 28.4, 28.3, 28.2.

m/z [M⁺]⁺ Calcd for C₁₆H₂₃NO₄ 293.16 Found 293.22

Synthesis of tert-butyl (2S,5R)-5-benzyl-2-(hydroxymethyl)morpholine-4-carboxylate (19b)



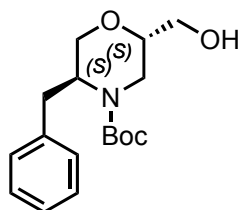
Yield 81%

^1H NMR (400 MHz, CDCl_3) δ 7.40-7.20 (m, 5H), 4.21 (s, 1H), 4.06 (dd, $J = 7.2, 4.8$ Hz, 1H), 3.93 (dd, $J = 13.4, 2.4$ Hz, 1H), 3.80-3.74 (m, 3H), 3.64 – 3.47 (m, 2H), 3.24 – 2.69 (m, 3H), 2.29 – 1.95 (m, 1H), 1.69 (s, 1H), 1.41 (s, 9H).

^{13}C NMR (101 MHz, CDCl_3) δ 154.6, 138.4, 138.2, 129.5, 129.4, 129.2, 128.5, 128.4, 126.4, 126.3, 80.0, 76.3, 75.8, 67.8, 67.3, 63.7, 53.1, 51.4, 41.3, 39.7, 35.3, 34.6, 28.3, 28.2.

m/z $[\text{M}]^+$ Calcd for $\text{C}_{17}\text{H}_{25}\text{NO}_4$ 307.18 Found 307.14

Synthesis of tert-butyl (2S,5S)-5-benzyl-2-(hydroxymethyl)morpholine-4-carboxylate (19c)



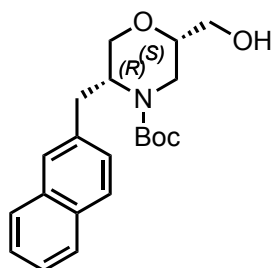
Yield 88%

^1H NMR (400 MHz, CDCl_3) δ 7.64 – 6.85 (m, 5H), 4.20-4.10 (m, 1H), 4.02 – 3.93 (m, 1H), 3.92-3.84 (m, 1H), 3.80-3.74(m, 2H), 3.65-3.55 (m, 1H), 3.51 (dd, $J = 12.0, 2.8$ Hz, 1H), 3.42 (dd, $J = 14.2, 4.8$ Hz, 1H), 3.08 – 2.91 (m, 1H), 2.17 (s, 1H), 1.42 (s, 2H).

^{13}C NMR (101 MHz, CDCl_3) δ 155.2, 138.0, 129.3, 128.5, 126.5, 80.7, 72.3, 61.4, 60.3, 53.2, 38.4, 35.7, 28.2.

m/z $[\text{M}^+]^+$ Calcd for $\text{C}_{17}\text{H}_{25}\text{NO}_4$ 307.18 Found 307.14

Synthesis of tert-butyl (2S,5R)-2-(hydroxymethyl)-5-(naphthalen-2-ylmethyl)morpholine-4-carboxylate (19d)



Yield 76%

^1H NMR (400 MHz, CDCl_3) δ 7.86-7.78 (m, 3H), 7.73 (s, 1H), 7.66 (s, 1H), 7.52-7.42 (m, 2H), 7.36 (d, $J = 8.1$ Hz, 1H), 4.31 (s, 1H), 4.16 (t, $J = 5.9$ Hz, 1H), 3.96 (dd, $J = 13.3, 2.3$ Hz, 1H), 3.91 – 3.66 (m, 3H), 3.59 (m, 2H), 3.28 – 2.94 (m, 3H), 2.07 (s, 2H), 1.68 (s, 2H), 1.38 (s, 9H).

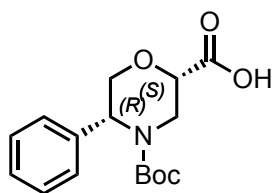
^{13}C NMR (101 MHz, CDCl_3) δ 154.6, 135.9, 135.8, 133.5, 132.2, 128.2, 128.1, 128.0, 127.9, 127.6, 127.6, 127.4, 126.1, 125.9, 125.5, 125.4, 80.1, 76.3, 75.8, 67.7, 67.2, 63.8, 53.1, 51.4, 41.4, 39.8, 35.4, 34.8, 28.3, 28.1.

m/z $[\text{M}+\text{Na}]^+$ Calcd for $\text{C}_{21}\text{H}_{27}\text{NO}_4\text{Na}$ 380.18 Found 381.14

General procedure for Boc-morpholino amino acid synthesis (20a-d)

To a vigorously stirred solution of Boc-morpholino amino alcohol (1.7 mmol) in DCM/H₂O (2:1) were added TEMPO (0.2 equiv) and BAIB (2 equiv) at 0 °C. After 6 h, the reaction was quenched with MeOH and the mixture was evaporated to dryness. Silica gel column chromatography (CH₂Cl₂/MeOH, 20:1) provided Boc-morpholino amino acid as a clear oil.

Synthesis of (2S,5R)-4-(tert-butoxycarbonyl)-5-phenylmorpholine-2-carboxylic acid (20a)



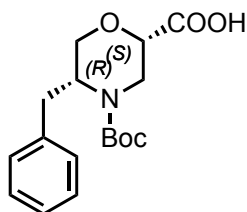
Yield 65%

¹H NMR (400 MHz, MeOD) δ 7.45 (d, *J* = 7.6 Hz, 2H), 7.37 (t, *J* = 7.4 Hz, 2H), 7.29 (d, *J* = 7.0 Hz, 1H), 5.11 (s, 1H), 4.48 (d, *J* = 11.6 Hz, 1H), 4.25 (d, *J* = 13.3 Hz, 1H), 4.13 (d, *J* = 11.1 Hz, 1H), 3.98 (d, *J* = 11.0 Hz, 1H), 3.00 (t, *J* = 12.2 Hz, 1H), 1.49 (s, 9H).

¹³C NMR (101 MHz, MeOD) δ 172.1, 155.0, 138.8, 128.5, 128.1, 127.0, 126.9, 125.8, 80.6, 75.0, 68.5, 52.8, 41.5, 29.5, 27.2.

m/z [M+Na]⁺ Calcd for C₁₆H₂₁NO₅Na 330.14 Found 331.15

Synthesis of (2S,5R)-5-benzyl-4-(tert-butoxycarbonyl)morpholine-2-carboxylic acid (20b)



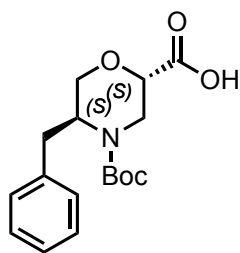
Yield 71%

^1H NMR (400 MHz, CDCl_3) δ 7.36 – 7.19 (m, 5H), 5.90 (s, 1H), 4.26 (d, $J = 45.6$ Hz, 2H), 4.12 (dd, $J = 11.4, 3.4$ Hz, 1H), 3.93 (dd, $J = 11.7, 1.0$ Hz, 1H), 3.64 (dd, $J = 11.7, 3.4$ Hz, 1H), 3.19 (dd, $J = 13.7, 11.4$ Hz, 1H), 3.05 – 2.89 (m, 2H), 1.42 (s, 9H).

^{13}C NMR (101 MHz, CDCl_3) δ 171.6, 154.3, 137.9, 129.4, 128.6, 126.6, 80.8, 77.3, 77.0, 76.2, 74.1, 73.9, 68.1, 68.0, 52.8, 51.1, 41.4, 40.0, 35.0, 34., 29.71, 28.2.

m/z $[\text{M}]^+$ Calcd for $\text{C}_{17}\text{H}_{23}\text{NO}_5$ 321.16 Found 321.15

Synthesis of (2S,5R)-5-benzyl-4-(tert-butoxycarbonyl)morpholine-2-carboxylic acid (20c)



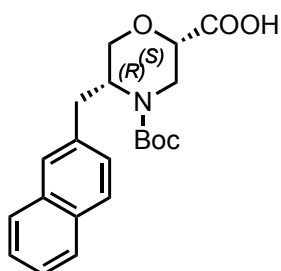
Yield 66%

^1H NMR (400 MHz, CDCl_3) δ 7.43 – 7.11 (m, 5H), 5.03 (s, 1H), 4.62 – 4.31 (m, 2H), 4.16 (s, 1H), 3.99 (dd, $J = 12.1, 3.7$ Hz, 1H), 3.64 (dd, $J = 12.1, 1.6$ Hz, 1H), 3.52 (dd, $J = 14.2, 5.3$ Hz, 1H), 3.00 (t, $J = 7.4$ Hz, 2H), 1.39 (s, 9H).

^{13}C NMR (101 MHz, CDCl_3) δ 173.9, 154.6, 137.9, 129.3, 128.6, 126.5, 80.7, 71.3, 63.7, 52.4, 39.1, 34.8, 29.7, 28.1.

m/z $[\text{M}]^+$ Calcd for $\text{C}_{17}\text{H}_{23}\text{NO}_5$ 321.16 Found 321.15

Synthesis of (2S,5R)-4-(tert-butoxycarbonyl)-5-(naphthalen-2-ylmethyl)morpholine-2-carboxylic acid (20d)



Yield 71%

^1H NMR (400 MHz, MeOD) δ 7.88 – 7.76 (m, 2H), 7.70 (s, 1H), 7.53 – 7.34 (m, 2H), 4.34– 4.24 (m, 1H), 4.10 (d, J = 10.9 Hz, 1H), 3.95 (d, J = 11.7 Hz, 1H), 3.75–3.6 (m, 1H), 3.32 – 2.96 (m, 3H), 1.32 (s, 9H).

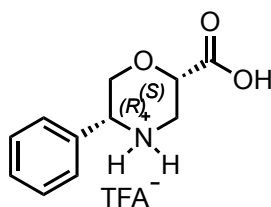
^{13}C NMR (101 MHz, MeOD) δ 171.0, 154.5, 133.7, 132.4, 127.6, 127.5, 127.2, 127.1, 125.6, 125.1, 80.1, 74.3, 68.5, 53.0, 39.9, 34.6, 29.3, 26.9, 26.7.

m/z $[\text{M}]^+$ Calcd for $\text{C}_{21}\text{H}_{25}\text{NO}_5$ 371.17 Found 371.17

General procedure deprotection of morpholino amino acid (7a-d)

To a round bottom flask equipped with magnetic stirring bar was added Boc-Morph-AA (1 equiv) and dissolved in DCM. The solution was cooled to 0°C and was added TFA (1 mL TFA: 25 mg reagent) slowly and dropwise, then the mixture was stirred for 3h. The crude mixture was concentrated in vacuo affording 30 in quantitative yield.

Synthesis of (2S,5R)-5-phenylmorpholine-2-carboxylic acid TFA salt (7a)



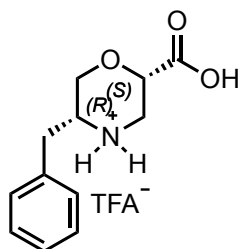
Yield: quantitative

^1H NMR (400 MHz, MeOD) δ 7.58 – 7.38 (m, 5H), 4.60 (t, J = 4.0 Hz, 1H), 4.55 (dd, J = 9.0, 3.6 Hz, 1H), 4.39 (dd, J = 13.0, 8.9 Hz, 1H), 4.08 (dd, J = 13.0, 3.6 Hz, 1H), 3.64 (ddd, J = 17.5, 12.8, 3.9 Hz, 2H)

^{13}C NMR (101 MHz, MeOD) δ 171.2, 161.5, 132.6, 129.6, 129.0, 127.9, 69.9, 64.8, 56.9, 42.9, 36.4.

m/z $[\text{M}]^+$ Calcd for $\text{C}_{11}\text{H}_{13}\text{NO}_3$ 209.09 Found 210.11

Synthesis of (2S,5R)-5-Benzylmorpholine 2-carboxylic acid TFA salt (7b)



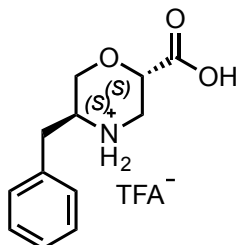
Yield: quantitative

¹H NMR (400 MHz, MeOD) δ 7.81 – 6.99 (m, 5H), 4.51 (t, J = 4.8 Hz, 1H), 3.95 – 3.76 (m, 2H), 3.73 – 3.57 (m, 2H), 3.56 – 3.40 (m, 1H), 3.02 (ddd, J = 20.0, 13.8, 7.5 Hz, 2H).

¹³C NMR (101 MHz, MeOD) δ 170.4, 134.7, 128.9, 128.9, 128.7, 127.2, 70.6, 65.5, 64.1, 54.4, 42.0, 33.7, 29.5.

m/z [M]⁺ Calcd for C₁₁H₁₃NO₃ 209.09 Found 210.13

Synthesis of (2S,5S)-5-Benzylmorpholine 2-carboxylic acid TFA salt (7c)



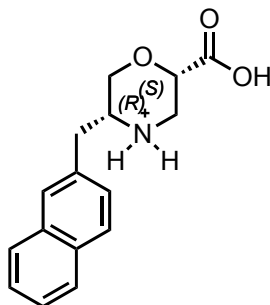
Yield: quantitative

^1H NMR (400 MHz, MeOD) δ 7.58 – 7.14 (m, 5H), 4.35 (d, J = 10.6 Hz, 1H), 4.08 (d, J = 11.2 Hz, 1H), 3.83 – 3.48 (m, 3H), 3.17 (t, J = 12.0 Hz, 1H), 3.05 – 2.79 (m, 2H).

^{13}C NMR (101 MHz, MeOD) δ 169.6, 134.2, 128.9, 128.8, 127.3, 72.0, 71.5, 67.6, 67.5, 55.1, 44.8, 34.6, 29.3.

m/z [M]⁺ Calcd for $\text{C}_{11}\text{H}_{13}\text{NO}_3$ 209.09 Found 210.11

Synthesis of (2S,5R)-5-(naphthalen-2-ylmethyl)Morpholine 2-carboxylic acid TFA(7d)



Yield: quantitative

^1H NMR (400 MHz, MeOD) δ 7.96 – 7.73 (m, 4H), 7.62 – 7.40 (m, 3H), 4.47 (s, 1H), 4.04 – 3.81 (m, 2H), 3.81 – 3.61 (m, 2H), 3.57 – 3.39 (m, 1H), 3.19 (ddd, $J = 20.1, 13.7, 7.4$ Hz, 2H).

^{13}C NMR (101 MHz, MeOD) δ 170.8, 133.6, 132.8, 132.1, 128.5, 128.0, 127.3, 127.2, 126.5, 126.1, 125.8, 71.0, 71.0, 64.3, 54.3, 42.2, 33.9, 29.3.

m/z $[\text{M}]^+$ Calcd for $\text{C}_{16}\text{H}_{18}\text{NO}_3$ 272.12 Found 272.13

General solid phase synthesis (SPPS) for peptides containing morpholino amino acid scaffold (Peptide 1-6)

1. **Swelling** of RINK-amide-N-Fmoc resin:

To a reactor was added 220 mg of RINK-amide-N-Fmoc (0.7 mmol/g; 0.154 mmol) and DCM (~6mL), then suspension was shaken for 20 min and filtrated under vacuum.

2. **Fmoc-deprotection** of RINK-amide-N-Fmoc resin. Synthesis of RINK-amide-NH₂:

To a reactor with swelled resin was added a solution of Piperidine 20% in DMF (~7mL) and shaken for 5 min and then filtered under vacuum. To the resin was added again the same quantity of Piperidine and shaken for 15 min. At the end of shaking was washed with DMF (x6) and DCM (x6).

3. **Activation and coupling** of N-Fmoc-AA-OH.

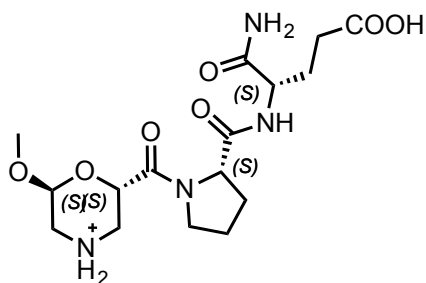
To a round bottom flask was added the N-Fmoc-AA-OH; (2.2 equiv.), 3 mL of DMF and the solution was cooled to 0°C than EtCN-oxime (3.3 equiv.) and DIC (3.33 equiv.) were added. The solution was stirred for 20 min and added to reactor. The reaction was shaken for 3h at r.t. Kaiser test is performed to investigate whether the coupling needs to be repeated. When the reaction is completed, the solvent was then filtrated under vacuum and the resin was washed with DMF (x6) and DCM (x6).

4. For tripeptide sequences, the steps 2–3 are repeated one time again.

5. **Cleavage** from the resin.

To the resin was added 3 mL of cleavage cocktail (2.85 mL TFA; 75 μ L TIS; 75 μ L H₂O) and shaken for 4h. The mixture was precipitated using Hexane/Methyl-tertButyl Ether (2:1) and centrifuged (3000rpm x5min) 3-4 times in order to obtain the final product as white solid without purification.

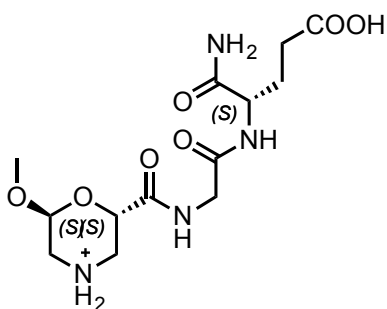
Synthesis of (2S,6S)-6-Methoxy-2-Morph-(L)-Pro-(L)-Glu-NH₂ (1)



Yield: 38%

m/z [M]⁺ Calcd for C₁₆H₂₇N₄O₇ 387.19; Found 388.20

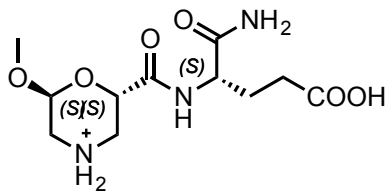
Synthesis of (2S,6S)-6-Methoxy-2-Morph-Gly-(L)-Glu-NH₂ (2)



Yield: 33%

m/z [M+Na]⁺ Calcd for C₁₃H₂₃N₄O₇Na 370.16; Found 371.20

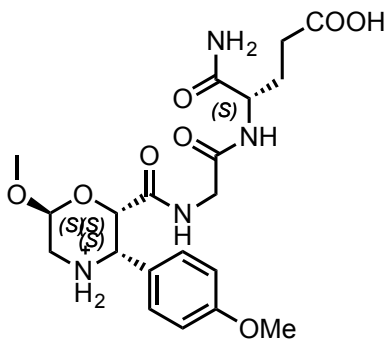
Synthesis of (2S,6S)-6-Methoxy-2-Morph-(L)-Glu-NH₂ (3)



Yield: 43%

m/z [M]⁺ Calcd for C₁₁H₂₀N₃O₆ 290.13; Found 291.13.

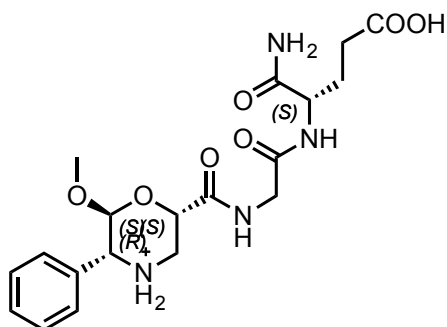
Synthesis of 3(S)-Aryl (2S,6S)-6-Methoxy-2-Morph-Gly-(L)-Glu-NH₂ (4)



Yield: 21%

m/z [M+Na]⁺ Calcd for C₂₀H₂₉N₄O₈Na 476.31; Found 477.32

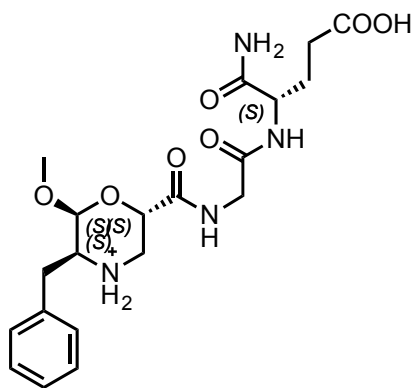
Synthesis of (2S, 5R) 5-Phenyl 2-Morph-Gly-(L)-Glu-NH₂ (5)



Yield: 45%

m/z [M+Na]⁺ Calcd for C₁₉H₂₇N₄O₇ 446.19; Found 446.22

Synthesis of (2S, 5S) 5-Benzyl 2-Morph-Gly-L-Glu-NH₂ (6)



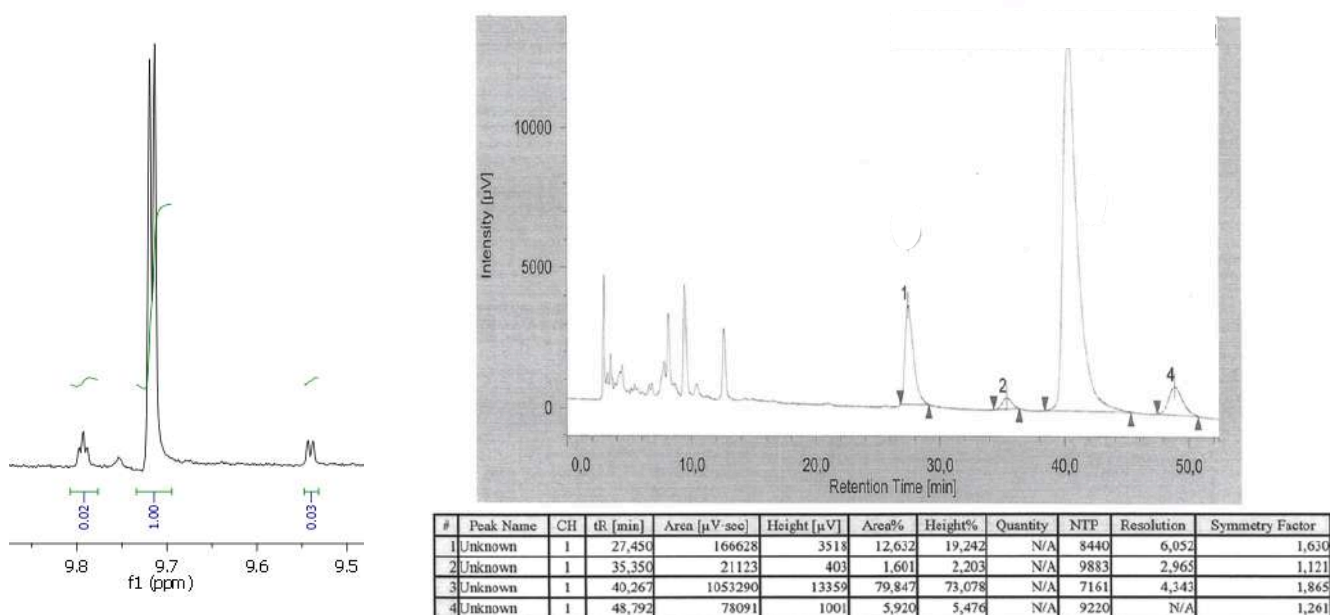
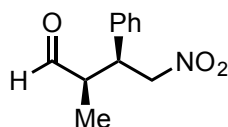
Yield: 38%

m/z [M]⁺ Calcd for C₁₉H₂₇N₄O₆ 407.19; Found 407.32

Synthesis and Analytical Data of γ -Nitroaldehydes

The catalyst TFA salt (1-10 mol%) was added to a solution of N-methylmorpholine (1-5 mol%), nitroolefin (1.5 equiv.) and aldehyde (1 equiv.) in the respective solvent (0.380 ml). The reaction mixture was stirred at $-10\text{ }^{\circ}\text{C}$ for 24/48 h. The solvent was removed under reduced pressure and the crude mixture was subjected to flash chromatography (5% \rightarrow 20% EtOAc in hexane, silica) to yield γ -nitroaldehyde. The diastereomeric ratio was determined by ^1H NMR spectroscopic analysis of the isolated product by comparison of the aldehyde R-CHO signals. The enantiomeric excess was determined by chiral stationary phase HPLC.

Synthesis of (2R,3S)-2-methyl-4-nitro-3-phenylbutanal (23b)



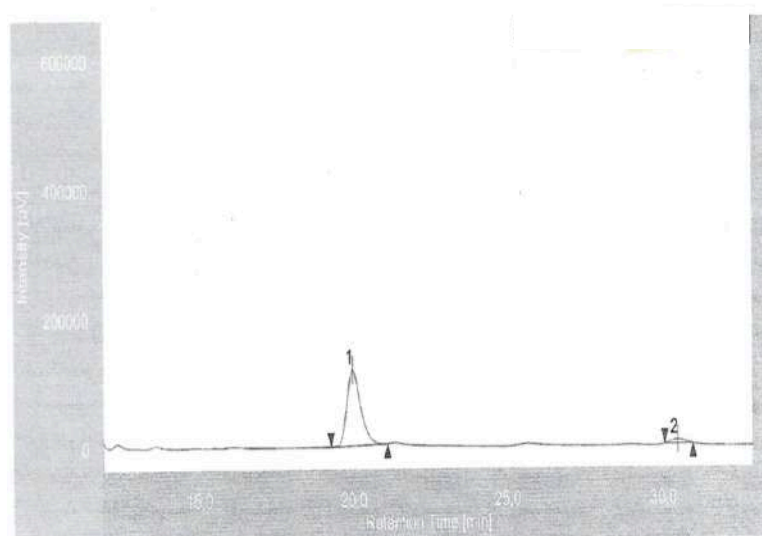
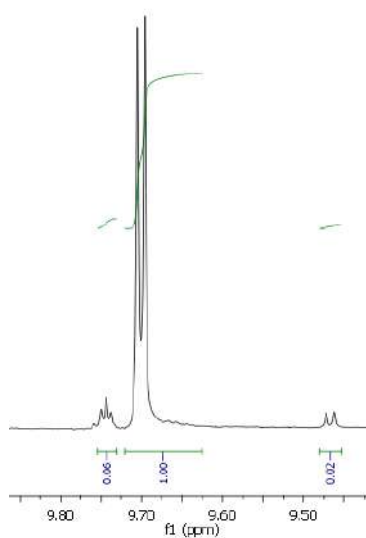
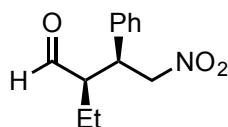
Conversion = quantitative, 94% d.r., 83% ee. The enantiomeric excess was determined by chiral stationary phase HPLC: Chiralcel OD-H, hexane/iPrOH 9:1, 1.0 ml/min, 25 °C, 254 nm, 27.2 min (syn, minor), 40.8 min (syn, major).

^1H NMR (300 MHz, CDCl_3) δ 9.72 (d, J = 1.7 Hz, 1H), 7.47 – 7.05 (m, 5H), 4.99 – 4.53 (m, 2H), 3.81 (td, J = 9.2, 5.6 Hz, 1H), 2.81 – 2.74 (m, 1H), 1.00 (d, J = 7.3 Hz, 3H).

^{13}C NMR (75 MHz, CDCl_3) δ 202.2, 136.5, 129.1, 129.0, 128.1, 128.0, 127.9, 78.0, 48.4, 44.0, 12.1.

(ESI): m/z calcd. for $[\text{M}]^+$ $\text{C}_{11}\text{H}_{13}\text{NO}_3$: 207.09; found: 207.09.

Synthesis of (2R,3S)-2-ethyl-4-nitro-3-phenylbutanal (23a)



#	Peak Name	CH	tR [min]	Area [μV·sec]	Height [μV]	Area%	Height%	Quantity	NTP	Resolution	Symmetry Factor
1	Unknown	1	19.973	3680065	117308	94.942	95.026	N/A	9699	12.140	1.310
2	Unknown	1	30.475	196054	6140	5.058	4.974	N/A	17440	N/A	1.079

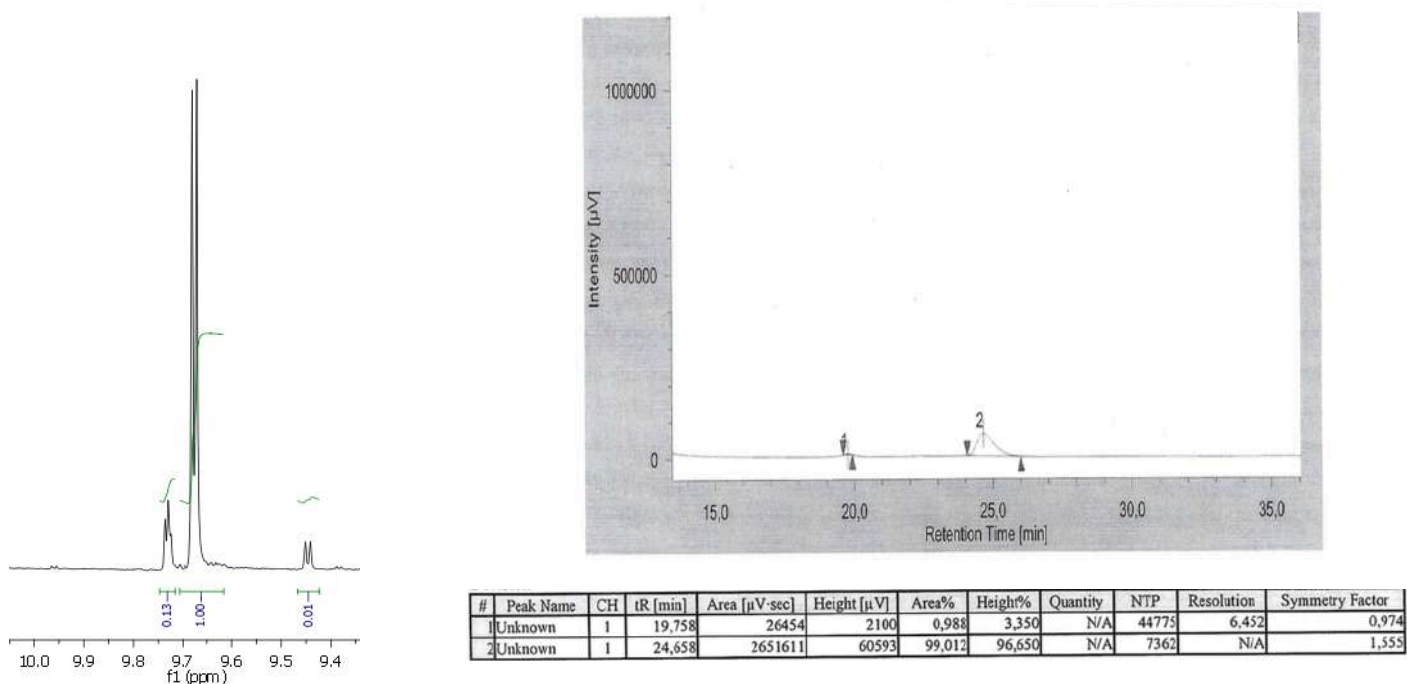
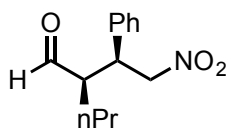
Conversion = 96%, 96% d.r., 92% ee. The enantiomeric excess was determined by chiral stationary phase HPLC: Chiralcel AD, hexane/EtOH 110:5, 0.8 ml/min, 25 °C, 220 nm, 19.9 min (syn, major), 30.4 min (syn, minor).

^1H NMR (300 MHz, CDCl_3) δ 9.71 (d, $J = 2.6$ Hz, 1H), 7.39 – 7.25 (m, 3H), 7.21 – 7.14 (m, 2H), 4.67 (dd, $J = 16.8, 7.4$ Hz, 2H), 3.79 (td, $J = 9.8, 5.1$ Hz, 1H), 2.68 (dddd, $J = 10.0, 7.6, 5.1, 2.6$ Hz, 1H), 1.82 – 1.33 (m, 2H), 0.83 (t, $J = 7.5$ Hz, 3H).

^{13}C NMR (75 MHz, CDCl_3) δ 203.1, 136.7, 129.1, 128.2, 128.1, 127.9, 78.5, 54.9, 42.6, 20.3, 10.6.

(ESI): m/z calcd. for $[\text{M} + \text{Na}]^+ \text{C}_{12}\text{H}_{15}\text{NO}_3$ 244.09; found: 244.09.

Synthesis of (R)-2-((S)-2-nitro-1-phenylethyl)pentanal (23c)



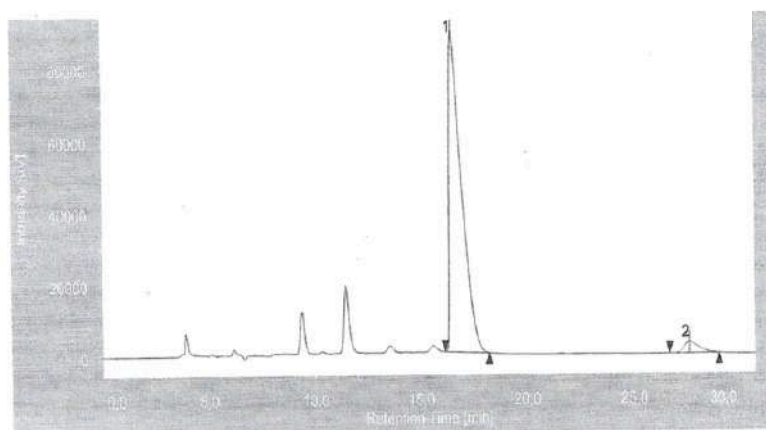
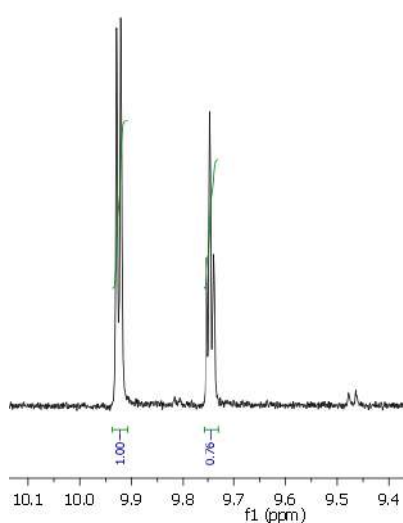
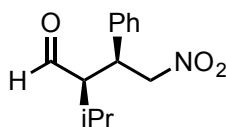
Conversion = 90%, 98% d.r., 99% ee. The enantiomeric excess was determined by chiral stationary phase HPLC: Chiralcel OD-H, hexane/iPrOH 9:1, 1.0 ml/min, 25 °C, 254 nm, 19.7 min (syn, major), 24.6 min (syn, minor).

^1H NMR (400 MHz, CDCl_3) δ 9.73 (d, $J = 2.8$ Hz, 1H), 7.40 – 7.29 (m, 3H), 7.20 (d, $J = 6.9$ Hz, 2H), 4.70 (dd, $J = 11.0, 7.4$ Hz, 2H), 3.80 (td, $J = 9.5, 5.4$ Hz, 1H), 2.73 (tt, $J = 9.5, 3.2$ Hz, 1H), 1.71 – 1.14 (m, 5H), 0.83 (t, $J = 7.1$ Hz, 3H).

^{13}C NMR (101 MHz, CDCl_3) δ 203.2, 136.8, 129.1, 129.1, 128.2, 128.1, 128.0, 78.4, 53.8, 43.2, 29.5, 19.7, 13.9.

(ESI): m/z calcd. for $[\text{M}]^+$ $\text{C}_{13}\text{H}_{17}\text{NO}_3$ 235.12; found: 236.13

Synthesis of (2R,3S)-2-isopropyl-4-nitro-3-phenylbutanal (23d)



#	Peak Name	CH	tR [min]	Area [μV-sec]	Height [μV]	Area%	Height%	Quantity	NTP	Resolution	Symmetry Factor
1	Unknown	1	16,517	3592592	89091	96,016	96,649	N/A	3882	9,543	3,178
2	Unknown	1	27,583	149056	3089	3,984	3,351	N/A	7607	N/A	1,639

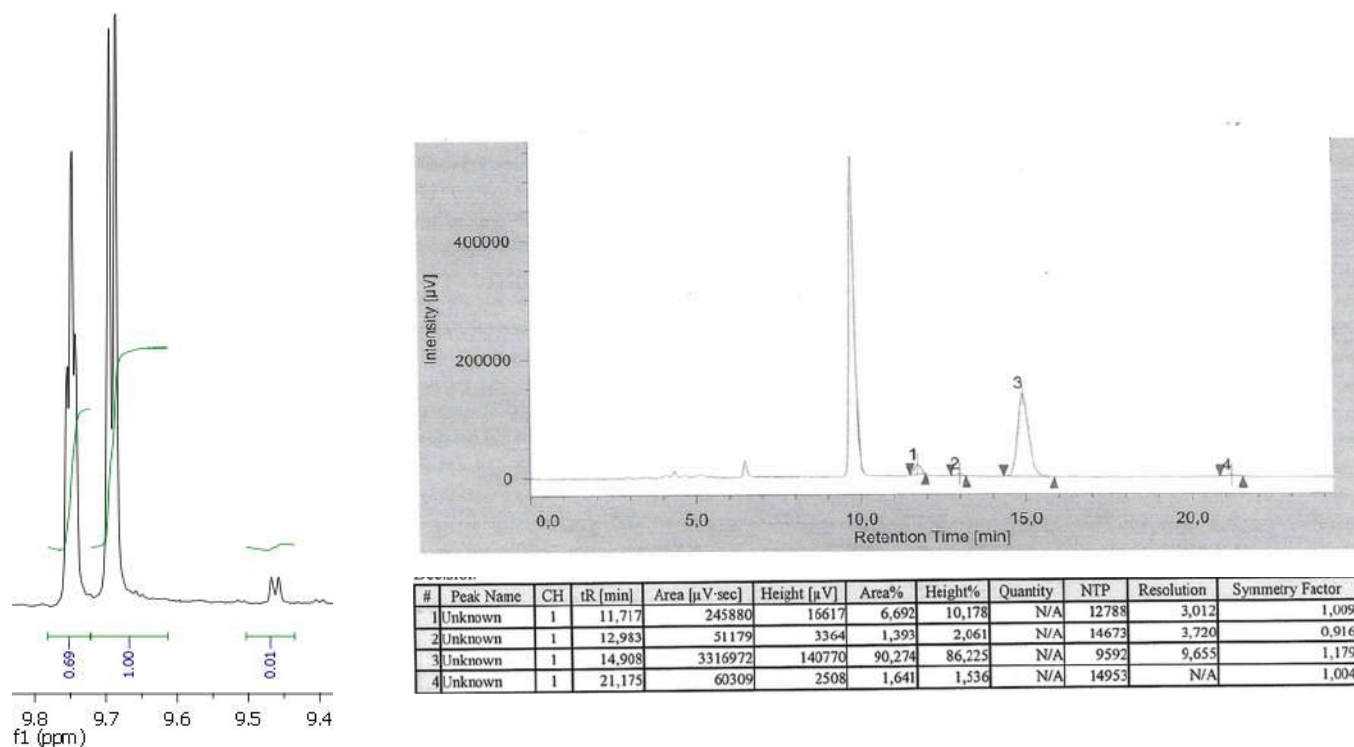
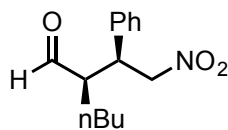
Conversion = 68%, 99% d.r., 95% ee. The enantiomeric excess was determined by chiral stationary phase HPLC Chiralcel AD, hexane/iPrOH 9:1, 0.8 ml/min, 25 °C, 254 nm, 16.5 min (syn, major), 27.5 min (syn, minor).

^1H NMR (400 MHz, CDCl_3) δ 9.95 (d, $J = 2.4$ Hz, 1H), 7.42 – 7.28 (m, 3H), 7.24 – 7.16 (m, 2H), 4.69 (dd, $J = 12.5, 4.4$ Hz, 1H), 4.60 (dd, $J = 12.5, 9.9$ Hz, 1H), 3.92 (td, $J = 10.3, 4.4$ Hz, 1H), 2.79 (ddd, $J = 10.7, 4.1, 2.5$ Hz, 1H), 1.75 (m, 1H), 1.12 (d, $J = 7.2$ Hz, 3H), 0.91 (d, $J = 7.0$ Hz, 3H).

^{13}C NMR (101 MHz, CDCl_3) δ 204.3, 137.1, 129.1, 128.1, 127.9, 78.9, 58.8, 41.9, 27.9, 21.6, 17.0.

(ESI): m/z calcd. for $[\text{M}]^+$ $\text{C}_{13}\text{H}_{17}\text{NO}_3$ 235.12; found: 236.13

Synthesis of (*R*)-2-((*S*)-2-nitro-1-phenylethyl)hexanal (23e)



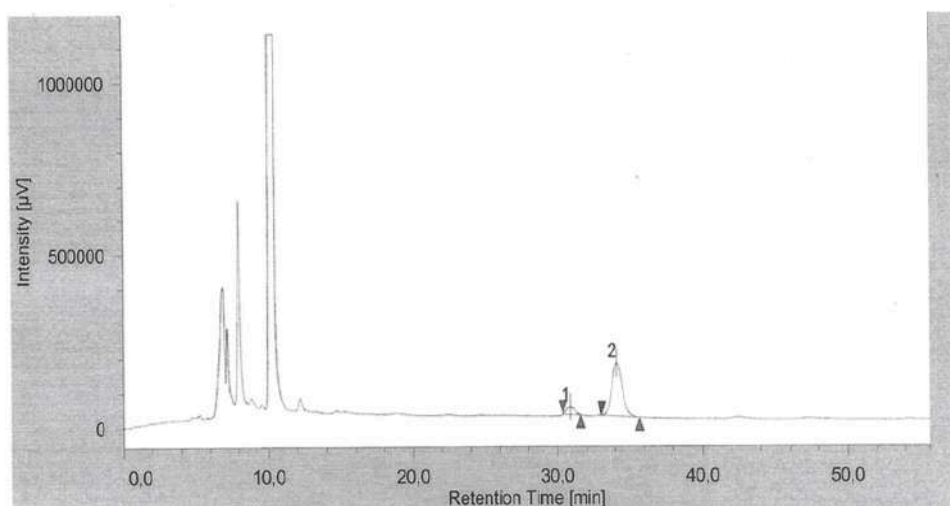
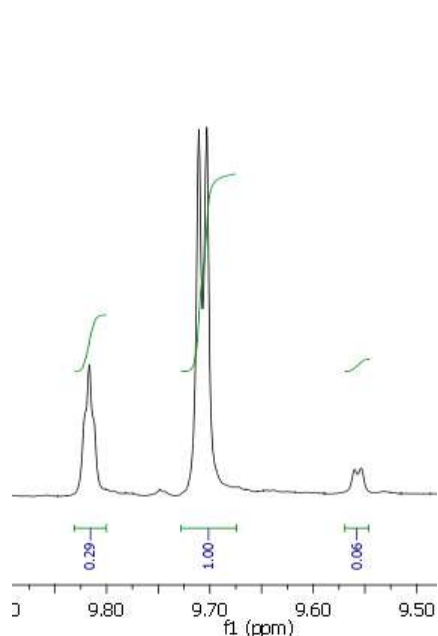
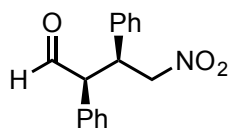
Conversion =60%, 98% d.r., 87% ee. The enantiomeric excess was determined by chiral stationary phase HPLC: Chiralcel OD-H, hexane/iPrOH 9:1, 1.0 ml/min, 25 °C, 216 nm, 11.7 min (syn, minor), 14.9 min (syn, major).

¹H NMR (300 MHz, cdcl₃) δ 9.70 (d, *J* = 2.8 Hz, 1H), 7.41 – 7.25 (m, 3H), 7.17 (dd, *J* = 7.9, 1.6 Hz, 2H), 4.67 (dd, *J* = 9.7, 7.4 Hz, 2H), 3.77 (td, *J* = 9.6, 5.4 Hz, 1H), 2.86 – 2.53 (m, 1H), 1.61 – 1.04 (m, 6H), 0.77 (t, *J* = 6.9 Hz, 3H).

¹³C NMR (75 MHz, cdcl₃) δ 203.2, 136.7, 129.0, 128.2, 128.1, 127.9, 78.4, 53.8, 43.1, 28.4, 27.0, 22.4, 13.6.

(ESI): [M + Na]⁺ C₁₄H₁₉NO₃Na: 272.12; found: 273.13

Synthesis of (2*S*,3*S*)-4-nitro-2,3-diphenylbutanal (23f)



#	Peak Name	CH	tR [min]	Area [µV-sec]	Height [µV]	Area%	Height%	Quantity	NTP	Resolution	Symmetry Factor
1	Unknown	1	30,875	854996	20896	9,955	12,008	N/A	11161	2,608	1,203
2	Unknown	1	34,108	7733657	153125	90,045	87,992	N/A	10723	N/A	1,102

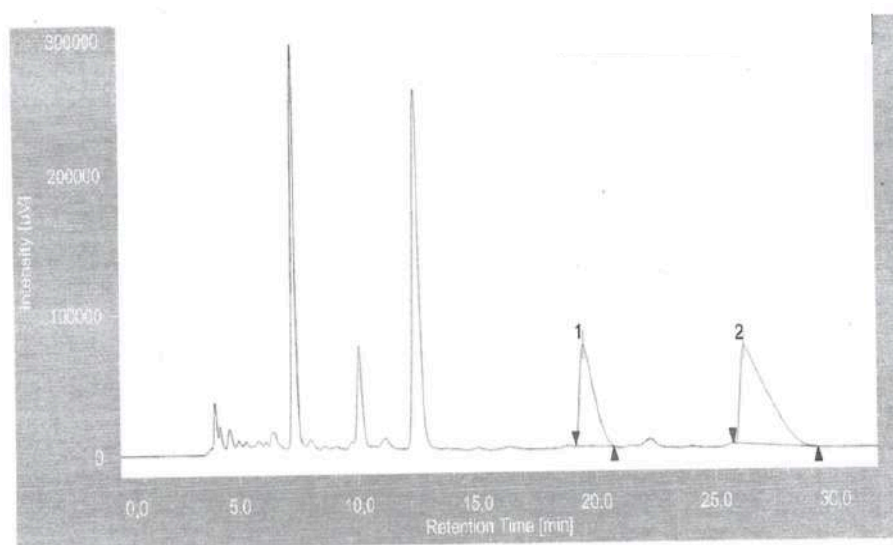
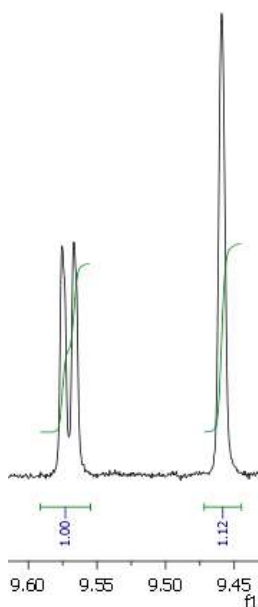
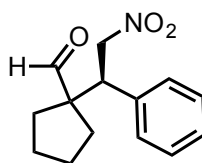
Conversion =80%, 89% d.r., 80% ee. The enantiomeric excess was determined by chiral stationary phase HPLC: Chiralcel OD-H, hexane/*i*PrOH 93:7, 1.0 ml/min, 25 °C, 220 nm, 30.8 min (syn, minor), 34.1 min (syn, major).

^1H NMR (400 MHz, CDCl_3) ^1H NMR (300 MHz, CDCl_3) δ 9.72 (d, $J = 2.3$ Hz, 1H), , 7.56 – 7.11 (m, 8H), 7.05 (dd, $J = 15.4, 13.7$ Hz, 2H), 5.05 – 4.53 (m, 2H), 3.83 (td, $J = 8.6, 6.4$ Hz, 1H), 3.19 – 2.99 (m, 1H), 2.81 – 2.73 (m, 2H).

^{13}C NMR (75 MHz, CDCl_3) δ 202.9, 137.1, 136.6, 129.2, 128.8, 128.7, 128.3, 128.0, 126.9, 78.0, 55.3, 43.4, 34.2.

(ESI): $[\text{M}]^+ \text{C}_{16}\text{H}_{15}\text{NO}_3$: 269.11; found: 270.13

Synthesis of (*R*)-1-(2-nitro-1-phenylethyl)cyclopentane-1-carbaldehyde (23g)



#	Peak Name	CH	tR [min]	Area [μV·sec]	Height [μV]	Area%	Height%	Quantity	NTP	Resolution	Symmetry Factor
1	Unknown	1	19,475	2891625	71546	35,068	50,884	N/A	5176	4,247	2,404
2	Unknown	1	26,175	5354145	69061	64,932	49,116	N/A	2531	N/A	4,380

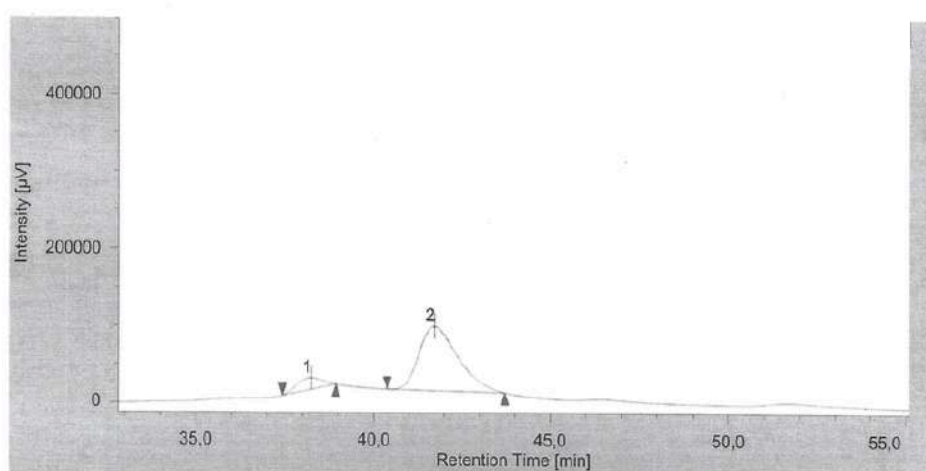
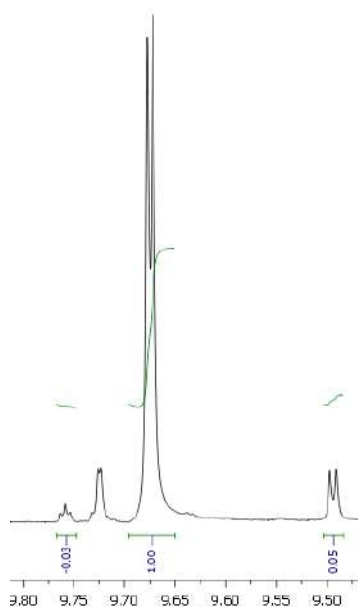
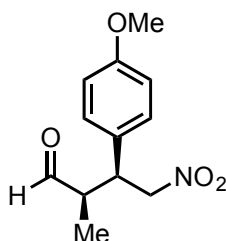
Conversion= 53%, 35% ee. The enantiomeric excess was determined by chiral stationary phase HPLC: Chiralcel AD, hexane/*i*PrOH 95:5, 0.8 ml/min, 25 °C, 254 nm, 19.4 min (syn, minor), 26.1 min (syn, major).

¹H NMR (300 MHz, CDCl₃) δ 9.49 (s, 1H), 7.36 – 7.24 (m, 4H), 7.19 (dd, *J* = 7.6, 1.9 Hz, 1H), 4.96 (dd, *J* = 13.1, 11.3 Hz, 1H), 4.69 (dd, *J* = 13.2, 3.9 Hz, 1H), 3.69 (dd, *J* = 11.3, 3.8 Hz, 1H), 2.15– 2.05 (m, 1H), 1.95– 1.87 (m, 1H), 1.77 – 1.43 (m, 6H).

¹³C NMR (75 MHz, CDCl₃) δ 204.5, 136.4, 128.8, 128.7, 128.1, 77.3, 60.2, 49.3, 32.6, 31.5, 24.8, 24.6.

HRMS (ESI): *m/z* calcd. for [M + Na C₁₄H₁₇NO₃Na: 270.09; found: 271.10

Synthesis of (2*R*,3*S*)-3-(4-methoxyphenyl)-2-methyl-4-nitrobutanal (23h)



#	Peak Name	CH	tR [min]	Area [μV·sec]	Height [μV]	Area%	Height%	Quantity	NTP	Resolution	Symmetry Factor
1	Unknown	1	38,242	761764	14970	10,620	15,172	N/A	11508	2,028	0,940
2	Unknown	1	41,717	6411429	83703	89,380	84,828	N/A	6890	N/A	1,429

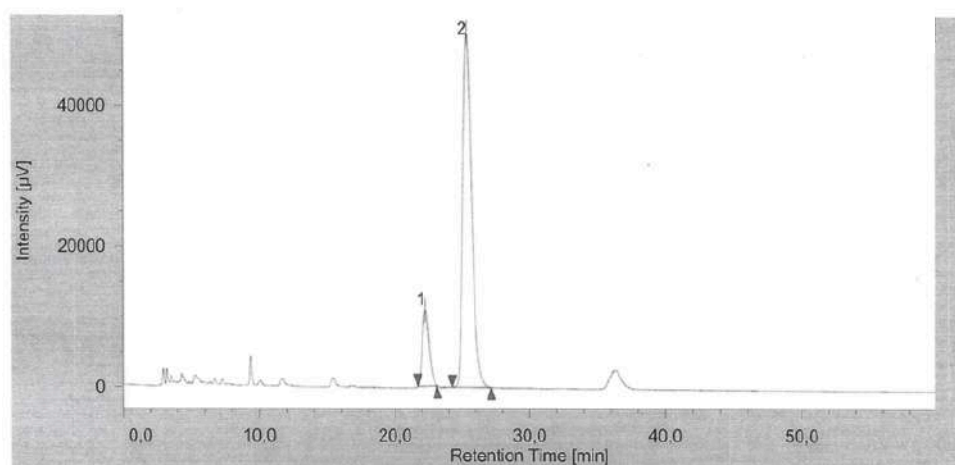
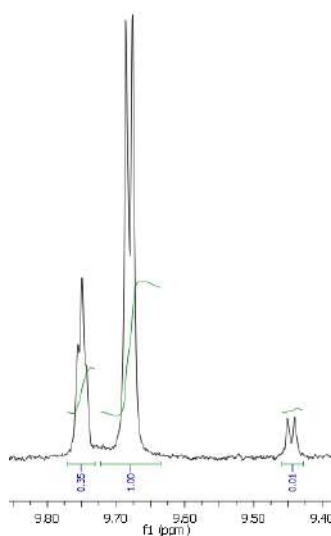
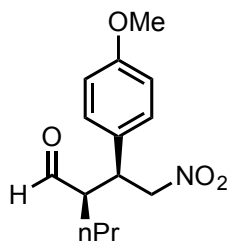
Conversion= quant%, 91% d.r., 80 ee%. The enantiomeric excess was determined by chiral stationary phase HPLC: Chiralcel OD-H, hexane/iPrOH 90:1, 1 ml/min, 25 °C, 210 nm, 33.4 min (syn, minor), 35.9 min (syn, major).

¹H NMR (300 MHz, CDCl₃) δ 9.70 (d, *J* = 1.8 Hz, 1H), 7.08 (d, *J* = 8.8 Hz, 2H), 6.86 (d, *J* = 8.8 Hz, 2H), 4.76 (dd, *J* = 12.5, 5.6 Hz, 1H), 4.63 (dd, *J* = 12.5, 9.4 Hz, 1H), 3.78 (s, 3H), 3.82 – 3.71 (m, 1H), 2.87 – 2.47 (m, 1H), 1.00 (d, *J* = 7.3 Hz, 3H).

¹³C NMR (75 MHz, CDCl₃) δ 202.3, 159.2, 129.0, 128.2, 114.4, 78.3, 55.2, 48.5, 43.3, 12.0.

HRMS (ESI): *m/z* calcd. for [M +]⁺ C₁₂H₁₅NO₄: 237.10; found: 238.10

Synthesis of (*R*)-2-((*S*)-1-(4-methoxyphenyl)-2-nitroethyl)pentanal (23i)



#	Peak Name	CH	tR [min]	Area [µV·sec]	Height [µV]	Area%	Height%	Quantity	NTP	Resolution	Symmetry Factor
1	Unknown	1	22,242	385927	10847	14,667	17,708	N/A	8912	2,953	1,234
2	Unknown	1	25,325	2245343	50409	85,333	82,292	N/A	7742	N/A	1,337

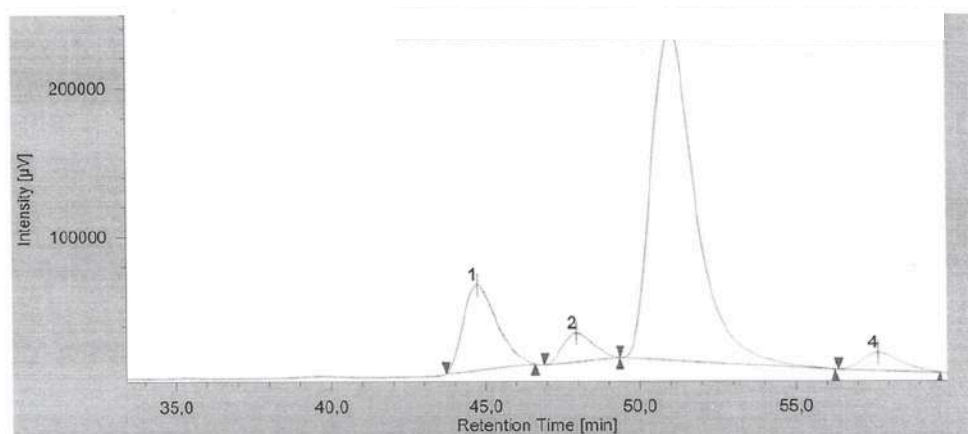
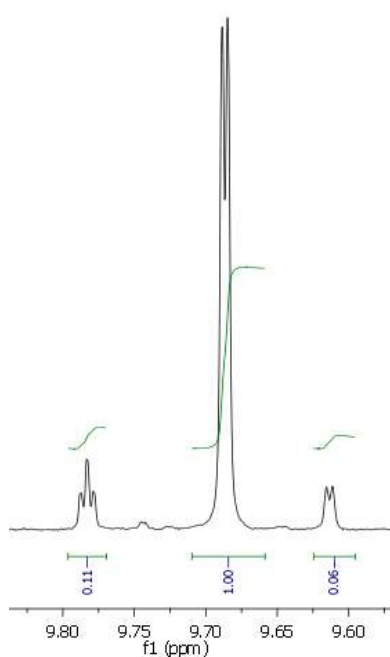
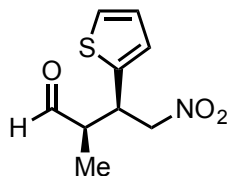
Conversion = 74%, 98% d.r., 70%, ee%. The enantiomeric excess was determined by chiral stationary phase HPLC: Chiralcel OD-H, hexane/iPrOH 9:1, 1.0 ml/min, 25 °C, 254 nm, 22.4 min (syn, minor), 25.3 min (syn, major).

¹H NMR (300 MHz, CDCl₃) δ 9.69 (d, *J* = 2.9 Hz, 1H), 7.08 (d, *J* = 8.7 Hz, 2H), 6.87 (d, *J* = 8.7 Hz, 2H), 4.63 (qd, *J* = 12.6, 7.4 Hz, 2H), 3.79 (s, 3H), 3.72 (td, *J* = 9.6, 5.4 Hz, 1H), 2.65 (tt, *J* = 9.5, 3.2 Hz, 1H), 1.61 – 1.03 (m, 4H), 0.81 (t, *J* = 7.1 Hz, 3H).

¹³C NMR (75 MHz, CDCl₃) δ 203.3, 159.2, 129.0, 128.4, 114.4, 78.6, 55.2, 53.9, 42.4, 29.4, 19.7, 13.9.

HRMS (ESI): *m/z* calcd. for [M]⁺ C₁₄H₁₉NO₄ 265.13; found: 266.13.

Synthesis of (2*R*,3*R*)-2-methyl-4-nitro-3-(thiophen-2-yl)butanal (23l)



#	Peak Name	CH	tR [min]	Area [μV·sec]	Height [μV]	Area%	Height%	Quantity	NTP	Resolution	Symmetry Factor
1	Unknown	1	44,717	4367591	57078	15,313	18,336	N/A	7707	1,640	1,410
2	Unknown	1	47,942	1323256	19088	4,639	6,132	N/A	10120	1,412	1,218
3	Unknown	1	51,017	21791148	223077	76,399	71,662	N/A	6883	2,776	1,444
4	Unknown	1	57,633	1040949	12048	3,650	3,870	N/A	9879	N/A	1,353

Conversion =91%, 89% d.r., 67% ee. The enantiomeric excess was determined by chiral stationary phase HPLC: Chiralcel OD-H, hexane/*i*PrOH 95:5, 1.0 ml/min, 25 °C, 254 nm, 44.7 min (syn, minor), 51.0 min (syn, major).

¹H NMR (300 MHz, CDCl₃) δ 9.69 (d, *J* = 1.0 Hz, 6H), 7.45 – 7.14 (m, 1H), 7.01– 6.93 (m, 2H), 5.00 – 4.53 (m, 2H), 4.21 (ddd, *J* = 20.0, 14.5, 7.2 Hz, 1H), 3.12 – 2.54 (m, 1H), 1.13 (d, *J* = 7.3 Hz, 3H).

¹³C NMR (75 MHz, CDCl₃) δ 201.6, 138.8, 127.0, 125.1, 78.6, 49.1, 39.8, 11.8.

HRMS (ESI): *m/z* calcd. for [M + Na]⁺ C₉H₁₁NO₃S: 236.05; found: 237.05

Synthesis of non-natural amino acid with isoxazoline core for the preparation of peptidomimetics

Introduction

The insertion of β -amino acids into peptides makes them more proteolytically stable to peptidase thanks to the stabilization of particularly secondary structures^{84,85,86,87,88,89}. Although the incorporation of various β -amino acids (symbolic.g., β^2 , β^3 , $\beta^{2,3}$, $\beta^{3,3}$, and $\beta^{2,2}$) in peptide foldamers is reported in literature⁹, only few cases are reported where $\beta^{2,2}$ -amino acids have been inserted into an α -peptide sequence to obtain hybrid or mixed peptides^{90,91}. The majority of them were synthesized by using achiral $\beta^{2,2}$ -amino acids^{92,93}, which limit the control of the conformational space of the resulting peptides.⁹⁴

Seebach and coworkers determined that a δ turn motif (8 members turn-forming) is adopted by a $\beta^{2,2}$ heptapeptide containing 1-(aminomethyl)cyclopropanecarboxylic acid residues (Figure 77A)⁹⁵. The repetitive eight-membered turn motif generates an 8-helix as predominant secondary structure (Figure 77B).

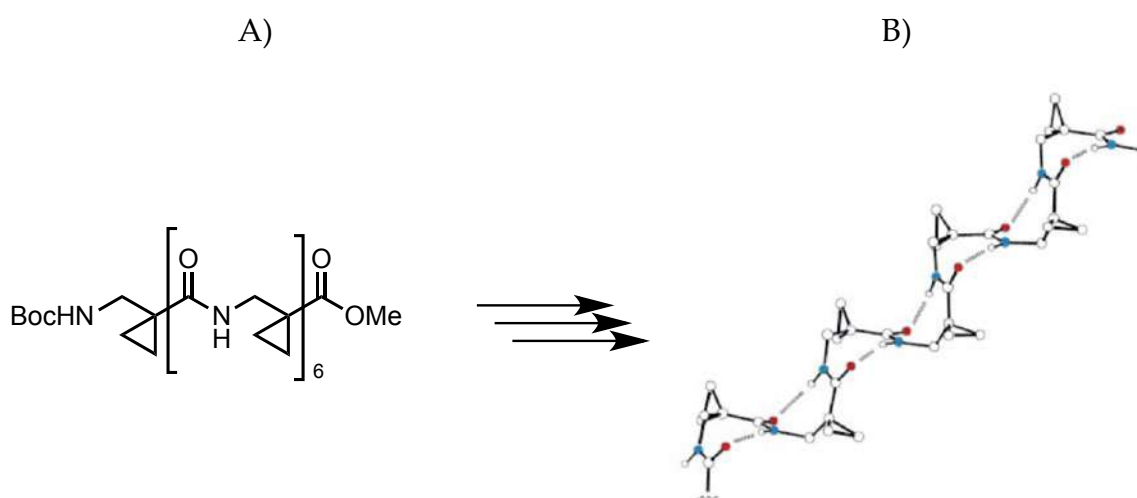


Figure 77 8-Helix generated by eight-membered turn motif containing 1-(aminomethyl)cyclopropanecarboxylic acid

Moreover, the effect of 1-aminomethylcycloalkane carboxylic acids on the stabilization of secondary structure has been studied (Figure 78A). β -Turn conformations and helical structures in short peptides have been stabilized using this particular gem-dialkyl $\beta^{2,2}$ AA (Figure 78B).⁹⁶

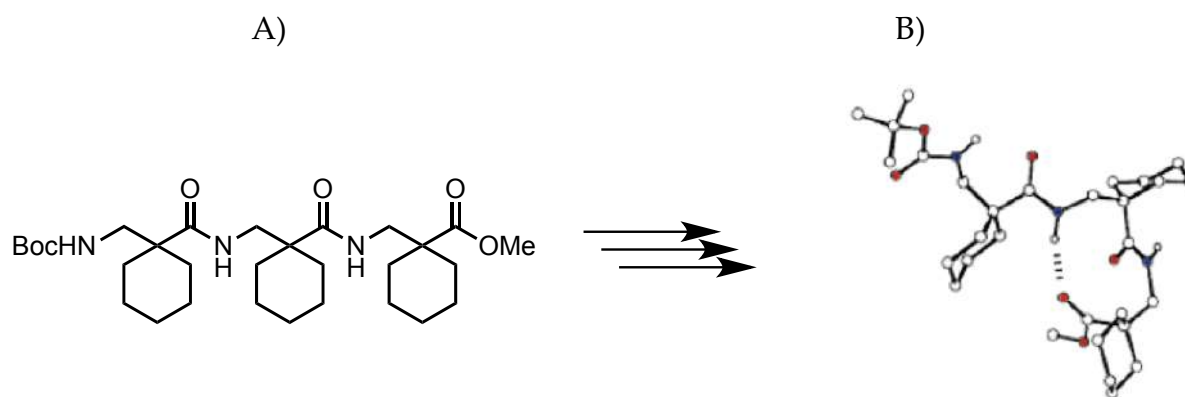


Figure 78 A) 1-Aminocycloalkane carboxylic acids tripeptide B) β -turn conformations

Recently new chiral $\beta^{2,2}$ -amino acids have been synthesized to study the effect of their chirality on the peptide conformation^{97,98,99,100} for potentially biological applications¹⁰¹. In particular, Fernando Rodriguez's group used α -methylisoserine, a chiral acyclic quaternary β -amino acid, to mimic secondary structures. They observed that this AA is a β -turn inducer when it is incorporated in a peptide model (Figure 79)¹⁰².

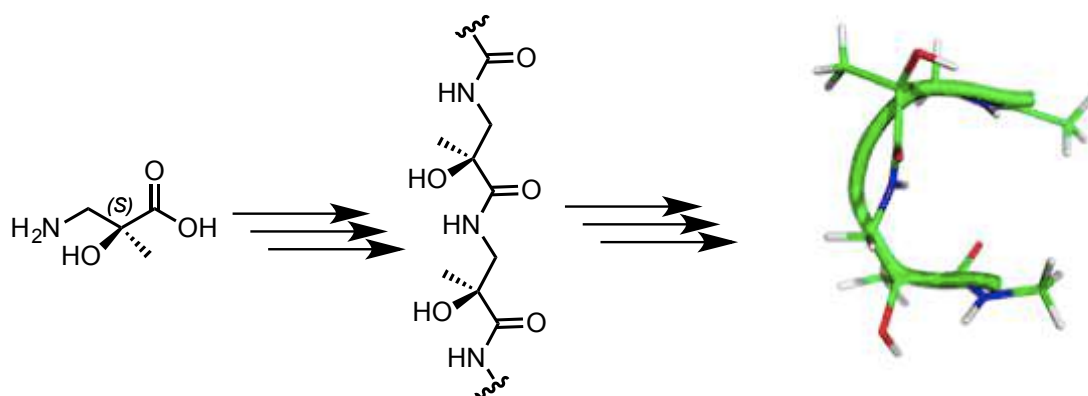


Figure 79 α -Methylisoserine as β -turn inducer

Aim of the work

As anticipated in the introduction, our research team is mainly involved in the synthesis of non-natural amino acids able to induce a particular secondary structure when inserted in model peptides¹⁰³, with the ultimate aim of preparing peptidomimetics for different applications. Here I report on the synthesis of the $\beta^{2,2}$ -amino acid with isoxazoline core, shown in Figure 80.

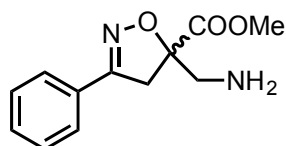


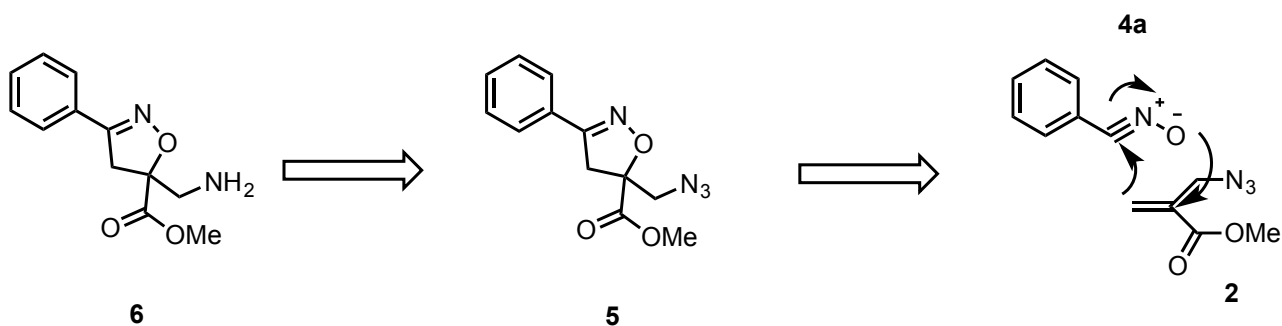
Figure 80 β -Amino acid with isoxazoline core

This new scaffold shows interesting features in its structure. First of all, the possibility of the N and O atoms in the isoxazoline core to accept H-bonds, which could potentially induce and/or stabilize the secondary structure of the peptide in which it is inserted. Moreover, the aryl moiety represents an important hydrophobic portion in the molecule for the non-covalent interactions. Last but not least, the structure represents a combination between flexible and constrained parts: the constrained portion could be able to induce a specific secondary structure, while the flexible part could confer adaptability to the molecule for example at the target binding site level.

Starting from the above information, our idea is to elaborate a synthetic strategy to achieve the above-described scaffold and then to evaluate the secondary structures that the two enantiomeric amino acids with opposite stereochemistry at position 5 of the isoxazoline ring can induce when inserted in model peptides.

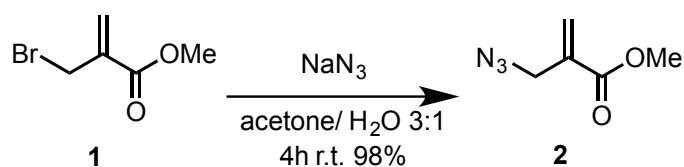
Scaffold synthesis

The regioselective 1,3-dipolar cycloaddition between methacrylate **2** and benzonitrile oxide, is the key step for the synthesis of the non-natural amino acid with isoxazoline core (Scheme 16). Thanks to this reaction, we were able to obtain azido compound **5**. Moreover, the cycloaddition was regioselective¹⁰⁴ being the carboxylic function of isoxazoline ring linked in position 5.



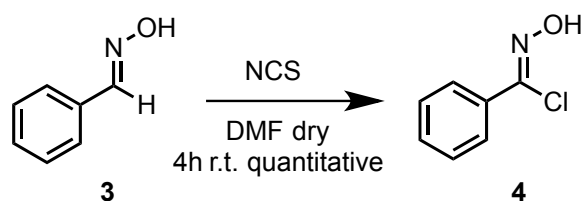
Scheme 16 Regioselective mechanism of 1,3-dipolar cycloaddition retrosynthetic scheme for the preparation of amino acid 6

The methacrylate **2** was obtained thanks to a nucleophile substitution reaction starting from bromo derivate **1**, in presence of sodium azide (acetone and water, 3:1; Scheme 17). The procedure reported in literature¹⁰⁵ suggests that the reaction leads to the desired compound in 10 minutes; however, it was observed that with higher reaction time until 4 hours, the yield became quantitative.



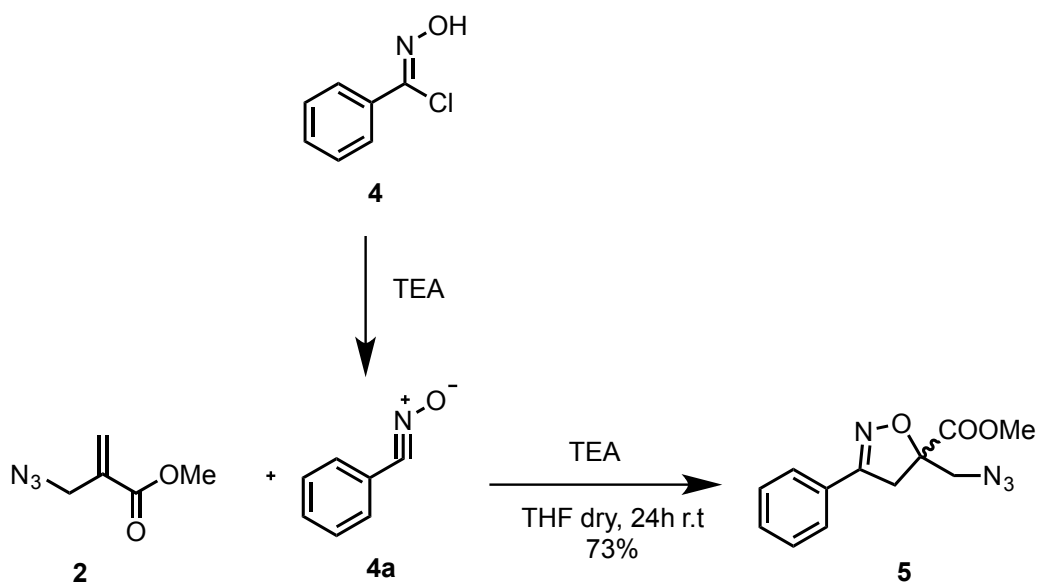
Scheme 17 Preparation of intermediate 2

Following the Werner and Buss synthesis (Scheme 18), chloroxime **4** was obtained. In particular, we decided to use NCS instead of Cl_2 and TEA instead of Na_2CO_3 , at room temperature¹⁰⁶. Commercially available benzaldoxime **3** was chlorinated using N-chlorosuccinimide at room temperature, under stirring for 4 hours. Firstly, we performed the reaction in dry THF, with the intention to use the same solvent planned for the cycloaddition, but better results were achieved in dry DMF (quantitative yield).



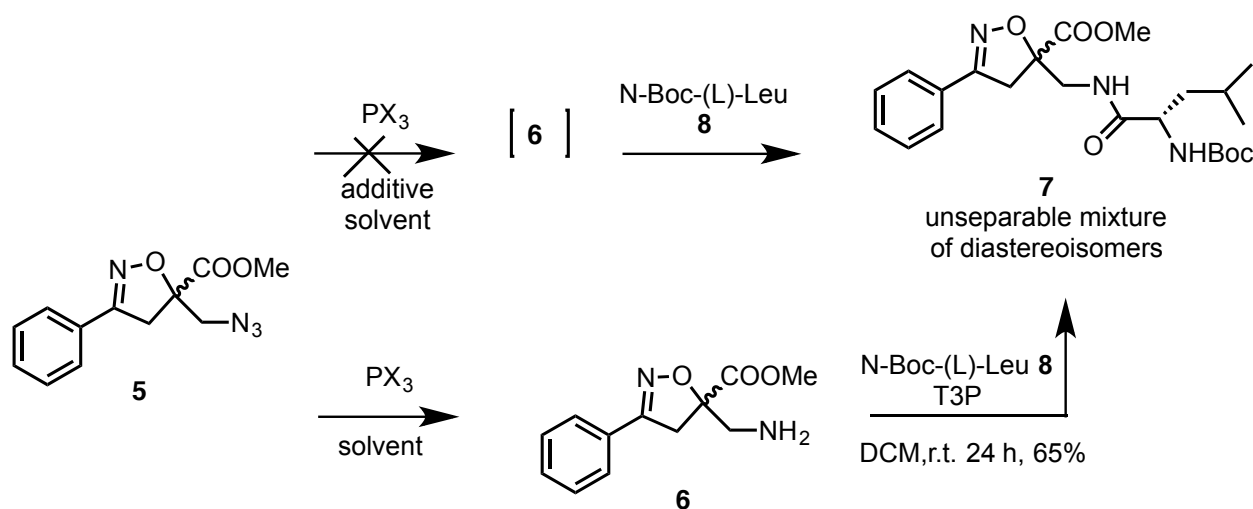
Scheme 18 Preparation of chloroxime 4 from benzaldoxime 3

1,3-Dipolar cycloaddition between **2** and benzonitrile oxide **4a** was performed in dry THF under nitrogen atmosphere. Intermediate **4a** was generated *in situ* starting from compound **4** by adding TEA to the reaction mixture (Scheme 19). Different reaction times were screened to find the right compromise between yield and quality of the reaction avoiding the formation of by-products. It was observed that leaving the reaction overnight allow the obtainment of compound **5** as single regioisomer with an overall yield of 73% after flash chromatography.



Scheme 19 Cycloaddition reaction between nitrile oxide **4a** and acrylate **2** affording a cyclic compound **5** with isoxazoline core

The new β-amino acid **6** was obtained using Staudinger reaction protocol to reduce the azido group to amino one. Furthermore, since compound **6** was obtained as a racemic mixture, it was necessary its transformation into a diastereoisomeric mixture in order to separate the enantiomers (Scheme 20).



Scheme 20 General strategies for the synthesis of dipeptide 7

Two different strategies were investigated, the first one consisting in the “one pot” transformation of azido compound **5**, in presence of *N*-Boc-(*L*)-Leucine, into diastereomers **7**, avoiding the isolation of amino intermediate **6** (Scheme 20). We tested different phosphine reagents, additives and reaction conditions in order to obtain directly **7** (Table 23, entries 1-3). Two different procedures were found in literature for this purpose. In the first one (entry 1, Table 23), an excess of PMe_3 was used in combination of PySSPy as additive to promote amidation.¹⁰⁷ The second one involves the use of catalytic amounts of PPh_3 in the presence of a reducing agent such as PhSiH_3 (entry 2) and Ph_2SiH_2 (entry 3). $\text{P}^{\text{III}}/\text{P}^{\text{V}}$ -redox-driven cycle exploiting the reactivity of silanes toward the chemo selective reduction of phosphine oxides to phosphine.¹⁰⁸

Unfortunately, all these approaches lead to the recovery of the starting materials.

Table 23 Summary of the Staudinger investigations

Entry	Reagent/s	Phosphine	Additive	Solvent	T (°C)	Compound (Yield)
1	5 + 8	PMe_3 (2.4 eq)	PySSPy (0.2 eq)	Toluene ^a	25	7 (-)
2	5 + 8	PPh_3 (0.1 eq)	PhSiH_3 (1 eq)	Toluene ^a	reflux	7 (-)
3	5 + 8	PPh_3 (0.1 eq)	Ph_2SiH_2 (1 eq)	Toluene ^a	reflux	7 (-)
4	5	$\text{P}(\text{OEt})_3$ (1.1 eq)	-	THF	25	6 (-)
5	5	PPh_3 (1.1 eq)	-	THF	25	6 (48%)

6	5	PMe ₃ (1.1 eq)	-	THF	25	6 (65%)
---	---	---------------------------	---	-----	----	---------

^aDry toluene;

Abandoned the idea of the one-pot ligation giving **7**, different phosphines were tested for the classic Staudinger reaction to obtain amine **6**, in particular P(OEt)₃ (entry 4), PPh₃ (entry 5), and PMe₃ (entry 6). Only triphenyl and trimethyl phosphines gave compound **6**. However, a significant difference in yield was observed by using the two reactants.

The reason behind this diversity could be ascribed to the different hydrolysis rate to convert the imino phosphorane intermediate to the amine. In fact, electronic and steric effects play multiple roles in determining the rate and yield of Staudinger reduction.¹⁰⁹ The resulting complex from the addition of PPh₃ is more sterically hindered than the complex from PMe₃ (Figure 81). Moreover, π -interactions between the aromatic group of the isoxazoline scaffold with the aryl moiety of the phosphine could make the complex very stable.

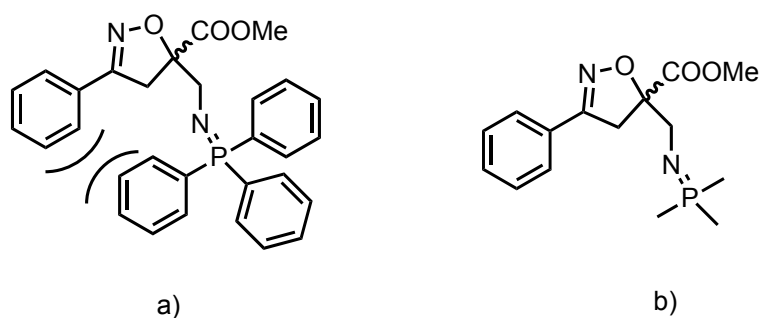


Figure 81 Iminophosphoranes obtained from triphenyl (a) and trimethyl (b) phosphines

We hypothesized that the complex resulting from the addition of PPh₃ is too stable for being release, or that water meets more difficulties reaching the N=P bond for the steric features, which explained the lower yield achieved of compound **6** when using this reagent. Our hypothesis was supported by the MS (ESI) analysis of the crude reaction mixture obtained with triphenyl phosphine: a significant peak representing the mass of the imino phosphorane (*m/z*: 495.09) is present, letting suppose that water could not perform the entirely release of the corresponding amine from the complex.

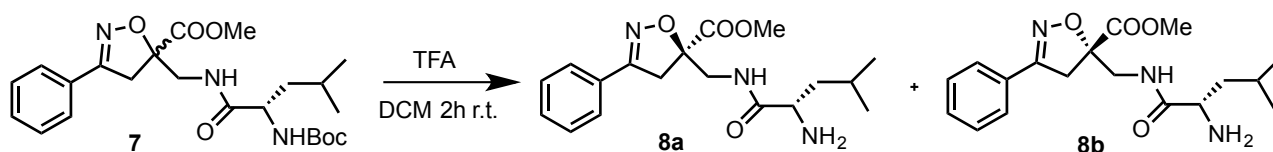
Based on the above-reported evidence, the best results for the Staudinger reaction consisted in use of THF and water (7 equiv.) with elected trimethyl phosphine, operating under stirring from a minimum of 24 hour to a maximum of 72 hours, which improved the yield of **6** to 65% (Table 23, entry 6).

Peptides synthesis

As underlined before, the resulting scaffold from the cycloaddition reaction was obtained as racemic mixture. Thus, a coupling reaction with *N*-Boc-(*L*)-Leu-OH was performed, combining the need to obtain two separable diastereomers and carry forward the intention to insert the scaffold into a model peptide to verify the ability of the new amino acid to generate a specific conformation according to its stereochemistry.

T3P was chosen as best coupling reagent for the activation of the carboxylic function of *N*-Boc-(*L*)-Leu¹¹⁰ in DCM. The peptide coupling reaction was performed for 24 hours and the crude product was purified through flash chromatography, affording compound **7** with 65% yield as a mixture of two diastereomers (Scheme 21). However, the dipeptide formation still did not allow the separation of the two isomers **7**.

Thus, starting from **7**, the *N*-terminus was deprotected affording compound **8**. Having the free *N*-terminus, it has been finally possible the separation of the two isomers (Scheme 21).



Scheme 21 Isomers **8a** and **8b** separation after the *N*-terminus deprotection

Optimal results were obtained conducting a separation with a gradient elution mixture, starting from 100% DCM to 10:1 DCM/MeOH adding 0.1% of TEA to the eluent mixture. This strategy turned out to be successful and the two isomers were efficiently separated with high yields.

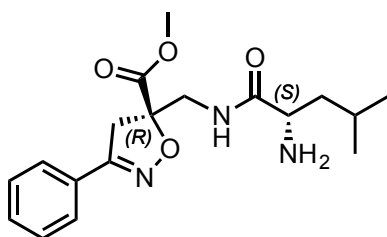
X-Ray analysis on a sample crystal of **8a** were performed in collaboration with Prof. Lo Presti (Chemistry Department of Milan University), with the aim of defining the absolute configuration at α,α -amino acid stereocenter. As described in Figure 82, the compound is chiral and crystallizes in the acentric polar space group, with one molecule for asymmetric unit. Figures 4a and 4b show the absolute configuration of the chiral centers, confirming the *S*-configuration for the Leucine and *R* that of isooxazoline moiety.

The crystal packing of this substance is likely dominated by permanent electrostatic interactions, which cause the alignment of neighboring molecules into a polar arrangement of iso-oriented dipoles. This aspect is worth of further studies, aimed at investigating

whether crystals of **8a** could display pyroelectric, piezoelectric or non-linear optical properties.

Puckering analysis¹¹¹, shows that the partially saturated isoxazole ring adopts a slightly distorted envelope configuration, with puckering amplitude and phase reading $Q_2 = 0.12$, $\phi_2 = 140.21$ deg, respectively.

A)



B)

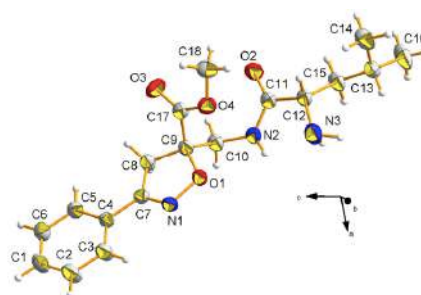
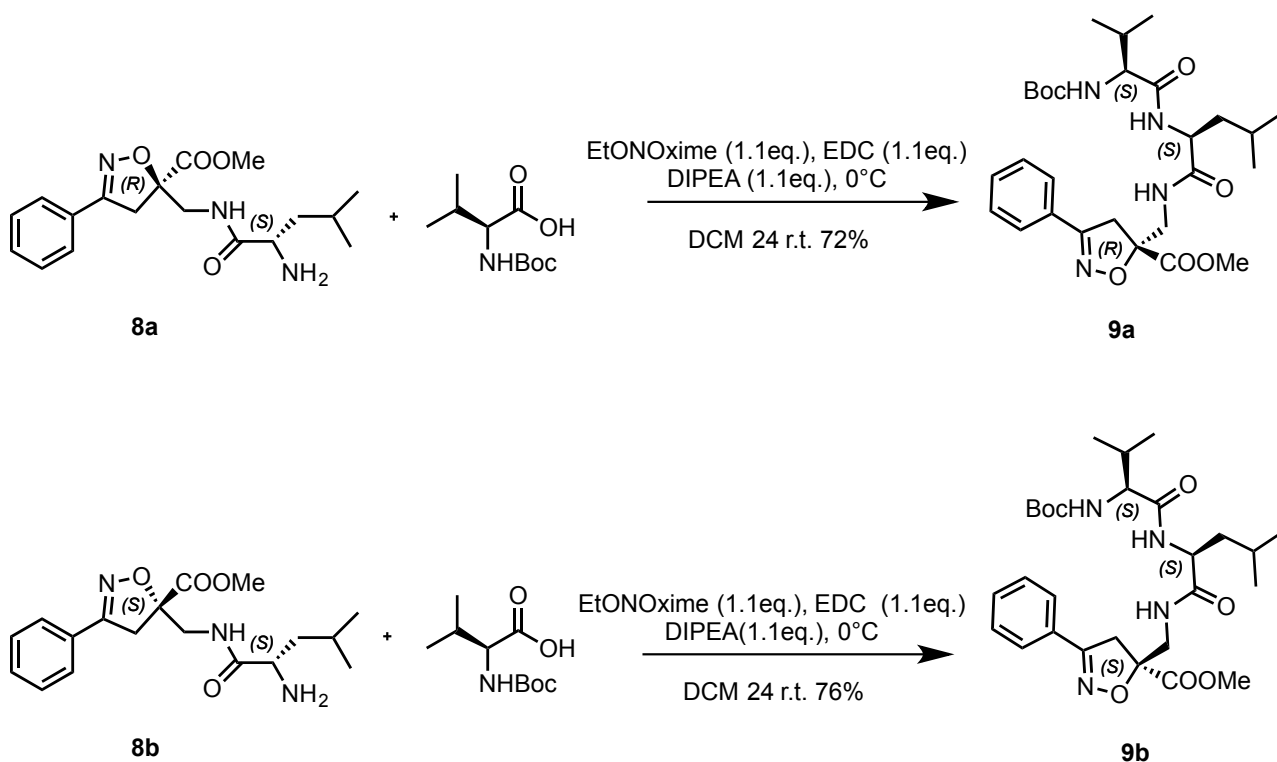


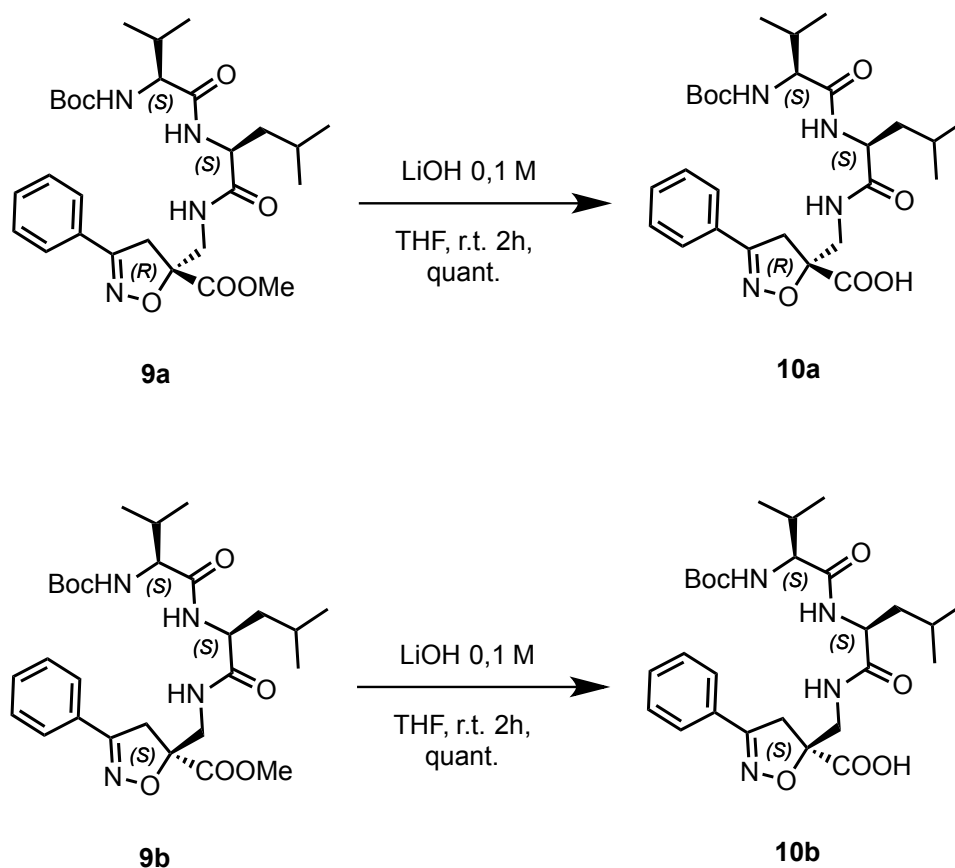
Figure 82 Asymmetric unit of **8a** at RT, with the atom-numbering scheme. The usual colour code was employed for atoms (grey: C; white: H; blue: N; red: O).

Starting from diastereomers **8a** and **8b**, a second coupling reaction was performed to elongate the peptide chain from *N*-terminus. *N*-Boc-(*L*)-Valine was chosen because it's well known that the Boc-*N*-Val-Leu-OH dipeptide assume an extended conformation in solution. For these reasons it would be possible to study the effect of $\beta^{2,2}$ -isox-AA on the secondary structure of the peptide. The coupling reaction was conducted on both **8a** and **8b** compounds in the same conditions previous reported in Scheme 5. On the other hand, we observed that setting up the reaction with different activators allowed the obtainment of the desired product in higher yields, with no purification requirements. Thus, EDC was used as activation agent (Scheme 22) instead of T3P, with EtONoxime as additive and again DIPEA as basic reagent. EtONoxime acts as a neutralizing reagent for the EDC by-product, preventing unwanted side reactions, *i.e.* racemization.



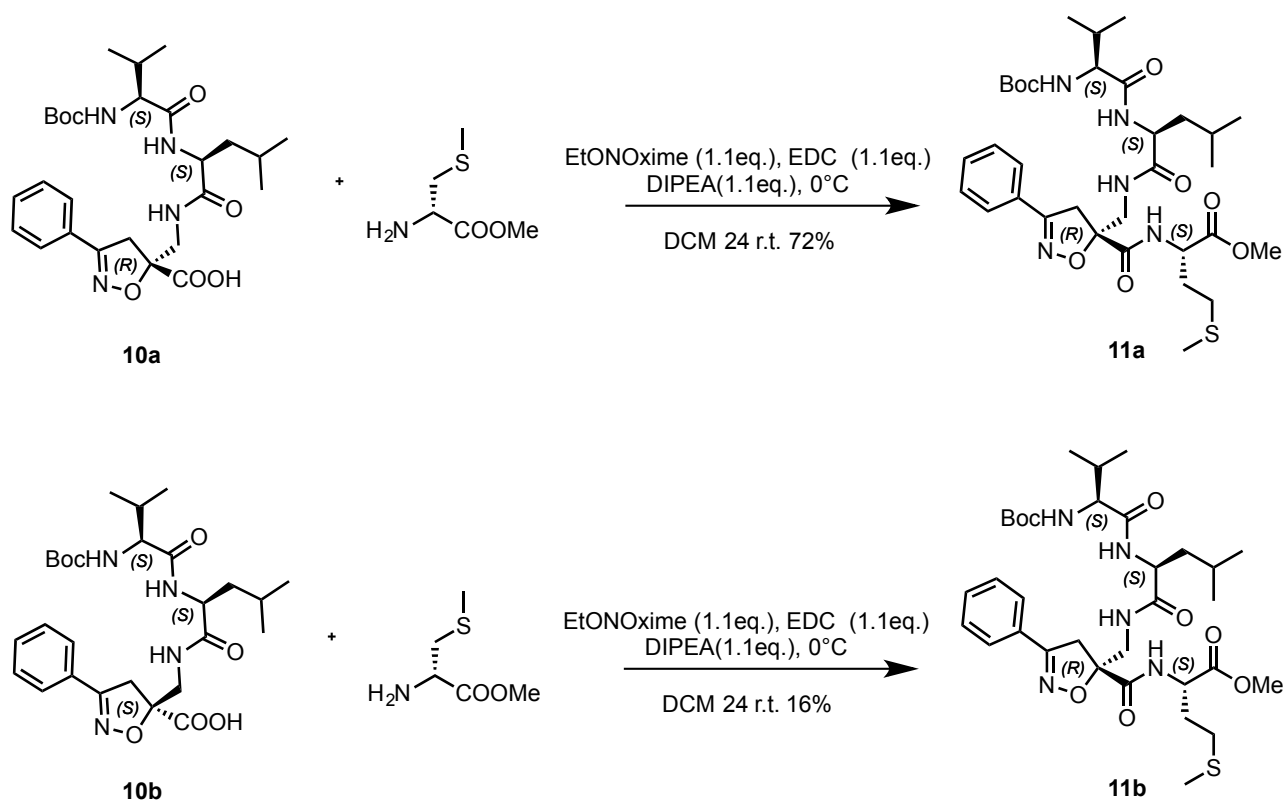
Scheme 22 Isomers **8a** and **8b** separation after coupling reaction

Afterwards, we worked to deprotect the C-terminus of the $\beta^{2,2}$ -isox-AA to elongate the peptide chain. Starting from both **9a** and **9b**, the deprotection of the C-terminus was performed using a 0.1 M solution of LiOH. After acidification, the acid intermediates **10a** and **10b** were obtained in quantitative yield (Scheme 23).



Scheme 23 Hydrolysis of tripeptide 9a and 9b

Tripeptide **10a** and **10b** coupled with methionine methyl ester using EDC/EtONoxime activation, as reported above, affording tetrapeptides **11a** (72%) and **11b** (16%). This second coupling reaction led to significantly different yields of the two isomers after purification. We think that this problem could be ascribe to the low solubility issue of **11b** in the eluent mixture (Scheme 24).



Scheme 24 Tetrapeptides **11a** and **11b**

NMR characterization

Tripeptides **9a** and **9b**, which differ for the configuration at isoxazoline stereocenter in position 5, showed different conformational behavior as it was observed from NMR analyses performed in the same condition (CDCl_3 , 150 mg in 750 μL). The chemical shift of the amide (5-7 ppm) and $\text{CH}\alpha$ (3.5-4.2 ppm) protons are well dispersed, indicating that the secondary structures of the two compounds resulted to be far away to the “lack of conformations”.

It is worth to underline the differences of the two diastereomers in terms of $\Delta\delta/\Delta T$. With NMR at variable temperature, it is possible to observe if the amidic protons are blocked in H-bonds or in steric situations not allowing the shift of the corresponding signal. This analysis is very useful to have a preliminary idea if the peptide can fold. According with these experiments (T: 273-323 K; Figure 83), compound **9a** showed low variation of $\Delta\delta/\Delta T$ for NH_{Leu} and NH_{Val} (NH_{Leu} -3.6 ppb/K; NH_{Val} -2.1 ppb/K), meaning that they are probably involved in strong H-bonds, while NH_{Isox} is not solvent shielded. On the other hand, all the NHs of **9b** are not involved in any H-bonds ($\text{NH} > -5$ ppb/K).

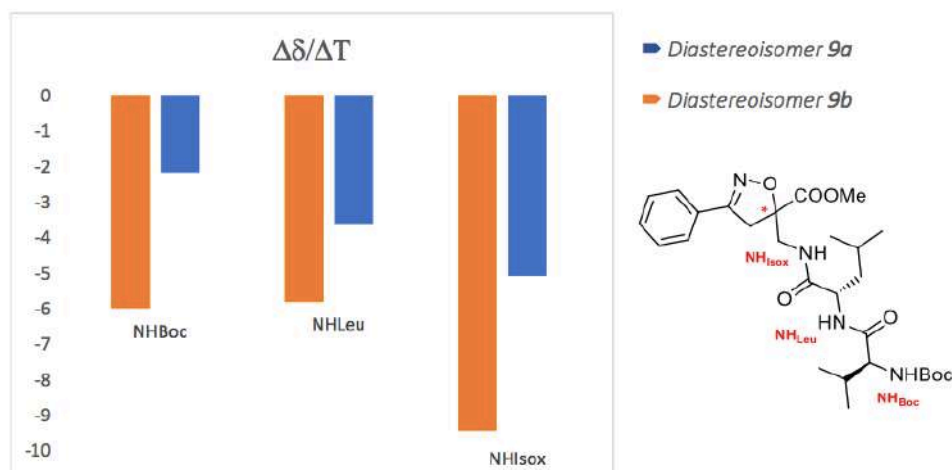


Figure 83 NH $\Delta\delta/\Delta T$ NMR analyses of the two diastereoisomers 9

NOESY experiment of peptide **9a** (Figure 84) presents strong CH_i/NH_{i+1} and weak NH_i/NH_{i+1} spatial proximity, suggesting the formation of turn. Furthermore, NH_{Isox} showed a weak NOE with Me_{Leu} suggesting that these two moieties point toward the same direction.

Considering that the C=N bond of isooxazoline ring is an isostere of a carbonyl function, our amino acid can be also considered a γ -AA. Our hypothesis is that a possible electrostatic or H-bond interaction between NH_{Val} and the nitrogen occurs forming a α -turn (Figure 84). This behavior is documented by some reported short peptides using heterocyclic.¹¹²

Considering the low $\Delta\delta/\Delta T$ for NH_{Leu} , the hypothesis is that it can interact with the oxygen of isooxazoline ring or this low value could be ascribed to an unfavorable steric situation preventing interaction with the solvent.

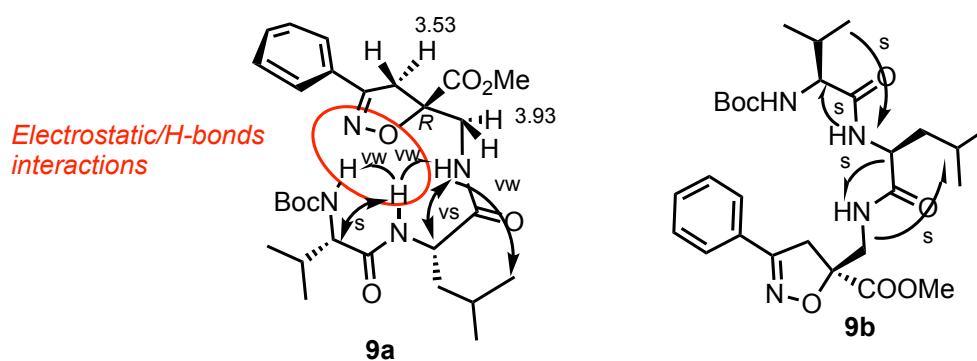


Figure 84 Structures of the tripeptides **9a** and **9b** and NOEs. Electrostatic/H-bonds interactions are described using arrows.

Even if the NH shifts of amide signals at different temperatures for the diastereomers **9b** show the absence of hydrogen bonds, this does not mean that it has not a preferred conformation: it is highly probable that **9b** assumed an extended conformation, as confirmed by $J_{HN\alpha}$, higher than 8 Hz for valine and leucine, and by strong CH_i/NH_{i+1} NOEs.

NMR analyses on tetrapeptides **11a** and **11b** are performed. With respect to **9a**, the experiments at variable temperature show a less strong H-bond for valine (-4.1 ppb/K), higher values for NH_{Leu} and NH_{Isox} (more then -7 ppb/K) and a medium value for methionine (-4.9 ppb/K) (Figure 85).

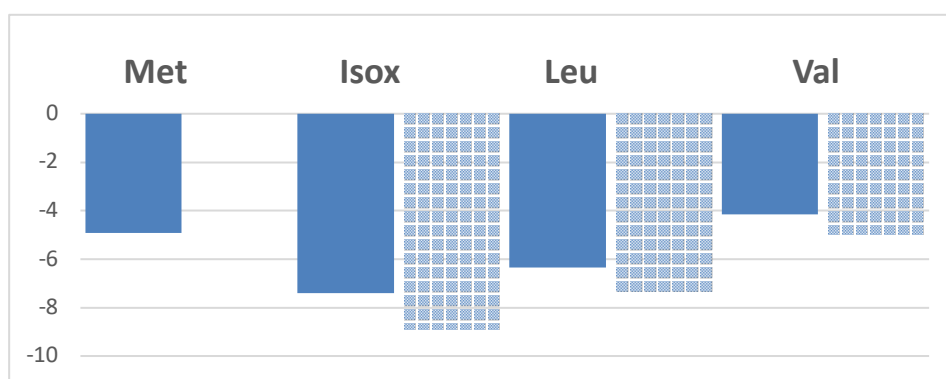


Figure 85 $NH \Delta\delta/\Delta T$ NMR analyses of the two diastereomers **11**

Focusing on the *N*-terminus chain of **11a**, a very good NHs dispersion was observed but with a significant lowering chemical shifts (mostly for isoxazoline moiety) respect to the corresponding tripeptide **9a**. NOESY experiment presents again, as for **9a** (Table 24), strong CH_i/NH_{i+1} and weak NH_i/NH_{i+1} spatial proximity. On the other hand, some weak intrastain NOEs were detected between NH_{Met} and both NH_{Isox} and Me_{Leu} (δ , 0.93), this last showing also proximity with NH_{Isox} (w9). Furthermore, Me_{Leu} resonating at δ 0.90, showed proximity with Ph. These NOEs are not compatible with **9a** conformation, suggesting that the presence of methionine can induce a different conformation. Considering that $\Delta\delta/\Delta T$ values of both methionine and valine are consistent with an equilibrium between an H- and a non H-bond, it is suggested that two conformers could be present, the first one similar to **9a**, the second, supported by intrastain NOE and by a possible NH-bond of methionine, in which the C- and N-terminus can face each other. The equilibrium between **11a** and **11a'** is made possible by the different dihedral angles of CH_2NH isoxazoline group which confers freedom to C-N bond (Figure 86).

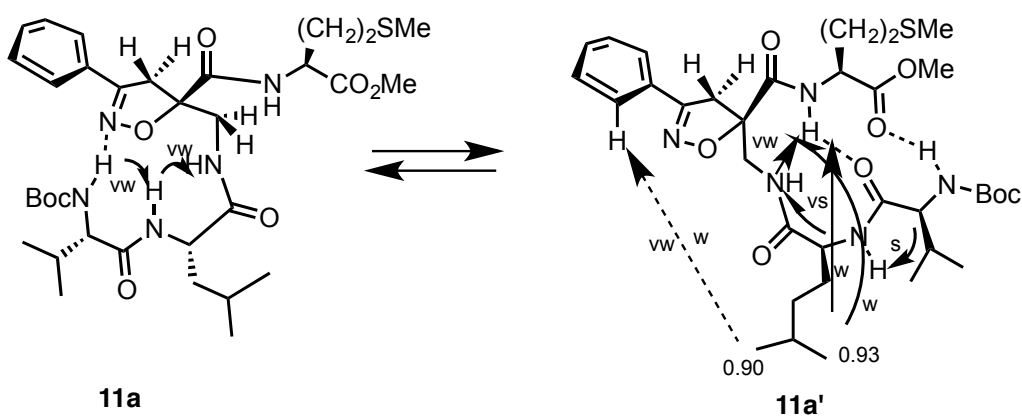


Figure 86 Conformational equilibrium between **11a** and **11a'** described using arrows and dotted line

Computational investigations are in progress to clarify this issue and to define the orientation of H-bonds, mostly for tripeptide **9a**.

Concerning peptide **11b**, it is to point out that no intrastrand NOEs were detected (Figure87).

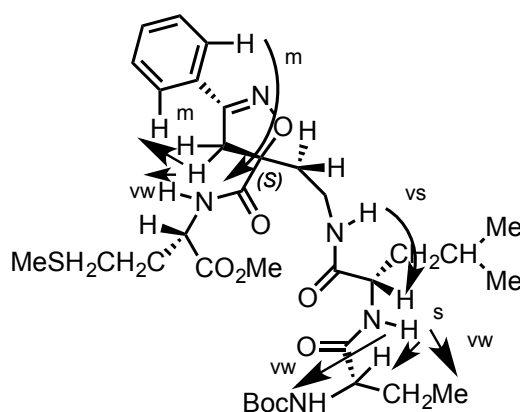


Figure 87 Conformational structure of tetrapeptide **11b**. Isoxazole ring, protons and amino acid side chain are described using arrows.

Table 24 Overview of NH and J_{NHCH} chemical shift

Amino Acid	9a		9b		11a		11b	
	NH (δ)	J_{NHCH}	NH (δ)	J_{NHCH}	NH (δ)	J_{NHCH}	NH (δ)	J_{NHCH}
Val	4.94	7.9	5.10	8.5	5.14	8.5	5.12	brs
Leu	6.37	7.5	6.44	8.1	6.58	7.4	6.47	brs
Isox	6.75	6.5 (t)	6.73	5.9 (t)	7.37	8.9/7.4	7.82	7.6/5.1
Met	-	-	-	-	7.77	7.7	7.48	8.4

Conclusion

In conclusion, we succeed in the synthesis of a new $\beta^{2,2}$ -amino acid with isoxazoline core with the aim of preparing peptidomimetics. We observed that the two isomers with opposite stereochemistry in position 5 are able to induce different stable secondary structures in tripeptide models **9a** and **9b**, being the first one is a turn mimic, while the second one an extended secondary structure mimic.

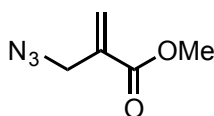
Preliminary conformational studies of tetrapeptides **11a** and **11b** describe a possible electrostatic interaction between NH_{Val} and/or NH_{Leu} with the conjugated π -system of isooxazoline ring suggesting the formation of α turn. Furthermore, to confirm our hypothesis, computational calculations are in our plan for the future.

Experimental part

General information

ESI mass spectra were recorded on an LCQESI MS on a LCQ Advantage spectrometer from Thermo Finnigan and a LCQ Fleet spectrometer from Thermo Scientific. The NMR spectroscopic experiments were carried out either on a Varian MERCURY 200 MHz (200 and 50 MHz for ^1H and ^{13}C , respectively), Varian OXFORD 300 MHz (300 and 75 MHz for ^1H and ^{13}C , respectively), or Bruker Avance 300 MHz spectrometers (300 and 75 MHz for ^1H and ^{13}C , respectively). Optical rotations were measured on a Perkin–Elmer 343 polarimeter at 20°C (concentration in g/100 mL). Chemical shifts δ are given in ppm relative to the CHCl_3 internal standard, and the coupling constants J are reported in Hertz (Hz).

Synthesis of methyl 2-(azidomethyl)acrylate (**2**)

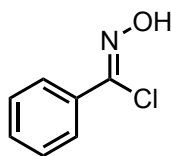


In a round bottom flask equipped with magnetic stirrer, **1** (74 mg, 4.13 mmol) was suspended in a mixture of $(\text{CH}_3)_2\text{CO}$ and H_2O 3:1 (16 mL). NaN_3 (537 mg, 8.26, 2 eq) was added to the solution. The reaction was stirred for 4 hours at room temperature. The reaction color turned slowly from colorless to pale orange. At the end of the reaction, the mixture was diluted with CH_2Cl_2 (15 mL) and the organic layer was extracted and washed with H_2O (5 mL), brine (5 mL) and then dried over Na_2SO_4 . Solvent was removed under reduced pressure, affording **2** as a pale-yellow oil with 98% yield.

R_f (hexane/AcOEt 6:4): 0.44

The NMR analysis are already reported in literature¹⁰⁵

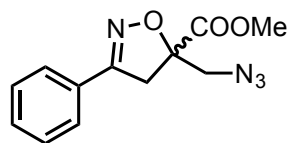
Synthesis of N-hydroxybenzimidoyl chloride (**4**)



In a two-necked round-bottom flask, equipped with magnetic stirrer and nitrogen inlet, corresponding oxime **3** (500 mg, 4.13 mmol) was suspended in dry DMF (6 mL). Afterwards, NCS (551 mg, 4.13 mmol, 1 eq) was added to the solution. The mixture turned quickly from colorless to bright yellow, and finally pale yellow. The reaction was stirred for 4 hours at room temperature under nitrogen atmosphere. Then, the reaction mixture was diluted with CH₂Cl₂ (15 mL) and the organic layer was extracted and wash with H₂O (10 mL), then dried over Na₂SO₄. The solvent was removed under reduced pressure, affording **4** as a pale-yellow oil with quantitative yield.

The NMR analysis are already reported in literature¹⁰⁶

Synthesis of methyl 5-(azidomethyl)-3-phenyl-4,5- dihydroisoxazole-5-carboxylate (5)



In a two-necked round-bottom flask, equipped with magnetic stirrer and nitrogen inlet, **2** (640 mg, 4.13 mmol) was suspended in dry THF (5 mL). Afterwards, **4** (580 mg, 4.13 mmol) was diluted in dry THF (7 mL) and added dropwise to the solution. TEA (1,15 mL, 8.26 mmol, 2 eq) was added dropwise to the mixture and the formation of a white solid precipitate was noticed. The reaction was stirred overnight at room temperature under nitrogen atmosphere. The reaction mixture was concentrated under reduced pressure, then the organic layer was extracted with AcOEt (10 mL) and washed with H₂O (15 mL), finally dried over Na₂SO₄. The solvent was removed under reduced pressure, affording a dark-yellow oil. Purification of the crude product by flash chromatography (gradient from 100% hexane to mixture hexane/AcOEt 8:2) affording compound **5** as a white solid (overall yield 73%).

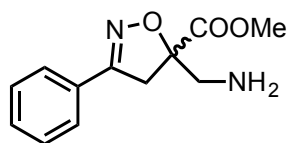
R_f (hexane/AcOEt 8:2): 0.40

¹H NMR: (300 MHz, CD₃Cl) δ 7.70-7.65 (m, 2H); 7.54-7.35 (m, 3H); 3.87 (s, 3H); 3.82-3.35 (AB system J=17 Hz); 3.75-3.69 (AB system J=17 Hz) ppm.

¹³C NMR: (75 MHz, CD₃Cl) δ 170.1, 156.4, 130.8, 128.9, 128.4, 127.0, 87.6, 54.2, 53.4, 41.5 ppm.

MS (ESI): *m/z*: 283.1 [M+Na]⁺

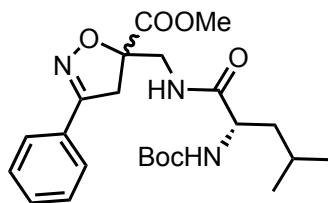
Synthesis of methyl 5-(aminomethyl)-3-phenyl-4,5- dihydroisoxazole-5-carboxylate (6)



In a round bottom flask equipped with magnetic stirrer, **5** (771 mg, 2.96 mmol) was suspended in THF (29.6 mL) to obtain a 0.1M solution. Afterwards, H₂O (0.37 mL, 20.72 mmol, 7 eq) and PMe₃ 0.1M in PhMe (3.26 mL, 3.26 mmol, 1.1 eq) were added to the solution. The reaction mixture turned from colorless to bright yellow. The reaction was stirred for 72 hours at room temperature under nitrogen atmosphere. At the end of the reaction, the mixture was filtered over cotton to remove trimethyl phosphine oxide as a white solid, then solvent was removed under reduced pressure and the obtained amine **6** was immediately used for the following coupling reaction.

R_f (DCM/MeOH 30:1): 0.24

Synthesis of methyl 5-(((S)-2-((tert-butoxycarbonyl)amino)-4-methylpentanamido)methyl)-3-phenyl-4,5-dihydroisoxazole-5- carboxylate (7)



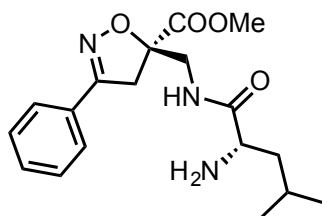
In a round bottom flask equipped with magnetic stirrer, **6** (693 mg, 2.96 mmol) was suspended in dry DCM (20 mL), then the solution was cooled to 0 °C. Afterwards, **N-Boc-(L)-Leucine** (1.369 g, 5.92 mmol, 2 eq) and T3P (3.2 mL 8.88 mmol, 3 eq) were added. Finally, DIPEA was added until pH = 8 (1.5 mL, 8.88 mmol, 3 eq). The reaction was stirred overnight at room temperature. After 12 hours at room temperature, the reaction mixture was washed with KHSO₄ 5% (20 mL), NaHCO₃ (20 mL), brine (25 mL), then the organic layer was dried over Na₂SO₄. The solvent was removed under reduced pressure, affording a pale-yellow oil. Purification of the crude product by flash chromatography (gradient from 100% hexane to mixture hexane/AcOEt 6:4) afforded the compound **7** as a white solid foam (overall yield 65%).

R_f (hexane/AcOEt 6:4): 0.44

¹H NMR: (300 MHz, CD₃Cl) δ 7.70-7.57 (m, 2H); 7.46-7.35 (m, 3H); 6.71-6.62 (m, 0.5 H); 6.58-6.47 (m, 0.5 H); 4.8 (d, J=7.5 Hz, 0.5 H); 4.7 (d, J=7.0, 0.5 H); 4.13-4.05 (m, 2H); 3.83 (s, 3H); 3.78-3.66 (m, 2H); 3.58-3.46 (m, 1H); 1.68-1.28 (13 H); 0.96-0.6 (m, 6H) ppm.

¹³C NMR: (75 MHz, CD₃Cl) δ 173.7; 170.6; 157.0; 156.8; 155.5; 130.6; 128.7 (x2); 126.97; 126.92; 87.8; 80.1; 53.2; 53.2; 42.7; 41.4; 41.2; 41.1; 28.2; 24.7; 22.9; 22.6; 21.7 ppm.

Synthesis of methyl 5-(((S)-2-amino-4-methylpentanamido)methyl)-3-phenyl-4,5-dihydroisoxazole-5-carboxylate (**8a**)



In a round bottom flask equipped with magnetic stirrer, **7** (850 mg, 1.91 mmol) was suspended in DCM (10 mL). Afterwards, the solution was cooled at 0 °C and TFA (10 mL) was added dropwise. The reaction was stirred for 2 hours at room temperature. Then, the reaction mixture was neutralized with NaHCO₃ and the organic layer was extracted with DCM and dried over Na₂SO₄. The solvent was removed under reduced pressure, affording the compound **8** as a pale- yellow foam (591 mg). The two diastereoisomers were separated through flash chromatography (DCM/MeOH 10:1 + 0.1% TEA) affording **8a** (266 mg) and **8b** (251 mg) as white solids.

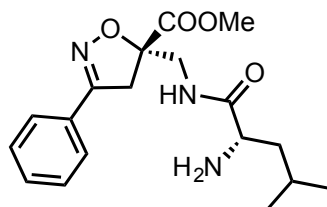
Rf **8a** (DCM/MeOH 10:1): 0.33

¹H NMR **8a**: (300 MHz, CD₃OD) δ 7.78-7.59 (m, 2H); 7.54-7.31 (m, 3H); 3.83 (s, 3H); 3.84- 3.57 (AB System, 17 Hz); 3.36-3.29 (m, 2H); 1.7-1.55 (m, 1H); 1.5-1.32 (m, 1H); 1.31-1.18 (m, 1H); 0.88-0.78 (m, 6H) ppm.

¹³C NMR **8a**: (75 MHz, CH₃OD) δ 177.66, 170.70, 156.85, 130.31, 128.60, 128.55, 126.53, 87.95, 53.19, 52.17, 44.18, 42.61, 40.74, 24.33, 21.89, 20.90.

[α]²⁰_D **8a**: +36° (22,2 · 10⁻³ g/mL in MeOH)

Synthesis of methyl 5-(((S)-2-amino-4-methylpentanamido)methyl)-3-phenyl-4,5-dihydroisoxazole-5-carboxylate (**8b**)



In a round bottom flask equipped with magnetic stirrer, **7** (850 mg, 1.91 mmol) was suspended in DCM (10 mL). Afterwards, the solution was cooled at 0 °C and TFA (10 mL) was added dropwise. The reaction was stirred for 2 hours at room temperature. Then, the reaction mixture was neutralized with NaHCO₃ and the organic layer was extracted with DCM and dried over Na₂SO₄. The solvent was removed under reduced pressure, affording the compound **8** as a pale- yellow foam (591 mg). The two diastereoisomers were separated through flash chromatography (DCM/MeOH 10:1 + 0.1% TEA) affording **8a** (266 mg) and **8b** (251 mg) as white solids.

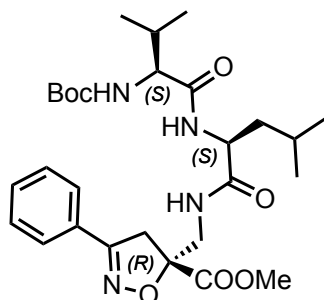
Rf **8b** (DCM/MeOH 10:1): 0.30

¹H NMR **8b**: (75 MHz, CH₃OD) δ 7.69-7.63; 7.49-7.40; 4.17-3.85 (AB System, 17 Hz); 3.83 (s, 3H); 3.58-3.44 (m, 2H); 1.48-1.34 (m, 3H); 0.64-0.74 (m, 6H) ppm.

¹³C NMR **8b**: (75 MHz, CD₃OD) δ 170.41, 156.57, 129.99, 129.04, 127.55, 127.00, 87.64, 52.23, 51.12, 42.82, 40.79, 40.51, 30.00, 24.56, 21.19, 20.38.

[α]²⁰_D **8b**: -91° (21,2 · 10⁻³ g/mL in MeOH)

Synthesis of N-Boc-(L)-Val-(L)-Leu-β-(R)-Isox-MetOMe (9a)



In a round bottom flask equipped with magnetic stirrer, **N-Boc-(L)-Valine** (176 mg, 0.811 mmol) was suspended in dry DCM (6 mL). Afterwards, the solution was cooled at 0 °C and EtONOXime (115 mg, 0.811 mmol) and EDC (160 mg, 0.811 mmol) were added. The reaction was stirred for 1 hour at 0 °C, then **8a** (256 mg, 0.737 mmol) was added. DIPEA was added until pH = 8 (0.14 mL, 0.811 mmol, 1.1 eq). The reaction was stirred overnight at room temperature. Then, the reaction mixture was washed with KHSO₄ 5% (20 mL), NaHCO₃ (20 mL), brine (25 mL), then the organic layer was dried over Na₂SO₄. The solvent was removed under reduced pressure, affording **9a** as white solid with 72% yield (292 mg). Detailed NMR data are reported in Table 25

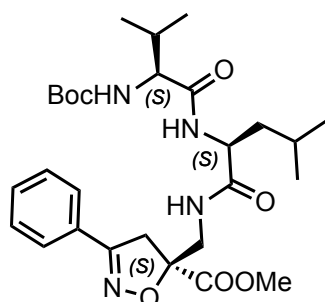
R_f (hexane/AcOEt 1:1): 0.42

[α]²⁰_D: -5°C (20.4 · 10⁻³ g/mL in MeOH)

Table 25 ^1H , ^{13}C NMR (CD_3CN , 750mL 0.033 mM) and NOEs (200 ms) data for **9a**

AA	atom	^1H δ	Moltepicity <i>J</i> (Hz)	^{13}C δ	Noesy (200 ms)
Val-1	CO			171.8	
	CH	3.81	overl.	53.2	NH _{Leu} (s)
	Me ₂ CH	2.12.-1.95	m	30.3	
	Me	0.90, 0.88	d, 8.5 d, 7.9	19.3 17.7	NH _{Boc} (vs)
	NH	4.94	d, 7.9	-	Me _{val} (0.89, vs) NH _{Leu} (vww)
	CO _{Boc}			156.1	
	<i>t</i> Bu	1.45	s	28.3, 80.3	
Leu-2	CO			172.9	
	CH ₂	1.58, 1.46	m	40.8	NH _{Leu} (m)
	CH	1.57	m	24.6	CH _{Leu} (s)
	Me	0.86 0.87	overl.	21.5, 22.9	0.86: NH _{Isox} (vw), CH _{Leu} (s) 0.87: NH _{Leu} (w),
	CH α	4.39	m	52.1	Me ₂ CHCH ₂ (s) NH _{Isox} (vs)
NH	6.37	d, 7.5		NH _{Boc} (w) Me ₂ CHCH ₂ CH (m) NH _{Isox} (w)	
Isox	CO			170.6	
	OMe	3.82	s	60.1	
	C-5	-		87.7	
	CH ₂ -4	3.73, 3.53	AB system 12.6	41.3	Ph (7.6, m) 3.53: CH ₂ N (3.93, m)
	CH ₂ N	3.93 3.78	dd, 14.5, 6.1 overl.	42.9	NH _{Isox} (m) 3.93: CH ₂ -4 _{Isox} (3.53, m)
	NH	6.75	t, 6.5	-	CH ₂ N (3.79 s, 3.93 (m)) CH _{Leu} (vs) Me ₂ CHCH ₂ (vww) NH _{Leu} (w)
	C-3			157.0	
Ph		7.7-7.6 7.4-7.3	m m	130.6 128.8 128.4 126.9	CH ₂ -4 _{Isox} (m)

Synthesis of N-Boc-(L)-Val-(L)-Leu-β-(S)-Isox-MetOMe (9b)



In a round bottom flask equipped with magnetic stirrer, **N-Boc-(L)-Valine** (166 mg, 0.763 mmol) was suspended in dry DCM (6 mL). Afterwards, the solution was cooled at 0 °C and EtONOXime (108 mg, 0.763 mmol) and EDC (151 mg, 0.763 mmol) were added. The reaction was stirred for 1 hour at 0 °C, then **8b** (256 mg, 0.737 mmol) was added. DIPEA was added till pH = 8 (0.13 mL, 0.763 mmol, 1.1 eq). The reaction was stirred overnight at room temperature. Next, the reaction mixture was washed with KHSO₄ 5% (20 mL), NaHCO₃ (20 mL), brine (25 mL), then the organic layer was dried over Na₂SO₄. Solvent was removed under reduced pressure, affording **9b** as white solid with 76% yield (289 mg). Detailed NMR data are reported in Table 26

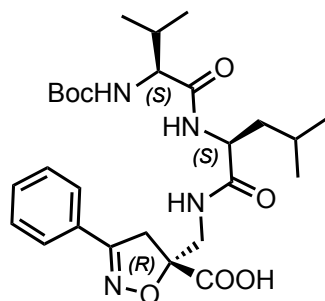
R_f (hexane/AcOEt 1:1): 0.42

[α]²⁰_D: -94°C (26.4 · 10⁻³ g/mL in MeOH)

Table 26 ^1H , ^{13}C NMR (CD_3CN , 750mL 0.019 mM) and NOEs (200 ms) data for **9b**

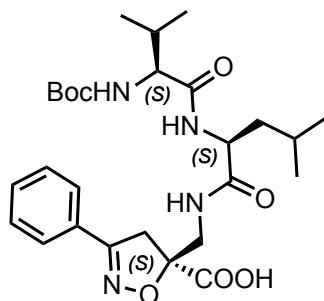
AA	atom	^1H δ	Molteplcity <i>J</i> (Hz)	^{13}C δ	Noesy (200 ms)
Val-1	CO			171.8	
	CH_α	3.87	m	60.1	Me (0.90, s) NH _{Leu} (s)
	Me ₂ CH	2.18-2.03	m	30.5	NH _{Leu} (vw) NH _{Val} (vw)
	Me	0.94	d, 6.8	19.3	NH _{Val} (m)
		0.90	d, 6.9	17.9	NH _{Leu} (w)
	NH	d, 5.10	8.5		<i>t</i> Bu (vw) Me _{Val} (0.90, m)
	CO _{Boc}			155.9	
<i>t</i> Bu	1.44	s	28.4, 80.1		
Leu-2	CO			172.9	
	CH	4.42	m	51.7	Me ₂ CHCH ₂ (s) NH _{Isox} (s)
	CHCH ₂	1.43,1.41	overl.	41.3, 24.7	CH _{Leu} (s) NH _{Leu} (m)
	Me	0.71	5.3	21.7	CH _{Leu} (s)
		0.67	5.1	22.4	
NH	6.44	8.1	-	CH _{Val} (s) CHCH ₂ Leu (m)	
Isox	CO			170.4	
	OMe	3.83	s	53.3	
	C-3			156.7	
	CH ₂ -4	3.77, 3.48	AB system, 17.5	41.1	Ph (7.63, w)
	C5			87.7	
	Ph	7.68-7.61 7.45-7.36		130.6 128.8 128.4 126.9	CH ₂ -4 (w)
	CH ₂ NH	4.13 3.61	dd, 14.4, 6.8 dd, 14.4, 6.8	42.9	NH _{Isox} (m/w) CH _{Leu} (s)
	NH	6.73	t, 5.9		CH _{Leu} (s) CH ₂ N (3.61 m, 4.13 (w))

Synthesis of N-Boc-(L)-Val-(L)-Leu- β -(R)-Isox-MetOH (10a)



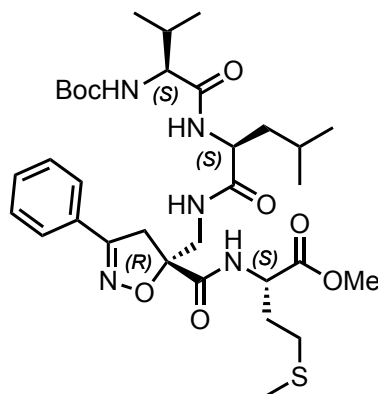
In a round bottom flask equipped with magnetic stirrer, **9a** (277 mg, 0.507 mmol) was suspended in dry THF (10 mL). Afterwards, LiOH 0,1 M (10.13 mL, 1.013 mmol, 2 eq) was added and the reaction was stirred for 2 hours at room temperature. At the end of the reaction, the mixture was washed with KHSO₄ 5% (20 mL) and the organic layer was extracted with DCM, then dried over Na₂SO₄. Solvent was removed under reduced pressure, affording **10a** as white solid with quantitative yield.

Synthesis of N-Boc-(L)-Val-(L)-Leu- β -(S)-Isox-MetOH (10b)



In a round bottom flask equipped with magnetic stirrer, **9b** (274 mg, 0.501 mmol) was suspended in dry THF (10 mL). Afterwards, LiOH 0,1 M (10 mL, 1 mmol, 2 eq) was added and the reaction was stirred for 2 hours at room temperature. At the end of the reaction, the mixture was washed with KHSO₄ 5% (20 mL) and the organic layer was extracted with DCM, then dried over Na₂SO₄. Solvent was removed under reduced pressure, affording a white solid with quantitative yield.

Synthesis of N-Boc-(L)-Val-(L)-Leu- β -(R)-Isox-MetOMe (11a)



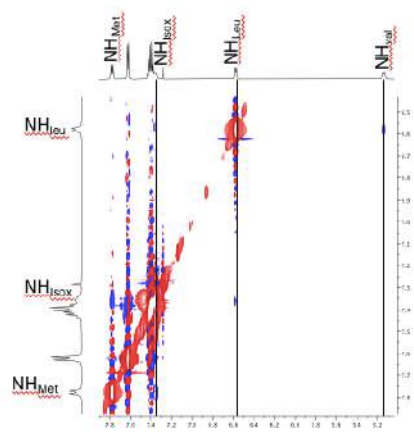
In a round bottom flask equipped with magnetic stirrer, **10a** (50 mg, 0.094 mmol) was suspended in dry DCM (3 mL). Afterwards, the solution was cooled at 0 °C and EtONoxime (13 mg, 0.094 mmol) and EDC (19 mg, 0.094 mmol) were added. The reaction was stirred for 1 hour at 0 °C, then (**L**)-Methionine-OMe (14 mg, 0.085 mmol) was added. DIPEA was added till pH = 8 (16 μ L, 0.094 mmol, 1.1 eq). The reaction was stirred overnight at room temperature. Next, the reaction mixture was washed with KHSO₄ 5% (10 mL), NaHCO₃ (10 mL), brine (15 mL), then the organic layer was dried over Na₂SO₄. Solvent was removed under reduced pressure, affording a white solid. Purification of the crude product by flash chromatography (gradient from 100% DCM to mixture DCM/AcOEt 6:4) afforded the compound **11a** as a white solid with 72% yield (46 mg). Detailed NMR data are reported in Table 27 and Figure 88.

R_f (DCM/MeOH 30:1): 0.47

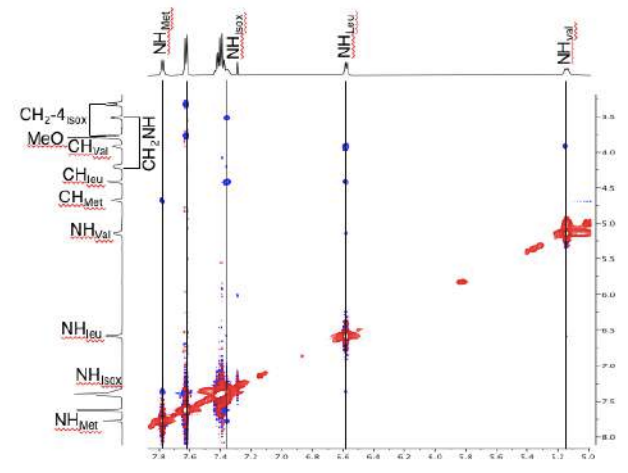
Table 27 ¹H, ¹³C NMR (CD₃CN, 750mL 0.016 mM) and NOEs (900 ms) data for **11a**

AA	atom	¹ H δ	Molteplicity <i>J</i> (Hz)	¹³ C δ	Noesy (900 ms)
Val-1	CO			171.9	
	CH _α	3.92	m	59.9	Me _{Val} (vs) NH _{Leu} (vs)
	Me ₂ CH	2.09-2.01	m, overl.	31.1	NH _{Leu} (m) NH _{Val} (m)
	Me	0.94, 0.92	d, 6.7 d, 6.8	22.7 19.2	0.94: CH _α (vs), NH _{Boc} (vs)
	NH	5.14	d, 8.5	-	Me ₂ CH _{Val} (vs) Boc (m) NH _{Leu} (vw)
	CO _{Boc}			155.8	
	<i>t</i> Bu	1.45	s	28.3, 79.7	
Leu-2	CO			172.5	
	CH ₂	1.66, 1.53	m (overl.), m	40.9	NH _{Leu} (m/s)
	CH	1.57-1.50	m, overl.	24.7	CH _{Leu} (s)
	Me	0.925 0.90	d, 6.2 d, 6.7	22.1, 22.7	CH _{Leu} (s) 0.925: NH _{Isox} (w), NH _{Met} (w) 0.90: Ph (7.6 vvw)
	CH _α	4.42	m	52.4	Me ₂ CHCH ₂ (s/m) NH _{Isox} (vs)
	NH	6.58	d, 7.4		NH _{Boc} (w) Me ₂ CHCH ₂ CH (s) Me ₂ CHCH _{Val} (s) NH _{Isox} (vvw)
Isox	CO			172.3	
	C-5	-		88.9	
	CH ₂₋₄	3.78, 3.33	AB system 17.6	41.6	3.78: Ph (7.6, m), 3.33: (Ph, m), CH ₂₋₄ _{Isox} (4.21, m)
	CH ₂ N	4.21 3.52	dd, 14.2, 8.9 dd, 14.2, 3.4	43.8	4.21: NH _{Isox} (vw); CH ₂₋₄ _{Isox} (3.33, m) 3.52: NH _{-Isox} (m)
	NH	7.35	br	-	CH ₂ N (3.52 m, 4.21 vvw), CH _{Leu} (vs) Me ₂ CHCH ₂ (vvw) NH _{Leu} (vvw) NH _{Met} (w)
	C-3			157.6	
	Ph	7.64-7.61 7.44-7.37	m m	130.6 128.8 128.6 126.9	7.63: Me _{Leu} (vw), CH ₂₋₄ _{Isox} (m)
Met	CO			172.9	
	OMe	3.80	s	52.8	
	CH	4.68	m	52.0	CH _{2-β} CH _{2-γ} (m/s) NH _{Met} (s)
	CH _{2-β}	2.19	m	30.3	NH _{Met} (m)
	CH _{2-γ}	2.57 2.48	m m	30.4	CH _{Met} (w) NH _{Met} (w)
	MeS	2.04	s	15.4	
	NH	7.77	d, 7.7	-	CH _{2β} -CH _{2γ} (s) NH _{Isox} (w) Me _{Leu} (w)

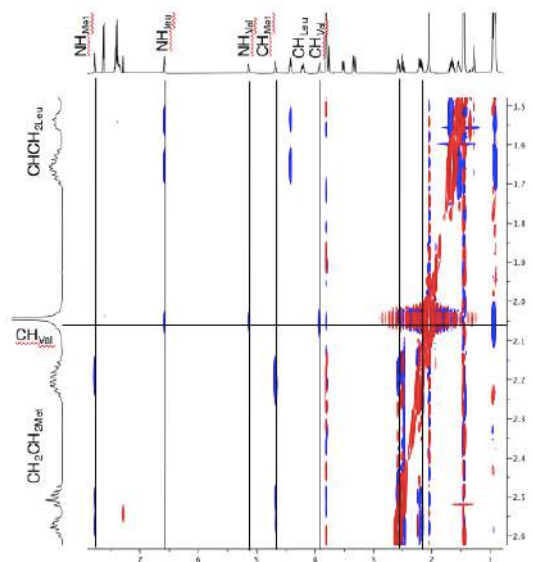
A)



B)



C)



D)

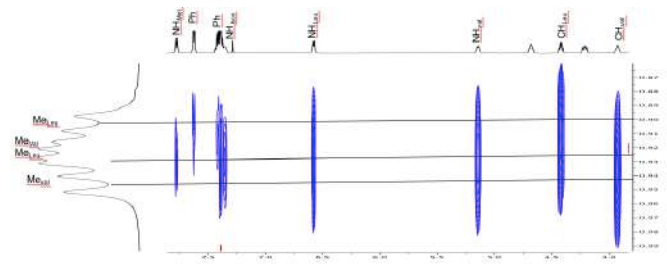
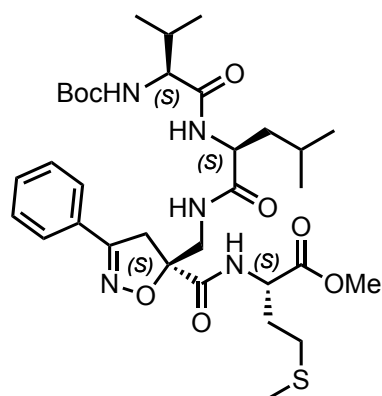


Figure 88 A) Zoom NH/NH region B) CH/Ar and CH/NH region. c) Zoom of CH-NH region. D) Zoom of Me_{L,Val}-NH region

Synthesis of N-Boc-(L)-Val-(L)-Leu-β-(S)-Isox-MetOMe (11b)



In a round bottom flask equipped with magnetic stirrer, **10b** (50 mg, 0.094 mmol) was suspended in dry DCM (3 mL). Afterwards, the solution was cooled at 0 °C and EtONOXime (13 mg, 0.094 mmol) and EDC (19 mg, 0.094 mmol) were added. The reaction was stirred for 1 hour at 0 °C, then (*L*)-Methionine-OMe (14 mg, 0.085 mmol) was added. DIPEA was added till pH = 8 (16 μL, 1.1 eq). The reaction was stirred overnight at room temperature. Next, the reaction mixture was washed with KHSO₄ 5% (10 mL), NaHCO₃ (10 mL), brine (15 mL), then the organic layer was dried over Na₂SO₄. Solvent was removed under reduced pressure, affording a white solid. Purification of the crude product by flash chromatography (gradient from 100% DCM to mixture DCM/AcOEt 6:4) afforded the compound **11b** as a white solid with 16% yield (8.6 mg). Detailed NMR data are reported in Table 28 and Figure 89.

R_f (DCM/MeOH 30:1): 0.47

Table 28 ¹H, ¹³C NMR (CD₃CN, 750mL 0.043 mM) and NOEs (700 ms) data for **11b**

AA	atom	¹ H δ	Molteplicity J (Hz)	¹³ C δ	Noesy (700 ms)
Val-1	CO			171.9	
	CH _a	3.87	m	60.1	Me _{Val} (s) NH _{Leu} (m)
	Me ₂ CH	2.07	overl.	30.7	
	Me	0.90, 0.88	d, 6.8 d, 6.0	19.4 19.2	CH _{Val} (vs), NH _{Boc} (s), NH _{Leu} (m)
	NH	5.12	brs	-	Me ₂ Val (s) NH _{Leu} (w)
	CO _{Boc}			155.9	
	<i>t</i> Bu	1.42	s	28.4, 79.9	
Leu-2	CO			172.6	
	CH ₂ CH	1.49, 1.39 2.04	m, m m	41.3 24.7	NH _{Leu} (m), NH _{Leu} (w), CH _{Leu} (m)
	Me	0.70	d, 6.4	21.9	CH _{Leu} (s), NH _{Leu} (w)
	CH _α	4.40	m	51.9	Me ₂ CHCH ₂ (s) NH _{Isox} (vs)
	NH	6.47	brs		NH _{Boc} (w), Me ₂ Val(vw), CH _{Val} (s)
Isox	CO			171.5	
	C-5	-		88.5	
	CH ₂ -4	3.66, 3.54	AB system 17.6	42.1	3.66: Ph (7.6, m), 3.54: CH ₂ N (4.19, m), Ph (7.6, m), NH _{Isox} (vw)
	CH ₂ N	4.19 3.47	dd, 14.3, 7.6 dd, 14.3, 5.1	43.6	4.19: NH _{Isox} (m), CH ₂ - 4 _{Isox} (3.54, m) 3.47: NH _{-Isox} (m)
	NH	6.82	brs	-	CH ₂ N (3.47 m, 4.19 m) CH _{Leu} (vs)
	C-3			157.7	
Met	Ph	7.65-7.62 7.44-7.36	m m	130.8 128.8 128.3 126.9	7.63: CH ₂ -4 _{Isox} (m)
	CO			171.5	
	OMe	3.70	s	52.6	
	CH	4.66	m	51.6	CH ₂ -βCH ₂ -γ(s) NH _{Met} (s)
	CH ₂ -β	2.23 2.09	m m	31.1	2.23: CH _{Met} (m) 2.09: CH _{Met} (m), NH _{Met} (w)
	CH ₂ -γ	2.55	m	30.1	CH _{Met} (m) NH _{Met} (m)
	MeS	2.10	s	30.6	
NH	7.48	d, 8.4	-	CH-CH ₂ -β (s)	

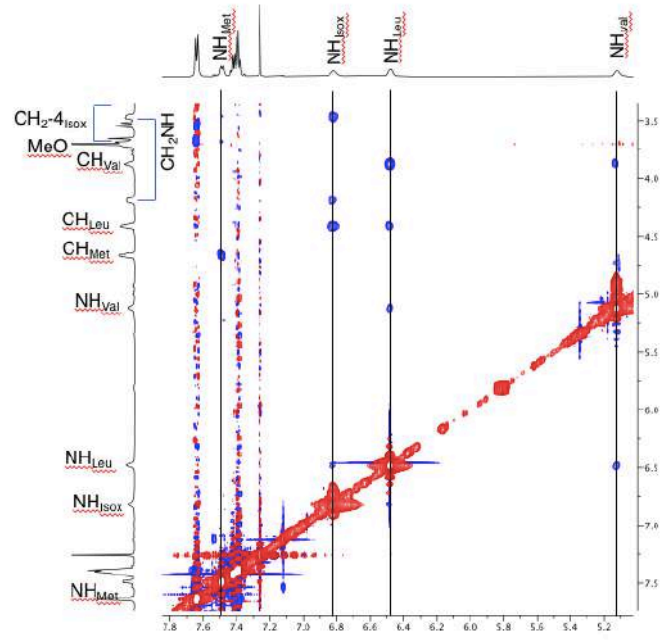
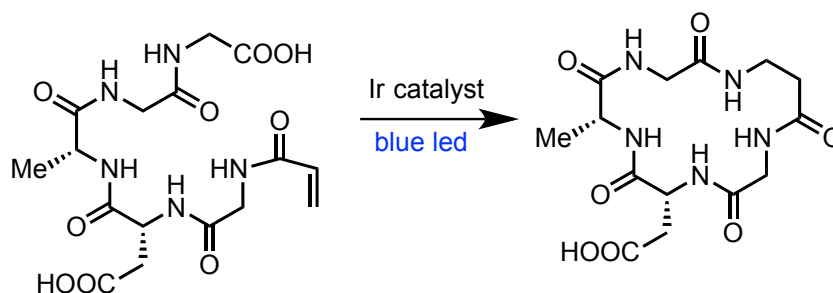


Figure 89 Zoom of CH-NH region

Photochemistry cyclization peptide

Introduction

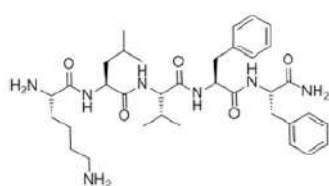
In the last ten years the interest on cyclic peptide has extremely increased due to their huge advantages; cyclic peptides are characterized by an improved biological activity and conformational rigidity if compared to the linear peptide. So far, ring closing metathesis (RCM) and 1,3 dipolar cycloaddition reactions are frequently reported as cyclization strategies, but in 2017 MacMillan's group was pioneer in peptide cyclization based on photochemical reactions (Scheme 25)¹¹³. It is important to point out that all the before mentioned strategies require the presence of at least one of not-natural amino acid to be successful.



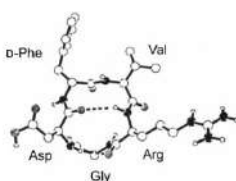
Scheme 25 MacMillan photochemical peptide cyclization

Starting from these premises during my visiting Ph.D. at University of Manchester, under the supervision of Prof. D. Leonori, I attempted the synthesis of cyclic peptides containing only natural amino acids through photoredox reactions. For this purpose, a new type of photochemistry reaction, just published in Nature Chemistry¹¹⁴ consisting N-C amination of aromatic group by general secondary amine, was exploited (Scheme 26).

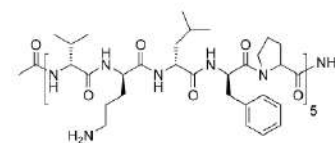
First of all, our idea was to evaluate the number of necessary AA to form a stable cycle then to try the functional group compatibility using different AA inserted in the peptide sequence. After that, the plan was used this new photochemical approach to cyclize linear peptide sequences already knew for their biological potency (Alzheimer's disease, Anticancer and Antimicrobial activity) in order to evaluate a possible improvement of the activity (Figure 90).



Alzheimer's disease



Anticancer activity



Antimicrobial activity

Figure 90 Example of linear peptide with biological activity

The preliminary results were very promising, in fact we obtained cyclic peptides from three to six AA residues. The project was unfortunately stopped due to external causes (Covid 19).

Bibliography

1. Seebach, D., Abele, S., Gademann, K. & Jaun, B. Pleated Sheets and Turns of β -Peptides with Proteinogenic Side Chains. *Angew. Chemie Int. Ed.* **38**, 1595–1597 (1999).
2. Cabrele, C., Martinek, T. A., Reiser, O. & Berlicki, Ł. Peptides Containing β -Amino Acid Patterns: Challenges and Successes in Medicinal Chemistry. *J. Med. Chem.* **57**, 9718–9739 (2014).
3. Nonn, M., Remete, A. M. & Kiss, L. Structural Diversity-Oriented Synthesis of Orthogonally Protected Cyclic Amino Acid Derivatives with Multiple Stereogenic Centers. *Helv. Chim. Acta* **103**, (2020).
4. Luo, G. *et al.* Access to Cyclic β -Amino Acids by Amine-Catalyzed Enantioselective Addition of the γ -Carbon Atoms of α,β -Unsaturated Imines to Enals. *Angew. Chemie - Int. Ed.* **58**, 17189–17193 (2019).
5. Appella, D. H., Christianson, L. A., Karle, I. L., Powell, D. R. & Gellman, S. H. β -Peptide Foldamers: Robust Helix Formation in a New Family of β -Amino Acid Oligomers. *J. Am. Chem. Soc.* **118**, 13071–13072 (1996).
6. Bode, K. A. & Applequist, J. Poly(β -amino acid) Helices. Theoretical π - π^* Absorption and Circular Dichroic Spectra. *Macromolecules* **30**, 2144–2150 (1997).
7. Appella, D. H., LePlae, P. R., Raguse, T. L. & Gellman, S. H. (R,R,R)-2,5-Diaminocyclohexanecarboxylic Acid, a Building Block for Water-Soluble, Helix-Forming β -Peptides. *J. Org. Chem.* **65**, 4766–4769 (2000).
8. Wang, X., Espinosa, J. F. & Gellman, S. H. 12-Helix Formation in Aqueous Solution with Short β -Peptides Containing Pyrrolidine-Based Residues. *J. Am. Chem. Soc.* **122**, 4821–4822 (2000).
9. Vasudev, P. G., Chatterjee, S., Shamala, N. & Balaran, P. Structural Chemistry of Peptides Containing Backbone Expanded Amino Acid Residues: Conformational Features of β , γ , and Hybrid Peptides. *Chem. Rev.* **111**, 657–687 (2011).
10. Jones, S. & Thornton, J. M. Principles of protein-protein interactions. *Proc. Natl. Acad. Sci.* **93**, 13 LP – 20 (1996).
11. Cheng, R. P., Gellman, S. H. & Degrado, W. F. β -Peptides : From Structure to Function. 40–43 (2001).
12. Cheng, P.-N., Liu, C., Zhao, M., Eisenberg, D. & Nowick, J. S. Amyloid β -sheet mimics that antagonize protein aggregation and reduce amyloid toxicity. *Nat. Chem.* **4**, 927–933 (2012).
13. Krauthäuser, S., Christianson, L. A., Powell, D. R. & Gellman, S. H. Antiparallel Sheet Formation in β -Peptide Foldamers: Effects of β -Amino Acid Substitution on Conformational Preference¹. *J. Am. Chem. Soc.* **119**, 11719–11720 (1997).

14. Robinson, J. A. β -Hairpin Peptidomimetics: Design, Structures and Biological Activities. *Acc. Chem. Res.* **41**, 1278–1288 (2008).
15. Whitby, L. R. *et al.* Design, Synthesis, and Validation of a β -Turn Mimetic Library Targeting Protein–Protein and Peptide–Receptor Interactions. *J. Am. Chem. Soc.* **133**, 10184–10194 (2011).
16. Guarna, A. & Trabocchi, A. *Peptidomimetics in Organic and Medicinal Chemistry: the art of transforming peptides in drugs.* (John Wiley & Sons, 2014).
17. Gellman, S. H. Foldamers : A Manifesto. **31**, 173–180 (1998).
18. Langer, O., Kählig, H., Zierler-Gould, K., Bats, J. W. & Mulzer, J. A Bicyclic Cispentacin Derivative as a Novel Reverse Turn Inducer in a GnRH Mimetic. *J. Org. Chem.* **67**, 6878–6883 (2002).
19. Pellegrino, S. *et al.* β -Hairpin mimics containing a piperidine-pyrrolidine scaffold modulate the β -amyloid aggregation process preserving the monomer species. *Chem. Sci.* **8**, 1295–1302 (2017).
20. Zhang, H., Zhong, H., Dou, F., Wang, C. & Wang, S. Electrospinning bifunctional polyphenylene-vinylene/heated graphene oxide composite nanofibers with luminescent-electrical performance. *Thin Solid Films* **725**, 138636 (2021).
21. Bucci, R. *et al.* Peptide grafting strategies before and after electrospinning of nanofibers. *Acta Biomater.* **122**, 82–100 (2021).
22. Bucci, R., Georgilis, E., Bittner, A. M., Gelmi, M. L. & Clerici, F. Peptide-based electrospun fibers: Current status and emerging developments. *Nanomaterials* **11**, 1–22 (2021).
23. Witty, M. Structure of the periplasmic domain of *Pseudomonas aeruginosa* TolA: evidence for an evolutionary relationship with the TonB transporter protein. *EMBO J.* **21**, (2002).
24. Kwon, S. *et al.* Self-Assembled Peptide Architecture with a Tooth Shape: Folding into Shape. *J. Am. Chem. Soc.* **133**, 17618–17621 (2011).
25. Xiang, S.-H. & Tan, B. Advances in asymmetric organocatalysis over the last 10 years. *Nat. Commun.* **11**, 3786 (2020).
26. List, B., Lerner, R. A. & Barbas, C. F. Proline-Catalyzed Direct Asymmetric Aldol Reactions. *J. Am. Chem. Soc.* **122**, 2395–2396 (2000).
27. Eder, U., Sauer, G. & Wiechert, R. New Type of Asymmetric Cyclization to Optically Active Steroid CD Partial Structures. *Angew. Chemie Int. Ed. English* **10**, 496–497 (1971).
28. Ahrendt, K. A., Borths, C. J. & MacMillan, D. W. C. New Strategies for Organic Catalysis: The First Highly Enantioselective Organocatalytic Diels–Alder Reaction. *J. Am. Chem. Soc.* **122**, 4243–4244 (2000).
29. Reyes, E. *et al.* How to Make Five Contiguous Stereocenters in One Reaction: Asymmetric Organocatalytic Synthesis of Pentasubstituted Cyclohexanes. *Angew.*

Chemie Int. Ed. **46**, 9202–9205 (2007).

30. Adzhubei, A. A., Sternberg, M. J. E. & Makarov, A. A. Polyproline-II Helix in Proteins: Structure and Function. *J. Mol. Biol.* **425**, 2100–2132 (2013).
31. Wilhelm, P., Lewandowski, B., Trapp, N. & Wennemers, H. A Crystal Structure of an Oligoproline PPII-Helix, at Last. *J. Am. Chem. Soc.* **136**, 15829–15832 (2014).
32. Moradi, M., Babin, V., Sagui, C. & Roland, C. A Statistical Analysis of the PPII Propensity of Amino Acid Guests in Proline-Rich Peptides. *Biophys. J.* **100**, 1083–1093 (2011).
33. Bonetti, A. *et al.* syn/anti Switching by Specific Heteroatom–Titanium Coordination in the Mannich-Like Synthesis of 2,3-Diaryl- β -amino Acid Derivatives. *European J. Org. Chem.* **2014**, 3203–3209 (2014).
34. Craven, T. W., Bonneau, R. & Kirshenbaum, K. PPII Helical Peptidomimetics Templated by Cation- π Interactions. *ChemBioChem* **17**, 1824–1828 (2016).
35. Bucci, R., Contini, A., Clerici, F., Pellegrino, S. & Gelmi, M. L. From glucose to enantiopure morpholino β -amino acid: a new tool for stabilizing γ -turns in peptides. *Org. Chem. Front.* **6**, 972–982 (2019).
36. Novotny, M. & Kleywegt, G. J. A Survey of Left-handed Helices in Protein Structures. *J. Mol. Biol.* **347**, 231–241 (2005).
37. Shang, M. *et al.* Modular, stereocontrolled C β -H/C α -C activation of alkyl carboxylic acids. *Proc. Natl. Acad. Sci.* **116**, 8721 LP – 8727 (2019).
38. Shang, M. *et al.* Modular, stereocontrolled C(β)-H/C(α)-C activation of alkyl carboxylic acids. *Proc. Natl. Acad. Sci. U. S. A.* **116**, 8721–8727 (2019).
39. Dukor, R. K. & Keiderling, T. A. Mutarotation studies of poly-L-proline using FTIR, electronic and vibrational circular dichroism. *Biospectroscopy* **2**, 83–100 (1996).
40. Mahoney, N. M., Janmey, P. A. & Almo, S. C. Structure of the profilin-poly-L-proline complex involved in morphogenesis and cytoskeletal regulation. *Nat. Struct. Biol.* **4**, 953–960 (1997).
41. Maffucci, I. & Contini, A. Improved Computation of Protein–Protein Relative Binding Energies with the Nwat-MMGBSA Method. *J. Chem. Inf. Model.* **56**, 1692–1704 (2016).
42. Vaghi, F., Bucci, R., Clerici, F., Contini, A. & Gelmi, M. L. Non-natural 3-Arylmorpholino- β -amino Acid as a PPII Helix Inducer. *Org. Lett.* **22**, 6197–6202 (2020).
43. Ren, X. *et al.* Correction: Surface modification and endothelialization of biomaterials as potential scaffolds for vascular tissue engineering applications. *Chem. Soc. Rev.* **44**, (2015).
44. Chow, L. W. *et al.* Peptide-Directed Spatial Organization of Biomolecules in Dynamic Gradient Scaffolds. *Adv. Healthc. Mater.* **3**, 1381–1386 (2014).

45. Singh, G., Bittner, A. M., Loscher, S., Malinowski, N. & Kern, K. Electrospinning of Diphenylalanine Nanotubes. *Adv. Mater.* **20**, 2332–2336 (2008).
46. Hamedani, Y. *et al.* Electrospinning of tyrosine-based oligopeptides: Self-assembly or forced assembly? *J. Biomed. Mater. Res. Part A* **108**, 829–838 (2020).
47. Nuansing, W. *et al.* Electrospinning of peptide and protein fibres: approaching the molecular scale. *Faraday Discuss.* **166**, 209–221 (2013).
48. Seebach, D. *et al.* β 2- and β 3-Peptides with Proteinaceous Side Chains: Synthesis and solution structures of constitutional isomers, a novel helical secondary structure and the influence of solvation and hydrophobic interactions on folding. *Helv. Chim. Acta* **81**, 932–982 (1998).
49. Ryakhovskii, V. V, Agafonov, S. V & Kosyrev, Y. M. Special features of the synthesis of peptides containing secondary amino acids. *Russ. Chem. Rev.* **60**, 924–933 (1991).
50. Hu, C. *et al.* Carbon Nanomaterials for Energy and Biorelated Catalysis: Recent Advances and Looking Forward. *ACS Cent. Sci.* **5**, 389–408 (2019).
51. Sang, W., Zhang, Z., Dai, Y. & Chen, X. Recent advances in nanomaterial-based synergistic combination cancer immunotherapy. *Chem. Soc. Rev.* **48**, 3771–3810 (2019).
52. Pelaz, B. *et al.* Diverse Applications of Nanomedicine. *ACS Nano* **11**, 2313–2381 (2017).
53. Locarno, S. *et al.* Self-assembled hydrophobic Ala-Aib peptide encapsulating curcumin: a convenient system for water insoluble drugs. *RSC Adv.* **10**, 9964–9975 (2020).
54. Ren, J. *et al.* Biological Material Interfaces as Inspiration for Mechanical and Optical Material Designs. *Chem. Rev.* **119**, 12279–12336 (2019).
55. Pu, F., Ren, J. & Qu, X. Nucleobases, nucleosides, and nucleotides: versatile biomolecules for generating functional nanomaterials. *Chem. Soc. Rev.* **47**, 1285–1306 (2018).
56. Bucci, R. *et al.* Self-assembly of an amphipathic $\alpha\alpha\beta$ -tripeptide into cationic spherical particles for intracellular delivery. *Org. Biomol. Chem.* 6773–6779 (2017) doi:10.1039/C7OB01693J.
57. Clerici, F., Erba, E., Gelmi, M. L. & Pellegrino, S. Non-standard amino acids and peptides: From self-assembly to nanomaterials. *Tetrahedron Lett.* **57**, 5540–5550 (2016).
58. Ruffoni, A. *et al.* Aqueous self-assembly of short hydrophobic peptides containing norbornene amino acid into supramolecular structures with spherical shape. *RSC Adv.* **6**, 90754–90759 (2016).
59. Bonetti, A. *et al.* Dipeptide Nanotubes Containing Unnatural Fluorine-Substituted beta2,3-Diarylamino Acid and l-Alanine as Candidates for Biomedical Applications. *Org. Lett.* **17**, 4468–4471 (2015).

60. Marchesan, S., Vargiu, A. V & Styan, K. E. The Phe-Phe Motif for Peptide Self-Assembly in Nanomedicine. *Molecules* vol. 20 (2015).
61. Yan, X., Zhu, P. & Li, J. Self-assembly and application of diphenylalanine-based nanostructures. *Chem. Soc. Rev.* **39**, 1877–1890 (2010).
62. Chen, Y. *et al.* High-Efficiency Fluorescence through Bioinspired Supramolecular Self-Assembly. *ACS Nano* **14**, 2798–2807 (2020).
63. Kol, N. *et al.* Self-Assembled Peptide Nanotubes Are Uniquely Rigid Bioinspired Supramolecular Structures. *Nano Lett.* **5**, 1343–1346 (2005).
64. Roviello, G. N., Benedetti, E., Pedone, C. & Bucci, E. M. Nucleobase-containing peptides: an overview of their characteristic features and applications. *Amino Acids* **39**, 45–57 (2010).
65. Marafon, G. *et al.* Tuning morphological architectures generated through living supramolecular assembly of a helical foldamer end-capped with two complementary nucleobases. *Soft Matter* **13**, 4231–4240 (2017).
66. Datta, D., Tiwari, O. & Ganesh, K. N. New archetypes in self-assembled Phe-Phe motif induced nanostructures from nucleoside conjugated-diphenylalanines. *Nanoscale* **10**, 3212–3224 (2018).
67. Tarasenko, Y. V, Abramova, T. V, Mamatuk, V. I. & Silnikov, V. N. Effective Synthesis of Fluorescently Labeled Morpholino Nucleoside Triphosphate Derivatives. *Nucleosides. Nucleotides Nucleic Acids* **35**, 32–42 (2016).
68. Abramova, T. V, Belov, S. S., Tarasenko, Y. V & Silnikov, V. N. Solid-phase-supported synthesis of morpholinoglycine oligonucleotide mimics. *Beilstein J. Org. Chem.* **10**, 1151–1158 (2014).
69. Pattanayak, S., Paul, S., Nandi, B. & Sinha, S. Improved Protocol for the Synthesis of Flexibly Protected Morpholino Monomers from Unprotected Ribonucleosides. *Nucleosides. Nucleotides Nucleic Acids* **31**, 763–782 (2012).
70. Zhang, N. *et al.* Synthesis and properties of morpholino chimeric oligonucleotides. *Tetrahedron Lett.* **49**, 3570–3573 (2008).
71. Tao, K., Levin, A., Adler-Abramovich, L. & Gazit, E. Fmoc-modified amino acids and short peptides: simple bio-inspired building blocks for the fabrication of functional materials. *Chem. Soc. Rev.* **45**, 3935–3953 (2016).
72. Nikitin, T., Kopyl, S., Shur, V. Y., Kopelevich, Y. V & Kholkin, A. L. Low-temperature photoluminescence in self-assembled diphenylalanine microtubes. *Phys. Lett. A* **380**, 1658–1662 (2016).
73. Ferré, M., Pleixats, R., Wong Chi Man, M. & Cattoën, X. Recyclable organocatalysts based on hybrid silicas. *Green Chem.* **18**, 881–922 (2016).
74. MacMillan, D. W. C. The advent and development of organocatalysis. *Nature* **455**, 304–308 (2008).
75. Mukherjee, S., Yang, J. W., Hoffmann, S. & List, B. Asymmetric Enamine Catalysis.

- Chem. Rev.* **107**, 5471–5569 (2007).
76. Sigman, M. S. & Jacobsen, E. N. Schiff Base Catalysts for the Asymmetric Strecker Reaction Identified and Optimized from Parallel Synthetic Libraries. *J. Am. Chem. Soc.* **120**, 4901–4902 (1998).
 77. Corey, E. J. & Grogan, M. J. Enantioselective Synthesis of α -Amino Nitriles from N-Benzhydryl Imines and HCN with a Chiral Bicyclic Guanidine as Catalyst. *Org. Lett.* **1**, 157–160 (1999).
 78. Reisman, S. E., Doyle, A. G. & Jacobsen, E. N. Enantioselective Thiourea-Catalyzed Additions to Oxocarbenium Ions. *J. Am. Chem. Soc.* **130**, 7198–7199 (2008).
 79. Tsogoeva, S. B. Recent Advances in Asymmetric Organocatalytic 1,4-Conjugate Additions. *European J. Org. Chem.* **2007**, 1701–1716 (2007).
 80. Kempf, B., Hampel, N., Ofial, A. R. & Mayr, H. Structure–Nucleophilicity Relationships for Enamines. *Chem. – A Eur. J.* **9**, 2209–2218 (2003).
 81. Maultzsch, J., Reich, S. & Thomsen, C. Raman scattering in carbon nanotubes revisited. *Phys. Rev. B* **65**, 233402 (2002).
 82. Schnitzer, T. & Wennemers, H. Effect of β -Amino Acids on the Performance of the Peptidic Catalyst H-dPro-Pro-Glu-NH₂. *Helv. Chim. Acta* **102**, e1900070 (2019).
 83. Breuning, M., Winnacker, M. & Steiner, M. Efficient One-Pot Synthesis of Enantiomerically Pure 2-(Hydroxymethyl)morpholines. *European J. Org. Chem.* **2007**, 2100–2106 (2007).
 84. Seebach, D. *et al.* β -Peptides: Synthesis by Arndt-Eistert homologation with concomitant peptide coupling. Structure determination by NMR and CD spectroscopy and by X-ray crystallography. Helical secondary structure of a β -hexapeptide in solution and its stability towards pe. *Helv. Chim. Acta* **79**, 913–941 (1996).
 85. Seebach, D. *et al.* Linear, Peptidase-Resistant β 2/ β 3-Di- and α / β 3-Tetrapeptide Derivatives with Nanomolar Affinities to a Human Somatostatin Receptor, Preliminary Communication. *Helv. Chim. Acta* **84**, 3503–3510 (2001).
 86. Frackenpohl, J., Arvidsson, P. I., Schreiber, J. V & Seebach, D. The Outstanding Biological Stability of β - and γ -Peptides toward Proteolytic Enzymes: An In Vitro Investigation with Fifteen Peptidases. *ChemBioChem* **2**, 445–455 (2001).
 87. Gopi, H. N. *et al.* Proteolytic stability of β -peptide bonds probed using quenched fluorescent substrates incorporating a hemoglobin cleavage site. *FEBS Lett.* **535**, 175–178 (2003).
 88. Sagan, S. *et al.* Structural and biological effects of a β 2- or β 3-amino acid insertion in a peptide. *Eur. J. Biochem.* **270**, 939–949 (2003).
 89. Wiegand, H. *et al.* The outstanding metabolic stability of a ¹⁴C-labeled β -nonapeptide in rats – in vitro and in vivo pharmacokinetic studies. *Biopharm. Drug Dispos.* **23**, 251–262 (2002).

90. Aguilar, M.-I. *et al.* β -Amino acid-containing hybrid peptides—new opportunities in peptidomimetics. *Org. Biomol. Chem.* **5**, 2884–2890 (2007).
91. Lengyel, G. A. & Horne, W. S. Design Strategies for the Sequence-Based Mimicry of Side-Chain Display in Protein β -Sheets by α/β -Peptides. *J. Am. Chem. Soc.* **134**, 15906–15913 (2012).
92. Dutot, L. *et al.* An extension of the ‘Bip method’: induced axial chirality in a series of dipeptides based on Bip/ β 2,2-HBip combined with Ala/ β 3-HAla. *Tetrahedron: Asymmetry* **17**, 363–371 (2006).
93. Hansen, T., Ausbacher, D., Flaten, G. E., Havelkova, M. & Strøm, M. B. Synthesis of Cationic Antimicrobial β 2,2-Amino Acid Derivatives with Potential for Oral Administration. *J. Med. Chem.* **54**, 858–868 (2011).
94. Seebach, D. *et al.* Preparation and Structure of β -Peptides Consisting of Geminally Disubstituted β 2,2- and β 3,3-Amino Acids: A Turn Motif for β -Peptides. *Helv. Chim. Acta* **81**, 2218–2243 (1998).
95. Abele, S., Seiler, P. & Seebach, D. Synthesis, Crystal Structures, and Modelling of β -Oligopeptides Consisting of 1-(Aminomethyl)cyclopropanecarboxylic Acid: Ribbon-Type Arrangement of Eight-Membered H-Bonded Rings. *Helv. Chim. Acta* **82**, 1559–1571 (1999).
96. Toniolo, C. *et al.* Peptide δ -Turn: Literature Survey and Recent Progress. *Chem. – A Eur. J.* **21**, 13866–13877 (2015).
97. Yu, J.-S., Noda, H. & Shibasaki, M. Quaternary β 2,2-Amino Acids: Catalytic Asymmetric Synthesis and Incorporation into Peptides by Fmoc-Based Solid-Phase Peptide Synthesis. *Angew. Chemie Int. Ed.* **57**, 818–822 (2018).
98. Sharma, G. V. M., Rajender, K., Sridhar, G., Reddy, P. S. & Kanakaraju, M. Synthesis of new β 2,2-amino acids with carbohydrate side chains: impact on the synthesis of peptides. *Carbohydr. Res.* **388**, 8–18 (2014).
99. Mata, L., Avenoz, A., Busto, J. H., Corzana, F. & Peregrina, J. M. Quaternary Chiral β 2,2-Amino Acids with Pyridinium and Imidazolium Substituents. *Chem. – A Eur. J.* **18**, 15822–15830 (2012).
100. Mazo, N. *et al.* Synthesis of Mixed α/β 2,2-Peptides by Site-Selective Ring-Opening of Cyclic Quaternary Sulfamidates. *Org. Lett.* **17**, 5804–5807 (2015).
101. Tyndall, J. D. A., Pfeiffer, B., Abbenante, G. & Fairlie, D. P. Over One Hundred Peptide-Activated G Protein-Coupled Receptors Recognize Ligands with Turn Structure. *Chem. Rev.* **105**, 793–826 (2005).
102. Rodríguez, F. *et al.* Conformational preferences of Chiral acyclic homooligomeric β 2,2-Peptides. *Curr. Top. Med. Chem.* **14**, 1225–1234 (2014).
103. Bucci, R. *et al.* Tetrahydro-4 H-(pyrrolo[3,4- d]isoxazol-3-yl)methanamine: A Bicyclic Diamino Scaffold Stabilizing Parallel Turn Conformations. *J. Org. Chem.* **83**, 11493–11501 (2018).

104. Houk, K. N., Sims, J., Watts, C. R. & Luskus, L. J. Origin of reactivity, regioselectivity, and periselectivity in 1,3-dipolar cycloadditions. *J. Am. Chem. Soc.* **95**, 7301–7315 (1973).
105. Sá, M. M., Ramos, M. D. & Fernandes, L. Fast and efficient preparation of Baylis–Hillman-derived (E)-allylic azides and related compounds in aqueous medium. *Tetrahedron* **62**, 11652–11656 (2006).
106. Tran, N. C., Dhondt, H., Flipo, M., Deprez, B. & Willand, N. Synthesis of functionalized 2-isoxazolines as three-dimensional fragments for fragment-based drug discovery. *Tetrahedron Lett.* **56**, 4119–4123 (2015).
107. Kosal, A. D., Wilson, E. E. & Ashfeld, B. L. Phosphine-based redox catalysis in the direct traceless Staudinger ligation of carboxylic acids and azides. *Angew. Chemie* **51** **48**, 12036–12040 (2012).
108. Burés, J., Martín, M., Urpí, F. & Vilarrasa, J. Catalytic Staudinger–Vilarrasa Reaction for the Direct Ligation of Carboxylic Acids and Azides. *J. Org. Chem.* **74**, 2203–2206 (2009).
109. Tam, A., Soellner, M. B. & Raines, R. T. Electronic and steric effects on the rate of the traceless Staudinger ligation. *Org. Biomol. Chem.* **6**, 1173–1175 (2008).
110. Waghmare, A. A., Hindupur, R. M. & Pati, H. N. Propylphosphonic anhydride (T3P®): An expedient reagent for organic synthesis. *Rev. J. Chem.* **4**, 53–131 (2014).
111. Cremer, D. & Pople, J. A. General definition of ring puckering coordinates. *J. Am. Chem. Soc.* **97**, 1354–1358 (1975).
112. Bucci, R. *et al.* Fishing in the Toolbox of Cyclic Turn Mimics: a Literature Overview of the Last Decade. *European J. Org. Chem.* **2021**, 2887–2900 (2021).
113. McCarver, S. J. *et al.* Decarboxylative Peptide Macrocyclization through Photoredox Catalysis. *Angew. Chemie Int. Ed.* **56**, 728–732 (2017).
114. Ruffoni, A. *et al.* Practical and regioselective amination of arenes using alkyl amines. *Nat. Chem.* **11**, 426–433 (2019).